Characterising Human Colorectal Mononuclear Phagocytes and Investigating their Role in Early HIV Infection

Erica Elizabeth Longmuir-Vine

A thesis submitted in fulfilment of the requirements for admission to the degree of Doctor of Philosophy at The University of Sydney

February 2025

Primary Supervisor: Dr Kirstie Bertram
Auxiliary Supervisor: Professor Andrew Harman
Auxiliary Supervisor: Professor Anthony Cunningham

Centre for Virus Research
The Westmead Institute for Medical Research

Faculty of Medicine and Health
School of Medical Science
The University of Sydney

Declaration

This is to certify that the content of this thesis is my own work. This thesis has not been submitted for any other degree or purpose.

I certify that the intellectual content of this thesis is the product of my own work, and that all assistance received in preparing this thesis and all sources have been acknowledged.

During the preparation of this thesis, OpenAI GPT-4o was minimally used for the purposes of research and text editing, including literature searches, thesaurus and paraphrasing. Where any text was modified by generative AI, I reviewed the resulting content for any errors, inaccuracies or biases, and modified it as required. I take full responsibility for the submitted thesis and ensure the work is my own and has used generative AI within the parameters of use, see University of Sydney generative AI guide for researchers.

The following publications are contained within this thesis:

- Doyle CM*, **Vine EE*** et al. Optimal Isolation Protocols for Examining and Interrogating Mononuclear Phagocytes From Human Intestinal Tissue. Front Immunol. 2021 Sep 1;12:727952. doi: 10.3389/fimmu.2021.727952. PMID: 34566985; PMCID: PMC8462295.
- **Vine EE***, Rhodes JW* et al. HIV transmitting mononuclear phagocytes; integrating the old and new. Mucosal Immunol. 2022 Apr;15(4):542-550. doi: 10.1038/s41385-022-00492-0. Epub 2022 Feb 16. PMID: 35173293; PMCID: PMC9259493.

Material written or published by other persons have been appropriately acknowledged and referenced in this thesis.

In addition to the statements above, in cases where I am not the corresponding author of a published item, permission to include the published material has been granted by the corresponding author.

Erica Elizabeth Longmuir-Vine

February 2025

As supervisor for the candidature upon which this thesis is based, I can confirm that the authorship attribution statements above are correct.

Dr Kirstie Bertram
February 2025

Abstract

In 2023, there was a HIV-related death every minute. HIV persists as a global pandemic, with 40 million people infected worldwide, and although antiretroviral therapies (ART) have made a significant impact on people living with HIV, transmission rates currently exceed a million new cases a year. ART can be utilised as pre-exposure prophylaxis (PrEP), though its minimal use in high-risk groups and its reduced efficiency in inflammation contributes to enduring HIV transmission. In the absence of a cure or vaccine, improving or supplementing current transmission prevention strategies could help mitigate PrEP non-compliance. The design of more targeted and varied prevention strategies requires an accurate and comprehensive understanding of the early events underlying HIV transmission. Mononuclear phagocytes (MNP), with their array of pattern recognition receptors, are the first cells to interact and bind HIV, facilitating the dissemination of virus to CD4 T cells as a consequence of their antigen presenting function. Despite the high risk and incidence of transmission occurring via receptive anal intercourse, early HIV interactions with key target cells in the human colon and rectum (colorectum) remain under-researched.

In this thesis, utilising optimised tissue digestion protocols in combination with high-parameter flow cytometry, human colorectal MNPs were categorised into three subsets of macrophage: monocyte-derived macrophage (MDM), transitional-MDM (t-MDM), and tissue-resident macrophage (Macrophage), and three subsets of DC: conventional DC1 (cDC1), $CD207^{+}$ cDC2, $CD207^{-}$ cDC2. These MNP subsets expressed unique profiles of HIV entry and HIV-binding lectin receptors and Macrophages and t-MDMs were the most capable at binding and taking up HIV over two hours. MNP interactions with HIV and CD4 T cells were investigated and though all MNPs were able to enhance the infection of CD4 T cells, DCs and t-MDM were more efficient in transferring HIV to CD4 T cells, while Macrophages were indicated to play a more crucial role in the establishment of the tissue HIV reservoir. A landmark high-parameter flow cytometry panel is also presented to interrogate and compare MNPs across both steady and inflammatory state sexual transmission tissues, as well as their capacity to take up HIV.

Identifying the MNPs that play a role in the HIV transmission in the human colorectum is essential for the development of additional PrEP options, potentially targeted at mucosal sites, which would increase PrEP compliance, reduce transmission rates, and aid in the eradication of this of this global pandemic.

Acknowledgements

First, and foremost, I would like to thank my supervisory team. The years that covered this project have personally been the hardest in my life. All of you provided me so much support in this project but also went above and beyond and provided me the personal support I needed to persevere and never give up. It is my relationships with you all that has made me sure that our lab is where I want to be. **Dr Kirstie Bertram**, your skills and talents in the lab are matched by your support out of the lab. None of the work we do here would be possible without you. You are truly a tissue and flow god, and I aspire to one day match the incredible standard you have set. **Professor Andrew Harman**, you have taught me more about presenting my work that anyone else. You gave me so many opportunities to practice my writing and presenting skills, and I am so grateful to have had you in my corner so that I could succeed. Thank you for always being available for a chat, and the many pieces of advice you gave me over the years. **Professor Tony Cunningham**, you are the only other person who truly loves macrophages as much as I do. You have taught me so much over the years with your endless memory for the literature. Thank you for all the laughs.

During my PhD, I was fortunate to collaborate with: **Dr Jake Rhodes** – you were my introduction into human tissue and HIV work. Your quiet, laidback confidence and willingness to work all hours to get the data, provided me with a standard that I have tried to live up to. **Dr Chloe Doyle** – you taught me everything I needed to know about intestinal tissue and how to have fun while doing it. I will always be grateful that we shared our first first-author paper together, as that crazy turn around gave me the best experience for all my writing that came after it. **Freja Warner van Dijk** – working on our panel together was a joy as much as it was a nightmare. The many challenges that we faced bringing it together would have been unbearable without your humour and support. **Dr Thomas O'Neil** – I am always impressed by your thirst for knowledge, and I have greatly benefitted from your willingness to share it. I am grateful that we will continue to collaborate and hope I can give back as much help as you have given me.

A huge thank you to the colorectal surgeons, particularly **Dr Graeme Cterctеko** and **Dr James Toh**, both of whom took a personal interest in the study and help to drive the rest of the surgical staff to ensure as many samples as possible made their way to me.

Suat Dervish, **Edwin Lau** and **Eve Diefenbach** of the WIMR Core flow facility. Thank you for sharing my joy of flow cytometry and for all the long hours sorting my very troublesome samples.

The year I worked as a facility technician with you all gave me so much insight and I will carry the knowledge with me in my career.

Dr Vicki Stylianou, **Dr Jason Herbert**, **Dr Emily McKinna** and **Wade Bocking** – at different times during my PhD, the four of you have been my go-to for support and laughs. Without you, these years would have been so much harder, and I am grateful that this project brought me into the lives of such amazing people. I would not have made it this far without all of you.

To the far-too-many people on level 6, and WIMR in general, thank you for always being around for a chat, whether it be about experimental issues or just blowing off steam. I am grateful for the supportive atmosphere that you all created; it really has been like working with friends and I feel grateful to be able to continue with you all for many years to come.

To my beautiful friends and family, who not only tried to understand my project but gave me a place to be away from it. Thank you for always reminding me what is important and providing me with the space I needed to get this done.

This research reported in this thesis was supported by the award of a Research Training Program scholarship to the PhD Candidate.

Publications, Presentations and Scholarships

Peer Reviewed Publications

1. Jake W. Rhodes*, Rachel A. Botting*, Kirstie M. Bertram, **Erica E. Vine**, Hafsa Rana, Heeva Baharlou, Peter Vegh, Thomas R. O'Neil, Anneliese S. Ashhurst, James Fletcher, Grant P. Parnell, J. Dinny Graham, Najla Nasr, Jake J. K. Lim, Laith Barnouti, Peter Haertsch, Martijn P. Gosselink, Angelina Di Re, Faizur Reza, Grahame Ctercteko, Gregory J. Jenkins, Andrew J. Brooks, Ellis Patrick, Scott N. Byrne, Eric Hunter, Muzlifah A. Haniffa, Anthony L. Cunningham, Andrew N. Harman. Identification of HIV-Transmitting Sub-Epithelial Mononuclear Phagocytes in Human Anogenital and Colorectal Tissues. *Nature Communications* (2021)

2. Chloe M. Doyle*, **Erica E. Vine***, Kirstie M. Bertram, Heeva Baharlou, Jake W. Rhodes, Suat Dervish, Martijn P. Gosselink, Angelina Di Re, Geoffrey P. Collins, Faizur Reza, James W. T. Toh, Nimalan Pathma-Nathan, Golo Ahlenstiel, Grahame Ctercteko, Anthony L. Cunningham, Andrew N. Harman, Scott N Byrne. Optimal Isolation Protocols for Examining and Interrogating Mononuclear Phagocytes From Human Intestinal Tissue. *Frontiers in Immunology* (2021)

3. **Erica E. Vine***, Jake W. Rhodes*, Freja A. Warner van Dijk, Scott N. Byrne, Kirstie M. Bertram, Anthony L. Cunningham, Andrew N. Harman. HIV transmitting mononuclear phagocytes; integrating the old and new. *Mucosal Immunology* (2022)

4. Heeva Baharlou, Nicolas Canete, **Erica E. Vine**, Kevin Hu, Di Yuan, Kerrie J. Sandgren, Kirstie M. Bertram, Najla Nasr, Jake W. Rhodes, Martijn P. Gosselink, Angelina Di Re, Faizur Reza, Grahame Ctercteko, Nimalan Pathma-Nathan, Geoff Collins, James Toh, Ellis Patrick, Muzlifah A. Haniffa, Jacob D. Estes, Scott N. Byrne, Anthony L. Cunningham, Andrew N. Harman. An *in-situ* analysis pipeline for initial host-pathogen interactions reveals signatures of human colorectal HIV transmission. *Cell Reports* (2022)

5. Wuji Zhang, Brendon Y. Chua, Kevin J. Selva, Lukasz Kedzierski, Thomas M. Ashhurst, Ebene R. Haycroft, Suzanne K. Shoffner-Beck, Luca Hensen, David F. Boyd, Fiona James, Effie Mouhtouris, Jason C. Kwong, Kyra Y. L. Chua, George Drewett, Ana Copaescu, Julie E Dobson, Louise C. Rowntree, Jennifer R. Habel, Lilith F. Allen, Hui-Fern Koay, Jessica A Neil, Matthew J. Gartner, Christina Y. Lee, Patiyan Andersson, Sadid F. Khan, Luke Blakeway, Jessica Wisniewski, James H. McMahon, **Erica E. Vine**, Anthony L. Cunningham, Jennifer Audsley, Irani Thevarajan, Torsten Seemann, Norelle L. Sherry, Fatima Amanat, Florian Krammer, Sarah L. Londrigan, Linda M. Wakim, Nicholas J. C. King, Dale I. Godfrey, Laura K. Mackay, Paul G. Thomas, Suellen Nicholson, Kelly B. Arnold, Amy W. Chung, Natasha E. Holmes, Olivia C. Smibert, Jason A. Trubiano, Claire L. Gordon, Thi H. O. Nguyen, Katherine Kedzierska. SARS-CoV-2 infection results in immune responses in the respiratory tract and peripheral blood that suggest mechanisms of disease severity. *Nature Communications* (2022)

6. Kirstie M. Bertram*, Thomas R. O'Neil*, **Erica E. Vine**, Heeva Baharlou, Anthony L. Cunningham, Andrew N. Harman. Defining the landscape of human epidermal mononuclear phagocytes. *Immunity* (2023)

7. Jayden A. O'Brien, Jackson F. Karrasch, Yun Huang, **Erica E. Vine**, Anthony L. Cunningham, Andrew N. Harman, Paul J. Austin. Nerve-myeloid cell interactions in persistent human pain: A reappraisal using updated cell subset classifications. *Pain* (2023)

8. **Erica E. Vine**, Paul J. Austin, Thomas R. O'Neil, Kirstie M. Bertram, Anthony L. Cunningham, Andrew N. Harman. Epithelial *dendritic* cells vs Langerhans cells; implications for mucosal vaccines. Cell Reports (2024)

9. Freja A. Warner van Dijk*, Orion Tong*, Thomas R. O'Neil, Kirstie M. Bertram, Kevin Hu, Heeva Baharlou, **Erica E. Vine**, Kate Jenns, Martijn P. Gosselink, James W. Toh, Tim Papadopoulos, Laith Barnouti, Gregory J. Jenkins, Gavin Sandercoe, Muzlifah Haniffa, Kerrie J. Sandgren, Andrew N. Harman, Anthony L. Cunningham, Najla Nasr. Characterising plasmacytoid and myeloid AXL+ SIGLEC6+ dendritic cell functions and their interactions with HIV. *PLoS Pathogens* (2024)

* co-first authors

Submitted for Publication

1. Daniel J. Buffa, Thomas R. O'Neil, **Erica E. Vine**, Lara Sarkawt, Freja A. Warner van Dijk, Oscar A. Dong, Najla Nasr, Anthony L. Cunningham, Kirstie M. Bertram, Andrew N. Harman. Current Understandings of Anogenital Dendritic Cells' Role in HIV Transmission. *Viruses* (2025). *under peer review*

2. **Erica E. Vine***, Freja A. Warner van Dijk*, Anthony L Cunningham, Najla Nasr, Andrew N Harman, Kirstie M Bertram. OMIP (unallocated): 26-parameter flow cytometry panel to characterise all homeostatic and inflammatory state mononuclear phagocytes in human skin, type II mucosa and type I mucosa. *Cytometry A* (2025). *submitted*

* co-first authors

Presentations and Chairs

1. Australian Centre for HIV and Hepatitis Virology Research (ACH4) annual meeting, oral presentation (2020)
2. Australian Centre for HIV and Hepatitis Virology Research (ACH4) annual meeting, oral presentation (2021)
3. Westmead Hospital Week Research Symposium, poster presentation (2022)
4. Westmead Research Hub Scientific Platforms Seminar Series, seminar (2022)
5. Australian Centre for HIV and Hepatitis Virology Research (ACH4) annual meeting, oral presentation (2022)
6. Society for Mucosal Immunology International Conference for Mucosal Immunology, oral presentation (2022), poster presentation (2022)
7. International Union of Immunological Societies 16th International Symposium on Dendritic Cells 2022, poster presentation (2022)
8. Kirby Institute HIV Science Symposium, session chair (2023)
9. Australian Centre for HIV and Hepatitis Virology Research (ACH4) annual meeting, oral presentation (2023)
10. Society for Mucosal Immunology International Conference for Mucosal Immunology, poster presentation x 2 (2024)
11. Early and Mid-Career Researcher Symposium, poster presentation (2024)
12. Westmead Research and Innovation Conference, oral presentation (2024)
13. Australian Society of Immunology conference, oral presentation (2024)

Awards and Scholarships

1. Australian Government Research Training Program Scholarship (2020)
2. Westmead Hospital Week Research Symposium, poster award (2022)
3. Australian Centre for HIV and Hepatitis Virology Research (ACH4) annual meeting, oral presentation award (2022)
4. Society for Mucosal Immunity, International Conference for Mucosal Immunologists, travel award (2022)
5. Society for Mucosal Immunity, International Conference for Mucosal Immunologists, travel award (2024)

Table of Contents

List of Figures

List of Tables

Abbreviations

Acronym	Definition
AIDS	Acquired Immunodeficiency Syndrome
APC	Antigen Presenting Cell
ART	Antiretroviral Therapy
AS-DC	AXL^+ $SIGLEC6^+$ Dendritic Cell
cDC	Conventional Dendritic Cell
CLR	C-type Lectin Receptors
DC	Dendritic Cell
DC-SIGN	Dendritic Cell-Specific Intercellular Adhesion Molecule-Grabbing Non-Integrin
ddH_20	Double-distilled Water
DMEM	Dulbecco's Modified Eagle Medium
DNase	Deoxyribonuclease
DPBS	Dulbecco's Phosphate Buffered Saline
DTT	1,4-dithiotreitol
E.coli	*Escherichia coli*
EDTA	Ethylenediaminetetraacetic Acid
FACS	Fluorescence Activated Cell Sorting
FCS	Fetal Calf Serum
FcεR1α	Human Anti-IgE Receptor
FMO	Fluorescence Minus One
FSC	Forward Scatter
FVS	Fixable Viability Stain
FXIIIA	Factor XIIIA
GM-CSF	Granulocyte-Macrophage Colony Stimulating Factor
gMFI	Geometric Mean Fluorescence Intensity
hAB	Human Type AB
HEPES	4-(2-Hydroxyethyl)-1-piperazineethanesulfonic Acid
HIV	Human Immunodeficiency Virus-1
HLA-DR	Human Leukocyte Antigen, Antigen D Related Receptor
IL	Interleukin
MACS	Magnetic Activated Cell Sorting
MDDC	Monocyte Derived Dendritic Cell
MDM	Monocyte Derived Macrophage
MHC-II	Major Histocompatibility Complex-Class II
MNP	Mononuclear Phagocytes
MOI	Multiplicity of Infection
MR	Mannose Receptor

Acronym	Definition
PBMC	Peripheral Blood Mononuclear Cell
PBS	Phosphate Buffered Saline
pDC	Plasmacytoid Dendritic Cell
PFA	Paraformaldehyde
PrEP	Pre-Exposure Prophylaxis
RF10	Roswell Park Memorial Institute supplemented with 10% Fetal Calf Serum
RH10	Roswell Park Memorial Institute supplemented with 10% Human AB Serum
RNA-seq	Ribonucleic Acid Sequencing
rpm	Revolutions per Minute
RPMI	Roswell Park Memorial Institute
RT	Room Temperature
SAMHD1	Sterile Alpha Motif and Histidine/Aspartic Acid Domain-Containing Protein 1
SIGLEC	Sialic Acid-Binding Immunoglobulin-Type Lectins
SSC	Side Scatter
Tat	HIV Transcriptional Activator Protein
t-MDM	Transitional Monocyte Derived Macrophage
t-SNE	t-Distributed Stochastic Neighbour Embedding
X-gal	5-Bromo-4-chloro-3-indolyl-β-D-galactopyranoside

Chapter 1. Literature Review

Publications incorporated into this chapter

Erica E. Vine*, Jake W. Rhodes*, Freja A. Warner Van Dijk, Scott N. Byrne, Kirstie M. Bertram, Anthony L. Cunningham and Andrew N. Harman, 2022. HIV transmitting mononuclear phagocytes; integrating the old and new. *Mucosal Immunology*, **15**, 542–550 (2022).

*Co-first Authors

To maintain consistency throughout this thesis, references to 'Siglec-1', 'Mannose Receptor', 'langerin' and 'DC-SIGN' have been changed from the published text to 'CD169', 'CD206', 'CD207' and 'CD209' respectively. Figures have not been amended. All text in this chapter was written by this author, including quoted text from the publication above.

1.1 Introductory statement

This thesis will investigate the populations of mononuclear phagocytes (MNPs) present in the colon and rectum (colorectum), utilising optimised tissue digestion protocols in combination with high-parameter flow cytometry. Firstly, it aims to identify and characterise all known subsets of dendritic cells (DC) and macrophages found in non-inflamed tissues. Secondly, it will examine the capacity of these MNP subsets to take up HIV, highlighting any correlations to the expression of HIV-binding lectin receptors. Furthermore, the interactions between macrophage subsets and CD4 T cells will be explored to assess their role in HIV transmission within this crucial transmission site. Finally, a high-parameter flow cytometry panel will be optimised to identify all known MNPs, including inflammatory MNPs, present in all sexual transmission tissues.

1.2 Introduction

"2021 marked the 40th anniversary of the first official report about AIDS and 35 – 43 million people have lost their lives to this disease. Despite this enduring pandemic, there is still no cure or vaccine for Human Immunodeficiency Virus (HIV). The introduction of antiretroviral therapies (ART) has improved patient outcomes and reduced the consequences of HIV infection from a terminal to a chronic illness (1). ART can reduce serum virus levels to undetectable levels and virtually eliminate the risk of transmission from ART-treated HIV^{+} individuals (2). However,

treatment is still lifelong (3) and HIV remains a substantial burden to the infected individual as well as national healthcare systems. Unfortunately, with approximately 16 million infected individuals worldwide not receiving ART, and the minimal use of pre-exposure prophylaxis (PrEP) in high-risk individuals (2,3), transmission rates remain stable. Therefore, the development of a cure and vaccine is still vital. In the meantime, an effective and fast-acting topical microbicide could be used on a per need basis. These could be incorporated into slow-release vaginal rings, lubricants, or a hygiene douche, complementing current PrEP regimes (4,5). However, designing effective prevention strategies requires an accurate and comprehensive understanding of the early events underlying HIV transmission."

"Sexual transmission across the human genital and anorectal (anogenital) mucosa is now the predominant route of HIV transmission, but the early transmission events and the immune cells involved remains under discussion (6–9). These transmission sites differ anatomically, physiologically and immunologically (7–12) but once the physical barriers of these tissues are breached, pathogens encounter a range of mucosal cell types that participate in HIV transmission, including sub-epithelial mucosal fibroblasts (13–15) and the cellular immune systems first line of defence, mononuclear phagocytes (MNP). MNPs are immune sentinels which bind pathogens via an array of cell surface receptors triggering an immune response. In the case of HIV these cells are actively involved in transmission, disseminating virus to CD4 T cells as a consequence of their antigen presenting cell function. MNPs are therefore potential key targets for blocking HIV transmission at mucosal sites and of key importance for vaccine design."

"Here we will review role the MNPs play in transmitting HIV in the tissues where sexual transmission occurs. In addition to providing a historical perspective, we will review recent advances in our understanding of the specific subsets of MNPs that transmit HIV as well as highlighting gaps in the literature that may impact on our understanding of early transmission events."

1.3 Anatomical characteristics of HIV transmission sites

The anogenital HIV transmission sites are comprised of three distinct tissue types: skin, type II mucosa and type I mucosa, which all contain an epithelial surface and an underlying layer of connective tissue (**Figure 1.1**).

The outer layer of skin (labia majora, labia minora, outer foreskin, glans penis and anal verge) is comprised of epidermis which is a stratified squamous epithelium made up of multiple layers of keratinocytes. The outermost surface (stratum corneum) is cornified and made up of dead cells that provide a formidable barrier to invading pathogens. Underlying the epidermis the layer of connective tissue is called the dermis which contains a rich array of immune cells.

The type II mucosa (vagina, ectocervix, inner foreskin, fossa naviculars and anal canal) are, like skin, protected by a surface epithelial stratified squamous epithelium. However, the type II mucosa lacks the protective stratum corneum making it more permeable to invading pathogens. Underlying this epithelial surface the layer of connective tissue is lamina propria which is similar to dermis but contains mucus producing cells and differs to dermis in its immune cell composition.

This contrasts with the type I mucosal surface (endocervix, penile urethra and colorectum) which is characterised by a thin and fragile single layer of columnar epithelial cells overlaying lamina propria. These epithelial cells form a barrier to the outside environment via the engagement of tight junction connections between adjacent cells. The barrier is further protected by a mucous layer that is deposited by goblet cells that are interspersed in the epithelium. “As mucosal trauma is highly associated with HIV transmission, it is likely that HIV encounters the rich array of immune cells in these tissues which include multiple subsets of MNPs.”

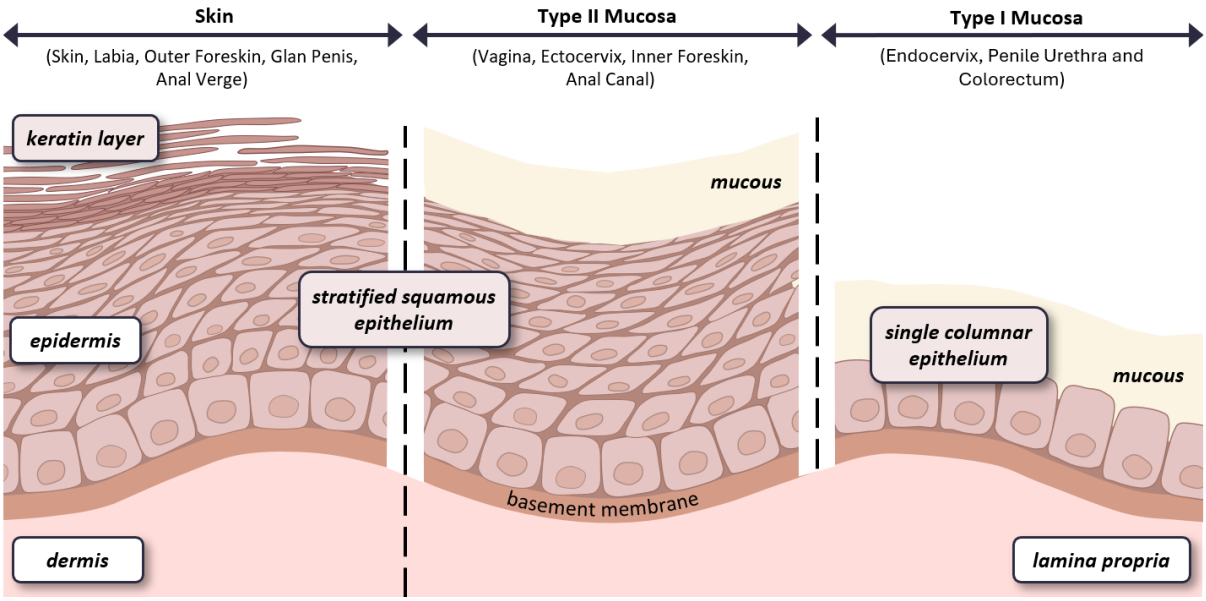

Figure 1.1: Tissue types of human sexual transmission tissues. Skin, type II mucosa and type I mucosa are divided into two distinct layers, an epithelial layer separated from the underlying connective tissue layer by a basement membrane. Skin contains an epidermis made up of a stratified squamous epithelium with an outer layer of dead keratinised cells, over a dermis. The type II mucosa also contains a stratified squamous epithelium over a lamina propria, while the lamina propria of the type I mucosa is covered by a single columnar epithelium.

1.4 Factors contributing to sexual transmission of HIV

The distinct differences between columnar and squamous epithelial surfaces represent significant challenges and unique opportunities for HIV to gain access to its target cells. The tightly packed cells of the stratified squamous epithelial layers of the vagina, inner foreskin, glans penis and anal canal represent a significant physical barrier for the virus. However, during intercourse these tissues can receive micro-abrasions leading to disruption of the physical protective barrier (16). Indeed, HIV penetration and infection across this surface type has been demonstrated in human ex vivo genital tissue explants from the vagina (17,18), ectocervix (19,20) and foreskin (7,9,17,18). Transmission across the anus is likely to be more efficient as the anus is more susceptible to mechanical abrasion as it lacks natural lubrication (unlike the vagina), and the external anal sphincter restricts the flexibility of this tissue. Although the adjacent rectum may undergo less mechanical damage as it is a more flexible and voluminous cavity, its thin and fragile columnar epithelial surface may present a pathway of lesser resistance for HIV transmission (6,21). The rectum is also vulnerable to infection due to its lack of acidic mucus (unlike the endocervix). Furthermore, the rectal mucosa undergoes osmotic stress in response to douching prior to intercourse (22) and is also prone to irritation from the use of lubricants (23,24). Importantly, HIV can penetrate across the type I mucosa of the rectum, endocervix and penile urethra (16,25) in the absence of tissue pathology via at least two known mechanisms. Firstly, lamina propria MNPs can sample HIV by extending processes between the epithelial cells into the intestinal lumen (26). Additionally, HIV can travel through epithelial cells via a mechanism called transcytosis, a process where the pathogen can be moved from the apical surface of the cell to basal surface via vesicle transfer (16,27). These factors mean HIV easily encounters its numerous target cells in the underlying tissue, contributing to the higher risk and incidence of HIV transmission via receptive anal, compared to receptive vaginal, intercourse (28,29). Therefore, characterising the MNPs in the human colorectum is critical to understanding the early events of HIV transmission, and will be investigated in **Chapter 3**.

1.5 The evolving mononuclear phagocyte system

“MNPs are a family of phagocytic cells, traditionally defined as macrophages, monocytes and dendritic cells (DC). Macrophages were the first MNP to be discovered by Élie Metchnikoff in 1884 for which he received the Nobel prize (30). In the 1920’s, monocytes were proposed to be precursors to macrophages (31,32) giving rise the idea of a multicellular mononuclear phagocyte system. Two years after the discovery of macrophages, Langerhans cells (LC) were discovered

by Paul Langerhans in 1884 (33). However, these were first thought to be nerve cells, due to their dendritic appearance and it was not until 1973 that Inga Silberberg showed that they played a role in immunity (34). Also in the 1970s, Nobel laureate Ralph Steinman discovered a novel cell type that did not look like macrophages and did not easily mediate endocytosis which he named DCs (35,36)."

"Since these early discoveries, multiple subsets of MNPs have been defined which have historically been classed based on their functional properties. **Dendritic cells** are potent APCs and function to sample pathogens and commensal microflora in tissue and then migrate to lymph nodes to present them to CD4 T cells via MHC-II and drive immune activation or immune tolerance. As **LCs** perform the same function as DCs and also have dendritic processes they have traditionally been considered a subset of these cells. **Macrophages** are weak APCs but play a key role in innate immunity by phagocytosing pathogens at the site of exposure and in maintaining tissue homeostasis. **Monocytes** are a population of cells in blood that migrate into tissue where they differentiate into effector DCs or macrophages based on the cytokine environment they encounter. It is of note that these monocyte-derived DCs (MDDC) and macrophages (MDM) differ to conventional DCs and macrophages."

"The advent of high parameter single cell technologies (especially RNA seq) has allowed for more robust ontological phenotyping leading to alternative classifications. Two key HIV target MNPs are of point here. Firstly, LCs have been shown to be derived from the yolk sac during embryogenesis similar to macrophages, as opposed to DCs which are derived from bone marrow derived progenitors. Thus, they can be thought of as either DCs or macrophages. For this reason, LCs are now best defined as their own class of MNP. Secondly, the $CD14^+$ tissue compartment, which has been undergoing an ongoing redefinition over the last decade. As will be discussed in detail later, tissue $CD14^+$ cells were originally believed to consist of tissue-resident yolk sac derived macrophage (defined by their autofluorescent properties) and a type of conventional DC (defined by their lack of autofluorescence) (37). The DC component was later redefined as MDMs (38) and more recently shown to consist of a heterologous population of MDMs and MDDCs (9). More recently still this compartment has also been shown to contain a new defined bona fide bone marrow derived DC population named DC3 (39–42)."

"Therefore, the MNP system is in reality a spectrum of cells derived from a variety of distinct precursors that perform a range of functions including pathogen detection and clearance, antigen presentation and tissue homeostasis. The full range of currently defined human MNPs is illustrated in **Table 1.1**."

"This review focusses on the functional role MNP play in sexual transmission of HIV which is highly dependent on their ability to capture the virus and then interact with CD4 T cells and transfer the virus to them. It is therefore the functional properties of these cells that will form the focus of our discussion."

Table 1.1: Human Mononuclear Phagocyte phenotypes and their known HIV uptake receptors

MNP subset	Defining markers			HIV uptake receptors	
Epithelial					
Langerhans Cells 	HLA-DR$^+$ **CD1a^{++}** E-Cadherin$^+$ CD1c^{low}	CD11c^{low} EpCAM$^+$ CD14$^-$ **Birbeck granules$^+$**	CD33$^+$	**Langerin** DC-SIGN MR Siglec-1	🟩 🟥 🟥 🟥
Epi CD11c$^+$ DC/VEDCs 	HLA-DR$^+$ **CD11c^{high}** HLA-DR$^+$ **CD1a$^+$**	MR$^+$ **CD1c$^+$** **CD14$^-$** **Birbeck granules$^-$**	CD1a^{low}	**Langerin** DC-SIGN MR Siglec-1	🟩🟥 🟥 🟩 🟩
Epi CD33^{low} MNPs 	**HLA-DR^{low}** **CD45^{low}** **CD33^{low}** CD1c^{low}	**CD1a$^+$** CD11c^{low} **CD14$^-$**		Langerin DC-SIGN MR Siglec-1	🟩 🟥 🟩 🟩
Sub-epithelial					
cDC1 	HLA-DR$^+$ **CADM1$^+$** CD141^{hi} **CLEC9A$^+$**	CD1c$^{-/low}$ **XCR1$^+$** CD11c^{low} **CD14$^-$**	SIRPα$^-$ CD103$^+$ (intestinal)	Langerin DC-SIGN MR Siglec-1	🟥 🟥 🟥 🟥
cDC2 	HLA-DR$^+$ CD14$^-$ **CD11c$^+$** **CD1a$^+$ (skin)**	**CD1c$^+$** **SIRPα$^+$** **HLA-DQ$^+$** **CD141$^-$**	CD88$^-$ CD163$^-$ **FcεRIα$^+$**	**Langerin** DC-SIGN MR Siglec-1	🟩🟥 🟥 🟩 🟩
pDC* 	HLA-DR$^+$ **CD123$^+$** **CD14$^-$**	CD11c$^-$ Axl$^-$ Siglec-6$^+$		Langerin DC-SIGN MR Siglec-1	🟨 🟨 🟨 🟨
AS DCs/Pre-DC* 	HLA-DR$^+$ **CD123$^+$** **CD14$^-$**	CD11c$^+$ **Axl$^+$** **Siglec-6$^+$**		Langerin DC-SIGN MR Siglec-1	🟨 🟨 🟨 🟩
DC3 	HLA-DR$^+$ **CD1c$^+$** **CD163$^+$** **CD88$^-$**	CD2 **CD14$^+$** (inflammatory only)		Langerin DC-SIGN MR Siglec-1	🟨 🟨 🟨 🟨
in vivo MDDC 	HLA-DR$^+$ **CD14$^+$** CD11c$^+$ **CD1c$^+$**	SIRPα$^+$ **Autofluorescence$^-$**		Langerin DC-SIGN MR Siglec-1	🟥 🟥 🟩 🟩
in vivo MDMs 	HLA-DR$^+$ **CD1c$^-$** CD11c$^-$ **CD14$^+$**	CD11b$^-$ CD16$^-$ CD163$^+$ **Autofluorescence$^-$**		Langerin DC-SIGN MR Siglec-1	🟥 🟩 🟩 🟩
Macrophages 	HLA-DR$^+$ **FXIIIA$^+$** **CD14$^+$** CD64$^+$	CD68+ CD163$^+$ **Autofluorescence$^+$**		Langerin DC-SIGN MR Siglec-1	🟥 🟩 🟩 🟩

*Key distinguishing markers in **bold*** *present* 🟩 *not present* 🟥 *unknown* 🟨

**Expression data from blood*

1.6 MNPs are key HIV transmitting target cells

"In tissue, almost all MNPs express the HIV entry receptors CD4 and CCR5 as well as a range of HIV-binding lectin receptors (**Figure 1.2**). MNPs are therefore key HIV target cells. Importantly, binding of HIV to CD4/CCR5 leads to HIV infection of the cell whereas binding to some lectin receptors results in rapid uptake into neutral pH Virus Containing Compartments (VCCs) which are invaginations of the plasma membrane (43–45). This compartment is phenotypically identical to the VCCs created in infected macrophages, where they are believed to contribute to viral reservoirs in mucosal tissues (46–48). Connections that link the VCC to the cell surface can be very tight and therefore protect the virus from host immunity (49–51)."

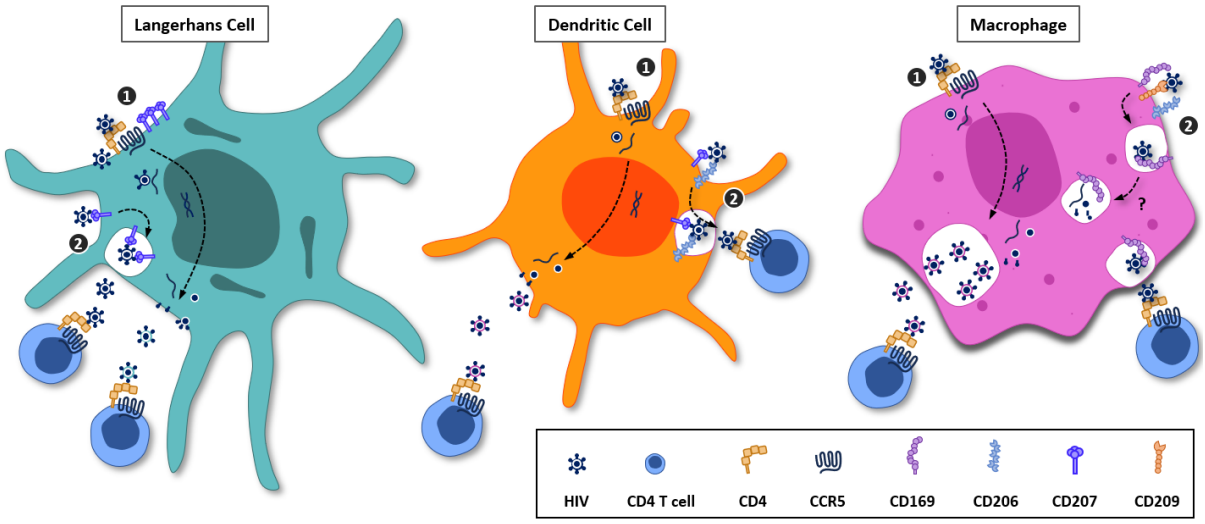

Figure 1.2: Mononuclear Phagocyte interactions with HIV In all MNPs, HIV productively infects cells via CD4 and CCR5. DCs express much higher levels of CCR5 and support much higher levels of infection than LCs and macrophages. CD207 has been shown to facilitate infection of LCs. 1. CD4/CCR5-dependent infection results in productive infection that can lead to the infection of other key HIV target cells, such as $CD4^+$ T cells. *De novo* virus is assembled in the cytoplasm of the cell near the cell surface, and in the case of LCs and DCs, buds from the surface of the cell once assembled. Macrophages assemble *de novo* virus into vesicles called Virus Containing Compartments (VCC) and can hold HIV in these VCCs for periods of time before its release outside of the cell. 2. All MNPs can transfer HIV in an infection-independent manner via lectin receptors (CD169 (Siglec-1), CD206 (Mannose Receptor), CD207 (langerin) and CD209(DC-SIGN)) to infect $CD4^+$ T cells. Epithelial DCs have a larger array of lectin receptors compared to LCs, though macrophages express the most. **Figure adapted from Vine et al. *Cell Reports* (2024)** (52) .

"Correlating with these two pathways of entry MNPs can transfer HIV to CD4 T cells in two successive phases (44,53). *Trans*-infection, (also called first-phase transfer) occurs when the MNP interacts with a CD4 T cell within 2-6 h, where virions are either held on the surface of the MNP (54,55) or discharged from VCCs in a pulsatile fashion (56). This most likely occurs in the tissues where transmission takes place. After 6 hours virions undergo acid proteolytic degradation over one or more days by a still undefined mechanism (56) and by 24 h no transfer of HIV to CD4 T cells occurs. It is well known that LCs and DCs can perform this function but the capacity for macrophages to act in this capacity is still unclear. *Cis*-infection (also called second-phase transfer) occurs when a CD4 T cell interacts with MNPs 72 h or longer after the MNP has been infected via the CD4/CCR5 pathway, with the MNP actively producing virus that buds from the plasma membrane. This newly synthesised virus is transported to the tips of filopodia via actin. The filopodia contact target CD4 T cells and transfer HIV by subsequently forming a virological synapse (57). In addition, HIV-infected macrophages can induce tunnelling nanotubes creating a bridge between cells and allowing for the transfer of virus separate from the extracellular environment (58). *Cis*-infection increases with time as more virions are produced by the infected cell."

1.7 HIV binding lectin receptors

"MNPs express a wide range of lectin receptors on their surface which enable them to capture incoming pathogens. Each subset of MNP expresses a unique repertoire of these receptors meaning they differ in the specific pathogens they can capture. CD207 (langerin), CD209 (DC-SIGN), CD206 (Mannose Receptor), and CD169 (Siglec-1), are currently the only MNP lectin receptors known to bind HIV (59–61). CD209 was initially thought to be the most important but was then shown to be only expressed on MNPs along with CD206 in the dermis whereas CD207 was expressed in the epidermis (62)."

"**CD207** (**Langerin)** is expressed most highly by LCs and has been extensively studied on authentic tissue-derived LCs and we refer the reader to the many reviews on this subject for a full historical perspective (7,8,63–65). HIV binds CD207 in its trimeric form (45) which has been shown by some to lead to the internalisation of the virus into Birbeck granules where it is degraded which led to the hypothesis that CD207 acts as a natural barrier to HIV infection (66). However, as discussed in detail below many others (17,67,68) have shown that LCs can transfer HIV to CD4 T cells following CD207 mediated uptake which can be blocked using soluble CD207 or a CD207 blocking monoclonal antibody (45)."

"**CD209 (DC-SIGN)** was first described by Geijtenbeek et al. in 2000 (69–71), and is the most extensively studied HIV binding lectin receptor. Using *in vitro* blood MDDCs, it has been shown to bind HIV in a tetrameric form (72) and to play a role in the formation of the MHC-II-independent (73) infectious synapse between DCs and T cells (74,75), whereby HIV is transferred to T cells in a protected environment while the cells are connected (76). Binding of HIV to CD209 on these model cells triggers a signalling cascade that enhances *trans*-infection (77). Many studies have shown that tissue CD209 expressing cells efficiently take up and transmit HIV (26,78–80)."

"**CD206** (**Mannose Receptor)** on *in vitro* blood MDDCs has been shown to bind HIV in a dimeric form (81) and mediate endocytic uptake which leads to trafficking into lysosomes (44). CD206 expressing *in vitro* blood MDDCs have been shown to transmit HIV to CD4 T cells. However, it is not clear if this process was mediated by CD206 or via an alternate lectin receptor such as CD209 which these cells also express (44)."

"**CD169 (Siglec-1)** is the most recent lectin receptor implicated in HIV uptake and *trans*-infection, with the mechanism of the capture, internalisation and retention of exogenous virus in 'vesicular caves' seen on MNPs (82–85) described before this interferon-inducible receptor was implicated (84,86–89). The formation of these caves sequesters the virus from the external environment, protecting it from neutralising antibodies and cellular immune responses, before it can be transferred to CD4 T cells. The cells' ability to transfer HIV via these lectin-mediated cell-to-cell contacts may contribute to the evasion of HIV from neutralising antibodies and ART (90)."

"These lectin receptors are found on a range of MNPs in transmission tissues, with differing expression levels (**Table 1.1**). The presence of these lectin receptors not only suggests their likely participation in HIV *trans*-infection but also provides an additional means of MNP subset classification. Furthermore, the influence of receptor expression on HIV uptake by MNP subsets into VCCs, including DC versus macrophage, and retention versus degradation (thus determining the degree and kinetics of HIV transfer to T cells), needs to be carefully examined."

1.8 Human tissue mononuclear phagocytes and HIV transmission

"The continuously changing landscape of the MNP system can, at times, make it difficult to fully understand what specific subsets of MNP are being investigated and has likely contributed to conflicting findings in the HIV literature. For example, recent work indicates that epidermal DCs

have been mis-defined. Most early studies of HIV and MNPs have made use of model *in vitro* derived MNPs and many studies still rely on these cells. These are most commonly derived *in vitro* from $CD14^+$ blood monocytes to produce MDDCs or MDM. Alternatively $CD34^+$ monocytes from cord blood can be used to generate monocyte-derived LCs (MDLC) and model LCs can also be derived from the MUTZ3 cell line (91). However, these model cells significantly differ from *bona fide* MNPs that reside within the anogenital tissue counterparts where transmission occurs. Notably, this particular model of MNP do not express the same repertoire of HIV binding lectin receptors as *in vivo* MNP. For example, in contrast to *bona fide* LCs, MDLCs express CD209 and CD206 while *in vitro* MDDC and MDM do not express CD169 in contrast to *in vivo* MDDC and MDM (9,92). In addition, compared to *bone fide* MNP, model MNPs express much higher levels of CD209 and CD206 as well as the HIV entry receptors CD4 and CCR5. Caution must therefore be applied in interpreting the findings of these studies (9)."

1.9 Epithelial HIV transmission

1.9.1 Langerhans Cells

"Until very recently LCs were believed to be the sole MNP subset present within steady state stratified squamous epithelium that covers human skin and genital tissues. LCs are currently best defined by their high expression of HLA-DR, CD207 and CD1a, low expression of CD11c, as well as the presence of distinct cytoplasmic structures known as Birbeck granules. They can be further distinguished from other MNPs by their lack of expression of CD206, CD209 and CD169 (7,8). Recent single cell transcriptomic analysis of the human stratified squamous epithelium has suggested that LCs exist as multiple subsets; two at steady state termed LC1 and LC2, an activated subset defined by high CD83 and low CCR7 expression termed LC3, and a migratory subset defined by high CCR7 expression termed LC4 (93). Of the two steady-state LCs, LC1 were delineated as classic LCs while LC2 were described as a novel and unique subset of LC."

"As LCs cells express the HIV entry receptor CD4 (94–97) and CCR5 in genital tissues and are found in closest proximity to the epithelial surface, they have been the most extensively studied MNP in the context of HIV transmission. Multiple early studies in the 1990s demonstrated that LCs within HIV exposed tissue contain HIV RNA (94,97,98) and also the p24 protein (95,99). Furthermore, LCs were shown to efficiently transfer HIV to T cells using skin explant models (100,101) and by co-culture of epidermal sheets with T cell lines (102). In 2007, Hladik and colleagues used human vaginal tissue explants to show that LCs rapidly took up HIV via endocytosis and were then able to migrate out of this tissue and interact with CD4 T cells.

Importantly, HIV was shown to concentrate at the point of contact between LCs and CD4 T cells (17). In a similar study in 2010, Ganor et al. used human foreskin explants to show that LCs take up HIV within 1 h of exposure and then migrate to the basement membrane where they interact with and transfer to CD4 T cells (67). They then went on to show that this migration was meditated by RANTES (103). These studies support the hypothesis that LCs are able to capture HIV and then transmit the virus to CD4 T cells. However, in 2007 de Witte et al. published a landmark study that challenged this hypothesis and concluded that LCs in fact act as a natural barrier to HIV by showing that they efficiently take up HIV via CD207 and traffic the virus to Birbeck granules where the virus become degraded (104). In 2014 Nasr et al. confirmed that LCs take up HIV via CD207 by showing that both soluble CD207 and a neutralising CD207 antibody were able to block HIV uptake. However, in their hands LCs did not act as a natural barrier as they were able to efficiently transfer HIV to CD4 T cells within two h of exposure, while transfer was blocked by both the soluble CD207 and the CD207 blocking antibody. Furthermore, these LCs were also able to become productively infected and transfer the virus again at later time points (45). Though these findings may appear contradictory, it is important to note that de Witte et al., used trypsin to isolate DCs cleaving the binding site on CD4 for HIV and Nasr et al. could reproduce their negative findings with similar trypsin treatment. Furthermore, when de Witte et al. used higher concentrations of HIV (similar to that of Nasr et al.) they showed that this effect could be overcome. These higher concentrations of HIV may be physiologically relevant due to the high burst size of HIV from infected CD4 T cells (105) that are present in semen and deposited on the anogenital mucosa during intercourse. Furthermore, amyloid fibrils in semen have been shown to increase the effective MOI of cell free virus by several orders of magnitude (106).”

1.9.2 Conventional dendritic cell 2 (cDC2) – a newly identified HIV transmitting MNP

“Misidentification of LCs in many of the studies described above may also explain the conflicting results on their role in HIV transmission. Recent studies have shown that LCs are not the only MNPs found in the stratified squamous epithelium in steady state. In 2018 Pena-Cruz et al. identified vaginal epithelial dendritic cells (VEDC) (18). Like LCs, VEDCs expressed CD1a, CD207, CD4, CCR5 and not CD209. However, they did not express Birkbeck granules which are a defining feature of LCs. Concurrently, Bertram, Botting, Baharlou et al. identified epidermal $CD11c^+$ DCs (7). These express the same markers as VEDC and can be discriminated from LCs by their (i) expression of CD206, (ii) higher expression of CD11c, CD11b, CD1c, FcεR1α and HLA-DR and (iii) lower expression of CD207 and CD1a. In abdominal tissue epidermal $CD11c^+$ DCs

are present in much lower proportions than LCs, but in foreskin they are present in roughly equal numbers and almost completely predominate over LCs in the epithelium of the vagina, fossa navicularis and anal canal (7,18). It is believed that VEDC/CD11c$^+$ DCs were erroneously overlooked due to the method of isolation and their overlapping expression of key surface markers with LCs (HLA-DR, CD1a and CD207). Many groups (except Nasr et al.) liberated LCs from tissue exclusively using trypsin enzymatic digestion. However, Botting at al. showed that trypsin significantly cleaves the key identifying surface receptors expressed by these cells, CD11c and CD1c as well as the HIV entry receptor CD4 (7,8,18). Therefore, unless CD11b, CD11c or CD1c are included as identification markers and trypsin is not used to liberate these cells from tissue, epidermal CD11c$^+$ DCs / VEDCs cannot be reliably discerned from LCs. This means that LCs have almost certainly been misidentified in many studies, especially those examining these cells in anogenital tissues where CD11c$^+$ DCs/VEDCs overwhelmingly predominate. Importantly, Bertram et al. showed that epidermal CD11c$^+$ DCs were morphologically and transcriptionally undistinguishable from dermal CD11c$^+$ conventional DC-2 (cDC2), suggesting these are in fact dermal cDC2 which have migrated into the stratified squamous epithelium. Functionally, however, epidermal CD11c$^+$ DCs are much more efficient APCs compared to their dermal CD11c$^+$ cDC2 counterparts. Furthermore, they secrete significantly higher levels of IL-1β, IL-6, IL-8, IL-10 and TNF than dermal CD11c$^+$ cDC2 and do not secrete IL-1α (7). Furthermore, as described above, in 2021 Liu, Zhu et al. identified four subsets of LCs by analysing the transcriptional profile of the vaginal stratified squamous epithelium (93). The cells they denote as LC2 showed many phenotypic similarities to epidermal CD11c$^+$ DCs in that they express the cDC2 specific transcription factor IRF4, lower levels of CD207 and CD1a and higher levels of CD1c and CD11b. Furthermore, both cells are enriched in foreskin epidermis. However, unlike Bertram et al., they did not compare the transcriptional profiles of these cells to sub-epithelial MNPs or any other MNP, explaining why the similarity to cDC2 was not revealed. Finally, a similar cell has been observed in inflamed stratified squamous epithelium, termed inflammatory epidermal dendritic cells (IDEC) (107,108). Similar to epidermal CD11c$^+$ DCs, these cells express CD11c and CD206. In conclusion, although further investigation is required, it is highly likely that epidermal CD11c$^+$ DC, VEDC, LC2 and IDEC are one and the same cell, namely, sub-epithelial cDC2s that migrate into the stratified squamous epithelium, especially in the context of inflammation and in mucosal tissues which are rich in microbiota."

"Importantly, both VEDCs and epidermal CD11c$^+$ DCs are important cellular targets for HIV. Pena-Cruz et al. showed that VEDCs are highly permissive to infection by R5 HIV strains, whereas X4 viruses replicated inefficiently. Interestingly, however HIV binding and fusion was comparable

for both R5 and X4 viruses, implying that the reduced replication was due to lower levels of integration and reverse transcription in addition to being influenced by restriction factor SAMHD1 which affects X4 viruses to a greater degree (18). Similarly, Bertram et al. showed that epidermal CD11c$^+$ DCs take up HIV much more efficiently than LCs within two h. Importantly, using foreskin explant models and the *in-situ* hybridisation RNAscope technology, they were able to visualise these cells interacting with HIV within 30 min of topical exposure. Correlating with their high capacity to take up HIV and present antigen to CD4 T cells, these cells were also much more efficient than LCs at first phase (*in trans)* transfer of the virus to CD4 T cells within two hours. Furthermore, epidermal CD11c$^+$ DCs expressed significantly higher levels of surface CCR5 than LCs and correspondingly supported higher levels of infection making them also more efficient than LCs at second phase (*in cis)* transfer of the virus to CD4 T cells at 72-96 h. Importantly second phase (*in cis)* transfer could be blocked with the CCR5-antagonist maraviroc confirming CD4/CCR5 meditated entry (7)."

"Further demonstrating the importance of cDC2 in HIV transmission, Rhodes, Botting et al. recently demonstrated that sub-epithelial CD207 expressing cDC2 are significantly more efficient at HIV uptake and transfer to CD4 T cells than their non-CD207 expressing counterparts (12). As Bertram et al. showed that the majority of anogenital epidermal CD11c$^+$ DC express CD207 and transcriptionally align with cDC2, it is highly probable that sub-epithelial CD207$^+$ cDC2 migrate to the epidermis where they capture HIV (7)." Colorectal epithelial cells will not be examined in this thesis, however, the ability to characterise them by high-parameter flow cytometry in other sexual transmission tissues will be discussed in **Chapter 4**.

1.10 Sub-epithelial HIV transmission

1.10.1 The changing classification of CD14+ MNPs

"In addition to CD11c$^+$ cDC2s, the dermis and lamina propria also contain CD14 expressing MNPs which, in contrast to skin, represent the bulk MNP population in all anogenital and intestinal mucosal tissues (9). These cells were historically classified as either macrophages (defined by their autofluorescent properties and/or CD68 expression) or non-autofluorescent CD14$^+$ DCs (37). In 2014, CD14$^+$ DCs were redefined as a transient population of MDMs derived from blood CD14$^+$ monocytes by McGovern, Schlitzer and colleagues (38). However, more recently Rhodes et al. showed that there are two populations of monocyte derived CD14$^+$ cells, discerned by their expression of CD1c and CD11c (9). In agreement with McGovern et al., CD14$^+$ CD1c$^-$ CD11c$^-$ cells were transcriptionally and morphologically macrophage-like and were also

non-migratory and therefore defined as MDMs. Meanwhile, $CD14^+$ $CD1c^+$ $CD11c^+$ cells were transcriptionally and morphologically DC-like and migrated out of tissue and therefore defined as MDDCs." Adding further complexity, Bujko et al. classified all CD14+ cells in the human jejunum as macrophages, defining both monocyte-like and tissue-resident like cells into four ($CD11c^-$ $CD11b^+$) (109).

CD209 has been well documented as a HIV binding receptor (70), and CD209 expressing cells are found in all anogenital transmission sites (62). However, following the recent re-classification of $CD14^+$ cells as *in vivo* MDMs and MDDCs it has been revealed that it is the MDM population that expresses CD209, and no currently known DC population express this molecule (9). Additionally, rectum and sigmoid colon CD209 expressing cells lack DC markers, but the majority co-express macrophage markers (61). Furthermore, the majority of HIV-capturing DCs in the human cervix were found to be CD209 negative (110). Similarly, CD169 was also believed to be a marker for DCs, being very highly expressed on *in vitro* MDDCs. However, as with CD209, transcriptional profiling in tissue MNPs has shown that this lectin receptor is predominately expressed on tissue-resident macrophages, with only very low expression on *in vivo* MDMs, (9). It is however expressed on inflammatory Axl^+ $Siglec\text{-}6^+$ DCs (ASDC) (111,112) . These findings support the re-examination of historic studies from a new perspective to match findings to our current understanding of MNP subset classification.

1.10.2 Re-evaluating the sub-epithelial MNP HIV transmission literature

In 2005, Gurney et al. were unknowingly the first to describe macrophage involvement in HIV transmission in human mucosal tissues, demonstrating that $CD209^+$ cells in the human rectum successfully captured HIV and facilitated transmission to CD4 T cells. According to MNP definitions at this time, these cells were defined as $CD14^+$ DCs, however, recent updates in the definition of the human MNP system reveals that these cells are a heterologous population of yolk sac derived and monocyte-derived macrophages (80). Similarly, in 2013 Ganor et al. compared penile urethral $CD68^+$ resident macrophages with T cells and showed that HIV preferentially interacted with macrophages (25).

"In 2010, Shen, Smythies et al. showed that CD13 and CD11c expressing MNPs in the small intestine could capture HIV and transfer it *in trans*- to CD4 T cells. This group went on to show similar findings in vaginal tissue (113). As CD14 and CD1c were not included as cell definition markers in either of these studies, these cells might consist of a heterologous population of cDC2 and MDDC as well as of MDM as they were shown to express low levels of CD209 (114). In 2013

Cavarelli et al. showed that CD209$^+$ *in vitro* derived MDDCs sampled HIV in a tissue model. Although they extended this study using colonic tissue explants, DCs were defined as CD11c$^+$ cells and thus, similar to the studies by Shen et al., these cells represented a heterologous population of cDC2 and MDDC (26) ."

"Three studies using human cervical tissue have demonstrated that MDDCs are preferential HIV target cells. In 2016, Rodriguez-Garcia et al. investigated HIV virus like particles capture on cervical CD11c$^+$ cells (110) and showed that HIV was exclusively captured by cells that co-expressed CD14, the majority of which did not express CD209. CD14$^+$ CD11c$^+$ CD209$^-$ cells are currently defined as *in vivo* MDDCs. However, within this study a small proportion of HIV$^+$ cells expressed CD209$^+$ implying that a small proportion of MDMs were also present in this population. In 2018, Trifonova et al. confirmed these findings showing that cervical CD14$^+$ CD11c$^+$ MDDCs could take up HIV more efficiently than CD14$^+$ CD11c$^-$ MDM and CD4 T cells (115). The following year, Perez-Zsolt, Cantero-Pérez et al. showed that CD169$^+$ CD14$^+$ CD11c$^+$ cervical MDDCs could efficiently *trans*-infect CD4 T cells and that transfer was partially blocked by CD169 antibodies (20)."

"Most recently, in 2021 Rhodes et al. showed that sub-epithelial MDDCs could be a key HIV target cell in the full range of human anogenital tissues. Although all CD14$^+$ cells were able to take up HIV within 2 h, become productively infected and transfer the virus to CD4 T cells, MDDCs carried out these functions preferentially (9). Importantly, using RNAscope they visualised both CD14$^+$ CD1c$^+$ MDDC and macrophages interacting with the virus 2 h post treatment in foreskin and urethral explants. Consistent with Perez-Zsolt et al., using a CD169 monoclonal antibody they could block up to 40% of HIV uptake on in vivo MDDCs, up to 60% on in vivo MDMs, and up to 85% on tissue-resident macrophages (9). The degree of blocking directly correlated to the expression of CD169, suggesting that CD169 is a key receptor for HIV uptake on tissue MNPs (9)."

Expanding from Rhodes et al., Baharlou et al. showed *in vivo* HIV:MNP interaction following HIV-1 topical application to the luminal surface of human colorectal explants (116). They showed that HIV was enriched in macrophages, as well as DCs, within the first two hours of inoculation and that these cells were able to sample more virus than other cells at the early time point. HIV-associated colorectal macrophages were preferentially localised to the submucosal layer, whereas uninfected controls showed macrophages enriched near the epithelial surface, suggesting migration deeper into tissue in response to HIV. Utilising neighbourhood analysis, Baharlou et al. found that macrophages have high HIV-transfer phenotype scores to CD4 T cells when exposed to HIV. However, only *in vivo* interactions of CD4 T cells with HIV carrying DCs

increased their viral load. Nevertheless, significant increase of autologous CD4 T cell viral loads were observed *ex vivo*, in co-culture with both macrophages and DCs.

The MNP subsets re-investigated in the above mentioned epithelial and sub-epithelial studies are summarised in **Figure 1.3**, according to the most recent literature.

Despite ongoing research to enhance our understanding of HIV transmission, the lack of consensus regarding which MNPs are interacting with HIV and CD4 T cells at each unique transmission site requires the re-evaluation and re-examination of published studies (52,117,118). The epithelial compartment has undergone extensive MNP characterisation, as have the dermis and lamina propria MNPs of the anogenital tract. While the colorectum has not be excluded from historic research, MNPs have been described either as bulk populations of DCs or macrophages or characterised based on findings in other sexual transmission tissues (9,26,116,119). At present, there is yet to be a definitive characterisation of the MNP subsets specific to colorectal tissue or an investigation of these subsets' interaction with HIV during transmission.

1.11 Have macrophages been overlooked in HIV transmission?

"Although macrophages have long been known to become infected by HIV, they have not been thought to play a role in HIV transmission as they are weak APCs. Instead, they have been thought to form part of the HIV reservoir (46–48,120–122). However, it is important to draw attention to the fact that two high affinity HIV binding lectin receptors that were historically considered to be classical DC markers are now known to be macrophage specific in tissues: CD209 and CD169. Although DC-like MNPs are more efficient at HIV uptake, infection, and transfer of the virus to CD4 T cells, macrophages can also perform these functions. Furthermore, as demonstrated by Rhodes et al., macrophage-like cells are significantly more abundant than DC-like cells across all anogenital tissues (9). Therefore, while macrophages may not be as efficient at transmitting HIV, they may be no less important due to their high abundance."

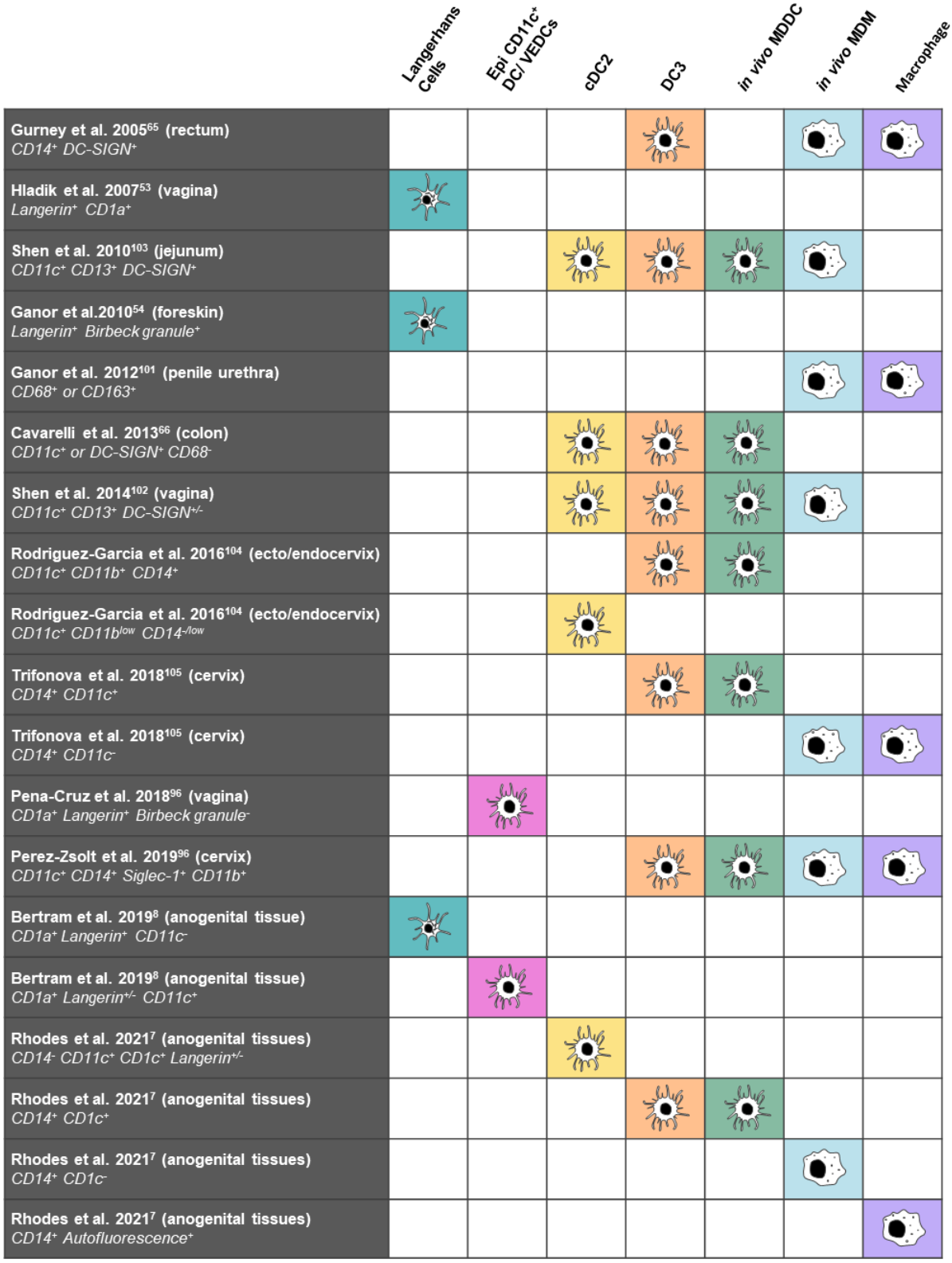

Figure 1.3: Current mononuclear phagocyte subsets represented in existing HIV literature. A selection of existing literature describing HIV interactions with transmission site mononuclear phagocytes were selected for re-examination. Based on the phenotypic data that was presented (left column lists the publications that were assessed, the tissue studied, and the defining phenotypic characteristics presented by the authors), key HIV transmitting mononuclear phagocytes from each study were categorised into the current mononuclear subsets (the columns on the right). This does not consider the proportional contribution that each subset represents, only whether each described mononuclear phagocyte matches the phenotypic profile of the current subset.

1.12 Inflammatory MNPs and HIV transmission

"Although the subsets of MNPs that inhabit steady state human tissues are now well defined, those present in inflamed tissues still need to be delineated. This is a key gap in the literature as HIV transmission is now known to be strongly associated with inflammation (123–125). Concerningly, current PrEP regimens have been shown to be ineffective in the context of inflammation and anogenital inflammation is prevalent in sub-Saharan Africa where most acquisition of HIV still occurs." This inflammation, particularly in the female genital tract, is driven by sexually transmitted infections and balance disruptions to the resident microbiota (126–129). "As cells migrate into inflamed tissues via CCR5 binding chemokine gradients, inflammatory cells therefore express higher levels of the HIV entry receptor CCR5, likely making them more permissive to HIV infection. This is evidenced by the recent findings by Liu et al. that LC2 are enriched in inflamed tissues (93) and the findings by Bertram et al. who showed high levels of CCR5 on epidermal $CD11c^+$ DCs (7) which are almost certainly the same cells as LC2. In addition, unlike their steady-state counterparts, *in vivo* MDDCs express the HIV binding lectin CD209 (130), likely enhancing their ability to take up HIV and transfer virus to CD4 T cells. Furthermore, the newly found inflammatory DC3s in blood have been shown to express high levels of CD209 and CD207 RNA, though this has not been investigated at the protein level or in tissue (40). Previously $CD123^+$ $BDCA2^+$ plasmacytoid DCs (pDCs) were the only known MNP cell type to exclusively inhabit inflamed tissues. Recently however, $CD123^+$ $BDCA2^+$ cells were shown to consist of a heterologous population of bona fide pDCs and Axl^+ $Siglec\text{-}6^+$ (AS) DCs (39,111) /pre-DC (42,131). In blood, AS DCs/pre-DCs have been shown to preferentially interact with HIV via CD169 (112)," as well participating in the *trans*- and *cis*-infection of CD4 T cells (111), though this is yet to be demonstrated in inflamed tissues.

"Therefore, as inflammatory MNP populations are better defined it is important to determine if these cells are present in the tissues where HIV transmission occurs and which HIV binding receptors they express. It will also be important to determine how efficiently they take up HIV, become infected, and transfer HIV to CD4 T cells. These findings will help in the development of modified PrEP strategies to block transmission of HIV in an inflamed setting. This could be particularly transformative for women in sub-Saharan Africa who are often disempowered to protect themselves." Although inflamed colorectal tissues will not be examined in this thesis, the optimisation of a high-parameter flow cytometry panel to identify inflammatory MNPs in all sexual transmissions tissues forms the basis for **Chapter 4**.

1.13 Concluding remarks

"There are still 1.5 million new HIV infections each year and up to 1 million HIV-associated deaths. Furthermore, the cost of lifetime ART for all individuals in low- and middle-income countries is estimated to be $30 billion USD per year by 2030. Therefore, the need to block transmission of this virus remains a high global health priority. With the rapid advancement of high parameter single cell technologies our understanding of the MNP system will continue to evolve, especially in inflamed tissues. As our understanding deepens it is important that we translate these advancements to better define the role these cells play in HIV transmission." Although anogenital MNPs have been extensively examined for their interactions with HIV, colorectal MNPs have been comparatively under-researched. Furthermore, since CD169 and CD209, key receptors for HIV binding and transfer, are now known to be present on macrophages rather than tissue DCs, tissue macrophages required more thorough investigation. "It is especially important that we accurately understand exactly which MNPs deliver HIV to CD4 T cells and the mechanism by which this occurs as this will guide designing vaccine strategies. Furthermore, prior to the development of an HIV vaccine this will also help in optimising PrEP regimens to block HIV acquisition."

1.14 Aims of this thesis

1. Define the subsets of MNPs present in the human colorectum.
2. Define the expression of HIV-binding receptors on these colorectal MNP and investigate their capacity for HIV binding and uptake.
3. Investigate the capacity for colorectal macrophage subsets to interact with CD4 T cells in early infection.
4. Design and optimise a high-parameter flow cytometry panel for the future comparison of sexual transmission tissue in steady and inflammatory states.

Chapter 2. Optimal isolation protocols for examining and interrogating mononuclear phagocytes from human intestinal tissue

Publications incorporated into this chapter

Chloe M. Doyle*, **Erica E. Vine***, Kirstie M. Bertram, Heeva Baharlou, Jake W. Rhodes, Suat Dervish, Martijn P. Gosselink, Angelina Di Re, Geoffrey P. Collins, Faizur Reza, James W. T. Toh, Nimalan Pathma-Nathan, Golo Ahlenstiel, Grahame Ctercteko, Anthony L. Cunningham, Andrew N. Harman, Scott N Byrne. Optimal Isolation Protocols for Examining and Interrogating Mononuclear Phagocytes From Human Intestinal Tissue. *Frontiers in Immunology* (2021)

*Co-first Authors

This chapter presents an optimised enzymatic digestion protocol for the extraction of viable, functionally intact mononuclear cells from human intestinal tissue. Additionally, it describes the development of flow cytometry panels, both for the characterisation of intestinal mononuclear phagocytes (MNP), and their isolation by FACS. These methods have been utilised throughout this thesis. Macrophage subsets in this publication were based on those identified in the human jejunum (109) , therefore, to maintain consistency throughout this thesis, references to 'Mf1', 'Mf2', and 'Mf3' have been altered from the original publication to include (MDM), (t-MDM), and (Macrophages) respectively. Additionally, references to 'langerin' have been changed to 'CD207'. Figures have not been amended. All experiments, analysis and writing contained herein were equally contributed to by this author, in collaboration with Chloe Doyle, PhD.

2.1 Abstract

"The human intestine contains numerous mononuclear phagocytes (MNP), including subsets of conventional dendritic cells (cDC), macrophages (Mf) and monocytes, each playing their own unique role within the intestinal immune system and homeostasis. The ability to isolate and interrogate MNPs from fresh human tissue is crucial if we are to understand the role of these cells in homeostasis, disease settings and immunotherapies. However, liberating these cells from tissue is problematic as many of the key surface identification markers they express are susceptible to enzymatic cleavage and they are highly susceptible to cell death. In addition, the extraction process triggers immunological activation/maturation which alters their functional phenotype. Identifying the evolving, complex and highly heterogenous repertoire of MNPs by flow cytometry therefore requires careful selection of digestive enzyme blends that liberate viable

cells and preserve recognition epitopes involving careful selection of antibody clones to enable analysis and sorting for functional assays. Here we describe a method for the anatomical separation of mucosa and submucosa as well as isolating lymphoid follicles from human jejunum, ileum and colon. We also describe in detail the optimised enzyme digestion methods needed to acquire functionally immature and biologically functional intestinal MNPs. A comprehensive list of screened antibody clones is also presented which allows for the development of high parameter flow cytometry panels to discriminate all currently identified human tissue MNP subsets including pDCs, cDC1, cDC2 (CD207 (langerin)$^{+}$ and CD207^{-}), newly described DC3, monocytes, Mf1 (MDM), Mf2 (t-MDM), Mf3 (Macrophage) and Mf4. We also present a novel method to account for autofluorescent signal from tissue macrophages. Finally, we demonstrate that these methods can successfully be used to sort functional, immature intestinal DCs that can be used for functional assays such as cytokine production assays."

2.2 Introduction

"Intestinal mononuclear phagocytes (MNPs), specifically dendritic cells (DC), macrophages and monocytes play a major role in maintaining tolerance to food-derived antigens and resident microbiota without compromising the hosts ability to respond to invading pathogens(132). DCs are professional antigen presenting cells (APC) capable of antigen uptake, processing and migration out of the tissue to draining lymph nodes where they present antigens and activate naïve T cells(133,134). In contrast, macrophages perform this antigen presenting function weakly and do not readily migrate out of the tissue. Their primary function is to phagocytose and destroy invading pathogens as well as secrete a variety of immune-modulating cytokines (133,134). Monocytes migrate into tissue from blood and differentiate into monocyte-derived macrophages or DCs. Embedded within these broad cell types are a diverse range of DC and macrophage subsets that each possess their own tissue-specific phenotype and function. Accurate identification of these subsets in the human intestine is required before we can understand their role in homeostasis and disease settings. Indeed, the misidentification of MNP subsets has caused much confusion in the literature (7,135–138)."

"Isolating MNPs from human tissues is a challenging task as the techniques used to liberate them can alter their phenotype and affect their viability (8). We have previously published optimised methods for isolating and interrogating immature DCs and macrophages from human abdominal skin via enzymatic digestion (8). However, skin and intestinal tissue have marked phenotypic, functional and structural differences which necessitates a modified approach to

isolating MNPs. Recent literature has described a suite of consistent markers used to define all currently known subsets of human tissue dendritic cells and macrophages (7–9,109,139,140). In human abdominal skin, these comprise XCR1$^+$ cDC1 (conventional DC), CD1c$^+$ cDC2 that includes CD207 expressing and CD207 negative populations and CD14-expressing cells including tissue-resident autofluorescent (AF) macrophages and monocyte-derived macrophages (9). In human intestinal tissue, three populations of DCs have been identified using CD103 and SIRPα (139,140) and four intestinal CD14$^+$ macrophage populations (Mf1-4) have been identified using HLA-DR, CD14, CD11c and CD11b (109). More recently, high-resolution analyses have revealed a subpopulation within human blood cDC2s (CD1c$^+$ DCs) that expresses CD14 and a monocyte-like gene signature termed DC3s (40,41). As defined by the literature, DC3s are CD88$^-$ CD1c$^+$ CD163$^+$ and express varying levels of CD14$^+$ (40,41)."

"In this study, we present an intestinal tissue specific MNP isolation protocol to liberate high yields of viable, immature and biologically active MNPs from human intestinal jejunum, ileum and colon as well as terminal ileum biopsies. We also present techniques to anatomically separate the mucosa and submucosa, including their associated lymphoid follicles being Peyer's Patches in the small bowel and lymphoid aggregates in the large bowel, to better understand these distinct immune compartments. We emphasize the importance of carefully selecting antibodies that target the appropriate epitope post-digestion as well as markers that accurately define intestinal-derived MNPs according to the most recent and reliable literature. Further, we present a high-parameter flow cytometry gating strategy to identify all currently known human MNPs in human tissues. We also include a method for correcting AF spillover from tissue-resident macrophages which considerably improves the accuracy of measuring cell surface expression levels and correct MNP definition."

2.3 Methods

2.3.1 Human Specimens

"This study was approved by the Western Sydney Local Area Health District (WSLHD) Human Research Ethics Committee (HREC); reference number (4192) AU RED HREC/15 WMEAD/11. Large human intestinal specimens were taken with informed consent from patients undergoing surgery for intestinal cancer, 10-20 cm away from tumours, where present. Samples were processed within 2 hours of collection except for samples destined for cell sorting which were covered in Roswell Park Memorial Institute (RPMI) (Lonza, Switzerland) 1640 supplemented with 0.25% gentamycin and stored overnight at 4°C for processing the following morning."

2.3.2 Tissue processing

"Typical whole tissue intestinal specimens ranged in size from 5-40 cm^2, with all data obtained with whole tissue specimens unless biopsies are stated. The muscularis externa was mechanically removed from the submucosa using curved surgical scissors and forceps. The tissue was then cut into approximately 25 mm^2 pieces and incubated for 15 mins twice in RPMI-1640 (Lonza, Switzerland) supplemented with 10% Foetal Bovine Serum (FBS) (Sigma-Aldrich, Missouri, USA), 0.3% Dithiothreitol (DTT) (Sigma-Aldrich) and 2 mM EDTA at 37°C (herein referred to as DTT treatment). The tissue was washed in Dulbecco's Phosphate Buffered Saline Mg^{++}/Ca^{++} free (DPBS) (Lonza, Switzerland) prior to incubation on a MACSmix Tube Rotator (Miltenyi Biotec, California, USA) 2-3 times in RPMI-1640 supplemented with 5 µL/mL DNase I (Worthington Industries, New Jersey, USA) and 3 mg/mL Collagenase IV (Worthington) for 30 min each time at 37°C. The supernatant was separated from undigested intestinal tissue using a tea strainer. The cell suspension was passed through a 100 µM cell strainer (Greiner Bio-One, North Carolina, USA) before being washed twice in DPBS. The single-cell suspension in RPMI-1640 was spun on a Ficoll-Paque PLUS (GE Healthcare, Illinois, USA) gradient and mononuclear cells were harvested from the RPMI-Ficoll interface. When required, the mucosa was anatomically separated from the submucosa using a dissection microscope and forceps. Lymphoid follicles present in the mucosa and submucosa were then dissected out using a scalpel. The mucosa was digested as above, with the submucosa not requiring the DTT treatment. For terminal ileum biopsies, a 10 min DTT treatment at 37°C was required. A single cell suspension from terminal ileum biopsies and isolated lymphoid follicles was generated by shaking them at 170 rpm in a 37°C incubator in RPMI-1640 supplemented with 5 µL/mL DNase I and 3 mg/mL Collagenase IV for 45 min."

2.3.3 Flow Cytometry

"Cells were labelled in aliquots of 1-3 x 10^6 cells per 100 µL of DPBS. Non-viable cells were excluded by staining with Fixable Viability Stain 700 (BD Biosciences, New Jersey, USA). Cells were washed with FACS wash (1% FBS (v/v), 2 mM EDTA, 0.1% sodium azide (w/v) in PBS) and surface stained with the antibodies indicated **Table 2.1** in 10 µL Brilliant stain buffer plus (BD Biosciences) for 30 mins on ice. Cells were washed twice with FACS wash prior to resuspension in 100 µL of CytoFix (BD Biosciences) for 15 mins at 4°C. Cells were washed and resuspended in 100 µL of FACS wash. Flow cytometry was performed on an LSR Fortessa or Symphony flow cytometers (BD Biosciences) with BD Diva Software (V8.0) and data analysed on FlowJo (TreeStar V10.7.1)."

2.3.4 Fluorescence Activated Cell Sorting (FACS)

"Single-cell suspensions to be sorted were enriched for $CD45^+$ cells using anti-CD45 microbeads (Miltenyi Biotec) as per the manufacturer's instructions. $CD45^+$ cells were stained with Live/ Dead Near IR dead cell stain kit (Life Technologies, California, USA) in DPBS for 30 mins on ice, and washed with magnetic-activated cell sorting (MACS) wash (1% FBS (v/v), 2 mM EDTA in DPBS) before surface staining with antibodies indicated in **Table 2.2**. Cells were washed twice with MACS wash and filtered prior to sorting on a BD FACS Aria (130μM nozzle) (BD Biosciences), with sorted cells collected into 1.5 mL Eppendorf tubes (Sigma-Aldrich) containing RPMI-1640 supplemented with 1 µM HEPES (Gibco, Massachusetts, USA), non-essential amino acids (Gibco), 1 mM sodium pyruvate (Gibco) 5 0 µM 2-mercaptoethanol (Gibco), 10 µg/mL gentamycin (Gibco) and 10% (v/v) FBS (herein referred to as DC culture media)."

Table 2.1: Symphony Mononuclear Phagocyte Phenotyping Panel

Marker	Company	Clone	Fluorophore	Purpose	Concentration (µL/100 µL)
Viability	BD Biosciences	-	FVS700	Live cells	1:10, 000
HLA-DR	BD Biosciences	G46-6	BUV395	Myeloid cells	0.5
CD45	BD Biosciences	HI30	BB755	Immune cells	0.5
CD3	BD Biosciences	UCTH1	BUV496	T lymphocytes	5
CD19	BioLegend	HIB19	BV750	B lymphocytes	5
CD14	BD Biosciences	M5E2	BUV737	Macrophages	2.5
Calprotectin	Invitrogen	MAC387	PE	Infiltrating monocytes	2.5
CD88	BioLegend	S5/1	PE Dazzle 594	Monocytes	0.5
CD1c	BD Biosciences	F10/21A3	BUV805	cDC2	2.5
FCεR1α	Novus Bio	9E1	AF488	cDC2	1.5
FCεR1α	BD Biosciences	AER-37	APC	cDC2	5
CD11b	BD Biosciences	ICRF44	BV711	MNPs	2
CD11c	BD Biosciences	B-Ly6	BB515	MNPs	1.5
CD123	BioLegend	6H6	PE/Cy5	pDCs	0.5
CD163	BioLegend	GHI/61	BV605	DC3	2.5
SIRPα	BioLegend	SE5A5	APC/Fire 750	DCs	2.5
CD207	Miltenyi	MB22-9F5	PE-Vio770	cDC2	1.5
XCR1	BioLegend	S15046E	BV421	cDC1	4
CD141	Miltenyi	AD5-14H2	APC	cDC1	2.5

2.3.5 Culturing of ex vivo mononuclear phagocytes

"Following dead cell depletion (STEMCELL Technologies, Vancouver, Canada) as per the manufacturer's instructions and $CD45^+$ enrichment, 5 x 10^5 cells per condition were taken as a time 0-hour aliquot. All remaining cells were cultured at 1 x 10^6 cells/mL for 14 hours in DC culture media. Cells were then washed once in DPBS and stained with Fixable Viability Stain 700. Cells were washed with FACS wash and surface stained with antibodies indicated in **Table 1.1**, with drop-in CD54-PE (clone: HA58; 2.5 µL/100 µL), CD80-PE (clone: L307.4; 3 µL/100 µL), CD83-APC (clone: HB15e; 2.5 µL/100 µL) and CD86-APC (clone: 2331 (FUN-1); 2.5 µL/100 µL). Cells were washed twice with FACS wash prior to resuspension in 100 µL of CytoFix (BD Biosciences) for 15 mins at 4°C. Cells were washed and resuspended in 100 µL of FACS wash for acquisition."

Table 2.2: FACs Aria Sort Panel

Marker	Company	Clone	Fluorophore	Purpose	Concentration (µL/100 µL)
Viability	ThermoFisher	-	NIR	Live cells	1: 500
HLA-DR	Miltenyi	G46-6	PerCP	Myeloid cells	2
CD45	BD Biosciences	HI30	BV786	Immune cells	1
CD3	Miltenyi	REA613	APC-Vio770	T lymphocytes	2.5
CD19	Miltenyi	REA674	APC-Vio770	B lymphocytes	1
CD14	BD Biosciences	M5E2	BV421	Macrophages	2.5
CD1c	BD Biosciences	F10/21A3	PE	cDC2	2
CD11c	BD Biosciences	B-Ly6	PE-CF594	MNPs	1.5
CD207	Miltenyi	MB22-9F5	PE-Vio770	cDC2	1.5
CD123	BD Biosciences	9F5	BV711	pDCs	1
XCR1	BioLegend	S15046E	APC	cDC1	4

2.3.6 Intracellular Cytokine Staining

"Sorted intestinal-derived MNPs were cultured in DC culture media and stimulated with 1 µg/mL of the TLR7/8 ligand, R848 (InvivoGen, California, USA). After 2 hours, 2.5 µg/mL Brefeldin A (Sigma-Aldrich) was added to prevent cytokine secretion into the supernatant. After a total of 16 hours, cells were washed with DPBS and stained with Live/ Dead Near IR dead cell stain kit. Cells were washed with FACS wash and resuspended in 100 µL of CytoFix/CytoPerm (BD Biosciences) for 15 mins at 22°C. Cells were washed twice with Perm Wash (1% FCS (v/v), 1% BSA (w/v), 0.1% saponin (w/v), 0.1% sodium azide (w/v) in PBS) and stained with anti-IL-6 APC (clone: MQ2-13A5;

2.5 µL/100 µL), anti-IL-23p40 PE (clone: C8.6; 0.25 µL/100 µL) and anti-TNF BV650 (clone: MAB11; 2.5 µL/100 µL) for 30 mins at 22˚C. Cells were washed and resuspended in 100 µL of FACS wash prior to acquisition."

2.3.7 Statistical analysis

"Statistical analysis was conducted using GraphPad Prism v9.1.2 (San Diego, CA). A Student's paired t test (comparing 2 groups) or a Kruskal Wallis test with Dunn's multiple comparisons test (comparing more than 2 groups) was used."

2.4 Results

2.4.1 Optimisation of enzymatic digestion protocols for the isolation and interrogation of intestinal mononuclear cells

"We optimised a protocol for the mechanical separation and enzymatic digestion of human intestinal tissue to liberate MNPs. Enzymatic access to the mucosal tissue was increased by removing the underlying muscle layer and fine dicing the tissue with a scalpel. The epithelium and any remnant mucus were removed with DTT treatment prior to digestion with collagenase type IV at 37°C which we previously showed to the best collagenase blend for MNP tissue isolation (8) (**Figure 2.1A**). Using this method, we compared the yield and proportions of MNPs ($CD3^-$ $CD19^-$ $HLA\text{-}DR^+$ $CD45^+$) from sequential 30-minute collagenase digestions (**Figure 2.1B**). Digestions were performed in sequence rather than one extended digestion to both limit the exposure of the liberated cells to the enzyme, and to replenish the enzyme for optimal activity. The first digestion resulted in significantly lower yield and proportion of MNPs than the subsequent digestions, suggesting that 30 mins was not long enough to liberate our cells of interest from whole tissue specimens. The second digestion provided the highest proportion of MNPs as well as the highest yield, in numbers suitable for phenotyping assays. (**Figure 2.1C&D**). A third digestion liberated additional cells which increased the total yield (Figure 2.1C), without compromising the proportion of $HLA\text{-}DR^+$ $CD45^+$ cells (**Figure 2.1D**) or their viability (**Figure 2.1E**). Two digestions were performed for phenotyping purposes, while three digestions were utilised when higher numbers of MNPs were required for cell sorting and functional assays."

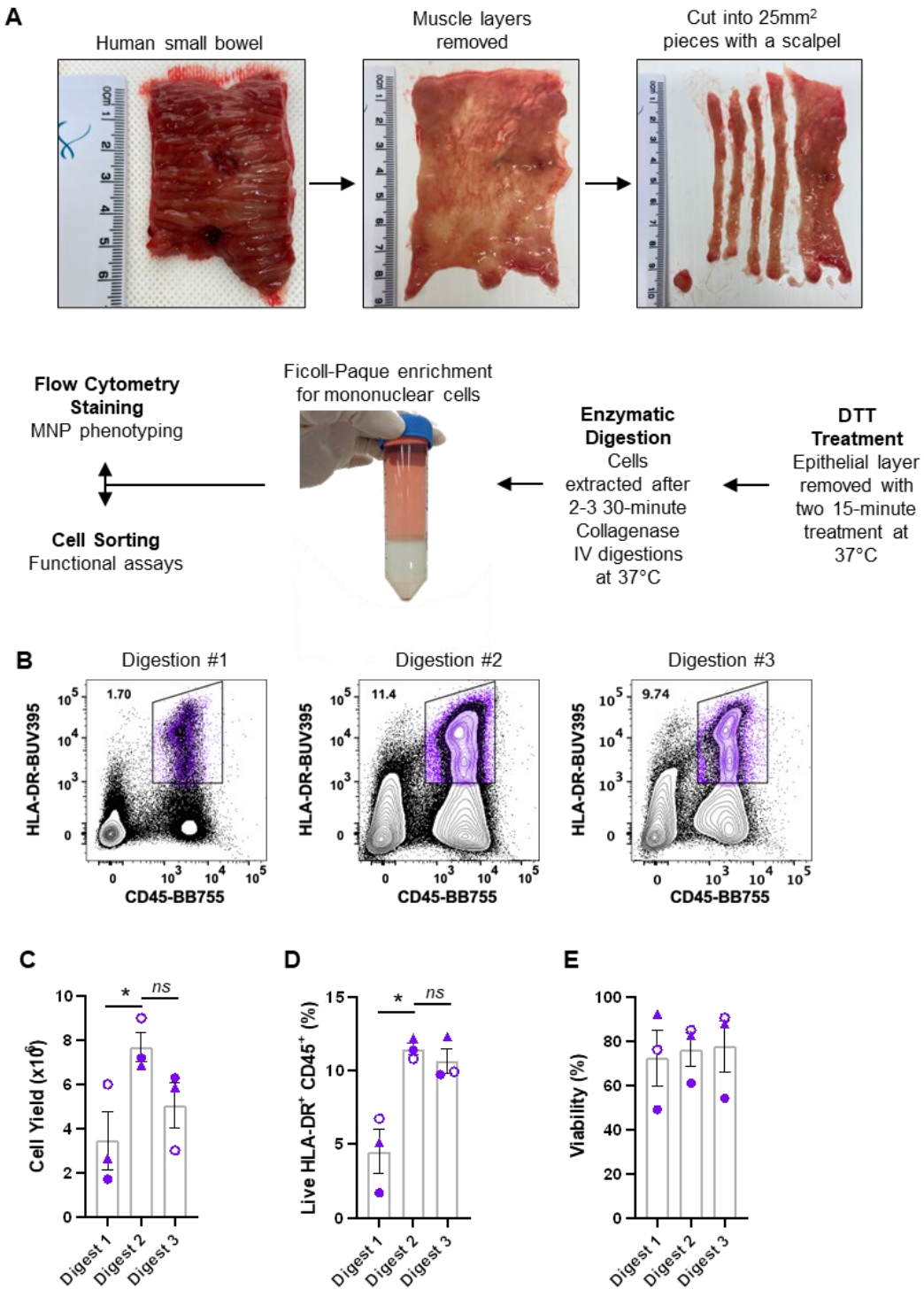

Figure 2.1: Isolation of immune cells from human intestinal tissues. "Discarded human intestinal tissues were obtained within one hour of surgery. **A** Underlying tissue was removed using curved surgical scissors before being diced into small pieces with a scalpel. Tissue was treated with DTT for two 15 min incubations at 37°C prior to 2-3 30 min digestions with collagenase type IV. Mononuclear cells were enriched using a Ficoll-Paque gradient before cells were stained for phenotyping or cell sorting. **B** Representative plot of live HLA-DR$^+$ CD45$^+$ proportions from each digestion. **C** Cell yields from each digestion, counted post-Ficoll on a haemocytometer. **D** Percentage of live HLA-DR$^+$ CD45$^+$ cells from total cells as determined by flow cytometry. **E** Percentage of viability of each digestion as determined by flow cytometry with mean ± SEM. Each symbol represents an individual donor (n=3). Statistics was by a Kruskal Wallis test with Dunn's multiple comparisons test comparing the sequential digests (*p<0.05)."

2.4.2 Manual separation of intestinal tissue compartments

"Intestinal mucosal tissue consists of multiple compartments that require separation to investigate their unique immune cell profiles (141). To achieve this, the mucosa and submucosa were mechanically separated along the biological border of the two layers, the muscularis mucosa, and lymphoid follicles were isolated prior to digestion (**Figure 2.2A**). This was performed under light microscopy without the need for tissue staining, with lymphoid follicles being visually identified and removed with a scalpel. The mucosa was digested as per the protocol for whole tissue (**Figure 2.1A**), with the submucosa digested without DTT treatment as it does not have an epithelial layer. Lymphoid follicles (<2 mm^2), like biopsies (<5 mm^2), are smaller than the diced pieces of whole tissue (25 mm^2) and as such were fully digested in a shorter, single digestion. The lymphoid follicles as well as terminal ileum biopsies underwent collagenase type IV digestion for 45 min at 37°C, with biopsies receiving a 10 min DTT treatment at 37°C before digestion as described in **Figure 2.2A**. Using tissue from 3 individual donors and a minimal staining panel we were able to show by flow cytometry that of the $CD45^+$ cells liberated, $CD3^+$ T cells, $CD19^+$ B cells and HLA-DR^+ MNPs were represented in different proportions in each compartment (**Figure** 2.2**B**), confirming that we can manually dissect intestinal tissue to enrich for specific tissue compartments using visual confirmation."

2.4.3 Accurate identification of tissue dendritic cell subsets via flow cytometry

"With the ever-changing classification of DCs (39,41,42,139,140), their identification by flow cytometry has required an increasing number of discriminatory markers. For tissue DCs this task is further complicated by the cleavage of surface identification markers that often occurs during enzymatic liberation. A subset of cDC2 that express FCεR1α have recently been described (41,42). We confirmed that FCεR1α was expressed on some cDC2s using the clone AER-37, though it was not until the same cells were stained with the clone 9E1 that we could confirm that the epitope recognised by AER-37 was being partially cleaved by collagenase Type IV (**Figure** 2.3**A**). In addition to epitope cleavage, a further consideration is whether markers found on the surface of circulating cells correspond to tissue DCs. Blood cDC1s have been classified as $CD141^+$ and $XCR1^+$ (142), however, this does not appear to be the case in intestinal tissues where only a small portion of $XCR1^+$ cells express CD141, the expression of which does not correlate to XCR1 expression **(Figure 2.3B**). Therefore, CD141 is not a reliable marker of cDC1s in the

intestine. Taken together, these results emphasise the importance of marker and antibody clone selection for the proper identification of enzyme-liberated intestinal DCs."

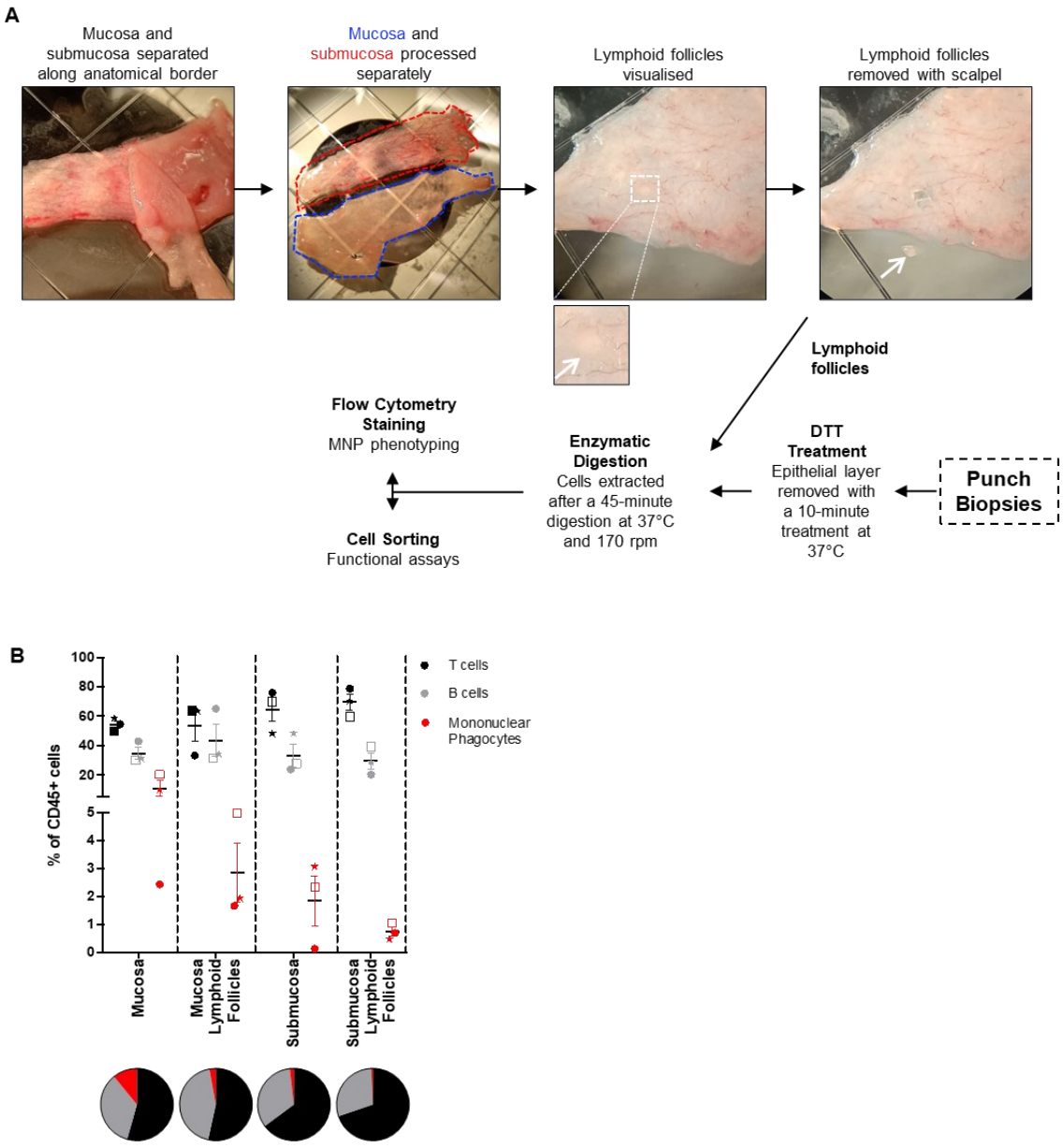

Figure 2.2: Separation of tissue compartments from intestinal tissue. "Discarded human intestinal tissues were obtained and underlying tissue removed as in Figure 1. **A** Under a dissecting microscope, the mucosa and submucosa were mechanically separated with forceps. Mucosa and submucosa were then processed separately for the removal of lymphoid follicles. Insert: magnified view of a lymphoid follicle. Follicles are visualised and removed from each tissue layer using a scalpel. Mucosa and submucosa were processed as per Figure 1, with no DTT treatment for the submucosa. Lymphoid follicles were digested for 45 mins at 37°C at 170 rpm. When obtained, punch biopsies were DTT-treated for 10 mins at 37°C, before being digested as per the lymphoid follicles. **B** Cells liberated from tissue compartments were analysed by flow cytometry. $CD3^+$ T cells, $CD19^+$ B cells and $HLA\text{-}DR^+$ mononuclear phagocytes were represented as a percentage of $CD45^+$ cells with mean ± SEM. Each symbol represents an individual donor (n=3). Pie charts represent the mean as parts of whole."

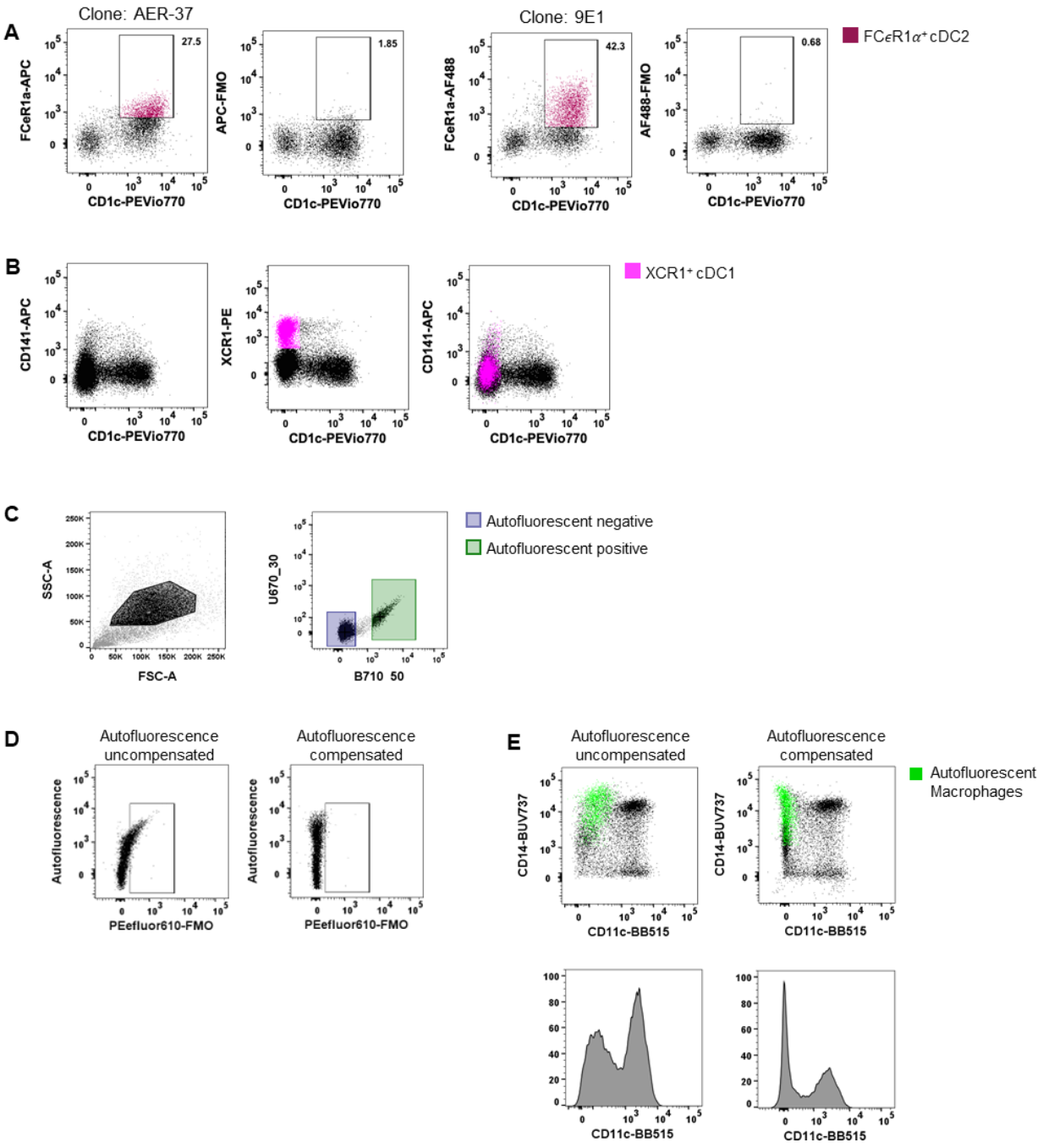

Figure 2.3: Optimisation of staining and acquisition parameters for flow cytometry. "Intestinal mononuclear phagocytes were isolated as per Figure 1**. A, B** Cells were stained to isolate HLA-DR$^+$ CD45$^+$ CD3$^-$ CD19$^-$ CD11c$^+$ DCs. **A** In the same donor, FCεR1α expression was compared between clones AER-37 and 9E1 for optimal expression, with corresponding Fluorescence Minus One (FMO) control. **B** Expression of defining conventional DC (cDC) 1 markers XCR1 and CD141 were compared in the same donor for correlation in intestinal tissue. **C, D** Unstained intestinal cells were acquired to show sample autofluorescence. **C** Representative plot of unstained intestinal cells, gated on events with higher side scatter. Autofluorescent negative and positive cells were gated and applied to un unused detector channel in FlowJo V10.7.1 to create the autofluorescent-corrected compensation matrix. **D** Representative plots for autofluorescent correction, showing correction of fluorescent signal for PEefluor610. **E** Representative plots of live HLA-DR$^+$ CD45$^+$ CD3$^-$ CD19$^-$ mononuclear phagocytes, comparing the CD11c BB515 signal with and without correction of autofluorescent signal. Autofluorescent macrophages overlaid, gated for CD14+ and autofluorescence."

2.4.4 Autofluorescent correction of tissue-resident macrophage subsets via flow cytometry

"Tissue-resident yolk sac derived macrophages are characteristically autofluorescent (AF) (37). This unique characteristic allows for their identification by flow cytometry as AF $CD14^+$ (9,37). However, as more subsets of macrophages are defined in the intestine (109), their AF properties can mask the expression of key defining markers as well as presenting false positives. Roca, Burton (143) recently described a method for AF correction using AutoSpill, an algorithm for calculating spillover coefficients, by assigning AF as an additional endogenous dye using an unstained sample. We acquired an unstained sample of intestinal-liberated cells in addition to single-colour controls on beads to facilitate AF correction for manual compensation. Using the compensation wizard in FlowJo, the unstained sample was allocated to an unused detector channel where autofluorescence spills naturally, for example B710_50 on the FACSymphony, treating the AF signal from tissue cells as a single-colour control. By setting positive and negative gates for AF **(**Figure 2.3**c)** and re-calculating the compensation matrix with AF as a measurable parameter, AF spillover into other detectors was minimised, as shown with the correction of false signal using Fluorescence Minus One (FMO) (**Figure 2.3D**) and on $CD45^+$ HLA-DR^+ $CD3^-$ $CD19^-$ cells (**Figure 2.3E**). Furthermore, not using this method leads to inaccurate determination of surface marker expression as indicated for key DC expression marker CD11c in **Figure 2.3E**. Here we show that the $CD14^+$ $CD11c^-$ AF macrophages can be corrected to display as $CD11c^-$, instead of spilling false signal into the detector allocated to CD11c."

2.4.5 Identification of intestinal-derived mononuclear phagocytes

"MNPs share several common markers in tissue making their definitive identification and characterisation challenging (7,109). Using flow cytometry, we were able to identify collagenase-liberated MNPs ($CD45^+$ HLA-DR^+ $CD3^-$ $CD19^-$) in intestinal tissue. We identified four subsets of $CD14^-$ DCs: cDC1s expressing XCR1; two subsets of $CD1c^+$ cDC2 divided by CD207 expression; and $CD123^+$ plasmacytoid DCs (pDCs) which, as expected, were more readily detectable in inflamed tissue (134) (**Figure 2.4A**). DC3s were identified as $CD11c^+$ $CD1c^+$ $CD163^+$ $CD88^-$ and $CD14^{+/-}$ (40,41). We also characterised intestinal DCs by their expression of CD103 and SIRPα (139,140). The $SIRP\alpha^+$ DCs correlate with the $CD207^+$ cDC2s, $CD103^-$ DCs correlate to $CD207^-$ cDC2s, and the $SIRP\alpha^-$ $CD103^+$ cells correlate with the $XCR1^+$ cDC1s (**Figure 2.4C**), showing that while there are distinct differences between human tissue DC phenotypes, there are overlapping similarities. In addition, $CD14^+$ macrophages could be divided into four subsets:

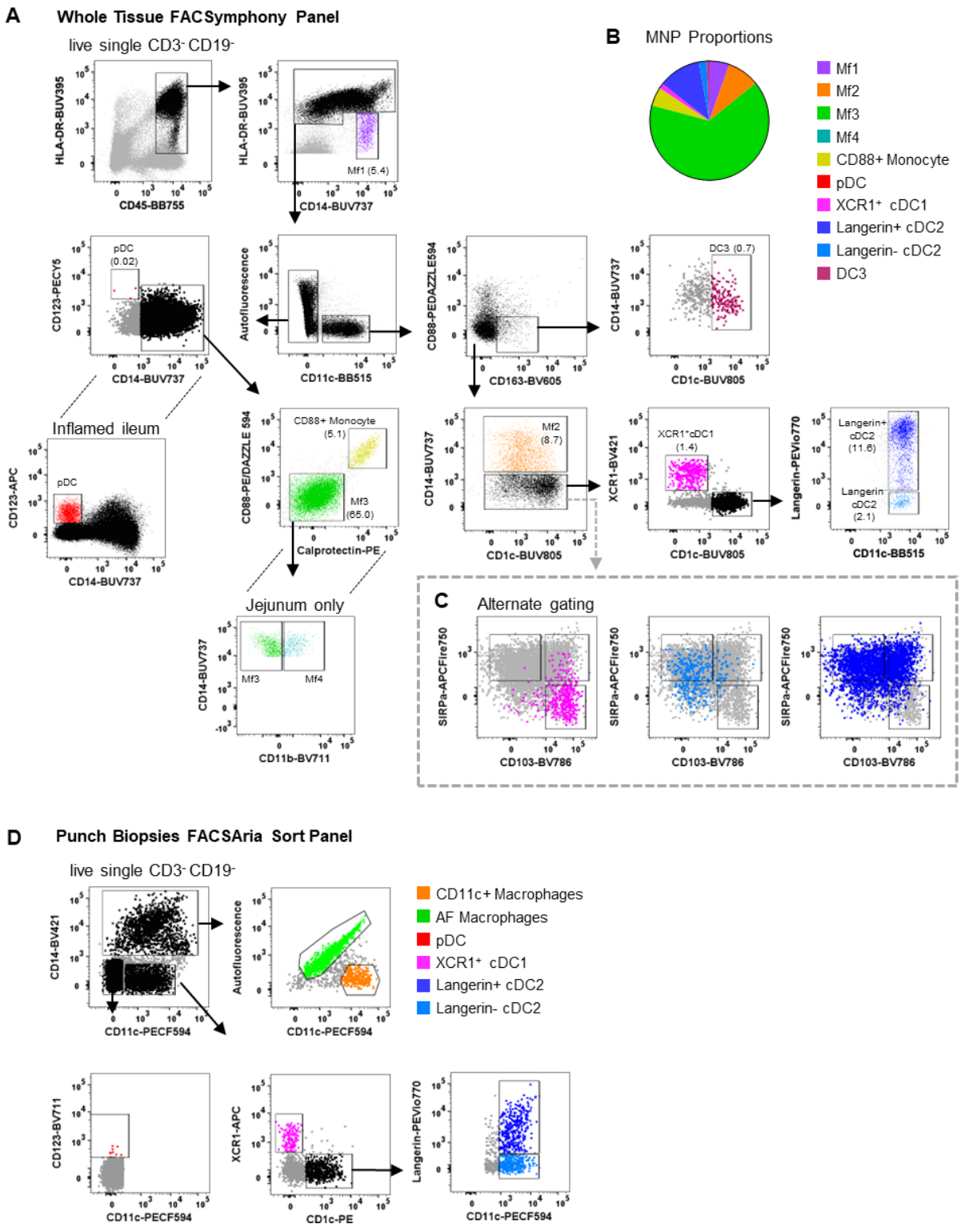

Figure 2.4: Identification of intestinal-derived mononuclear phagocytes by flow cytometry. "Intestinal mononuclear phagocytes were isolated as per Figure 1. **A** Cells were stained with FACSymphony Phenotyping Panel **(Table 1)**. All mononuclear phagocytes were gated within the live, single, CD45$^+$ CD3$^-$ CD19$^-$ population. Intestinal mononuclear phagocytes (MNP) were gated in sequential order with percentage of total mononuclear phagocytes in brackets. Macrophage (**Mf) 1** (MDM) were defined as CD14$^+$ HLA-DR^{low}, with all sequential MNPs gated as HLA-DR$^+$. Cells were then divided by their expression of CD11c. CD11c$^-$ cells included CD14$^-$ CD123$^+$ plasmacytoid DCs (**pDCs**), CD14$^+$ Calprotectin$^+$ **CD88$^+$ monocytes** and CD14$^+$ autofluorescent$^+$ **Mf3**s (Macrophage) which could be further subdivided into CD11b$^+$ **Mf4** detectable only in the jejunum. CD11c$^+$ cells were divided as follows: CD88$^-$ CD163$^+$ CD1c$^+$

DC3s, CD14$^+$ **Mf2**s (t-MDM), CD14$^-$ CD1c$^-$ XCR1$^+$ **cDC1**s, CD14$^-$ XCR1$^-$ CD1c$^+$ **cDC2**s divided by their expression of **CD207**. **B** Alternative gating for CD11c$^+$ CD14$^-$ cells, characterised by SIRPα and CD103, overlaid with cDC1 and cDC2s from the main gating strategy for comparison. **B** Pie cart representation of proportion of mononuclear phagocyte subsets as part of whole of all mononuclear phagocytes **C** Cells isolated from intestinal biopsies were positively selected for CD45 and stained with FACS Sort Panel **(Table 2)**. Live, single CD45$^+$ HLADR$^+$ cells were divided by CD14 expression. CD14$^+$ cells were sorted as CD11c$^-$ autofluorescent$^+$ macrophages and CD11c$^+$ macrophages. CD14$^-$ cells were sorted as CD123$^+$ plasmacytoid DCs, XCR1$^+$ cDC1s, CD1c$^+$ cDC2s CD207$^{+/-}$."

Mf1 (MDM, HLA-DR^{low}), Mf2 (t-MDM, CD11c$^+$), Mf3 (Macrophage, CD11c$^-$) and Mf4 (CD11c$^-$ CD11b$^+$) (109), with Mf3 macrophages representing the largest proportion of mononuclear phagocytes (**Figure 2.4B**). We identified the Mf4 population in human jejunum (109), however have consistently been unable to identify these cells in lower intestinal tissues. Also identified were CD14$^+$ CD88$^+$ monocytes which can be further separated from macrophages by their expression of calprotectin (42). As whole tissue samples are not always abundantly available, we optimised a FACSort panel that would allow for the identification and isolation of MNPs from terminal ileum biopsies. As AF correction occurs post-acquisition, a gating strategy was devised to utilise AF spillover. We identified XCR1$^+$ cDC1, CD207$^{+/-}$ cDC2, pDCs as well as AF macrophages (Mf3, Macrophage) and CD11c$^+$ macrophages (Mf1 (MDM) and Mf2 (t-MDM)) for use in functional assays. (**Figure 2.4D**)."

2.4.6 Mononuclear phagocytes are phenotypically immature at the time of liberation

"A complication of the digestion process can be the inadvertent activation or maturation of cells (8,92,144). We investigated the maturation status of MNPs isolated by our digestion protocol, by assessing the surface expression of adhesion (CD54) and co-stimulatory molecules (CD80, CD83 and CD86), which are upregulated upon maturation (145). Immediately after isolation, all MNP subsets expressed low levels of CD54, CD80, CD83 and CD86 (**Figure 2.5A**). In two of three donors, Mf1 (MDM), Mf3 (Macrophage) and cDC1s did not survive the 14-hour culture and therefore their maturation status at this time was not determined. However, significant upregulation of CD54 was seen on Mf2 (t-MDM), CD54, CD83 and CD86 on CD207$^{+/-}$ cDC2s, with CD207$^-$ cDC2 also upregulating CD80 post-culture (n=3) (**Figure 2.5B**). This culture-induced upregulation of maturation markers suggests that not only were the tissue-liberated MNPs viable, but they also remained immature throughout the enzymatic digestion."

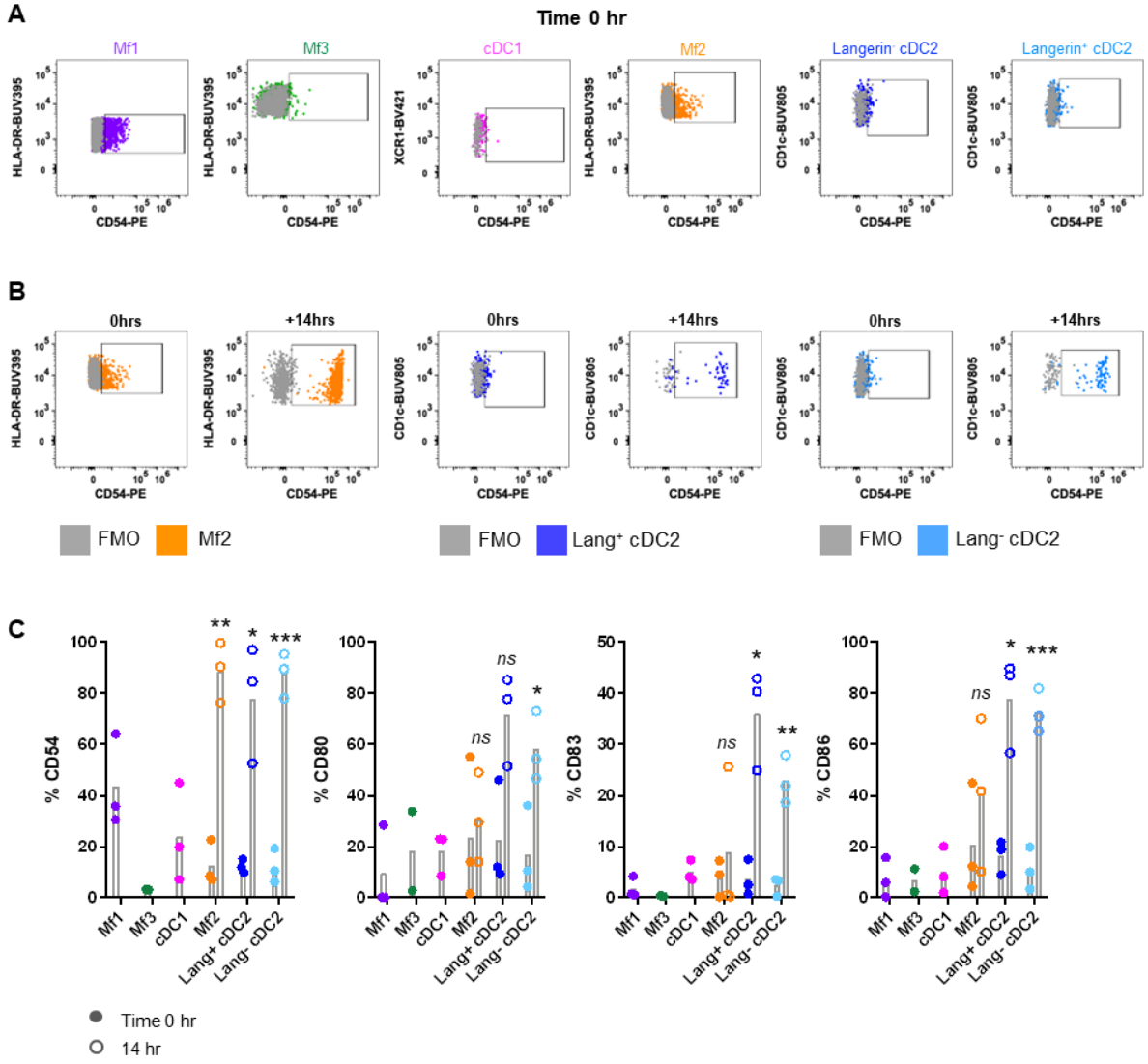

Figure 2.5: Investigating the maturation phenotype of tissue MNPs liberated by enzymatic digestion. **"**Intestinal mononuclear phagocytes (MNP) were isolated as per Figure 1. Cells were stained for flow cytometry with FACSymphony Phenotyping Panel **(Table 1)** with drop-ins for CD54, CD80, CD83 and CD86, immediately following liberation (time 0 hr) as well as 14 hr post-liberation. **A** Cells were gated as per Figure 4a, with representative plots of time 0 hr expression of CD54 shown, compared to Fluorescence Minus One (FMO). **B** Representative plot for Mf2 (t-MDM), CD207^{+} cDC2 and CD207^{-} cDC2 showing expression of CD54 at time 0 hr compared to 14 hr post-liberation, compared to FMO. **C** Expression of CD54, CD80, CD83 and CD86 on MNP subsets at time of liberation (closed circles), with 14-hr comparison (open circles) for Mf2 (t-MDM), CD207^{+} cDC2 and CD207^{-} cDC2 (n=3). Statistics was by a paired Student's t-test comparing each marker for each cell type at 0h with 14h (*p<0.05, **p<0.01, ***p<0.001)."

2.4.7 Liberated intestinal mononuclear phagocytes can be used for functional assays ex vivo

"Having isolated and identified immature MNPs, we next confirmed that their biological functionality had been maintained. Sorted MNPs were stimulated and cultured for 16 hrs to determine their cytokine response. We observed, via intracellular staining, that AF macrophages, cDC1s and cDC2s could produce TNF, IL-23p40 and IL-6 in response to R848 (**Figure 2.6**). This cytokine response suggests that the intestinal-derived MNPs were liberated in a functional state."

2.5 Discussion

"The ability to interrogate immune cells from fresh human tissue is critical for advancing our understanding of the role these cells play in human disease settings. This is especially the case with intestinal MNPs, which are integral components of the mucosal innate immune system. Here, they play a crucial role in maintaining tolerance of the commensal microbiota while also remaining poised to respond to invading pathogens. While sophisticated animal models have greatly expanded our knowledge of intestinal MNPs, they are not able to completely recapitulate human tissue with many cells differing phenotypically and functionally (140,146). Translating the data generated from these animal models requires the development of isolation methods to interrogate human immune cells *ex vivo* while maintaining their biological state. We previously described tissue digestion protocols for the isolation of MNPs from human abdominal skin (8) and anogenital tissues (7,9). However, given the distinct phenotypic, functional and structural differences between skin and mucosal tissue, we present an isolation protocol to extract functionally immature MNPs from human intestinal tissue. We have carefully selected the optimal antibody clones and corrected AF spillover to develop high-parameter flow cytometry gating strategies to accurately identify all currently known subsets of MNPs in fresh human intestinal tissue."

"An important consideration when isolating cells via enzymatic digestion is the delicate balance between cell yield and viability. Many groups perform one round of enzymatic digestion (109,139), however, Lefrançois and Lycke (147) showed the advantages of performing a second round of digestion in murine mucosal tissues to enhance cell yield and viability. Our findings show that we can digest human intestinal tissue for a total of 90 mins without compromising cell viability or proportions. As a result, we can liberate a higher quantity of total cells for downstream functional assays, which can be a limiting factor when working with human tissue-

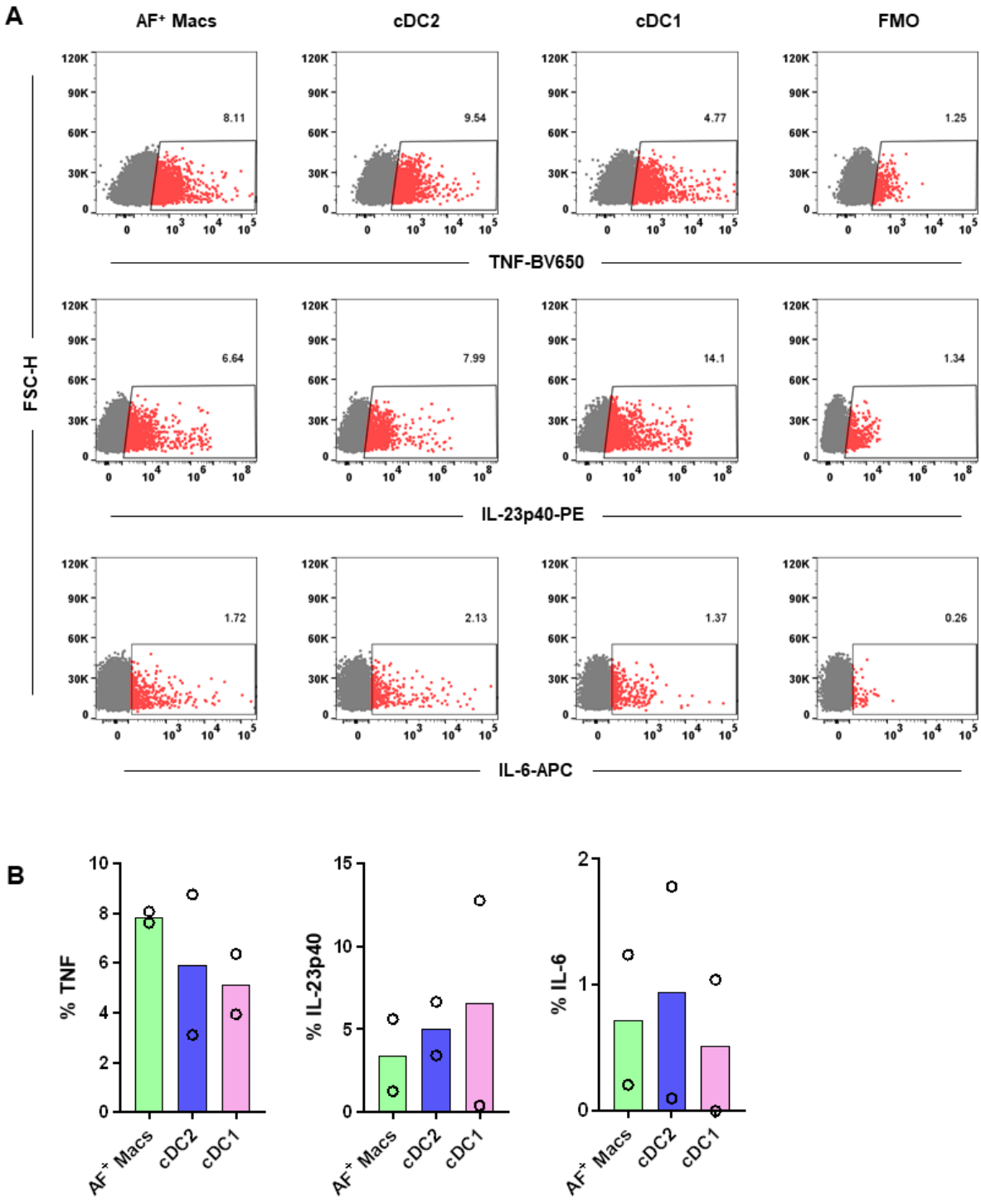

Figure 2.6: Investigation of the cytokine responses of tissue MNPs liberated by enzymatic digestion. "Intestinal mononuclear phagocytes were isolated as per Figure 1. Cells were positively selected for CD45 and stained with FACS Sort Panel (Table 2). Autofluorescent (AF) macrophages (Macs), conventional DC (cDC) 1 and cDC2s were sorted based on gating in Figure 4c. Sorted cells were cultured at $1x10^6$ cells/mL in DC Culture Media with 1μg/mL R848 for 2 hours. 2.5μg/mL Brefeldin A was added, and the cells cultured for a further 14 hours. Cells were then stained with Fixable Viability Stain 700 and intracellularly stained with anti-TNF, anti-IL-23p40 and anti-IL-6. Cells were acquired on a FACSymphony. A Representative plots for expression of TNF, IL-23p40 and IL-6 on all subsets compared to Fluorescence Minus One (FMO). B Expression of TNF, IL-23p40 and IL-6 as a percentage of live single cells minus FMO, columns represent mean expression (n=2)."

derived cells (9,45). Most of the data we have presented here has taken advantage of our privileged access to whole pieces of intestinal tissue. While these larger tissue samples are often required to perform sorting for functional assays *ex vivo*, it is far more common to receive surgical biopsies from patients. To that end, we have shown that using our protocols it is possible to liberate, phenotype and even sort MNPs from human punch biopsies. Due to punch biopsies being smaller, a shorter digestion protocol is sufficient to liberate the cells which will make the interrogation of DC and macrophages from the intestine easier and far more accessible."

"In the intestine, there are several different anatomical compartments containing varying ratios of functionally specialised immune cells each with their own unique interactions with the local intestinal environment (148). To interrogate these immunological compartments and the unique role each plays in disease settings it is crucial to isolate and interrogate them separately. The four primary compartments investigated in this study are the mucosal and submucosal layers, and their associated lymphoid follicles. Posing the greatest obstacle to deepening our knowledge of these immune compartments has been the difficultly in delicately separating the tissue layers and correctly identifying and removing the small lymphoid follicles. Other groups have attempted to expedite this task by using dyes to better visualise the lymphoid follicles (141), however, here we present an alternative method that removes this step and the risk it may pose in altering their function (149). Based on the method of Fenton, Jørgensen (141,150), we were able to separate these compartments and show their unique immune profiles."

"A known complication of enzymatic digestion is the cleavage of cell surface proteins, which can lead to the misidentification of cell subsets. We have previously shown that type IV collagenase best preserved the cell surface proteins used to identify tissue MNPs which led to the discovery of previously unidentified epidermal DC subset (7,8). However, even with this collagenase blend, surface proteins can be partially cleaved, leading to underrepresentation of cell subsets within the tissue or their loss of function. It has proven particularly challenging to identify tissue-specific cDC2s as their markers overlap with monocytes and macrophages. Dutertre, Becht (42) revealed that FCεR1α was one of two exclusive markers used to identify tissue cDC2s. Upon reviewing the literature, we selected FCεR1α clone AER-37 as this was the most widely used clone. By using this specific antibody clone and type IV enzyme combination, we observed that FCεR1α was partially sensitive to enzymatic cleavage as an unusually low proportion of cDC2s were FCεR1α^{+}. It wasn't until we selected a new FCεR1α antibody clone: 9E1, that we were able to detect a much higher proportion of FCεR1α expression on cDC2s in the intestine. Hence, FCεR1α clone 9E1 with collagenase type IV is the superior combination."

"Another consideration is the change in the pattern of marker expression on MNPs from different tissue compartments. In human blood and cutaneous abdominal tissue, cDC1s have been shown to express both CD141 and XCR1 (151). However, in human intestinal tissue we found that the expression of CD141 on cDC1s is extremely low and does not correlate with expression of XCR1. In addition, tissue cDC2s can upregulate their expression of CD141 (152). Peripheral blood cDC1s are defined by their CD141 and CADM1 expression, although CADM1 is not expressed by human skin cDC1s (8). We show here that CD141 is an unreliable marker in human intestine, therefore, we recommend XCR1 as the optimal marker for identifying cDC1, with the S154046E clone, in our experience as the only reproducibly reliable antibody that currently works on tissue-derived cells. This highlights the importance of carefully selecting antibodies that not only target preserved receptor epitopes post-digestion but reflect the expression of cell surface receptors in the tissue of interest."

"The classification of MNPs is a rapidly evolving field of research and identifying them by flow cytometry can be challenging as subsets of MNPs share common markers (7,109). This is further complicated by the AF properties of tissue-resident macrophages. Here we were able to correct AF by using an unstained tissue-derived control sample, allowing us to differentiate between real and false signal and improve resolution of surface markers used to identify MNPs. We could identify all currently known subsets of intestinal DCs using CD103 and SIRPα (139,140) as well as the newly published DC3s (40,41) in the same tissue. Furthermore, the SIRPα^- CD103$^+$ cells could be identified as XCR1$^+$ cDC1 and SIRPα^+ CD103$^{+/-}$ cells as CD1c$^+$ (CD207$^{+/-}$) cDC2, which is more relevant across different tissue types."

"Following enzymatic extraction of MNPs from human intestinal tissue we have optimised methods to interrogate the function of these cells. This is important as extraction of MNPs from the tissue by enzymatic digestion can alter their biological function. Mature tissue MNPs have been shown to express elevated levels of leukocyte adhesion molecule CD54 (ICAM-1) and co-stimulatory molecules such as CD80, CD83 and CD86 (145). Conversely, immature MNPs freshly isolated from healthy human intestinal tissue should express low levels of these receptors on their surface. Following overnight culture, we showed that Mf2s and cDC2s had a substantial increase in maturation marker expression confirming that the cells were in an immature state upon liberation. Interestingly, we observed that Mf2s and cDC2s survived the culture, whereas Mf1 (MDM), Mf3 (Macrophage) and cDC1 did not survive in two out of three donors. This suggests that cDC2 and Mf2 (t-MDM), which are phenotypically very similar (109), share a propensity for survival outside of their tissue environment. We also showed that tissue liberated MNPs could

produce cytokines in response to a TLR7/8 ligand. These findings confirm that intestinal MNPs liberated by enzymatic digestion following our optimised mucosal tissue digestion protocol are in an immature and biologically functional state. This is advantageous over other isolation methods such as spontaneous migration of DCs out of tissue during culture, which triggers the maturation of DCs limiting their use in functional assays (8)."

"In summary, our study demonstrates an enzymatic digestion protocol for the isolation of human intestinal MNPs in an immature state from tissue and biopsies while maintaining their biological function. We provide a method for the anatomical separation of the different gut-associated lymphoid tissues without the use of dyes. We also demonstrate the need for careful selection of antibodies that target preserved receptor epitopes and reflect their unique tissue-specific phenotype. These optimised protocols will greatly enhance our ability to interrogate APCs in human tissue, which will be important to understanding their role in homeostasis and diseases of the intestine."

Chapter 3. Defining colorectal mononuclear phagocytes and investigating macrophage interactions with HIV in early infection

This chapter identifies all known non-inflamed mononuclear phagocytes (MNPs) present in the human colon and rectum (colorectum), utilising high-parameter flow cytometry and single-cell RNA sequencing (ScRNA). Furthermore, colorectal MNP expression profiles of HIV entry (CD4, CCR5) and HIV-binding lectin receptors (CD169, CD206, CD207, CD209) were examined. The MNP subsets were assessed for their capacity to take up HIV, as well as their efficiency at transferring HIV to CD4 T cells. All experiments, analysis and writing contained herein were completed by this author, the sole exemption being the ScRNA processing. Data was aligned by Brian Glass and the pre-processing performed by Thomas O'Neil, however, all ScRNA analysis included in this chapter was performed by this author.

3.1 Introduction

HIV/AIDS still has no cure or vaccine, and infection persists globally in 40 million people. Fortunately, outcomes have improved since the introduction of antiretroviral therapies (ART), converting a terminal diagnosis to chronic illness (121) . Individuals with undetectable HIV loads while on ART have almost no risk of transmission and transmission rates in countries with adequate ART coverage have markedly reduced as a result. However, as this is a lifelong treatment (3) , HIV remains a substantial burden to national healthcare systems, and of course the infected individual, as well as drug toxicity, residual disease and social stigma. But with approximately one third of HIV^+ individuals worldwide not receiving ART, and the minimal use of pre-exposure prophylaxis (PrEP) in high-risk groups (2,3) HIV transmission continues. Moreover, recently it has become clear that genital inflammation markedly enhances the efficiency of HIV transmission and PrEP is inefficient in this context (126,153). The long-term effects of PrEP use on healthy individuals are unknown and even those on effective ART may experience persistent health problems (154) . These can include an increased risk of non-communicable diseases such as osteoporosis, renal disease, cardiovascular disease and liver complication, especially in the cases of hepatitis co-infection. Moreover, cessation of treatment results in rapid viral rebound and the eventual progression to AIDS. Although the development of a vaccine and cure remain key priorities, improving current transmission prevention strategies for high-risk individuals for whom current strategies are not viable is an important interim goal. However, the design of more targeted prevention strategies is contingent upon a comprehensive and accurate understanding of early HIV transmission events.

Sexual transmission of HIV via the human genital and anorectal (anogenital) skin and mucosa is the principal mode of transmission. However, although there have been several key recent developments in our understanding of the immune cells involved in the early events of transmission in these tissues (7,9,18,116,155), the precise sequential mechanisms are still being debated (52,118). Physiologically, anatomically and immunologically HIV transmission sites are varied, but once the protective barriers are breached, HIV encounters a range of cell types that contribute to transmission, notably the cellular immune sentinels, mononuclear phagocytes (MNP) consisting of dendritic cells (DC), Langerhans cells, macrophages and monocytes. MNPs are a family of antigen presenting cells (APC) that form the first line of defence against invading pathogens, binding them via a variety of cell surface lectin receptors leading to pathogen uptake, processing and presentation to T cells to drive an immune response. Importantly, APCs spread HIV to CD4 T cells as a consequence of their APC function. Therefore, MNPs present a prospective target for blocking HIV transmission at mucosal sites, and given their role in driving adaptive immunity, may also be a critical factor in the design of next generation mucosal vaccines.

Despite the higher risk and incidence of HIV transmission via receptive anal intercourse compared to vaginal intercourse (28,156), there are still gaps in our understanding of how HIV transmission occurs across the colorectal mucosa, as well as the specific MNPs HIV is likely to encounter. Furthermore, while DCs have been a focus for anogenital HIV transmission studies (7,18,155), macrophages being the weakest APCs of the MNP family have historically been overlooked as vehicles for HIV sexual transmission. However, recent studies have demonstrated that macrophages take up HIV and interact with $CD4^+$ T cells within tissue (9,116) highlighting them as a potential key player in the establishment of HIV infection. Though HIV interactions in intestinal tissue have been previously investigated (9,116,157), DCs and particularly macrophages have been examined either as a bulk population or subdivided based on skin or Type II mucosa definitions. Additionally, while macrophage subsets have been well defined in human jejunum (109) , macrophages in the colorectum have only been investigated by single-cell transcriptomics (158).

In this study, human colorectal MNPs were thoroughly investigated in non-inflamed tissue, with three subsets of macrophage: monocyte-derived macrophage (MDM); transitional-MDM (t-MDM); and tissue-resident macrophage (Macrophage), as well as three subsets of DC: conventional DC1 (cDC1); $CD207^+$ cDC2; $CD207^-$ cDC2. Macrophages were found to be significantly more abundant than the other MNPs and expressed the highest levels of the HIV

binding lectin receptors CD169 (Siglec-1) and CD209 (DC-SIGN), resulting in significantly more HIV uptake within 2 hours of exposure. Interestingly, while all MNPs were able to enhance the infection of CD4 T cells, DCs and t-MDM were more efficient in transferring HIV to CD4 T cells.

3.2 Methods and materials

3.2.1 Reagents

Table 3.1: Antibodies

Marker	Clone	Conjugation	Company	Volume / 2.5×10^6 cells in 50 µL (µL)
Axl	108724	BV605	BD Biosciences	1
CD1a	HI149	BV510	BD Biosciences	1
CD1c	F10/21A3	BV650	Biolegend	3
CD3	REA613	APC-Vio770	Miltenyi Biotec	2.5
	SK7	APC Cy-7	BD Biosciences	2.5
	UCHT1	BUV496	BD Biosciences	5
CD4	OKT4	BV570	Biolegend	5
	OKT4	BV650	Biolegend	2
	OKT4	BV786	Biolegend	2.5
CD11b	D12	BV711	BD Biosciences	1
	ICRF44	BV711	Biolegend	2
	ICRF44	BV421	Biolegend	2.5
CD11c	B-ly6	BB515	BD Biosciences	1.5
	B-ly6	BUV661	BD Biosciences	2
	B-ly6	PE-CF594	BD Biosciences	2.5
CD14	M5E2	BV421	BD Biosciences	2.5
	M5E2	BUV737	BD Biosciences	2.5
CD19	L719	APC-Vio770	Miltenyi Biotec	2.5
	SJ25C1	APC Cy-7	BD Biosciences	2.5
	HI819	BV750	Biolegend	1
CD45	HI30	PE-Cy7	BD Biosciences	1.5
	HI30	BV480	BD Biosciences	0.2
	Polyclonal	Dylight800	SICGEN (Portugal)	-
	QA17A19	CF770	Biotium (California, US)	-
CD69	FN50	BV480	BD Biosciences	0.2
CD103	Ber-ACT8	BUV563	BD Biosciences	5
	Ber-ACT8	BV711	BD Biosciences	2.5
	B-ly7	SB780	Invitogen (TF)	2.5

Marker	Clone	Conjugation	Company	Volume / 2.5 x 10^6 cells in 50 µL (µL)
CD123	6H6	PE-Cy5	Biolegend	0.5
CD141 (BDCA-3)	AD5-14H12	APC	Miltenyi	0.5
CD169 (Siglec-1)	7-239	PE-efluor610	Invitogen (TF)	2.5
CD172a (SIRPα)	SE5A5	Fire APC750	Biolegend	3
CD195 (CCR5)	REA245	PE	Miltenyi Biotec	2.5
CD206 (MR)	19.2	BUV805	BD Biosciences	0.5
CD207 (Langerin)	REA770	PE Vio770	Miltenyi Biotec	1.5
CD209 (DC-SIGN)	DCN46	BV421	BD Biosciences	2.5
	DCN46	PerCP Cy5.5	BD Biosciences	-
CD327 (Siglec-6)	REA852	Biotin	Miltenyi Biotec	2
HLA-DR	AC122	PerCP	Miltenyi Biotec	2
	L243	BUV395	Biolegend	1
p24	KC57-RD1	PE	Beckman Coulter	1
	28b7	APC	Medimabs (Canada)	1
Streptavidin	All species	BV510	Biolegend	1
XCR1	S15046E	BV421	Biolegend	4
	S15046E	APC	Biolegend	4

Table 3.2: Equipment

Equipment	Source
BD FACSymphony	BD Biosciences
BD Aria Cell Sorter	BD Biosciences
BD Influx Cell Sorter	BD Biosciences
Centrifuge 5418, 5424R, 5427R, 5810R	Eppendorf, Hamburg, Germany
EasySep Magnet	StemCell Technologies
QuadroMACS Separator	Miltenyi Biotec
Sorvall Legend XTR Centrifuge	Thermo Scientific, California, US
Spintron GT-20	Spintron, Victoria, Australia

Table 3.3: Software

Software	Source
BD FACSDiva	BD Biosciences
FlowJo v10.10.0	BD Biosciences
Graphpad Prism 10	Graphpad Software, California, US

3.2.2 Cell line maintenance

3.2.2.1 TZM-bls

TZM-bl cells (NIH AIDS Reagent Program) are an adherent reporter cell line derived from HeLa cells. They express large amounts of CD4 and CCR5, and express Tat-dependent Luciferase and β-galactosidase. This cell line is highly sensitive to infection by R5 strains of HIV-1. TZM-bl cells are cultured in Dulbecco's Modified Eagle Medium (DMEM, Lonza, Basel, Switzerland) supplemented with 10% Fetal calf serum (FCS, Sigma-Aldrich (Merck), St Louis, US) (DMEM10) at 37°C. They were passaged with a 1:10 dilution twice a week using TrypLE (Gibco) dissociation.

3.2.2.2 HEK293Ts

HEK293T (ATCC) cells are adenovirus-immortalized human embryonic kidney cells that are favourable for viral transfection, producing high titres. HEK293Ts were cultured in DMEM10 and were passaged with a 1:10 dilution three times a week using TrypLE dissociation.

3.2.3 Primary cells

3.2.3.1 Freezing of primary cells

All primary cells were resuspended in FCS supplemented with 10% Dimethyl sulfoxide (DMSO), aliquoted into 2 mL cryovials at $<10^6$ cells/ml, and frozen by placing in a CoolCell (Corning). Cells were stored at -80°C.

3.2.3.2 Isolation of peripheral blood mononuclear cells (PBMCs) from blood

Blood products were obtained in partnership with the Australian Red Cross Blood Service. PBMCs from leukoreduction system chambers (LRSC) were collected and processed on the same day as platelet donation.

LRSCs were drained into a 50 mL Falcon tube and flushed with Dulbecco's Phosphate Buffered Saline (DPBS) (Lonzo, Switzerland). Blood was diluted 1:5 with DPBS and separated into three 50 mL Falcon tubes in a volume of 35 mL. 15 ml Ficoll-Paque PLUS (GE Healthcare, Illinois, US) was underlayed and centrifuged at 1800 rpm for 20 mins without brakes. PBMCs from the blood:Ficoll interface were collected and washed twice with DPBS. Any remaining red blood cells were removed with an incubation in 5 ml of 1x Red Cell Lysis buffer (150 mM ammonium chloride (v/v), 10mM potassium bicarbonate (v/v), 0.1 mM EDTA (v/v) in ddH_20) at room temperature (RT) for 4 mins. Cells were either resuspended in DPBS for immediate use, or frozen as per **Section 3.2.3.1**.

3.2.3.3 Differentiation into monocyte derived dendritic cells (MDDCs) and monocyte derived macrophages (MDMs)

PBMCs underwent CD14 selection using a Human CD14 Microbead Enrichment Kit (Miltenyi Biotec, Cologne, Germany) as per the manufacturer's instruction, separated on LS columns (Miltenyi Biotec).

MDDCs: $CD14^+$ PBMCs were resuspended at 2 x 10^6/mL in RF10 supplemented with 500 U/mL of Interleukin-4 (IL-4, Peprotech, Israel) and 300 U/mL Granulocyte-Macrophage Colony-Stimulating Factor (GM-SCF, Miltenyi Biotec). Cells were seeded into T75 flasks and incubated on end at 37°C for 6 days with cytokines replenished at day 3. Cells were collected and washed in RF10 supplemented with IL-4 and GM-CSF immediate use, or frozen as per **Section 3.2.3.1.**

MDMs: $CD14^+$ PBMCs were resuspended in RPMI and plated at 1 x 10^6 cells in 0.5 mL/well in an uncoated 24-well plate. Plates were centrifuged at 700 rpm for 10 mins and incubated at 37°C for 1 hour. Media was replaced with RPMI supplemented with 10% filtered Human AB Serum (RH10, Sigma-Aldrich (Merck)) and incubated for 6 days. The wells were gently washed twice with DPBS, and 250 µL of Cell Dissociation Buffer (Gibco (Life Technologies), California, US) added to and incubated at 37°C for 30 mins. 1 mL of DPBS was added to each well and the cells were lifted with a small cell scraper. Cells were washed in RH10 for immediate use, or frozen as per **Section 3.2.3.1**.

3.2.3.4 Activation of CD4 T cells

PBMCs were cultured at 1 x 10^6 cells/mL in RF10 with Phytohaemagglutinin (PHA, Sigma-Aldrich (Merck)) (5 µg/mL) and Interleukin-2 (IL-2, Peprotech) (150 IU/mL) at 37°C for 3 days. Activated PBMCs underwent CD4 selection using a EasySep Human CD4+ T Cell Enrichment Kit (StemCell Technologies, Vancouver, Canada) as per the manufacturer's instruction, separated on LS columns. These activated $CD4^+$ T cells were frozen in aliquots as per **Section 3.2.3.1**.

3.2.4 Preparation of high-titre HIV virus stocks

3.2.4.1 Clinical HIV Strain Z3678M

The infectious molecular clone (IMC) for HIV-1 transmitted founder (TF) virus Z2678M was gifted by Prof. Eric Hunter, Emory University, Georgia USA (GenBank: KR820393). The IMC was sourced from an acutely infected individual in Zambia following a heterosexual transmission event. The cloning vector is a Bluescript backbone with the 9,055 base pair insert cloned using ligation-

independent cloning. The plasmid contains ampicillin resistance and was propagated in *Escherichia coli* (*E. coli*), strain Stbl2, before being transfected into HEK293T cells using calcium phosphate transfection. This particular Clade C stain was selected as it was shown to infect both T cells and monocyte-derived dendritic cells (MDDC) (159), and had been shown to be taken up by and infect tissue macrophages (12).

3.2.4.2 Transfection and expansion of HIV plasmid

Glycerol stocks of HIV_{Z3678M}-transfected *E.coli* (Plasmid - $HIV_{3678MTF}$: Eric Hunter, Genbank ascension number: KR820393) were grown overnight at 37°C on Luria-Bertani (LB) Agar (Invitrogen, California, US) supplemented with 100 µg/ml ampicillin (Sigma-Aldrich (Merck)). Single colonies were inoculated into LB Broth (Gibco (Life Technologies)) supplemented with 100 µg/ml ampicillin and incubated at 37°C for 8 hours at 250 rpm before expansion to 250 ml at 37°C overnight at 250 rpm. The bacteria were pelleted at 6000 x g for 20 mins at 4°C. The plasmid was isolated and purified using Nucleobond Xtra Maxi Plasmid Purification Kit (Macherey-Nagel, Düren, Germany) as per the manufacturer's instruction.

3.2.4.3 Transfection of HEK293T cells

HEK293Ts were seeded at 8 x 10^6 per T150 flask in 20 mL DMEM10 and incubated at 37°C for 24 hours. Cells were transfected with 80 µg of plasmid DNA, 1 ml of 10% TE (1 mM Tris, 0.1 mL EDTA, pH 8.0), 128 µL of 2 M $CaCl_2$, 1 ml of 2x HEPES-buffered saline (280 mM NaCl, 50 mM HEPES, pH 7.1) in 13 mL DMEM10. Cells were incubated at 37°C, with 13 mL media replaced at 18 hours, and further incubated for 24 hours. Virus containing media (VCM) was collected at day 2, 3, 4 and 5. VCM was concentrated using Vivaspin 20 Filters, 300,000 MW (Sartorius, Göttingen, Germany) before ultracentrifugation (28,000 x g for 2 hours). The supernatants were aspirated, and the pelleted virus resuspended in 300 µL of DPBS and stored at -80°C in aliquots. Virus was titred on TZM-bls in RF10 and incubated at 37°C for 3 days. Media was removed and 50 µL of X-gal staining solution (1% X-gal (v/v), 1% potassium ferricyanide (w/v), 1% potassium hexacyanoferrate trihydrate (w/v) in PBS) added and incubated at 37°C for 1 hour. Cells were fixed in 4% PFA at room temperature (RT) for 20 mins. Infected cells were imaged using the EliSPOT Reader Classic (AID Autoimmun Diagnostika GmbH, Straßerg, Germany). TCID50/mL was determined using the Spearman & Kärber algorithm.

3.2.4.4 Testing Infectivity of Virus

Virus was added to MDDCs in a titration of MOI 1-10 and cultured in 150 µL of RPMI supplemented with IL-4 and GM-CSF (both at 0.5 µL/mL) at 37°C for 2 hours. MDDCs were washed thrice before being resuspended and cultured at 37°C for 4 days. Cells were washed in DPBS and stained with viability stain FVS700 (BD) at 4°C for 20 mins. The cells were washed in FACS wash (1% FCS (v/v), 2 mM EDTA, 0.1% sodium azide (w/v) in PBS) before being permeabilised with 100 µL of Cytofix/Cytoperm (BD Biosciences, New Jersey, US) at RT for 20 mins. Cells were washed in PERM Wash (1% FCS (v/v), 1% BSA (w/v), 0.1% saponin (w/v), 0.1% sodium azide (w/v) in PBS) and intracellularly stained with dual antibodies for HIV p24 protein p24-PE (KC57, Beckman Coulter) and p24-APC (28b7, Medimabs, Canada) at RT for 30 mins. Cells were washed twice with PERM Wash prior to acquisition on the FACSymphony A5 flow cytometer using single colour compensations.

3.2.5 Identification of human colorectal mononuclear phagocyte subsets

3.2.5.1 Human colorectal tissue

This study was approved by the Western Sydney Local Area Health District (WSLHD) Human Research Ethics Committee (HREC); reference number (4192) AU RED HREC/15 WMEAD/11. Human colorectal tissue was sourced via collaboration with colorectal surgeons at the Westmead Hospital and private hospital in the greater Sydney area. Non-inflamed (by surgical staff visual assessment) portions of pathology samples were collected no later than 30 mins after surgical removal from the patient (**Table 3.4**). Samples were de-identified. Tissue samples that were allocated to HIV assays were covered in RPMI supplemented with 1% gentamycin and stored overnight at 4°C for early morning processing.

3.2.5.2 Enzymatic digestion of human colorectal tissue

Cells were isolated as per **Chapter 2**. In brief, the muscle propria was first mechanically separated from the submucosa using surgical scissors before the tissue was cut into approximately 5x5 mm^2 pieces. The epithelium and surface mucus were removed by two incubations of 20 mL of RPMI supplemented with 10% FBS (v/v), 0.3% DTT (w/v) and 2 mM EDTA at 37°C for 15 mins. The tissue was washed in DPSB and twice digested in 20 ml RPMI supplemented with 0.3% Collagenase Type 4 (w/v) and 0.5% DNase (v/v) at 37°C for 30 mins. The cell solution was filtered through a 100 µm cell strainer and washed twice with DPBS.

Table 3.4: List of Human Tissue Samples

Tissue No.	Hospital	Surgery	Sample Type	Sex	Age
152	Westmead Public	Anterior resection	Colon	Female	64
154	Blacktown Public	Endoscopy	Duodenum (biopsies)	Male	69
155	Blacktown Public	Endoscopy	Duodenum & ileum (biopsies)	Female	50
156	Blacktown Public	Endoscopy	Duodenum & ileum (biopsies)	Female	47
158	Westmead Public	Anterior Resection	Colon	Male	77
193	Westmead Public	Anterior Resection	Colon	Female	80
198	Westmead Public	Anterior Resection	Colon	Male	68
199	Norwest Private	Anterior Resection	Colon	Male	63
215	Westmead Public	Anterior Resection	Colon	Female	68
221	Westmead Public	Anterior Resection	Ileum	Female	74
232	Westmead Public	Anterior Resection	Colon	Male	63
233	Westmead Public	Anterior Resection	Colon	Male	49
234	Westmead Public	Anterior Resection	Colon	Male	59
237	Westmead Public	Anterior Resection	Colon	Female	42
238	Westmead Public	Anterior Resection	Colon	Male	68
247	Westmead Public	Anterior Resection	Colon	Female	73
255	Westmead Private	Anterior Resection	Colon	Female	50
272	Westmead Public	Anterior Resection	Colon	Female	76
281	Westmead Public	Anterior Resection	Rectum	Female	81
285	Westmead Public	Anterior Resection	Colon	Male	43
286	Lakeview Private	Anterior Resection	Rectum	Female	72
287	Westmead Private	Anterior Resection	Rectum	Female	23
288	Westmead Public	Anterior Resection	Colon	Male	79
294	Westmead Public	Anterior Resection	Colon	Male	60
298	Westmead Public	Anterior Resection	Colon	Male	51
304	Westmead Public	Anterior Resection	Rectum	Female	74

3.2.5.3 Selection of target cells

Cells were resuspended in 35 ml RPMI, underlaid with 15 ml Ficoll-Paque and centrifuged at 4°C at 1800 rpm for 20 mins without brakes. Cells from the RPMI:Ficoll interface were collected and washed twice with DPBS at 1800 rpm. Remnant red blood cells were removed in 5 ml of 1x Red Cell Lysis buffer in sterile H_2O at RT for 4 mins.

When required, cells were counted and selected using the EasySep Human CD45 Cell Enrichment Kit (Miltenyi), as per the manufacturer's instruction using LS columns and the QuadroMACS Separator (Miltenyi).

3.2.5.4 Staining preparation for flow cytometry

Cells were resuspended in 100 µL DPBS per 2.5 x 10^6 cells and stained with fixable viability stain FVS700 at 4°C for 30 mins. Cells were washed, resuspended in 50 µL of FACS wash, and stained with an optimised panel for BD FACSymphony (**Table 3.5**) in 10 µL Brilliant Stain Buffer (BD) at 4°C for 30 mins. The cells were washed twice with FACS wash and fixed with Cytofix (BD) at 4°C for 15 mins. Cells were washed again in FACS wash prior to acquisition on a flow cytometer. Cells were filtered through a 100 µm cell strainer prior to acquisition. Flow cytometry was performed on BD Symphony with BD Diva Software (V8.0). All data was acquired on application settings to mitigate fluorescence intensity fluctuations between donors.

Flow cytometry compensation controls were stained on beads using 1 µL of antibody per 1 drop of beads unless optimised to a different concentration (**Table 3.5**). Beads were vortexed prior to use, washed in FACS Wash prior to staining at RT for 15 mins, and washed twice with FACS wash before acquisition. An unstained human tissue cell control was acquired for autofluorescence compensation.

3.2.6 Analysis of human CD14+ cells using single cell RNA sequencing analysis from colorectal tissue

A publicly available single-cell RNA sequencing (ScRNA) data was download from authors Domanska et al. (2023) (https://pubmed.ncbi.nlm.nih.gov/35139155/). It was accessible by EGAD00001007765. Data was aligned by Brian Gloss. This dataset contained scRNA data from four human colon donors who underwent a resection procedure for colorectal cancer. Cells underwent CD14 selection prior to sequencing. Methods for processing of explants and the generation of the data is described here (Domanska et al. 2022). The method used for single-cell dissociation only differed from the methods presented in this thesis in the digestive enzyme used: Liberase TL (Roche). This enzyme was tested and resulted in comparable yield and viability as for collagenase Type 4 (data not shown).

A typical Seurat v5 pipline (R package) (160) was utilised for data processing, with analysis in the R programming language (v4.4.2) and RStudio (v2023.06.1+524). Scripts used for pre-processing (performed by Thomas O'Neil) and data analysis are available on GitHubhttps://github.com/CVR-MucosalImmunology/StudentScripts/tree/main/EricaVine.

All heatmaps, UMAP visualizations, and dot plots were produced using Seurat functions in conjunction with the ggplot2 (R package).

Table 3.5: BD FACSymphony – Phenotype and HIV Uptake Panel

Marker	Conjugation	Optimal volume ($2.5x10^6$ cells / 50µl) (µL)	Compensation beads	Optimal volume on beads (µl / 50µl)
Viability	FVS700	0.05/200ul	Arc Reactive	1
CD19	BV750	1	CompBead Plus	1
CD3	BUV496	5	CompBead Plus	1
CD4	BV570	10	CompBead	1
CD69	BV480	0.2	CompBead Plus	1
HLA-DR	BUV395	1	CompBead Plus	1
CD14	BUV737	2.5	CompBead Plus	1
CD11c	BB515	2	CompBead Plus	1
SIRPα	Fire APC750	3	CompBead Plus	1
CD1c	BV650	3	CompBead	1
CD123	PE-Cy5	0.5	CompBead Plus	1
Axl	BV605	1	CompBead	1
Siglec-6	Biotin	2	-	-
Streptavidin	BV510	0.1	CompBead	1*
MR	BUV805	0.5	CompBead Plus	1
Siglec-1	PEefluor610	2.5	CompBead	1.5
Langerin	PE Vio770	1.5	CompBead Plus	1.5
Drop-ins				
p24	APC	1	CompBead	0.5**
XCR1	APC	4		
p24	PE	1	Anti-REA Bead	1
CCR5	PE	2.5		
CD11b	BV711	2	CompBead	1
DC-SIGN	BV421	2.5	CompBead	1
CD4	BV786	2.5	CompBead	1

We generated pseudotime developmental trajectories using the Monocle3 (R package) (161), scaling the pseudotime values between 0 and 1, and mapping them onto UMAP visualizations in conjunction with ggplot2 (R package). Differentially expressed genes (DEGs) along this trajectory were identified with Moran's I test.

3.2.7 Assessment of HIV binding and entry by intracellular HIV p24 protein staining from colorectal tissue

3.2.7.1 Isolation of CD4 T cells, DCs and macrophage subtypes

CD45 positive selected cells were resuspended in 100 µl DPBS per 2.5 x 10^6 cells and stained with FVS700 at 4°C for 30 mins. Cells were washed in MACS Wash or other wash depending on cell selection method before being resuspended in 50 µl MACS Wash and 10 µl Brilliant Stain Buffer per 2.5 x 10^6 cells. Cells were antibody stained with FACS panel (**Table 3.6**) at 4°C for 30 mins and washed in MACS wash and again in Pre-Sort Buffer (BD). Cells were resuspended in 1 mL of Pre-Sort Buffer and filtered through a 100 µm cell strainer prior to sorting on the BDAriaIII or BDInflux Cell Sorter in the Westmead Research Hub Flow Core Facility. All compensation controls were stained on CompBead PLUS (BD) using 1 µL of antibody per 1 drop of bead, except FVS700 which was 1 µL of antibody on 1 drop ArcReactive beads.

CD4 T cells were defined as live $CD3^+$ $CD4^+$. Bulk DCs were defined as live HLA-DR^+ $CD3^-$ $CD19^-$ $CD14^-$ $CD11c^+$. Macrophages were defined as live, HLA-DR^+ $CD3^-$ $CD19^-$ $CD14^+$ and separated for sorting into MDM ($CD11c^+$ HLA-DR^{low}), t-MDM ($CD11c^+$ HLA-DR^+) and Macrophages ($CD11c^-$). Cells were collected in 500 µl of DC Media and kept on ice until used.

Table 3.6: Optimised flow cytometry panel for FACS

Marker	Purpose	Conjugation	Optimal volume in gut ($2.5x10^6$ cells / 50µl) (µL)
Viability	Live cells	FVS700	0.05/200 µl
CD19	B Lymphocytes	APC Vio770	2.5
CD3	T Lymphocytes	APC Vio770	2.5
CD4	CD4 T cells	BV650	2
HLA-DR	Myeloid cells	PerCP	1
CD14	Macrophages	BV421	2.5
CD11c	MNPs	PE CF594	1.5

3.2.7.2 Mononuclear phagocyte to CD4 T cell transfer assay

FACSorted cells were resuspended in 150 µL of RPMI-1640 supplemented with 1 µM HEPES (Gibco, Massachusetts, USA), non-essential amino acids (Gibco), 1 mM sodium pyruvate (Gibco) 5 0 µM 2-mercaptoethanol (Gibco), 10 µg/mL gentamycin (Gibco) and 10% (v/v) FBS (herein referred to as DC culture media) and exposed to the HIV_{Z3678M} (MOI=1) and incubated at 37°C for

2 hours. Cells were thrice washed with DC Culture Media, with the third wash supplemented with 0.02% Normocin (v/v). Activated CD4 T cells were added in a ratio of 2:1 and co-cultured in 200 µL at 37°C for 2 hours. Activated CD4 T cells were cultured alone as a mock treated control. Activated CD4 T cells were infected with HIV (MOI=1) as an infection control. Infection of the CD4 T cells was determined by intracellular p24 expression by flow cytometry as described in **Section 3.2.4.4**.

3.2.7.3 HIV uptake assay

Cells liberated from tissues underwent selection by Ficoll-Paque density gradient and CD45 positive magnetic selection on LS columns (Miltenyi). 5 x 10^5 cells were resuspended in 150 µL of DC Culture Media and exposed to HIV_{Z3678M} (MOI=5) and incubated at 37°C for 2 hours. Cells were washed thrice in DPBS and stained with the FACSymphony Uptake panel (**Table 3.5**), before intracellular p24 staining as described in **Section 3.2.4.4**.

3.2.7.4 HIV blocking assay

Prior to HIV uptake assay, cells were incubated with either 20 µg/mL Anti-CD169 (Siglec-1) monoclonal antibody (Mab, Invitrogen, clone-Hsn7D2), or dual Anti-DC-SIGN Mab (CD209, R&D Systems, clone-120612 and AIDS Research and Reference Reagent Program, NIH, clone-DC28) at 10 µg/mL (162) each in DC Culture Media. Cells were incubated at 37°C for 30 mins prior to HIV inoculation, then followed the protocol for HIV uptake Assay (**Section 3.2.7.3**).

3.2.8 Statistics

Graphs and statistical analysis were produced with GraphPad Prism 10. To account for donor variability, when normalised distribution could not be assumed, statistics were calculated using un-paired, non-parametric Mann–Whitney t tests, or Wilcoxon tests for paired data. Grouped data was calculated by the One-way analysis of variance (ANOVA), utilising Tukey's Multiple Comparisons, or Dunnett's Multiple Comparisons if comparing to a control. Results were considered statistically significant when $p \leq 0.05$.

3.3 Results

This project is focused on the isolation and classification of MNP subsets from human colon and rectal (colorectal) tissues and investigating their early infection interactions with HIV, predominantly macrophages, with a clinically relevant transmitted/founder HIV strain. Multiple flow cytometry panels were utilised to achieve the aims of this project, supported by a publicly available RNAseq dataset on $CD14^+$ cells extracted from human colon.

3.3.1 Phenotyping mononuclear phagocyte subsets in human colorectal tissue

Human colorectal MNPs isolated from human tissue were examined for their surface receptor expression for phenotypic characterisation. RNAseq analysis from CD14+ colorectal cells assisted in confirming these phenotypes and suggested differing functions of the macrophage subsets.

3.3.1.1 Determining the optimal lot of collagenase Type 4 for colorectal tissue digestion

The most notable complication of the isolation of immune cells from tissue by enzymatic digestion is the cleavage of cell surface proteins, importantly, surface markers used to identify them. Generally speaking, enzymes that produce higher yields of liberated cells (e.g. trypsin) cleave more surface markers than those that produce lower yields (e.g. collagenase). Different enzyme blends differ as to which markers they cleave, and their efficiency at digesting specific tissues. As such, the enzyme blend and lot used to digest intestinal tissue needed to be carefully selected to ensure good yields and viability, whilst leaving immune cell definition markers intact. Collagenase Type 4 (Worthington Industries) is specifically designed to have a high collagenase and low tryptic activity, which limits damage to cell membrane receptors, and has been shown to be the most reliable digestion enzyme to perform flow cytometry on tissue-liberated cells, both providing good viability and sufficient yields (7,8,163). Even so, with manufacturing variations, similar lots of enzyme blends can result in different levels of cleavage of key markers, specifically HIV binding receptors CCR5 and CD209 (DC-SIGN) which are prone to cleavage (8). To ensure consistent data collection, one lot of collagenase Type 4 was used for all phenotyping and HIV assays.

Four test lots of collagenase Type 4 were received from the manufacturer and used to digest equal portions of a single colorectal sample. The extracted cells were stained with an optimised

panel for BD FACSymphony A5 flow cytometer. There were noticeable differences between the lots in yield, viability, proportion of CD45$^+$ HLA-DR$^+$ cells, and expression of HIV binding receptors (**Figure 3.1**). Two lots (X8669, X8714) were excluded due to poor yields and viability, which would prevent samples from being suitable for FACS and effect the *ex vivo* MNPs performance in functional assays. While lot X8668 provided the best viability and yield, it partially cleaved CCR5 in additional to the almost complete cleavage of CD209. With CCR5 critical for HIV entry and CD209 important for endocytic HIV uptake, this lot was also excluded. Fortunately, lot X9043 gave rise to an acceptable yield and viability, while showing minimal cleavage of key markers. As such, large quantities of X9043 were purchased and used for all further experiments in this chapter.

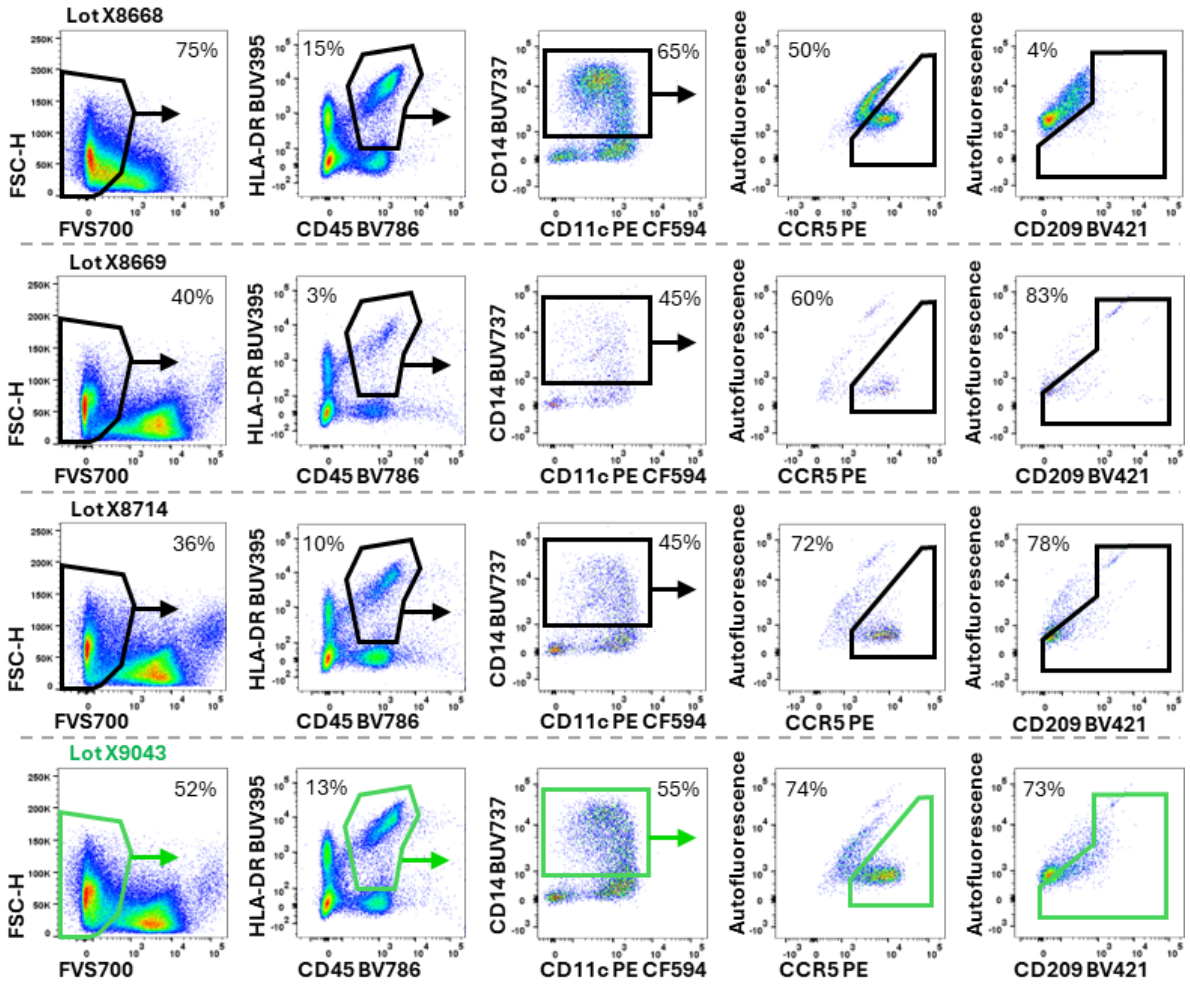

Figure 3.1: Lot testing for collagenase type 4. Cells were isolated from colorectal tissue using the techniques described in Section 3.2.5.2. A single colorectal sample was digested using four lots of collagenase type 4 (Worthington). Column 1 indicates cell viability based on Fixable Viability Stain (FVS700), while column 2 illustrates the proportion of HLA-DR$^+$ CD45$^+$ cells. Column 3 shows the frequency of CD14$^+$ cells. Columns 4 and 5 depict the expression of CCR5 and CD209 within the CD14$^+$ population. Dot plot density represents digestion yields, with numbers indicating the percentage of each gate relative to the parent population. Selection prioritised both yield and the expression of CCR5 and CD209, with green coloured gates indicating the chosen lot.

3.3.1.2 Definition of colorectal mononuclear phagocyte subsets by flow cytometry

To define the MNP subsets present in human colorectal tissue, mononuclear cells were isolated from fresh non-inflamed tissues, as described in **Chapter 2** in this thesis (163) (**Figure 3.2**). A 24-parameter FACSymphony panel (**Table 3.5**) was used to define the colorectal MNPs using the progressive flow cytometry gating strategy outlined in **Figure 3.3**. Three macrophage subsets were identified, closely corresponding to subsets defined in the human jejunum (109): a newly infiltrated monocyte-derived macrophage defined as $CD14^+$ $CD11c^+$ $HLA\text{-}DR^{low}$ (MDM), a monocyte-derived macrophage transitioning into a tissue-resident macrophage phenotype defined as $CD14^+$ $CD11c^+$ $HLA\text{-}DR^+$ (transitional-MDM, t-MDM), and a tissue-resident macrophage defined as $CD14^+$ $CD11c^-$ (Macrophage). Additionally, cDC subsets were identified: $XCR1^+$ $CD1c^-$ cDC1, and $CD11c^+$ $CD1c^+$ cDC2, further divided by CD207 expression. The newly defined $CD163^+$ $CD1c^+$ DC3 were not detected in these non-inflamed tissues.

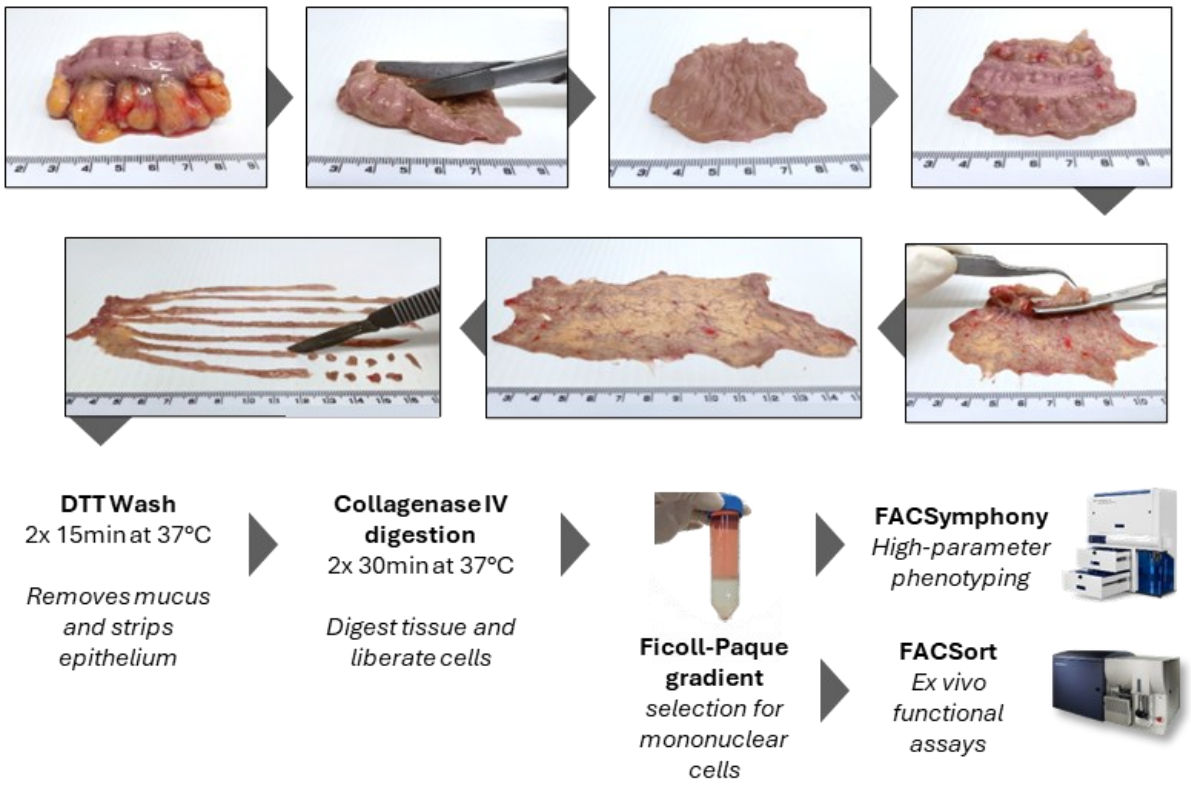

Figure 3.2: Protocol for extraction of mononuclear cells from human colorectal tissue. Representative pictorial breakdown of tissue from all gut donors is shown. Samples were collected within 30 mins post-surgery and underwent the following procedures: visual inspection, removal of fat and mesentery, tube opened, mucosal surface cleaned, tissue flipped to expose and remove muscle layer. Subsequently, the mucosa was cut into 5x5 mm^2 pieces for collagenase digestion, followed by Ficoll-Paque enrichment in preparation for antibody staining.

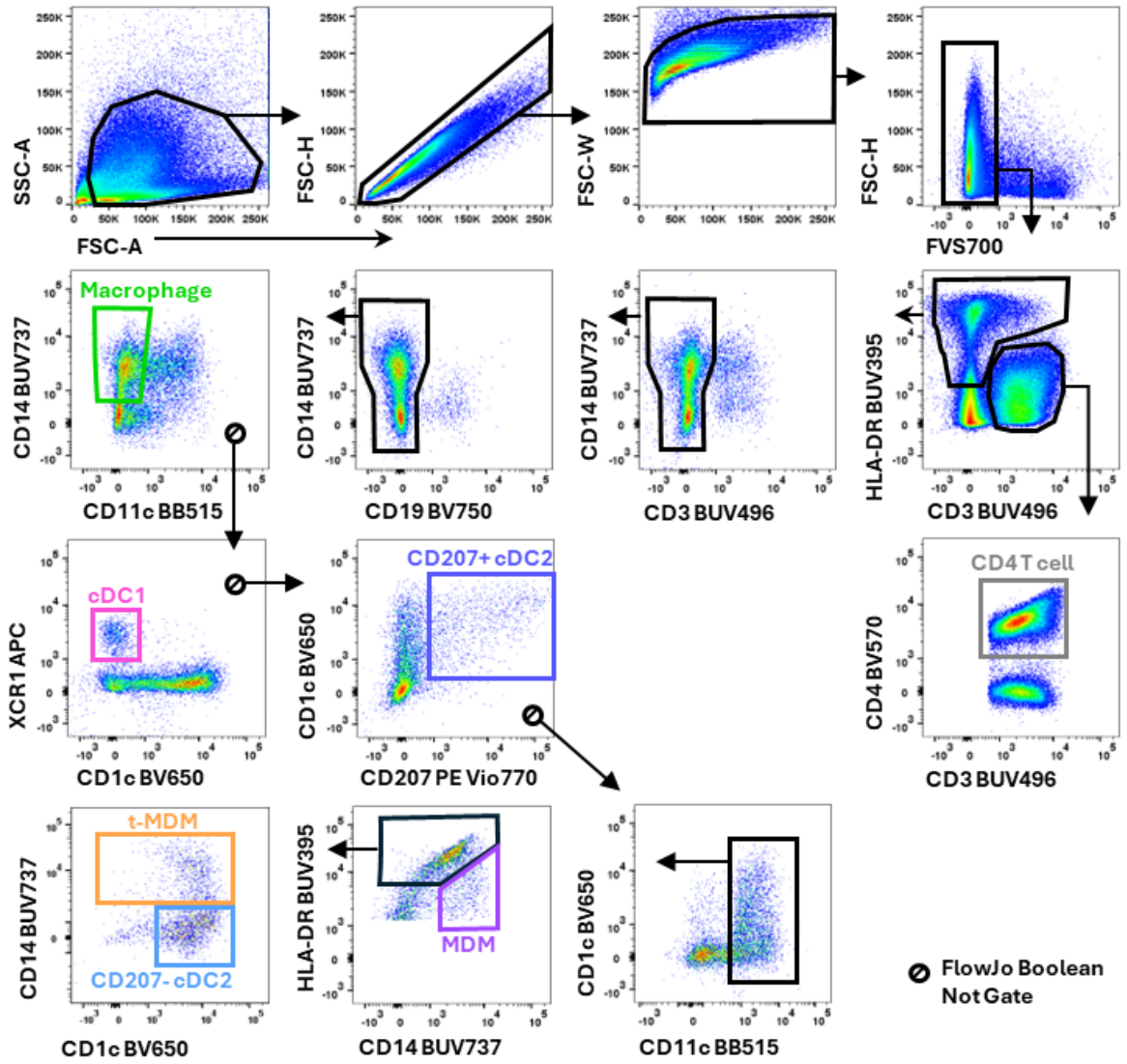

Figure 3.3: FACSymphony gating strategy to define human colorectal mononuclear phagocytes. Cells were isolated from colorectal tissue using the techniques described in Section 3.2.5.2. Cell size, singlet, and viability gates were established using forward scatter (FSC), side scatter (SSC), and FVS700. CD4 T cells were identified as $CD3^+$ $CD4^+$. MNPs were gated as HLA-DR^+ $CD3^-$ $CD19^-$ and subsequently separated into macrophage and DC subsets. Initially, three populations were defined using a series of Boolean Not Gates: Macrophages ($CD14^+$, $CD11c^-$), conventional DC1 (cDC1; $XCR1^+$ $CD1c^-$), and $CD207^+$ cDC2 ($CD1c^+$ $CD207^+$). CD11c+ cells were gated from the remaining population and further stratified by HLA-DR, with MDM classified as HLA-DR^{low}. Cells were then divided based on CD14 and CD1c into tissue-resident transitional-MDM (t-MDM; $CD14^+$) and $CD207^-$ cDC2 ($CD14^-$ $CD1c^+$). Gating strategy is a composite of multiple donors to demonstrate all MNP populations.

The relative proportions of each MNP subset were calculated as a percentage of $CD45^+$ HLA-DR^+ cells. We observed Macrophages (mean 31.6% ±52.0) to be the most abundant MNP (**Figure 3.4A**). t-MDMs and bulk DCs showed comparable proportions (mean 7.9% ±14.8 and 8.6% ±11.5 respectively) both significantly more abundant than MDMs (mean 1.5% ±4.2). As these macrophage subsets proportions were similar to those in the human jejunum (109), samples

from the duodenum, ileum and rectum were processed to determine if the macrophage dominance over DCs was present throughout the entire gastro-intestinal tract. All three additional gut compartments demonstrated similar proportional trends, though with limited donor numbers, statistical significance was not achieved. When comparing the average proportion of the MNP subsets as a total of the MNPs, the proportion of total macrophages to DCs can be seen to favour macrophages more as the gut compartment becomes more distal (**Figure 3.4B**).

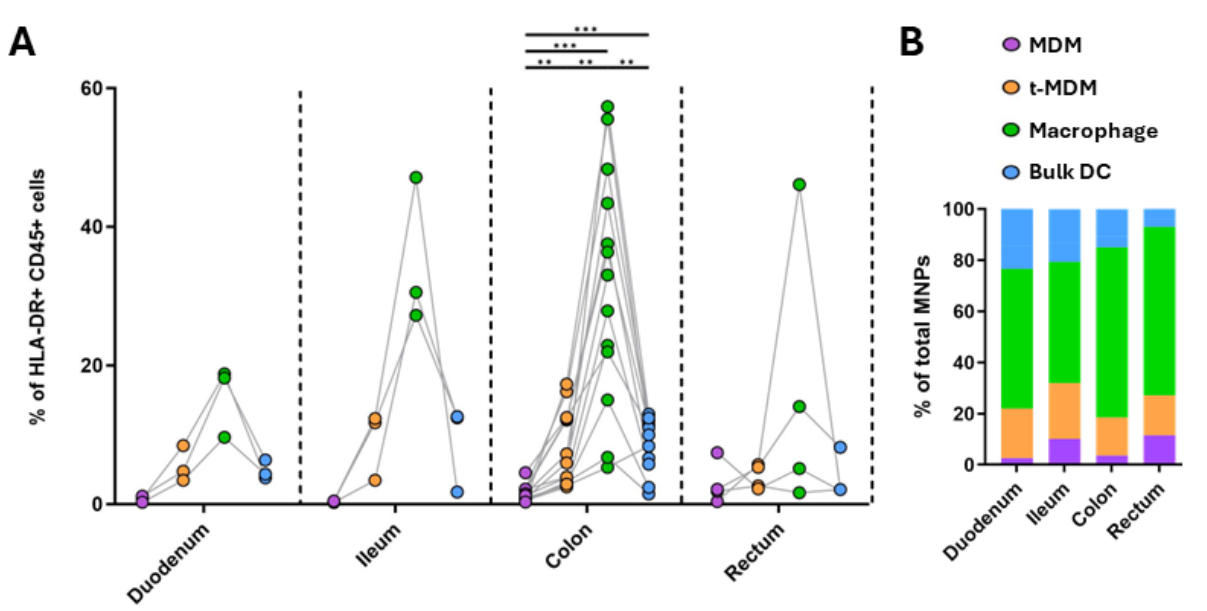

Figure 3.4: Proportion of human gut mononuclear phagocytes. Cells were extracted from tissue as outlined in Section 3.2.5.2 and subsequently surface-stained for flow cytometry. **A** The data represents the proportion of MNP subsets relative to HLA-DR$^+$ CD45$^+$ cells from the following sites: duodenum (n=3), ileum (n=4), colon (n=13), and rectum (n=4). Grey lines represent each distinct donor. Statistical analysis was performed for colon only using repeated measures ANOVA mixed-effects analysis with the Geisser-Greenhouse correction, and Tukey's multiple comparisons (***p = 0.001, **p = 0.01). **B** Proportions of total MNPs from data presented in A.

3.3.1.3 Colorectal mononuclear phagocytes express unique HIV-binding receptor profiles

Following definition of the colorectal MNPs, data from the FACSymphony panel was analysed to determine the expression of HIV-associated MNP receptors. CD4 and CCR5 are the main HIV entry receptor and co-receptor, and lectin receptors CD169 (Siglec-1), CD206 (Mannose Receptor), CD207 (Langerin) and CD209 (DC-SIGN) are known to bind HIV. Therefore, these receptors were included in the design of the FACSymphony flow cytometry panel to inform the likelihood of the MNP subsets to become infected by, or take up, HIV.

MNP subsets were defined as above, and the geometric means of fluorescence intensity (gMFI) expression for all HIV-binding receptors were calculated. As CD4 T cells are the primary HIV target cells for viral replication, their expression of HIV entry receptors was included as a reference. All colorectal MNP subsets expressed CD4, though CD4 T cells expressed significantly higher CD4 than any of the MNPs (**Figure 3.5A**). CD4 expression was comparable between all MNPs, however t-MDMs had significantly higher expression than $CD207^-$ cDC2, and both t-MDM and $CD207^-$ cDC2 had significantly higher expression than MDM. CCR5 was expressed significantly higher on CD4 T cells and both subsets of cDC2. t-MDM had significantly higher CCR5 than MDM, Macrophages and cDC1, with Macrophage CCR5 expression only significantly higher than cDC1. CCR5 was significantly lower on MDMs and cDC1, with most donors for cDC1s falling below the limit of detection for the panel, as described previously (8,9). Altogether, this suggests that cDC2 and t-MDM are susceptible to CD4/CCR5 mediated HIV infection, as well as macrophages though to a lesser extent. cDC1 and MDMs appear to be unlikely to be susceptible to HIV infection due to their lack of/relatively low CCR5 expression.

MNP HIV-binding lectin receptors were more discriminatory than the HIV-entry receptors CD4 and CC55. CD169 was only expressed on t-MDM and macrophages, most highly by Macrophages (**Figure 3.5B**). CD206 was highly expressed on t-MDM, macrophages and both cDC2 subsets, though it was significantly higher on the $CD207^+$ subset. CD206 (Mannose Receptor) was not expressed on MDM or cDC1. CD207 (langerin) was only expressed by $CD207^+$ cDC2s. Similar to CD169 (Siglec-1), CD209 (DC-SIGN) was highly expressed on t-MDM and Macrophages, with expression on Macrophages significantly higher. However, unlike CD169, there was low expression of CD209 on $CD207^+$ cDC2, though significantly lower than t-MDM.

3.3.1.4 Distinct colorectal macrophage subsets confirmed by single-cell RNAseq

To independently verify the distinct phenotypic profiles of the macrophage subsets determined by flow cytometry, a publicly available single-cell RNAseq data set (Domanska et al. 2022) derived from CD14+ human colon cells was sourced and analysed. In this study, while clusters were identified by unbiased algorithms and extensively investigated, no attempt was made to fit these macrophage clusters into any known classification structure. Using unbiased algorithms, alongside comparisons to protein expression observed in the above flow cytometry data, allowed for a more objective exploration of colorectal macrophage subsets.

In the original study, Domanska et al. confirmed that macrophages in the gut were able to be subdivided into two general subsets that their group had previously observed in human small

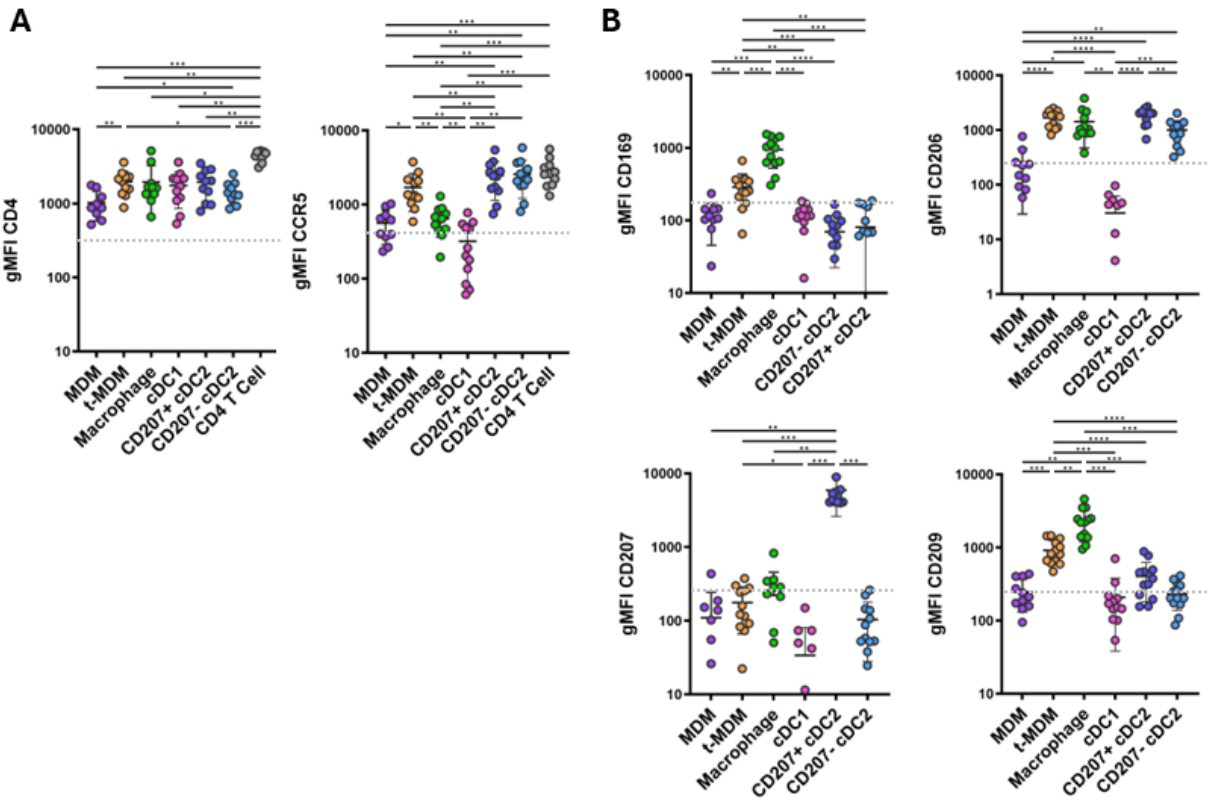

Figure 3.5: Expression of HIV- binding receptors on colorectal mononuclear phagocytes. Cells were isolated from colorectal tissue using the techniques detailed in Section 3.2.5.2 and subsequently enriched following the optimised protocol outlined in Section 3.2.5.3 before staining for acquisition on the FACSymphony. The geometric mean of fluorescence intensity (gMFI) values for each MNP subset were obtained using FlowJo V10.10.0 for **A** HIV entry receptors CD4 and CCR5, and **B** HIV-binding uptake receptors CD169, CD206, CD207 and CD209. Statistical analysis was performed using the One-way analysis of variance (ANOVA) with Tukey's multiple comparisons (****p = <0.0001, ***p = <0.001, **p = <0.01, *p = <0.05).

intestine: a monocyte-like macrophage defined by high levels of calprotectin (S100A8/9), and a tissue-resident macrophage expressing complement component 1 chains (C1QA, CIQB and C1QC). Using cluster analysis, they identified 13 clusters based on differentially expressed genes (DEGs) and explored each cluster individually. However, to use this data to confirm the subsets observed by surface protein expression, similarities in phenotypic profiles became the primary focus.

Identification of distinct macrophage clusters

Initially, a Uniform Manifold Approximation and Projection (UMAP) plot was constructed for the pre-processed data, and Seurat used to identify 16 clusters (**Figure 3.6A**). On first appearance, two clusters stood out spatially: **cluster 9** was spilt across opposite sides of the UMAP, and

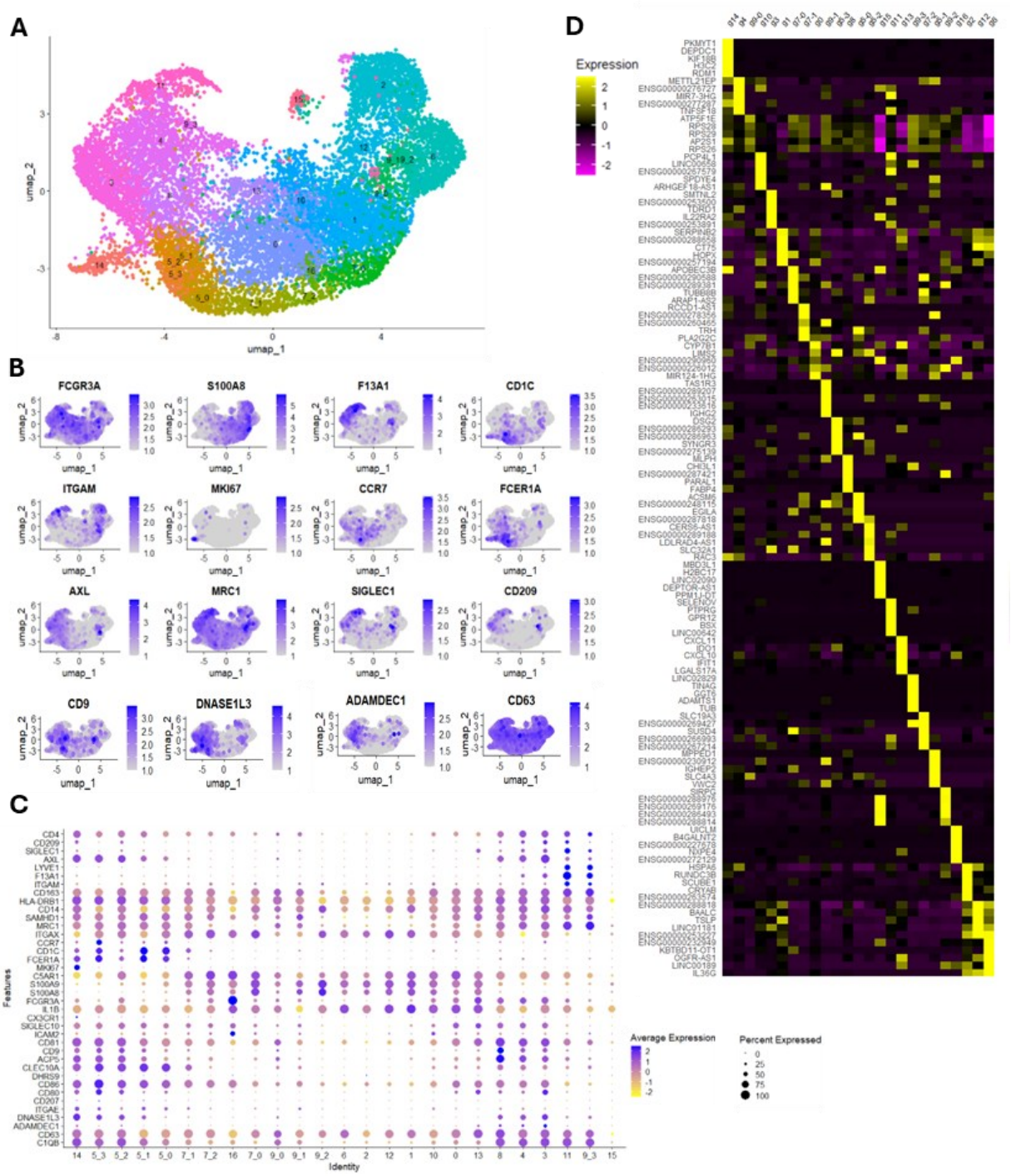

Figure 3.6: Identification of colonic MNP subsets via cluster analysis. Data was obtained from Domanska et al. (2022) and processed as described in Section 3.2.6. **A** Dimension reduction was performed to generate a uniform manifold approximation and projection (UMAP). 16 clusters were identified. **B** UMAP visualisation of selected genes. Expression levels are visualised from low (grey) to high (purple) expression. **C** DotPlot of expression selected genes. Expression levels are visualised from low (yellow) to high (blue) expression, with percentage of cluster expressing gene visualised by size of dot. **D** Top5 genes differentially expressed genes (DEG) were visualised in heatmap for all clusters.

cluster 7 traversed the length of four other clusters. These two clusters were sub-clustered before detailed analysis.

The spatial location and expression intensity of certain genes were overlayed on the UMAP to provide an initial understanding of what type of CD14+ cells each segment of the UMAP might contain (**Figure 3.6B**). Some genes, namely *FCGR3A*, *MRC1* and *CD63*, were expressed throughout all clusters and while they would not be useful for cluster identification, they did confirm that the majority of cells in the data were of monocyte or macrophage lineage. *S100A8* and *ITGAM* (CD11b) were visualised to confirm the locations of monocyte-like macrophages, and *F13A1*, *AXL*, *SIGLEC1*, *CD209*, and embryonic development associated genes *DNASE1L3* and *ADAMDEC1* (O'Shea et al. 2016; Schepper et al. 2018; Shaw et al. 2018) used to locate tissue-resident macrophages. *CD1C* and *FCER1A* were used next to explore the presence of CD14+ DC, followed by *CCR7* for lymph-tissue migration, *CD9* for activation, and *MKI67* for proliferation. From these visual observations, suspected monocyte-like and macrophage-like cells, as well as DC-like cells could be seen in discrete locations on the UMAP, and the clusters were re-ordered to group similar clusters for more detailed investigation.

To utilise existing knowledge of colorectal macrophage subsets, a dot plot was created for all clusters showing the gene expression of all receptors that were present in the FACSymphony panel as well as a selection of DEGs reported by Domanska et al. (**Figure 3.6C**). **Cluster 5** was observed to have high *CD1C* and *FCER1A* expression, suggesting that the cells were DCs. As this dataset was produced from CD14 selected cells, Domanska et al. posited that these cells were DC3s. However, as these cells have yet to be definitively shown to reside in non-inflamed gut tissue and given the low expression of CD14, these cells could also include cDC2, therefore cluster 5 was sub-clustered for more detailed analysis. Working to exclude all non-macrophage-like clusters, **cluster 15** was addressed first. As it was clustered separately from the main UMAP structure, expressed almost none of the genes investigated, the cluster was dismissed and termed 'Junk'. Next, the subclusters of **cluster 5** were investigated, and while there were subtle differences between all four subclusters, only one was noticeably different to the others with lower CD1C and FCER1A and higher CD14, C5AR1. However, as this combination of genes did not allow for the separation of cDC2 and DC3 and no delineating DEGs were noted in the top5 analysis (**Figure 3.6D**), **cluster 5** was re-combined and termed generally 'DC'. Having a similar transcriptomic profile was **cluster 14**, expressing *CD1C* and *FCER1A*. **Cluster 14** formed a distinct cluster and defined by *MKI67*, led to it being termed 'Proliferating DC'. The subclusters of **cluster 7** also showed similarities to DC, with the notable addition of *S100A8* and *S100A9*,

suggesting monocyte origin. This cluster formed the lower boundary of the main UMAP structure and connected the monocyte-like cells to DC, and it was observed that as the subclusters transitioned between the two there was increasing expression of *HLA-DRB1* and decreasing expression of *S100A8/9*, suggesting differentiation. Therefore, **cluster 7** was re-combined and termed 'MDDC'.

Of the remaining clusters, six were identifiable by their expression of *S100A8/9* and low expression of *HLA-DRB1* as recently infiltrating monocytes. All had low expression of *CD14* except for **cluster 9_2**, which also had the highest *S100A8/9*, leading to it being termed 'CD14 monocyte'. **Cluster 16** was high for the expression of *FCGR3A* (CD16), *C5AR1* (CD88) and *ICAM2*, resulting in it being termed 'CD16 Monocyte'. The remaining four clusters, while expressing minor differences in gene expression, all displayed a clear MDM signature, expressing *S100A8/9* and *ITGAX* (CD11c), low *HLA-DRB1* and *CD14*, and no *MRC1* (MR) or *C1QB*. While these MDMs form a single population by flow cytometry, based on differences in *CD14* expression, and similarities in the top10 DEGs, **clusters 6** and **2** were combined into 'MDM1' and **clusters 12** and **1** combined into 'MDM2'.

Two of the remaining ten clusters (**9_0** and **9_1**) had expression of most of the genes that were investigated, including monocyte-like and macrophage-like genes, and analysis of the top 5 DEGs only highlighted high ribosomal activity. As these cells were not easily identifiable, due to their high ribosomal content and small size, cluster 9_0 and 9_1 were termed 'Mystery1' and 'Mystery2' and left out of the main macrophage subset clusters.

The final eight clusters represented three clear macrophage signatures. When compared to the MDMs, **clusters 10**, **0** and **13** had less expression of *S100A8/9* and *ITGAX*, and higher expression of *HLA-DRB1* and macrophage-associated *CD14*, *C1QB*, *CD81* and *CD163*. As these clusters expressed both monocyte- and macrophage-associated genes, they were termed 't-MDM'. The final five clusters had no *S100A8/9* expression and are tissue-resident macrophages. They express *CD14*, *C1QB*, *CD81*, *CD163* and *MRC1*. However, there are two distinct subsets of these macrophages. **Clusters 8**, **4** and **3** had higher expression of *CD86* and *CD80*, suggesting a more activated state, whereas **clusters 11** and **9_3** had high expression of *CD163* and *MRC1*, suggesting a more homeostatic state. These clusters were grouped as reported and termed 'Macrophage1' and 'Macrophage2' respectively.

Differentiation pathway confirmed by pseudotime analysis

Following cluster identification, Monocle3 was employed to create a pseudotime trajectory for unbiased indication of the development path between the macrophage subset clusters, with the user-chosen MDM1 cluster location selected as the base branch point (**Figure 3.7A**). Analysis was performed with all clusters included rather than only the clusters annotated as macrophages. As expected, there was a clear path from monocyte-like to macrophage-like cells. The path moved through the macrophages from MDM1, via MDM2 and t-MDM to Macrophage1 and Macrophage2 (**Figure 3.7A**). By analysing the top 20 DEGs with the strongest correlations to the pseudotime, it was observed that complement genes *C1QA/B/C* as well as *HLA-DQA1* were defining Macrophages (**Figure 3.7B**). As for MDMs, they were defined by genes associated with inflammation, *FCN1* (Chen et al. 2023) and *FTH1* (Michalides et al. 2024), or tumour infiltration *AQP9* (Liu et al. 2020), which was expected given the nature of the samples. These results reinforce the differentiation gradient from MDM, via t-MDM, to Macrophage, and highlight the changes macrophages undergo to adapt to the tissue environment.

Expression of HIV-binding receptor genes highest in Macrophages

Lastly, HIV binding receptors were investigated on the five macrophage clusters. The expression of HIV-entry receptor *CD4* showed an increase in average expression from MDM1 to Macrophage2 (**Figure 3.8A**), matching the trends seen in the surface protein expression (**Figure** 3.8**B**). While the average expression of *CCR5* is highest in t-MDMs, again matching the flow cytometry data, the percentage of cells expressing *CCR5* was less than 25% in all macrophage clusters, with Macrophage2 showing no expression. HIV X4 strain binding co-receptor *CXCR4*, and HIV restriction factor *SAMHD1* were both expressed at low levels in MDMs and most highly in Macrophage1. The expression of HIV-binding uptake receptor genes closely matched their surface protein expression for *CD209*, *SIGLEC1* (CD169), *MRC1* (CD206) and *CD207*. Both technologies showed that the expression of these lectin receptors was increased in correlation with the degree to differentiation from the monocyte-like to tissue-resident macrophage-like phenotype. Each of these markers was plotted in relation to pseudotime, confirming increasing expression that peaks in cluster Macrophage1 (**Figure 3.8C**). This data taken together with the corresponding flow cytometry data strongly suggests that macrophage subsets are more susceptible to HIV infection and more like to take up the virus as they approach terminal differentiation.

Interestingly, while gene expression and surface protein expression in cells did not always correlate perfectly, these results confirm that three distinct macrophage subsets are present in the human colorectum, and that Macrophages are the most likely to interact with HIV.

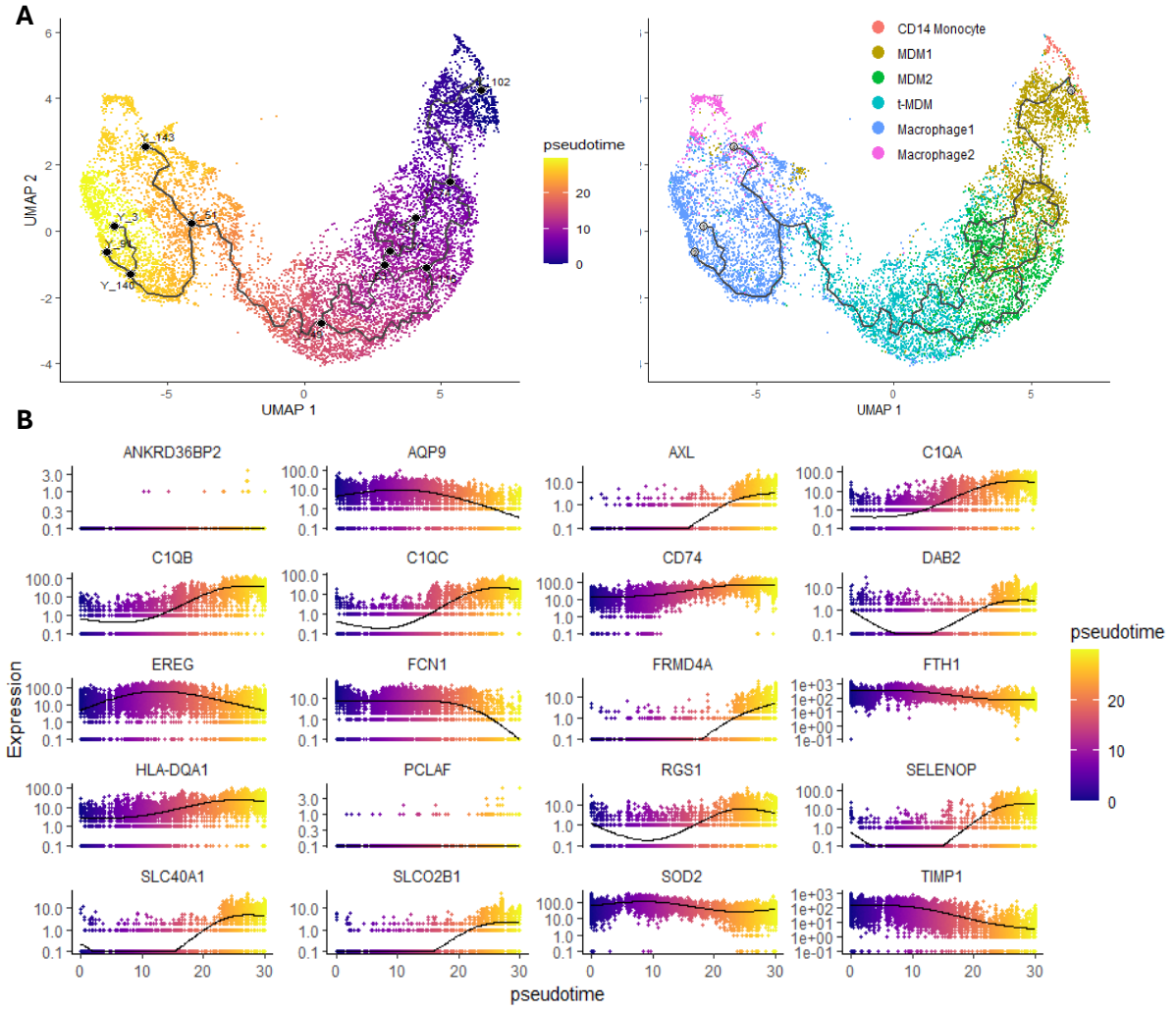

Figure 3.7: Pseudotime trajectories for colonic MNPs. Data was obtained from Domanska et al. (2022) and processed as described in Section 3.2.6. **A** Reconstructed developmental trajectory of colonic MNPs showing pseudotime from blue to yellow (left). Overlay of annotated clusters over pseudotime trajectory UMAP (right). **B** Gene expression of top20 genes with highest correlation to pseudotime trajectory, average expression shown as trend line, pseudotime coloured blue to yellow.

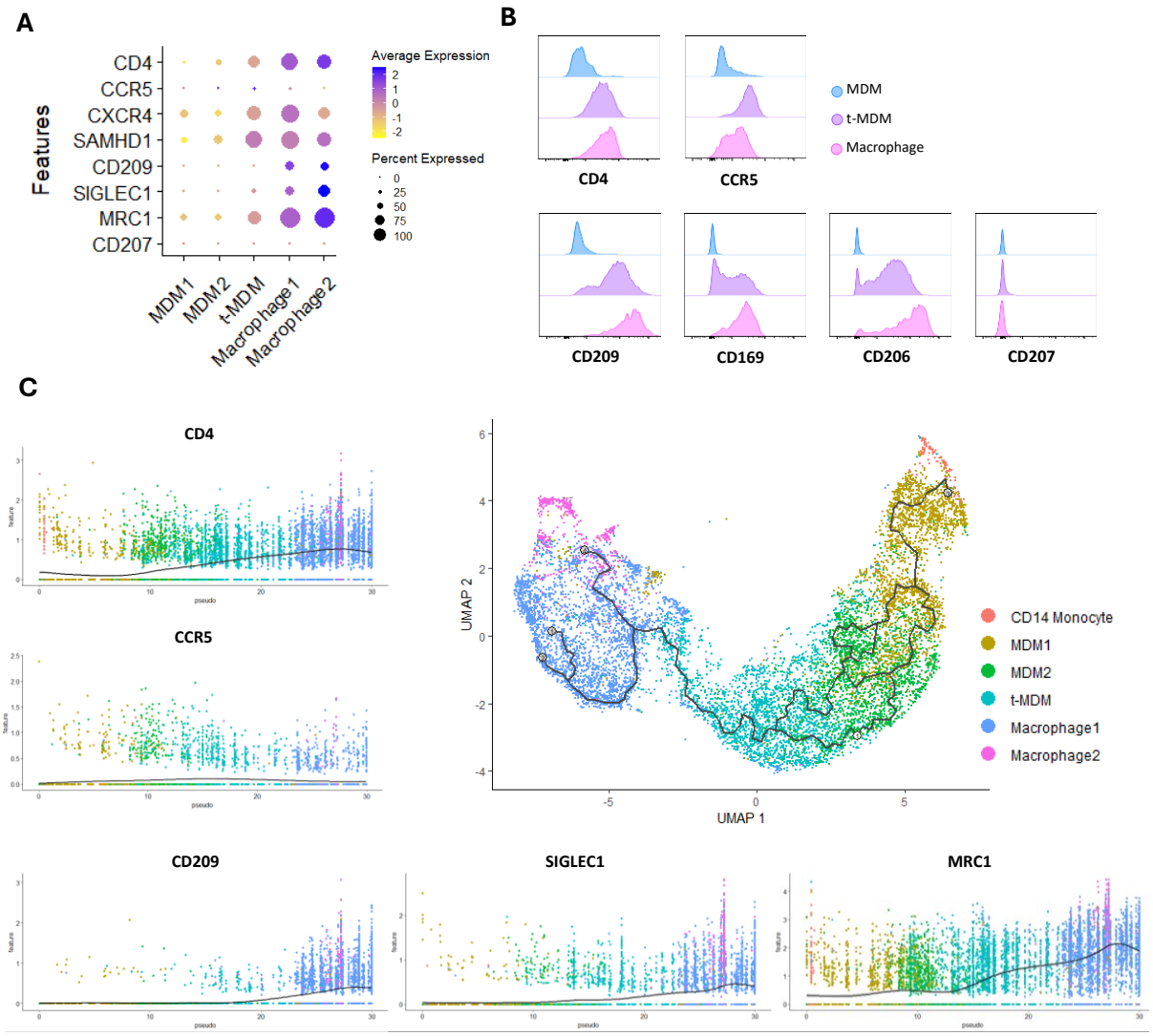

Figure 3.8: HIV receptor comparison of RNA to surface protein, and pseudotime trajectories of HIV-binding receptors. Data was obtained from Domanska et al. (2022) and processed as described in Section 3.2.6 **A** DotPlot of expression of selected genes: HIV-entry receptor (*CD4*, *CCR5*, *CXCR4*), HIV restriction factor (*SAMHD1*), HIV-binding lectin receptor (*CD209*, *SIGLEC1*, *MRC1*, *CD207*). **B** Representative plot of surface expression for HIV-entry and HIV-binding lectin receptors by flow cytometry in MDM (blue), t-MDM (purple) and Macrophages (pink). **C** Overlay of annotated clusters over pseudotime trajectory for HIV-binding receptors (left and below), Overlay of annotated clusters over developmental trajectory UMAP (right top).

3.3.2 Defining HIV interactions with colorectal mononuclear phagocytes and CD4 T cells

With the colorectal MNP subsets defined, functional HIV assays were performed using a clinical strain of HIV. The *ex vivo* MNPs were either defined post-HIV exposure via high-parameter flow cytometry, or FACSorted into subsets prior to HIV exposure.

3.3.2.1 Optimisation of virus preparation

To limit variability in HIV assays, it was preferred to use one virus preparation to complete all infection assays, with plasmids resulting from the amplification of a single transformed *E. coli* bacterium. Infectious virus yields from the lab's existing protocol were adequate, however they were designed to ensure that the preparation did not require attention outside of normal working hours. Specifically, following transfection, virus containing media (VCM) was collected on day 3 and day 6, corresponding to Friday and Monday. This meant that virus remained in suspension at 37°C for up to 3 days before collection, where it remained at 4°C for additional days during the sterilisation and concentration steps in the protocol. Having previously lost infectious virus from collected supernatants left at 37°C, a protocol with daily VCM collections was proposed and tested.

HEK293Ts were seeded into 12 T150 flasks and transfected as per **Section 3.2.4**. Following the day 1 media change, 6 flasks were allocated for collections on day 3 and 6 (staggered) as per the existing protocol, and 6 flasks allocated for collections every day from day 2 to day 6 (daily). Aliquots of VCM from each collection were kept at 4°C until day 6 when they were titred on TZM-bls. Due to higher-than-expected concentrations in the initial collections, titres for the first collection for each condition could not be calculated. The daily collections resulted in higher total titre (TCID50/ mL >8.58 x 10^6) compared to the staggered collections (TCID50/ mL >5.45 x 10^6) (**Figure 3.9**). Consequently, the new protocol with daily collections was adopted. The subsequent virus preparations were tested on activated CD4 T cells and *in vitro* MDDCs prior to use on colorectal MNPs to confirm they could infect primary cells.

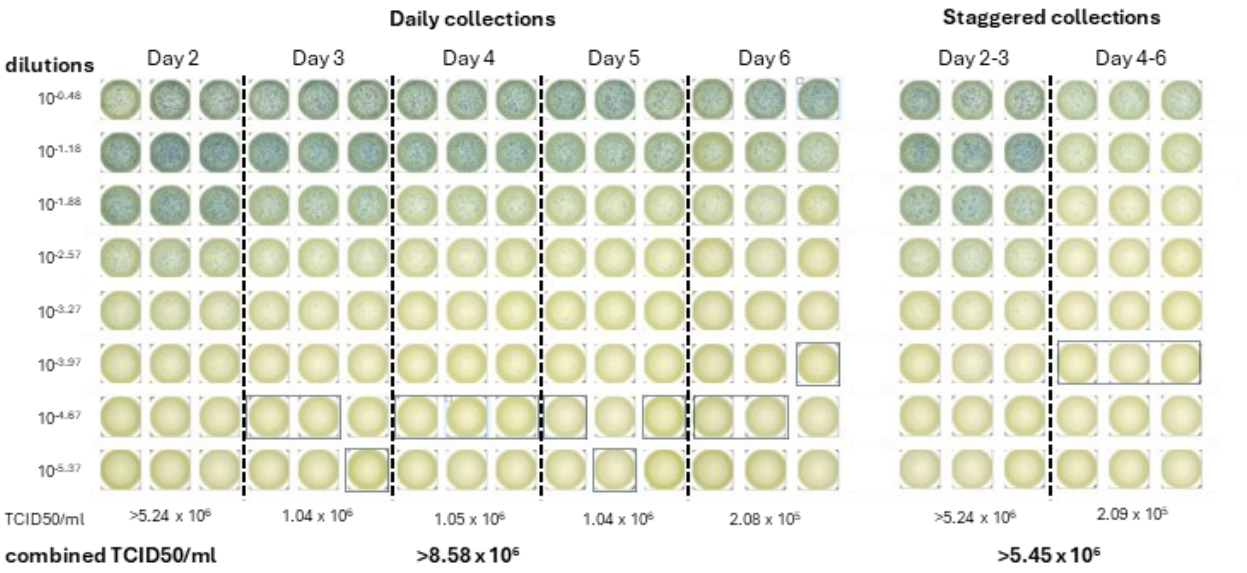

Figure 3.9: Virus preparation optimisation, comparison of viral titres. Comparison of TCID50/ml for 6 days of virus containing media (VCM). Aliquots from collections from virus preparation flasks were stored at 4°C until day 6. Daily collections were collected day 2, 3, 4, 5 and 6. Staggered collections were collected day 3 and day 6. On day 6, VCM aliquots were added to TZM-bls at a 1:3 dilution and titrated at 1:5 dilution. TZM-bls were cultured and developed as per Section 3.2.4.4. Dotted boxes denote last well in dilution series to contain 3 or more infected cells. Day 2 and Day 2-3 were too concentrated for accurate titre calculation. Combined total represents lowest TCID50/ml per each collected condition.

3.3.2.2 Colorectal macrophages take up more HIV than DCs and CD4 T cells

To investigate the ability of the MNP subsets to bind and take up HIV, mononuclear colorectal cells were incubated with HIV (MOI 5) for two hours prior to high-parameter flow cytometry staining. Following surface staining, cells were intracellularly stained with two antibodies against HIV capsid protein, p24, with a mock condition gating control (**Figure 3.10A**). As this assay was performed on CD45+ selected cells, as opposed to FACSorted cells, relatively large cell numbers and virus quantities were required. Therefore, for these assays, a lab adapted strain of HIV_{BAL} was used to reserve the more clinically relevant HIV_{Z3678M} for assays using FACSorted cells. XCR1 was removed from the staining panel to allow dual p24 staining, therefore uptake data for cDC1s was not collected. However, we have previously demonstrated that colorectal cDC1 do not express CCR5 or HIV binding lectin receptors and correspondingly do not take up or become infected by HIV (9) .

All MNP subsets were significantly more efficient at taking up HIV than $CD4^+$ T cells at the 2-hour time point, with CD4 T cells expressing mean 5.9% (± 7.4) p24 **Figure 3.10B**, **left**). As a comparison, $CD4^-$ T cells (0.3% ± 0.3) and $CD19^+$ B cells (0.4% ± 0.3) (**Figure 3.10B**, **right**) did not take up HIV. MDMs and $CD207^-$ cDC2s took up the least HIV of the MNPs, with mean uptake of

46.1% (±11.9) and 52.9% (± 28.0) respectively. CD207$^+$ cDC2 (60.8% ± 10.8), t-MDM (78.1% ± 21.0) and Macrophages (87.7% ± 5.9) took up the most HIV. t-MDM and Macrophages took up significantly more HIV than any other cell. Additionally, as a proportion of all p24$^+$ cells, Macrophages contained 65.0% of all HIV taken up, significantly more than the other reported MNPs and CD4 T cells (**Figure 3.10C**). Taken together, these results show that Macrophages are the most efficient of all colorectal MNP subsets at HIV uptake.

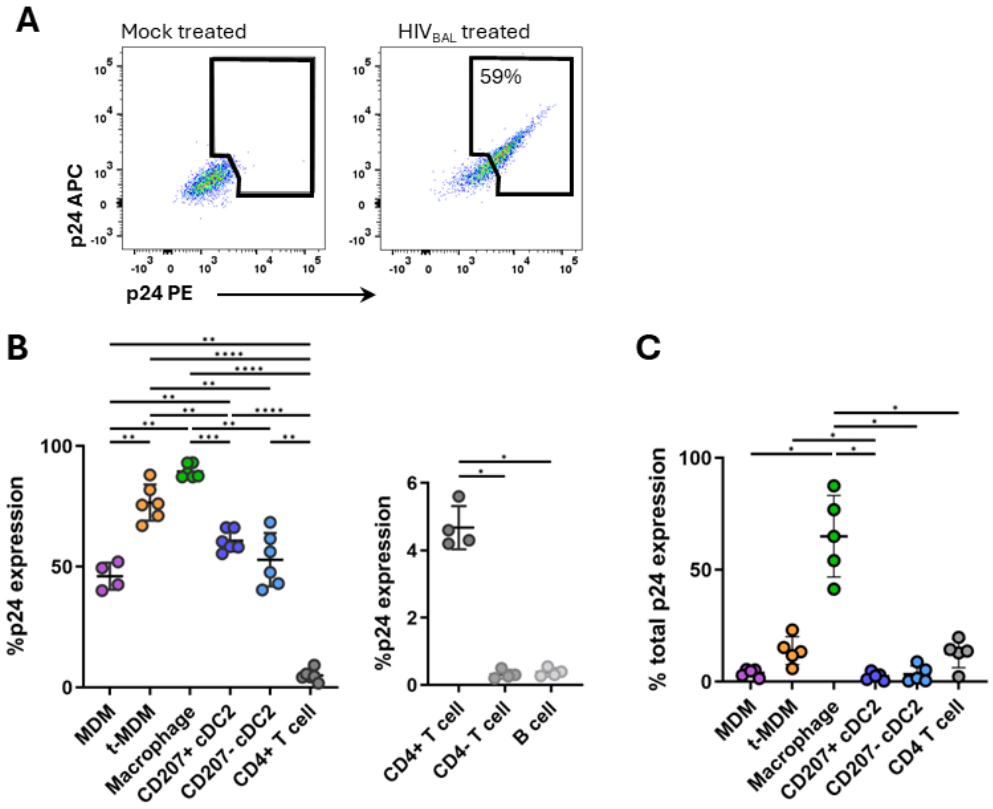

Figure 3.10: Uptake of HIV by p24 expression on colorectal mononuclear phagocytes. Cells were isolated from colorectal tissue using the techniques described in Section 3.2.5.2, enriched for CD45$^+$ cells, and exposed to HIV$_{BAL}$ (MOI=5) for 2 hours before staining for acquisition on the FACSymphony. **A** Representative gating illustrating dual p24 expression, with the mock-treated sample used to set p24$^+$ gate. **B** Percentage of dual p24 expression across MNP subsets and CD4$^+$ T cells (left) and CD4$^+$ T cells, CD4$^-$ T cells and CD19$^+$ B cells (right). **C** Percentage of dual p24 expression across MNP subset and CD4$^+$ T cells as a proportion of total dual p24$^+$ cells. Statistical analysis was performed using Ordinary one-way analysis of variance (ANOVA) with Tukey's multiple comparisons (****p = <0.0001, ***p = <0.001, **p = <0.01, *p = <0.05).

3.3.2.3 Blocking CD169 reduces HIV uptake in Macrophages

While conducting exploratory analysis of the HIV uptake flow cytometry data, it was noticed that CD169 fluorescence intensity was lower in HIV exposed samples when compared to mock. This was investigated in all macrophage subsets, and while t-MDMs trended lower for CD169 after HIV exposure, only Macrophages demonstrated significantly lower surface CD169 (**Figure 3.11A**). CD206 and CD209 were also investigated for this phenomenon, but it appeared to be CD169 specific. This confirms previous findings that CD169 is internalised with HIV during uptake (56) .

To determine the extent that CD169 contributes to HIV uptake on Macrophages, $CD45^+$ cells were blocked with a monoclonal anti-CD169 antibody for 30 mins prior to HIV exposure. CD209, being the other key HIV-binding lectin receptor highly expression only on colorectal macrophages, was blocked with two anti-CD209 monoclonal antibodies as the combination had been shown to be more effective at blocking CD209 than any single antibody (162) .

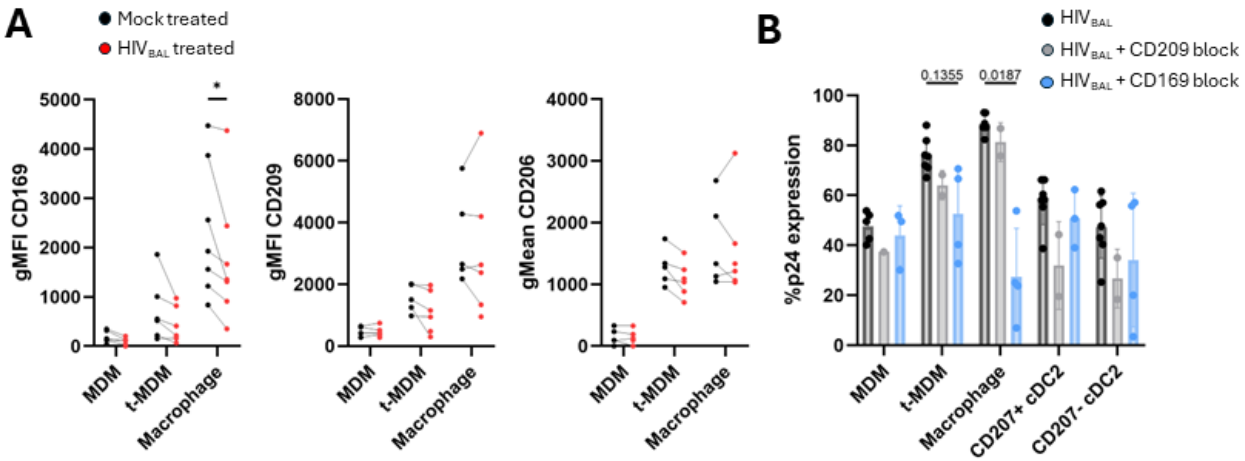

Figure 3.11: CD169 internalised with HIV uptake. Cells were isolated from colorectal tissue using the techniques described in Section 3.2.5.2, enriched for $CD45^+$ cells, and exposed to HIV_{BAL} (MOI=5) for 2 hours before staining for acquisition on the FACSymphony. **A** Geometric mean of fluorescence intensity (gMFI) of CD169 expression on macrophage subsets for mock-treated samples and HIV-treated samples. Statistical analysis was conducted using Wilcoxon matched-pairs signed rank test (*p = <0.05). **B** CD45+ cells were incubated with monoclonal anti-CD169 or dual monoclonal anti-C209 for 30 mins prior to exposure to HIV. Percentage of dual p24 expression across MNP subsets, using $CD169^-/CD209^-$ cDC2 subsets as non-specific binding control. Statistical analysis was performed using the One-way analysis of variance (ANOVA) with Geisser-Greenhouse correction and Sidak's multiple comparisons (significant = <0.05).

Blocking with CD209 showed no significant difference on the percentage of macrophages or cDC2s taking up HIV. However, blocking with CD169 reduced the $p24^+$ t-MDMs from 73.0% to 52.6% (**Figure 3.11B**). Additionally, CD169 blocking significantly decreased uptake in Macrophages from 87.5% to 27.4%, a total reduction of 60%. The degree of blocked HIV uptake in t-MDMs and Macrophages evidently correlates with their expression of CD169 (**Figure 3.5**). Therefore, it can be concluded that CD169 is a key HIV-binding receptor on colorectal Macrophages, and the intracellular pathway of HIV in macrophages from CD169-mediated uptake should be further explored.

3.3.2.4 Development of a FACSort panel to isolate colorectal MNPs

To understand how each MNP subset interacts with HIV as well as CD4 T cells, MNPs needed to be accurately isolated while remaining live and functional. To achieve this, a panel for FACSorting was optimised taking into account the downstream applications. Specifically, the clone of the anti-CD4 antibody was selected to be non-competitive with the HIV binding site, and cytometer detectors for APC and PE were left unallocated to allow for dual p24 staining. The optimised panel and gating strategy can be found in **Table 3.6** and **Figure 3.12** respectively. It should be noted that due to the very low proportions of DC subsets compared to macrophage subsets, DCs were FACSorted as a bulk $HLA\text{-}DR^+$ $CD11c^+$ population to ensure sufficient sort yields for their inclusion in the below assays.

3.3.2.5 Colorectal MNPs enhance the infection of CD4 T cells

MNPs are the first to encounter HIV in the colorectum, and DCs and macrophages interacting with CD4 T cells has been observed *in situ* within 2 hours (116). With the ability of the MNPs to take up HIV confirmed, the specific interactions between colorectal MNPs and CD4 T cells remained to be investigated. *Ex vivo* FACSorted MNPs were co-cultured with autologous CD4 T cells to determine what effect the MNPs would have on the infection of the CD4 T cells. To be as physiologically relevant as possible, all remaining assays were performed with the transmitted founder HIV_{Z3678M} strain.

Live T cells were gated using a minimal strategy (**Figure 3.13A**), with $p24^+$ cells gated using the mock sample. To normalise the variability seen between donors, the p24 expression was calculated as fold change in expression compared to the positive control with only CD4 T cells (mean 5.38% ± 3.7 SEM). CD4 T cells co-cultured with DCs had significantly greater infection than the positive control (**Figure 3.13B**). This is consistent with previous studies in human skin (7,9).

Interestingly, MDMs, t-MDMs and Macrophages also enhanced the infection of co-cultured CD4 T cells.

Unexpectedly, there was no noticeable difference between any of the macrophage subset co-cultures, and more surprisingly there was no difference between the infection enhancement of the macrophages and DCs.

Culture supernatants from the co-cultures were added to a HIV infection reporter cell line, TZM-bls, to confirm productive infection by quantifying cell-free virus. Interestingly, while there was more p24 in CD4 T cells co-cultured with the colorectal MNPs, there was no significant increase in the cell-free virus found in the supernatants (**Figure 3.13C**).

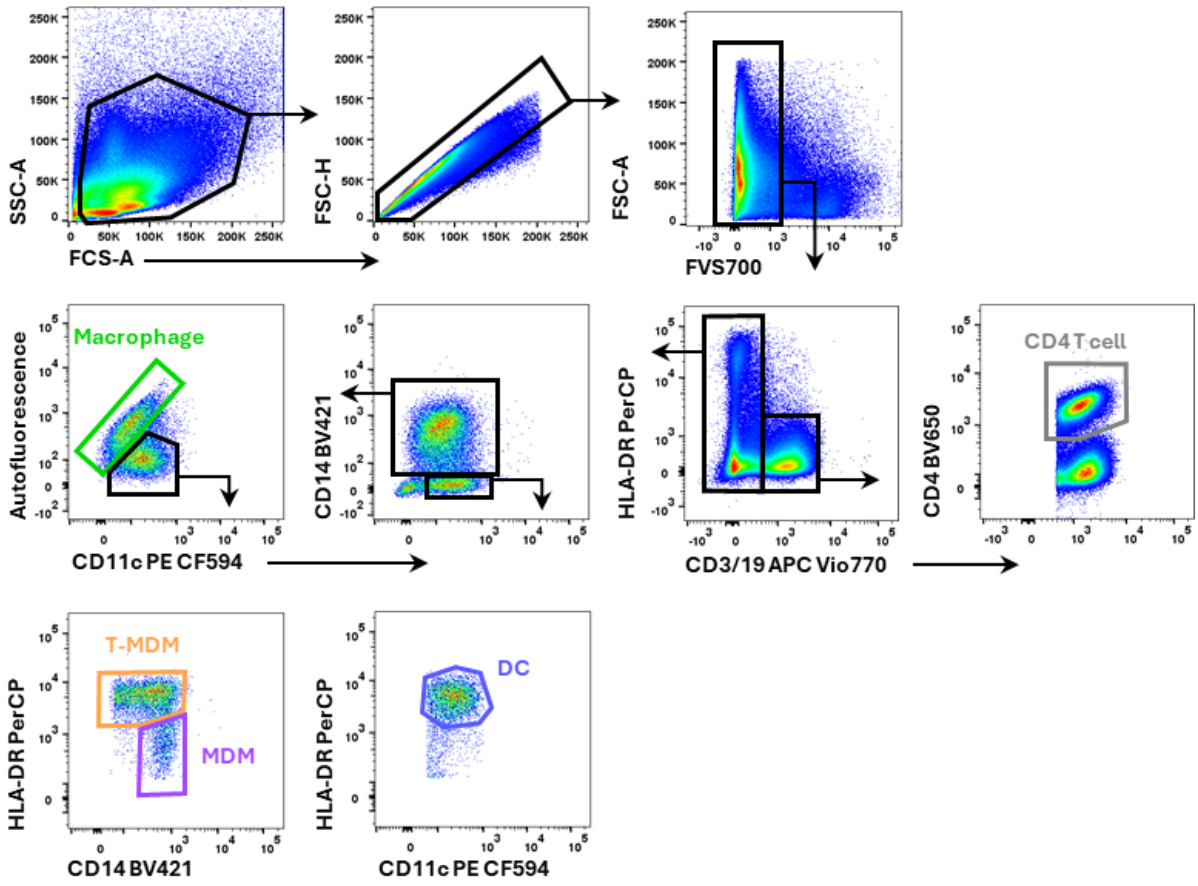

Figure 3.12: FACS gating strategy to isolate colorectal mononuclear phagocytes. Representative gating strategy for CD45+ cells isolated from colorectal tissue using the techniques described Section 3.2.5.2. Single live cells were gated using forward scatter (FSC), side scatter (SSC) and FVS700. CD4 T cells were identified as $CD4^+$ $CD3^+$. MNP populations were gated as $CD3^-$ $CD19^-$ and sorted as follows: bulk DC ($CD14^-$ $CD11c^+$ $HLA\text{-}DR^+$), MDM (CD11c+ $HLA\text{-}DR^{low}$ $CD14^{hi}$), t-MDM ($CD11c^+$ $HLA\text{-}DR^+$, $CD14^+$), and Macrophages ($CD11c^-$ $CD14^+$ $Autofluorescence^+$).

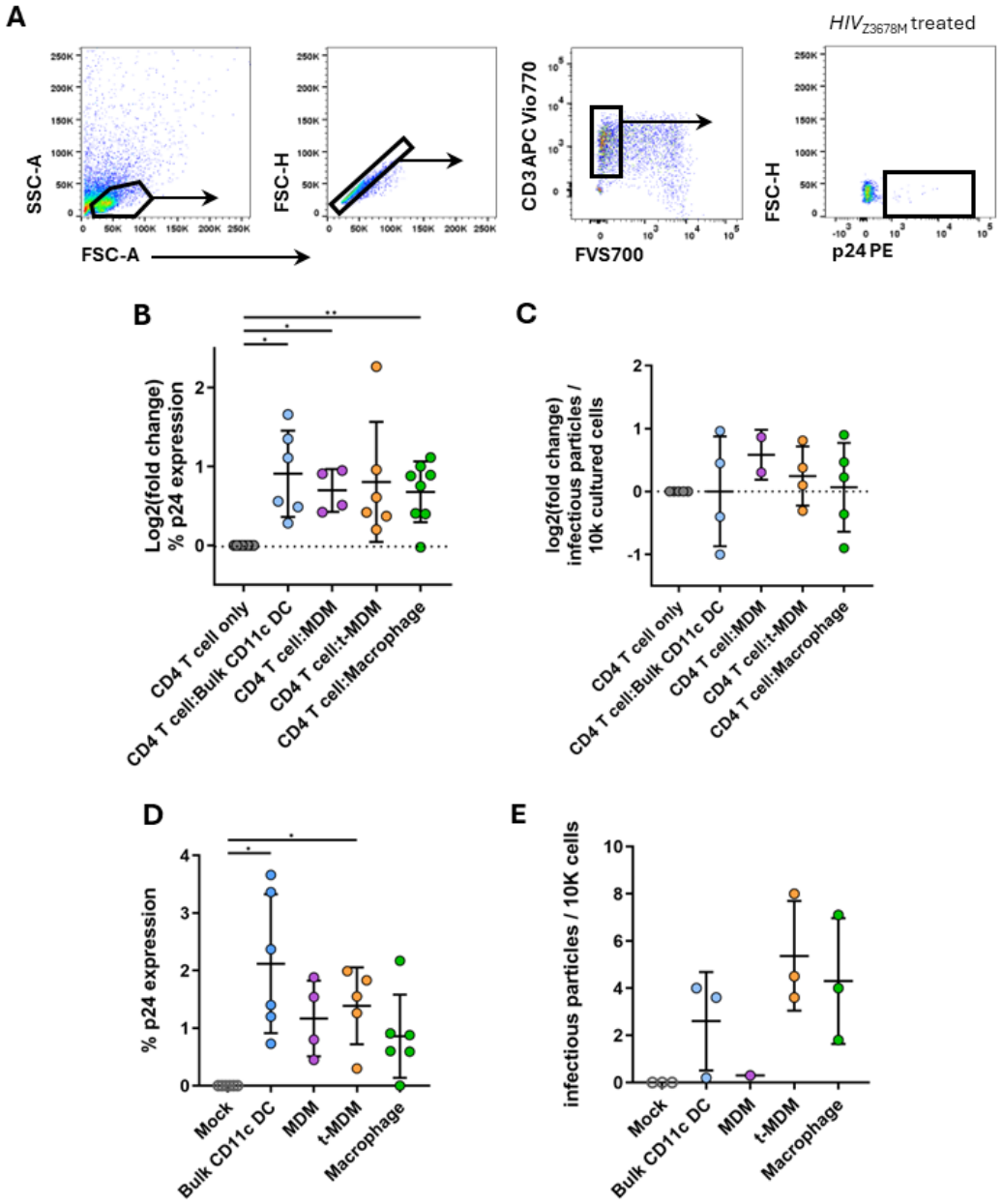

Figure 3.13: HIV infection of colorectal CD4 T cells with mononuclear phagocyte in co-culture and transfer. A Representative gating strategy for post-infection CD4 T cells. Representative gating to single, live $CD3^+$ T cells. HIV infection at day 3 was evaluated by p24 expression, using mock treated sample as gating control. **B** FACSorted colorectal MNP subsets were added to autologous CD4 T cells in a ratio of 1:10 and exposed to clinical strain HIV_{Z2678M} (MOI=1) for 2 hours, washed and incubated for 3 days at 37°C. Supernatants were collected and cultures on TZM-bls, with cells stained for flow cytometry. Data shows the fold change of the p24 expression in CD4 T cells from MNP co-cultures compared to the CD4 T cell only condition, adjusted for background staining from the mock. **C** Supernatants from B were cultured on TZM-bls for 3 days before being developed as described in Section 3.2.4.4. Data shows the fold change of the number of infectious particles/10k cells in CD4 T cells from MNP co-cultures compared to the CD4 T cell only condition. **D** FACSorted colorectal MNP subsets were exposed to clinical strain HIV_{Z2678M} (MOI=1) for 2 hours, washed 3 times, and added to allogeneic Activated CD4 T cells in a ratio of 1:2, then incubated for 3 days at 37°C. Data shows percentage of p24 expression in CD4 T cells compared to mock. **E** Supernatants from D were cultured on TZM-bls for 3 days before being developed as described in Section 3.2.4.4. Data shows the number of infectious particles/10k cells in MNP transfer cultures compared to the mock. Error bars indicate mean ± SD. Statistical analysis was conducted using Ordinary one-way analysis of variance (ANOVA) with Dunnett's multiple comparisons (**p = <0.01, *p = <0.05).

3.3.2.6 Colorectal t-MDM as efficient as DCs in HIV transfer to CD4 T cells

To better understand the demonstrated enhancement of CD4 T cell infection by MNPs, our MNP-T cell transfer assay using activated allogeneic T cells (7,9,44,45) was utilised to determine how MNP transfer to CD4 T cells contributes to the enhancement. Activated cells from a single donor were used for all transfers to minimise variability in the assay.

After CD4 T cells were incubated with the MNPs for 3 days, live CD4 T cells were gated using a simple strategy (**Figure 3.13A**), with p24+ cells gated using the mock sample. DC and all macrophage subsets were capable of transferring HIV to CD4 T cells, though MDMs and Macrophages did not reach significance compared to mock (mean 1.2%, 0.9%) (**Figure 3.13D**). In line with previous studies on skin-derived DCs (7,9) , *ex vivo* colorectal DCs transfer of HIV to CD4 T cells was significant against the mock (mean 2.1%). Remarkably, significant transfer was also demonstrated by the t-MDMs (mean 1.4%). Additionally, there was no significant difference noted in the level of transfer displayed by DC and t-MDMs. This is the first time that a tissue-derived macrophage has shown comparable transfer of HIV to a CD4 T cell as a tissue-derived DC.

As with the co-cultures, culture supernatants from the transfer assay were added to TZM-bls to confirm productive infection by quantifying cell-free virus. Statistical significance was not achieved with only 3 donors collected. MDMs were not present in high enough numbers in 2 of the collected donors to make any conclusions. Supernatants from DCs, t-MDMs and Macrophages transfer assays all contained cell-free virus (**Figure 3.13E**). Interestingly, though the p24 expression was highest from DC transfer, the quantity of virus in the supernatants were higher from the t-MDM and Macrophage transfers. Given the 2:1 ratio of CD4 T cells to MNPs in this assay, this result may suggest that the cell-free virus reported was not only the virus produced by the CD4 T cell infection but could be contributed to by de novo virus production or the release of virus from VCCs from the macrophages in culture.

3.4 Discussion

In this study, utilising high-parameter single-cell technologies and our privileged access to human intestinal tissues, we have defined a full array of MNP subsets present in non-inflamed colorectal tissue and identified which subsets take up HIV and transmit the virus to CD4 T cells. In doing so, we have shown three distinct macrophage subsets MDM, t-MDM and Macrophages, as well as three DC subsets, cDC1, CD207^{+} cDC2, and CD207^{-} cDC2. These MNP subsets exhibited unique profiles of HIV-binding receptors both for HIV entry and HIV uptake. Macrophages were shown to be the most abundant MNP in intestinal tissues and were the most efficient at taking up HIV, having the highest level of expression of lectin receptors, particularly CD169 and CD209. We demonstrated that blocking CD169 resulted in significant reduction in HIV uptake in Macrophages. All macrophage subsets were shown to enhance the infection of CD4 T cells in co-culture, though MDMs and Macrophages were not efficient at first-phase transfer. As expected, DCs were efficient at transferring HIV to CD4 T cells, though surprisingly, t-MDMs were also as efficient.

While DC classifications are expanding (7,39,40,42,111), cDC subsets are maintained throughout tissue types, with cDC1s and cDC2s in the colorectum showing similar profiles of defining markers and HIV-binding entry and uptake receptors (9). The classification of macrophages, however, is dependent on the specialised requirements of their tissue of residence. To date, Bujko et al. has provided the most extensive investigation into intestinal macrophages, identifying four distinct subsets in human jejunum (109). It is these subsets, termed Mf1-4, that were the initial starting point for our colorectal subsets, and MDMs (HLA-DR^{low}, CD14^{+} CD11c^{+}), t-MDMs (HLA-DR^{+} CD14^{+} CD11c^{+}) and Macrophages (HLA-DR^{+} CD14^{+} CD11c^{-}) correspond to Mf1, Mf2 and Mf3 respectively. They identified Mf4 that was distinguished from Mf3s (referred to here as Macrophages) by the surface expression of CD11b. While some colorectal donors did have CD11b^{+} Macrophages, the majority did not. Transcriptionally, we were able to confirm that these subsets represented different stages of macrophage differentiation, with MDMs and t-MDMs expressing S100A8/9, and t-MDMs and Macrophages expressing C1QA/B/C **(Figure 3.6**), suggesting a transition from a monocyte-like cell to a tissue-resident phenotype, which was further confirmed by pseudotime analysis (**Figure 3.7**). While this study has focussed on steady-state tissues, it is important to note that inflammation is closely associated with an increased risk of sexually transmitted diseases (164–168). The subsequent chapter will focus on the optimisation of a flow cytometry panel to enhance the classification of colorectal MNP subsets to include all known inflammatory tissue MNPs (169). This panel has

been designed to be compatible with all tissues involved in sexual transmission, enabling direct comparisons of HIV uptake in comparable MNPs across various transmission sites.

In line with our previous findings (9) , we have shown that macrophages are the sole MNP in steady-state colorectal tissues that express lectin receptor CD169 (Siglec-1) (**Figure 3.5**). Pseudotime analysis of the transcriptional signatures of the macrophages confirmed what has been seen by surface protein, showing that *SIGLEC1* is upregulated in tissue, with higher expression corresponding to the state of differentiation towards a tissue-resident phenotype (**Figure 3.8**). Therefore, it was not surprising that MDMs did not express CD169, t-MDMs expressed a moderate amount, and the highest expression seen in Macrophages. This correlated to significantly higher HIV uptake seen in both t-MDM and Macrophages compared to MDM, cCD2s and CD4 T cells; uptake that could be significantly blocked in Macrophages by targeting CD169 specifically. The significantly higher expression of CD169 in conjunction with the high abundance of Macrophages resulted in them containing the majority of HIV within $CD45^+$ cells. CD169 has long been known to bind and internalise HIV into non-degradative intracellular Virus-Containing Compartments (VCC) (20,56,170), as well as being involved in the transfer of HIV to CD4 T cells (171–173). Surprisingly, despite the level of HIV uptake in Macrophages, this did not correspond to transfer of HIV to CD4 T cells (**Figure 3.13D**), in contrast, t-MDMs did prove to be as efficient in transfer as $CD11c^+$ DCs. Mechanisms to inhibit the release of HIV from VCCs, such as soluble anti-CD36 antibodies (174) or silencing microtubule-associated kinesin KIF3A by RNA interference (175) have been investigated in *in vitro* derived MDMs, suggesting that HIV release can be interrupted in macrophages. However, the trend to higher quantity of cell-free virus from the transfer cultures does suggest that Macrophages, as well as t-MDMs, released internalised HIV into the culture over the three-day incubation period. As the kinetics of this release has not been described in tissue macrophages, it can only be suggested that the release from VCC by Macrophages occurred later in the incubation. This could mean that any transfer to and subsequent infection of CD4 T cells may not have completed a full replication cycle at the time of the assay collection, contributing to the low intracellular p24. Consequently, further investigation would be required to fully interpret these results, such as blocking CD169 in the transfer assay to prevent uptake into VCCs to understand their contribution to the present result. However, these are extremely difficult experiments to perform due to viability of *ex vivo* derived tissue MNP post liberation from tissue. Given that tissue macrophages have been demonstrated to contribute to the HIV reservoir in the human intestine (176,177) and urethral mucosa (47) in ART-suppressed HIV^+ individuals, the observation that macrophages retain rather than release

HIV is less surprising than initially believed. Additionally, CD169-mediated uptake may play a role in establishing latent infection.

Interestingly, a portion of t-MDMs expressed *CD1C and FCER1A*, genes that were used to define DCs (**Figure 3.6**). Surface expression of CD1c on a portion of t-MDMs is also seen on most donors (**Figure 3.3**). Interestingly, although all $CD14^+$ cells in the intestine have been reported as macrophages (109), these $CD1c^+$ t-MDM share defining phenotypic markers with MDDCs found in skin and type II mucosa (9). These MDDCs were shown to be preferential HIV target cells and, like t-MDMs, were capable of transferring HIV to CD4 T cells. Interestingly, these *ex vivo* MDDCs did not express CD169, and CD169 and CD1c are mutually exclusive on t-MDMs by flow cytometry (data not shown), suggesting that an $CD1c^+$ MDDC population could be contained with the t-MDM subset. This is further supported by the presence of an MDDC-like cluster identified in the analysed RNA dataset, also expressing *CD1C*. Additionally, DC3s share defining receptors with t-MDMs, namely HLA-DR, CD11c, CD1c, CD163 and CD14 (40–42,111). Currently, $CD14^+$ DC3 are implicated in inflammatory disease settings (169), which could explain their absence in the colorectal samples included in this study. However, it might be the case that their steady-state tissue phenotype remains incompletely understood. Conversely, a recent study in female genital tissues posited that all $CD14^+$ $CD1c^+$ cells were DC3 (155), implying that the previously defined *ex vivo* $CD14^+$ DC (9,110,178) and DC3 were the same cell and were not defined by CD163. Therefore, t-MDMs should be re-evaluated to verify their expression of $CD1c^+$ and whether this $CD1c^+$ portion can be discerned as MDDC and/or DC3s. Unfortunately, due to the time constraints of this PhD, this evaluation remains a future direction of this study.

Access to human colorectal tissues represents a significant strength of this study; however, the use of human tissue also presents inherent limitations that are not limited to potential donor-related variation. We are fortunate to receive explants of colorectal tissue from a network of collaborating surgeons, yet the variability in explant size poses challenges. MNPs constitute less than 1% of the $CD45^+$ selected cells in this tissue (data not shown), resulting in many samples being unsuitable for further processing via FACS for functional HIV assays based solely on post-digestion cell yield. The limited number of donors for some experiments reflects the limitations of using *bona fide* colorectal MNPs; the experiments carried out here took over 4 years to perform. Although we successfully separated macrophage subsets for cell sorting, there were too few DCs to sort them by subsets for functional assays, meaning we could not investigate $CD207^+$ cDC2, a subset previously shown to play a dominant role in HIV transmission within skin and mucosa (9). While we were successful in sorting macrophages from eligible donors, the

limited survival rates of *ex vivo* tissue-derived MNPs in culture posed significant challenges to our research. This particularly affected our ability to assess the permissibility of macrophage subsets to HIV infection and to further investigate CD169 uptake. Unfortunately, this challenge was not overcome in the time constraints of this PhD, although attempts were made. Notably, using media conditioned overnight on cultured human dermal fibroblasts enhanced cell viability; however, the majority of cells still did not survive the requisite 96-hour timeframe for the infection assay (data not shown) (9) . In light of these challenges, we adjusted our approach to allow macrophages to adhere to treated slides, with plans to subsequently measure infection through immunofluorescence (IF) microscopy. *Ex vivo* macrophages were cultured in Yssel's Media (179) for three days to facilitate adhesion, resulting in marked improvements in viability (data not shown), though optimisation did not progress further and remains a future direction. Our initial objective was to identify HIV infection in *ex vivo* derived cells via p24 protein expression or HIV RNA *in situ* hybridization (RNAscope); however, previous functional assays revealed a complication. CD169-mediated uptake resulted in the presence of intracellular HIV that was independent of productive infection, indicating that assessments of intracellular p24 and RNAscope would not reliably (180) reflect actual infection status. A future direction is to use a dual-fluorescent HIV construct containing two distinct sequences: one near-infrared fluorescent protein (iRFP) which is constitutively expressed to confirm the presence of HIV RNA, and green fluorescent protein (GFP) expressed only upon HIV DNA integration into the host cell (180). As this construct lacks an envelope (Env) gene, the construct will be packaged with a R5 envelope. The use of this HIV construct will enable us to differentiate between macrophages that are productively infected, those retaining HIV due to CD169-mediated uptake, as well as those latently infected. Once this protocol is optimised, it could serve as a vital tool for investigating the kinetics of CD169-mediated uptake in tissue macrophages. Furthermore, it may provide valuable insights into the dynamics and trajectory of the VCC, potentially identifying mechanistic targets to hinder the establishment of HIV reservoirs within these cells.

In conclusion, enhancing our understanding of the classifications of MNPs in the human colorectum, as well as their interactions with HIV and CD4 T cells, is crucial for elucidating HIV transmission across the colorectal mucosa. This knowledge could not only aid in the development of targeted mucosal prevention therapies, including topical microbicides, but also to the formulation and delivery of cure strategies and an effective mucosal vaccine.

Chapter 4. OMIP: 26-parameter flow cytometry panel to characterise all homeostatic and inflammatory state mononuclear phagocytes in human skin, type II mucosa and type I mucosa

This manuscript has been submitted to *Cytometry Part A* and is awaiting review

Erica E. Vine*, Freja A. Warner van Dijk*, Tony L. Cunningham, Najla Nasr, Andrew N. Harman, Kirstie M. Bertram. Chapter 4. OMIP: 26-parameter flow cytometry panel to characterise all homeostatic and inflammatory state mononuclear phagocytes in human skin, type II mucosa and type I mucosa. *Cytometry A* (2025) *submitted*

*Co-first Authors

This chapter, presented in Cytometry Part A Optimised Multicolour Immunofluorescence Panel (OMIP) manuscript format, details the design and optimisation of a 26-parameter conventional flow cytometry panel for the BD FACSymphony A5. This optimised panel is something that has not been attempted previously: one panel that will allow for the identification of all known steady and inflammatory state MNPs in all human sexual transmission tissues (skin, type I mucosa, type II mucosa). This chapter represents more than three years of optimisations including trouble-shooting and exploratory analysis. While not presented in this version for publication, this panel has been designed to include two antibodies against HIV capsid protein p24. This will enable detection and comparison of HIV uptake in all MNPs in non-inflamed and inflamed sexual transmission tissues.

All experiments, analysis and writing contained herein were equally contributed to by this author, in collaboration with Freja Warner van Dijk, PhD Student.

4.1 Abstract

We developed a 26-colour flow cytometry panel to comprehensively characterise mononuclear phagocytes (MNP) in steady and inflammatory states for human skin, type II and type I mucosal tissues. The capacity to isolate and define Langerhans cells, dendritic cells, macrophages and monocytes from fresh human tissue is critical to understanding their roles as antigen presenting cells. Liberating MNPs from tissue via enzymatic digestion requires careful consideration to prevent cleavage of surface proteins, particularly those markers necessary for identification. Additionally, tissue-resident cells emit unique and varied autofluorescent signatures that further complicate design and analysis. Furthermore, the expression levels of key surface receptors vary

across different tissues, ranging from low to extremely high, making fluorophore selection and cytometer setup crucial. Here we present an optimised multicolour immunofluorescence flow cytometry panel capable of defining LC, conventional (c) DC1, cDC2, DC3, plasmacytoid DC, Axl^+ $Siglec\text{-}6^+$ (AS)DC, monocytes and a variety of macrophages across a range of human peripheral tissues including skin, type II mucosae and intestine.

4.2 Introduction

The first cellular line of defence in the human immune system is dependent on the action of antigen presenting cells (**APCs**), which distinguish between antigens of pathogenic or commensal microbes. Mononuclear phagocytes (**MNPs**) are a phagocytic subgroup of professional APCs responsible for detecting and binding exogenous antigens via surface receptors and presenting them to naïve T cells. In human tissue, MNPs comprise of Langerhans cells (**LC**), macrophages, dendritic cells (**DC**) and monocytes. These cells are the sentinels of the innate immune response and are crucial for triggering adaptive immunity, including against the sexually transmitted viruses HIV and HSV.

MNP subsets and definitions, particularly in blood, are continuously evolving. When MNPs migrate into peripheral tissues, their phenotype and function can be altered by the micro-environment. Homeostatic human tissue-derived MNPs have been relatively well investigated, however, across different tissue types, MNP subsets have been defined using an inconsistent variety of markers. Furthermore, tissue MNPs from an inflammatory milieu remain poorly understood (9,39,181,182), specifically those that reside in anal and genital (anogenital) and colon and rectal (colorectal) tissues. Crucially, anogenital inflammation is highly associated with increased HIV and HSV transmission (164–168). This highlights the critical need to identify and characterise the MNPs residing not only in steady state but also inflamed human anogenital tissues. Utilising a flow cytometry panel that can consistently identify MNP subsets across different mucosal tissues will allow for a direct comparison of populations. This thorough characterisation will aid the development of improved mucosal vaccines and immunotherapy that target inflammatory MNPs (52) . Therefore, we have designed a 26-colour phenotyping panel to comprehensively phenotype all MNP subsets in both steady state and inflamed human tissues from both male and female genital tracts and the intestinal tract (**Table 4.1** and **Table 4.2**). Additionally, it should be emphasised that this phenotyping of MNP subsets across different tissue types, particularly the inflammatory subsets, is both novel and highly exploratory. This represents the first investigation of these cells in these tissues. While some populations

were not detected during optimisation, the limited number of samples analysed limits any definitive conclusions about their presence or absence.

Human sexual transmission sites are either skin, type II mucosa or type I mucosa. All three tissues consist of a surface epithelium and an underlying layer of connective tissue referred to as dermis for skin and lamina propria for type I and II mucosa. Skin (trunk skin, often used as a model, outer foreskin, labia, glans penis and the anal verge) is relatively impermeable to pathogens as it contains a stratified squamous epithelium and a surface layer of keratinized dead cells (stratum corneum). Type II mucosa (vagina, ectocervix, inner foreskin, fossa naviculars and anal canal) similarly comprises a stratified squamous epithelium but lacks or has a thin stratum corneum. Type I mucosa (endocervix, penile urethra, rectum and all intestinal tissues) comprises a single layer of fragile columnar epithelium and is most vulnerable to pathogen invasion. Importantly, inflamed skin and mucosa often loses integrity of the tissue barrier (183–185). This results in pathogens having direct access to the underlying tissues and the complement of MNPs found therein, including inflammation specific MNP subsets. Access to all human anogenital and colorectal tissues in this study was facilitated by extensive collaborations with surgeons across the Western Sydney Local Health district. Using our previously optimised tissue digestion protocols (8,163), MNPs were liberated from these tissues in a functionally intact state (**Figure** 4.1).

To ensure the accurate assessment of the MNP compartment, lymphocyte markers CD3 and CD19 were included to omit T cells and B cells respectively. HLA-DR, the marker of all APCs was also an essential inclusion.

LCs reside in the stratified squamous epithelium of skin and are defined by high expression of HLA-DR, CD207 (langerin) and CD1a, and low expression of CD11c (7,118). They are found in smaller proportions in type II mucosa and are absent from type I mucosa. Previously, it was thought that LCs were the only MNP residing in epithelium, however Bertram et al. (7) revealed a previously overlooked steady-state MNP subset, the epidermal CD11c^{+} DC (HLA-DR^{+} CD11c^{hi} CD207$^{+/-}$ CD1a^{+}), which shared similarities with an epidermal DC previously identified in inflamed tissues (18,108). These epidermal CD11c^{+} DCs predominate over LCs in type II mucosal tissue (7) and are enriched in inflammation (18,108) . With CD11c being the key distinguishing marker between these epithelial LCs and DCs, its inclusion in this panel was crucial.

DCs predominantly reside in deeper dermal/lamina propria layers of human tissues. They are HLA-DR^{hi} expressing cells and can be divided into subgroups of conventional DCs (cDC) cDC1

and cDC2, as well as the recently defined DC3 (39–42). cDC1s are functionally and phenotypically quite distinct from other DCs, as they are resistant to HIV infection (186). They are clearly distinguishable by their expression of XCR1 (39,182). In skin and type II mucosa, cDC2 identification has become increasingly difficult. They share a distinctive phenotypic similarity with DC3s and *in vivo* monocyte-derived DCs (**MDDC**), all of which are $CD11c^{+}$ and $CD1c^{+}$, markers which were previously used to exclusively identify cDC2s. Therefore, historical cDC2 classifications need re-evaluation to ensure their accurate isolation from other MNPs (39–42,117,118). Adding further complexity, MDDC and DC3 populations both express CD14 (9,38,39), and DC3s and MDMs both express CD163 (39). However, when comparing between these three $CD11c^{+}$ $CD1c^{+}$ DC subsets, precise identification of cDC2s is achieved by first isolating DC3s based on their CD163 expression ($CD163^{+}$ $CD14^{+/-}$), before dividing the remaining cells according to their CD14 expression: MDDC (CD14+) and cDC2 ($CD14^{-}$ $CD207^{+/-}$). In type I mucosa, cDC2s are distinguishable from DC3s and MDM subsets ($CD14^{+}$) by these markers, in addition to CD172a (139,140,163) .

In human skin and type II mucosa, $CD14^{+}$ macrophages are divided broadly into tissue resident macrophages (**Macrophage**) identified by their high autofluorescence, and non-autofluorescent monocyte-derived macrophages (**MDM**), derived from migrated monocytes. In type I mucosal tissues, based on intestinal macrophage subsets defined by Bujko et al (109), macrophages were divided into **MDM**s ($CD11c^{+}$ HLA-DR^{lo}), MDMs transitioning to a tissue-resident phenotype: transitional-MDMs (**t-MDM**) ($CD11c^{+}$ HLA-DR^{+}), and tissue-resident macrophages (**Macrophage**) ($CD11c^{-}$ HLA-DR^{+}). Calprotectin (S100A8/S100A9), in addition to CD88 and CD16, were included to identify and characterise infiltrating monocytes and monocyte-derived cells (41,109,187). To further assist in macrophage subset differentiation, lectin receptors CD169 (Siglec-1), CD206 (Mannose Receptor) and CD209 (DC-SIGN) were included as they are associated with a tissue-resident phenotype. Previously, CD169 and CD209 were thought to be markers specific to DCs (20,72,80), however, Rhodes et al. (9) revealed that they are important phenotypic markers for tissue macrophages.

One of the central aims of this panel was to more comprehensively identify and phenotype inflammatory MNPs present in inflamed anogenital tissues (169). $CD123^{+}$ pDCs are a known MNP that infiltrate into inflamed tissues. However, owing to the advances of single-cell RNA sequencing technologies a novel population of cells was distinguished from the pDC lineage, identifiable by their expression of Axl and CD327 (Siglec-6), termed ASDCs (39)/pre-pDCs (112,131). These ASDCs can be further divided into $CD123^{hi}$ and $CD11c^{low}$ populations.

Importantly, a recent study demonstrated that ASDCs reside in human anogenital tissues exclusively in the context of inflammation, revealing their presence in inflamed rectums of ulcerative colitis and diverticulitis patients, and their absence in healthy rectum (111). In inflammation, MDDCs are recruited to affected tissue sites and have been previously reported in skin (188), nasal mucosa (189) and anogenital tissues (12). As detailed earlier, these cells are $CD14^{+}$ $CD1c^{+}$ cells, but in an inflammatory context they have also been described to express CD1a, CD206 and CD11b (181,190). CD14 expression has also been linked to inflammatory DC3s ($CD5^{-}CD163^{+}CD14^{+}$) which have been shown to accumulate in the blood and kidneys of lupus patients when compared to healthy donors (42,191), and they increased in numbers in psoriatic skin (192) and inflamed broncho-alveolar lavage (193). Another key feature of tissue inflammation is cell cycling and division, and migration out of tissue. To evaluate DC proliferation and migration, we included the intracellular marker KI67 to assess cellular proliferation (194) and the chemokine receptor CCR7 required for DC maturation and migration to lymph nodes (195).

4.2.1 Similarity to other OMIPs

Several previously published OMIPs have focused on broadly characterising the immune cell composition of human PBMCs, in which some DC subsets and monocytes were identified (OMIP-024, OMIP-042, OMIP-051, OMIP-069, OMIP-078, OMIP-102, OMIP-104). OMIP-044 is the only other OMIP which comprehensively phenotypes APCs, and was demonstrated in PBMCs, fresh human blood and fresh human non-lymphoid tissues. OMIP-102 only included PBMC samples, however, the marker CD45, a human tissue-derived leukocyte marker, was included for future tissue use. The only other three previous OMIPs specifically designed for and assessed in human tissue are, OMIP-070, identifying NK cells in human tumours, OMIP-082, identifying lymphoid cells in human intestinal tissue and OMIP-096, identifying T cells in human skin, intestine and type II mucosa. This OMIP is the first to characterise human tissue APCs and MNPs, across a range of human tissues (skin, type II and type I mucosa), specifically in the context of inflammation – making it broadly applicable to many human disease settings.

Table 4.1: Summary table for application of OMIP.

Purpose	Characterisation of human mononuclear phagocytes isolated from skin, type I and Type II mucosa.
Species	Human
Cell types	Colon, rectum, foreskin, vagina
Cross reference	OMIP-044, OMIP-070, OMIP-082, OMIP-096

Table 4.2: Reagents used for OMIP.

Specificity	Fluorochrome	Clone	Purpose
HLA-DR	BUV395	G46-6	MNP
CD16	BUV496	3GB	Monocyte
Siglec-1	BUV615	7-239	Macrophage
CCR7	BUV661	2-L1-A	Lymph node homing
CD14	BUV737	B-ly6	Macrophage, monocyte, MDM, MDDC
CD163	BUV805	GHI/61	DC3, macrophage
CD209	BV421	DCN46	Macrophage
Siglec-6	BV480	767329	ASDC
CD1a	BV510	HI149	Epidermal DC and LC
CD4	BV605	OKT4	Conventional CD4+ T cells
CD1c	BV650	F10/21A3	DC
CD11b	BV711	ICRF44	Macrophage, DC
Axl	BV785	108724	ASDC
CD11c	BB515	B-ly6	DC
CD3	NovaFluor Blue 660-120S	UCHT1	T cell dump
CD19	NovaFluor Blue 660-120S	HIB19	B cell dump
CD88	PerCP eFluor710	20/70	MDDC
CD206	RB780	19.2	DC, macrophage
Calprotectin	PE	MAC387	Monocyte, MDM
CD103	PE Vio615	REA803	Colorectal DC
CD123	PE-Cy5	6H6	pDC and ASDC
CD5	PE-Cy5.5	CD5-5D7	ASDC
CD207	PE Vio770	REA770	LC and CD207+ cDC2
XCR1	APC	S15046E	cDC1
Viability	FVS700	N/A	Live cells
KI67 biotin	Streptavidin Dylight800	MKI67/2465	Proliferating cells

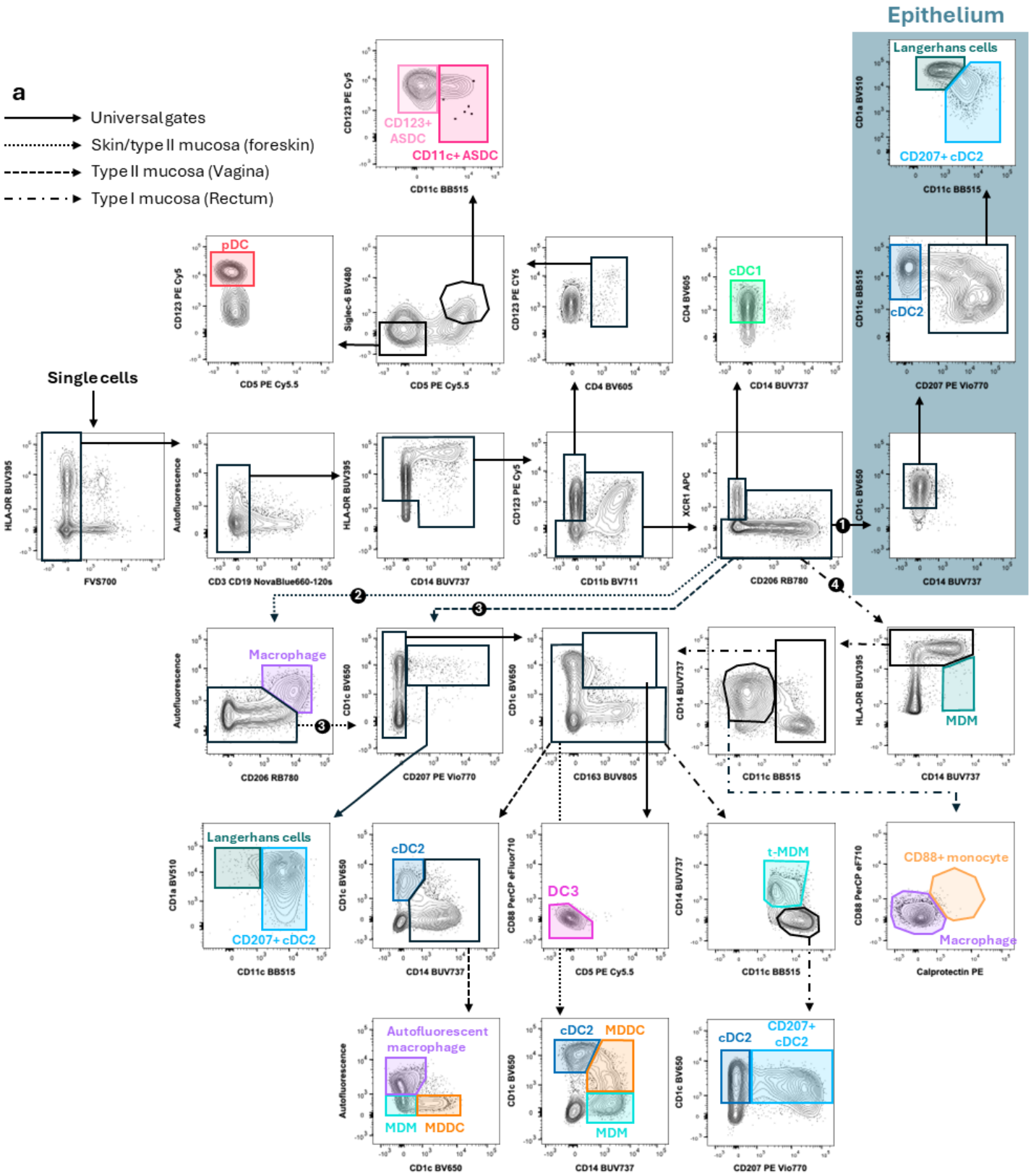

continued over page

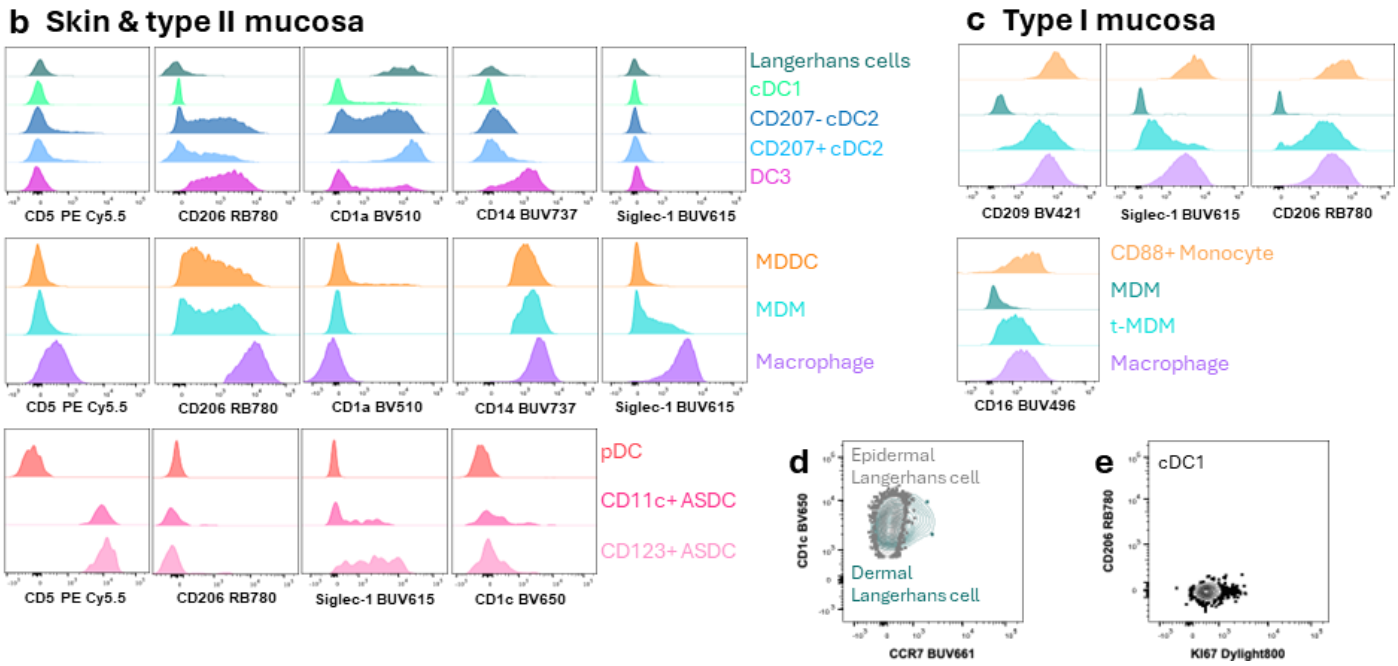

Figure 4.1: Gating strategy to identify mononuclear phagocytes (MNP) in human skin, type II and type I mucosal tissues. a) Cells were isolated from fresh colorectal and anogenital tissues, stained and acquired on a BD FACSymphony A5 instrument. Cells were gated on single cells (FSC-H vs FSC-A and SSC-W vs SSC-A), live cells (FVS700$^-$) and HLA-DR$^+$ cells. T and B cells were excluded using a CD3/CD19 dump gate against autofluorescence to account for any autofluorescent MNPs spreading into the CD3/CD19 channel. The infiltrating inflammatory cells are identified as CD123$^{+/int}$ CD11b$^-$ CD4$^+$. **pDC** are defined as Siglec-6$^-$ CD5$^-$ CD123$^+$, whilst **ASDC** are Siglec-6$^+$ CD5$^+$ and further divided by expression of CD11c. **cDC1** are gated as a population of XCR1$^+$ CD206$^-$ cells and defined as CD4$^+$ CD14$^-$. The XCR1$^-$ vs CD206 gate is divided into 4 different pathways. 1) Following the unbroken line is the gating strategy for the epithelium (highlighted in blue). After gating on CD1c$^+$ CD14$^-$ cells the **epidermal cDC2** are identified as CD11c$^+$ CD207$^-$, the **epidermal CD207$^+$ cDC2** as CD207$^+$ CD11c$^+$ CD1a^{lo} and **Langerhans cells** as CD207$^+$ CD11c^{lo} CD1a$^+$. 2) Following the dotted line for skin and type II mucosal tissues of the foreskin identifies the **macrophage** as autofluorescent$^+$ CD206$^+$, the autofluorescent$^-$ gate flows onto pathway number 3. 3) Following the dashed line for type II vaginal mucosa and dotted line for foreskin leads to the identification of CD207$^+$ CD1c$^+$ CD11c$^+$ **cDC2s** and migrated epithelial **Langerhans cells** as CD207$^+$ CD1c$^+$ CD11c^{lo} CD1a$^+$. 4) Following the dot-dash line of type I mucosa leads to the identification of HLA-DR^{lo} CD14+ MDMs and the remaining HLA-DR+ population flows onto a CD14 vs CD11c plot. The CD11c- CD14+ cells leads to the identification of Calprotectin$^+$ CD88$^+$ **monocytes** and Calprotectin$^-$ CD88$^-$ **Macrophages**. The CD11c+ portion of the CD14 vs CD11c plot along with pathways 2 and 3 all lead to the CD1c vs CD163 plot. **DC3** are defined as CD1c$^+$ CD163$^+$ CD88$^-$ CD5$^-$. The dashed line of type II vaginal mucosa identifies **cDC2** as CD1c$^+$ CD14$^-$, **MDDC** as CD14$^+$ CD1c$^+$ autofluorescent$^-$, **MDM** as CD14$^+$ CD1c$^-$ autofluorescent$^-$ and **autofluorescent macrophages** as CD14$^+$ CD1c$^-$ autofluorescent+. The dotted line of foreskin skin and type II mucosa identifies **cDC2s** as CD1c$^+$ CD14$^-$, **MDDC** as CD14$^+$ CD1c$^+$ and **MDM** as CD14$^+$ CD1c$^-$. The dot-dashed line of type I mucosa identifies t-MDM CD14$^+$ CD11c+, whilst the CD14$^-$ cells define the CD1c$^+$ **cDC2**, further split by their expression of CD207. **b)** Histograms of markers expressed by MNPs in skin and type II mucosa divided into dendritic cell subsets, monocytes and macrophages and inflammatory cells. **c)** Histograms of markers expressed by monocytes and macrophages in type I mucosa. **d)** Representative outer foreskin plot of the expression of migratory marker CCR7 on Langerhans cells in the epidermis compared to the Langerhans cells that migrate into the dermis. **e)** Representative inner foreskin lamina propria plot of cellular proliferation marker KI67 on a cDC1 population.

4.3 Supplemental: Development Plan

We developed a 26-parameter human tissue mononuclear phagocyte (MNP) panel for a BD FACSymphony A5 cytometer, equipped with 8 lasers and 48 detectors. The configuration of this cytometer can be found in **Online Table 1**. All reagents for the final panel are listed in **Online Table 2**. All iterations of the panel are summarised in **Online Table 3**. All reagents tested but not present in the final panel are listed in **Online Table 4**. All compensation controls are listed in **Online Table 5**. All titration staining panels are listed in **Online Table 6**. All reagents were titrated on fresh human abdomen, labia, colon, small bowel, lymph node, or Pan-DC selected PBMC as outlined in **Online Figure 1**.

4.3.1 Considerations for flow cytometry on MNPs isolated from human tissues

The main objective of this panel was to define all known mononuclear phagocytes (MNP) in all tissues associated with sexual transmission of disease. This consists of three tissue types: skin (labia, outer foreskin, glans penis and anal verge), type II mucosa (vagina, ectocervix, inner foreskin, fossa navicularis and anal canal) and mucosa type I (endocervix, penile urethra, colon and rectum). Markers were included that would be able to isolate specific inflammatory MNPs found exclusively in inflamed tissue, as well as markers known to have variable expression across different tissues and disease states to ensure that this panel could be used not only on homeostatic or steady-state samples, but also in a variety of different inflammatory and disease settings. Importantly, this panel was designed to work with specific tissue digestion protocols. Utilising a low-tryptic activity digestive enzyme, namely collagenase type 4 (Worthington) and neutral protease (Dispase, Worthington), limits the cleavage of surface protein markers for accurate characterisation, while short digestive incubations enable the isolated cells to be preserved in their *in situ* state (8,163,196,197). These digestion protocols, optimised for each unique tissue, are specified in this document.

4.3.2 Marker selection and expression on tissue MNPs

The challenges for designing a comprehensive dendritic cell (DC) and macrophage fluorescent flow cytometry panel that work across a range of human tissues, including skin, type II mucosa and type I mucosa is three-fold:

1. Understanding the biological expression patterns of all markers across each cell population in such varied tissue settings.

2. Designing a panel that accounts for the variation in antigen expression across tissue-types and tissue donors, ranging from extremely high, to very low or no expression.
3. Accounting for the high autofluorescent of some MNPs, particularly macrophages.

Our lab has spent 30 years isolating and researching DCs and macrophages from a vast range of human tissues, and through experience working with these cells, have accumulated an extensive knowledge of biological expression patterns. However, as the panel included a novel combination of markers and fluorophores, some marker expressions across different cell populations and tissues were initially uncertain. Specifically, several newly defined MNP populations in human blood or skin had not yet been characterised in mucosal tissues. it was unclear whether these populations were (1) present in mucosal tissues, and (2) whether their defining markers displayed the same expression patterns in mucosa. To address this, we relied on known expression patterns and conducted iterative testing to clarify the expression of each marker on specific cell types across various tissues to accurately identify the similar MNP subsets in different tissues. Optimisations for this panel were performed on both non-inflamed and inflamed samples at each iteration to ensure that all marker expression differences were considered.

4.3.3 Iteration 1

To start, utilising our experience and knowledge, and references from the literature, we investigated the marker expression across all our target cell populations (**Online Table 7**). After identifying which markers were expressed by each cell type, together with the preliminary stain index run on our BD Symphony A5 (**Online Table 8**), we first assigned the markers HLA-DR (as it is high on all cell types), all markers that were exclusive to only 1-2 cell types, or those of limited fluorophore availability. Additionally, as we have experience with autofluorescent macrophages, and understood that while autofluorescence can be excited by all lasers and emits over a broad range of wavelengths, the 700-800 emission detectors captured less autofluorescence across all the tissues (**Online Figure 2)**. Therefore, the important macrophage markers were allocated to the 700-800nm emission range. As we had previously designed panels for the Symphony to identify MNPs in various tissues, we already had optimised fluorophore/marker combinations for the backbone of MNP defining markers, which we utilised where possible.

HLA-DR BUV395 (U379) – HLA-DR is highly expressed by all MNPs. BUV395 was considered the best place for this marker as it has minimal spectral spillover into other channels and has been successfully used in our lab previously across multiple MNP panels.

CD123 PE-Cy5 (Y670) – CD123 is highly expressed by pDCs and ASDCs (and basophils). PE-Cy5 is a very bright fluorophore that can cause problematic spread. As pDCs and ASDCs represent a very small proportion of MNPs in inflamed tissue and have mutually exclusive defining markers to other DCs and macrophages, CD123 was assigned to PE-Cy5.

XCR1 APC Fire 750 (R780) – XCR1 is the only marker we found to consistently work in identifying human tissue conventional (c) DC1s, having previously tested and found CLEC9A and CADM1 to be poor DC markers when isolated from human skin (8). Whilst CD141 (BDCA3) works well in human body skin, we found it does not work well in human intestine (163). Additionally, CD141 is problematic as its expression can be induced on maturing cDC2 (8). The XCR1 clone S15046E is the only clone we have found to work successfully in tissue isolated DCs and has limited fluorophore availability. We assigned XCR1 to APC Fire 750 with the objective that XCR1 positive cDC1s would not be impacted by the mutually exclusive cDC2 and macrophage markers assigned to the 750 – 800 emission detectors.

CD207 (langerin) PE Vio770 (Y780) – CD207 is highly expressed by Langerhans cells (LC), with a spread of low to high expression on some cDC2s. As CD207 is a C-type lectin binding receptor capable of antigen capture, we wanted to capture all $CD207^{+}$ cDC2s, even at low expression levels. Both the Beckman Coulter clone DCGM4 (198) and the Miltenyi clone MB22-9F5 (8,163) are effective in human tissue. With limited fluorophore availability and previous success using PE Vio770 to detect low expression, we assigned CD207 to PE Vio770.

Since there are multiple highly expressed markers on MNP from human tissue, we minimised spread into lowly expressed markers by saturating one wavelength range with the highest expressed markers. We chose to detect these markers on a higher wavelength (around 750-800nm) due to significant spectral spillover in this range. Since CD207 and XCR1 were already within this range, we chose markers that would either be higher in the gating strategy or not expressed on LCs, cDC2s and cDC1s, ensuring optimal resolution for these markers.

Axl BV786 (V820) – Axl was needed to define ASDCs. As there is considerable spread into the BV786 channel from other fluorophores, and it was initially thought ASDCs did not express many macrophage markers we intended to allocate to the 780-800 emission detectors, we assigned Axl to BV786. However, Axl is also expressed by macrophages, and since it was allocated to a saturated wavelength, the resolution of Axl on macrophages was somewhat sacrificed.

CD14 APC Fire 810 (R820) – CD14 is a critical macrophage marker with variable expression and hence it was important to choose a fluorophore that was moderately bright and not greatly

affected by autofluorescence. Additionally, very few markers were available on APC Fire 810 when this panel was initially designed. As CD14 is not expressed by cDC1s (with XCR1 APC Fire 750 assigned on R780), and there is limited expression of CD207 (assigned to PE Vio770 on Y780) on $CD14^+$ cells, CD14 APC Fire 810 was chosen.

CD11c BUV737 (U740) – CD11c is predominantly a marker for DCs, although it has variable expression on some macrophages. This made high resolution and accurate identification of CD11c+ cells crucial. BUV737 is a bright fluorophore and has little spillover into other channels, hence, CD11c was placed on BUV737.

CD163 BUV805 (U820) – CD163 is traditionally recognised as being highly expressed by macrophages. However, recently CD163 has been determined a key identifying marker for DC3s, though it's expression on these cells is dimmer. As BUV805 is a relatively bright fluorophore, has little autofluorescent signal, and minimal spillover into other channels, it was chosen for CD163.

Viability stain (FVS700, R730) – As this panel is designed for enzymatically digested tissue, there is generally a higher proportion of cell death, so definitively identifying live cells is crucial. FVS700 has consistent and accurate staining and importantly, has limited macrophage autofluorescence interference, which we experienced with other viability stains such as FVS UV440. Additionally, the fluorophores available on the Red 730/45 detector are relatively dim or suboptimal, making FVS700 a suitable choice.

CD11b BV711 (V710) – CD11b is a useful marker for gating macrophage populations and is occasionally expressed by cDC2s and DC3s. BV711 is not impacted by our main macrophage marker CD14 on APC Fire 810, so CD11b BV711 was objectively a good choice.

CD209 (DC-SIGN) BV421 (V427) – CD209 is a C-type lectin receptor important for antigen capture (particularly HIV). Importantly, we have previously found this marker to be sensitive to cleavage and difficult to detect when on a dull fluorophore. Therefore, we assigned CD209 to BV421, as it is a very bright fluorophore with limited spillover.

CD1a BV510 (V525) – CD1a is an antigen presentation marker extremely highly expressed by LCs and highly expressed by cDC2s. While BV510 can be a challenging fluorophore due to its dullness, our decade long experience using CD1a on BV510 has consistently yielded excellent detection of LCs and cDC2 from skin. Therefore, we opted to keep this reliable marker/fluorophore pair.

CD327 (Siglec-6) BV480 (V474) – CD327 is exclusive to ASDCs (also expressed on some granulocytes and B cells) and an important marker to delineate these cells. ASDCs had not been identified in human tissues when this panel was first designed so biological expression patterns had only been identified from blood-derived ASDCs. We assumed these cells did not express CD209 or CD1a, which were already assigned to either side of BV480 and would cause some spillover into this channel. Therefore, we assigned CD327 to BV480.

Slan (M-DC8) PE (Y586) – Slan/ M-DC8 is exclusive to Slan+ inflammatory monocytes and when this panel was designed, PE was the only fluorophore conjugate available for this marker.

FcεR1α AF488 (B515) - FcεR1α was identified by Duterte et al (42) as an important marker for defining tissue cDC2s, later confirmed in blood by Mair & Liechti et al (182). We had previously shown that the clone 9E1 worked well in human intestine and was vastly superior to the clone AER-37 (163). Clone 9E1 had limited availability so was assigned to AF488, which received minimal spillover from other channels.

CD103 PE Vio615 (Y610) – CD103 is an important marker previously used to identify cDC1s and a subset of cDC2s in human intestine (139,163). It is also present on lymphocytes including intraepithelial ILC1-like cells (196) and T cells (197). We had previously identified the REA803 clone to be more resistant to enzymatic cleavage and more reliable in detecting CD103+ cells isolated from tissue compared to the Ber-ACT8 clone (197). The REA803 clone had limited availability, therefore we assigned it to PE Vio615. Importantly, it was thought that CD103+ DCs would not express Slan (PE fluorophore).

CD1c BV650 (V677) – CD1c is an essential marker for defining cDC2s and DC3s. The primary sources of spillover into this channel were markers expressed on other cell types or at low levels. Additionally, our previous experience with this antibody-fluorophore combination demonstrated reliable resolution.

CD16 BV570 (V586) – CD16 is predominantly expressed by certain macrophage populations (and useful for distinguishing neutrophils in inflamed tissues). Although dull, we had previously used BV570 in another panel to detect $CD16^{+}$ macrophages in human lymph nodes.

CD3/CD19 NovaBlue660/120S (B670) (dump) – The predominant immune cell populations from digested tissue are T cells and B cells. As these cells express markers that are co-expressed by MNPs, their identification and exclusion was necessary. The Blue 670/30 channel has limited fluorochrome availability and presents challenges with other channels, particularly

autofluorescence, making it a suitable place for a dump channel. CD3 and CD19 were both available on NovaBlue660/120S and were assigned accordingly.

CD89 BB700 (B710) – CD89 was included to aid in identifying monocytes, as CD88 and CD89 have recently been described as monocyte markers (42,182). Since the expression of CD89 was low, a bright fluorophore was chosen. BB700 spills into multiple channels, however, since CD89 is only expressed on newly emigrated monocytes, spillover from this channel is expected to have minimal impact.

CD169 (Siglec-1) BUV615 (U610) – CD169 is a pattern binding receptor, important in binding pathogens such as HIV (52,169), with moderate to high expression on tissue macrophages. Since $CD103^+$ populations (assigned to PE Vio615 on Y610) exhibit little to no CD169 expression, BUV615 was deemed a suitable option for this marker.

Calprotectin (S100A8/9) AF594 (O616) – Calprotectin, traditionally an intracellular marker, was included to gate newly emigrated blood monocytes, though it is also highly expressed by intestinal monocyte-derived macrophages (MDM) (109,163). Calprotectin can also be upregulated in DCs in inflammation (199).

CD45 BB790-P (B820) – CD45, present on all immune cells, had previously performed well on BB790-P when the antibody titre was kept low to limit spread into other channels (196). At the time of initial panel design, fluorophore availability on this channel was limited. Therefore, we maintained a low antibody concentration to just sufficiently resolve $CD45^+$ cells while minimising impact on other detectors.

CD5 PerCP Cy5.5 (Y710) – CD5 is a key defining marker for ASDCs and used to identify a subpopulation of cDC2. This CD5 PerCP Cy5.5 antibody was successfully used on a blood myeloid panel by Mair & Liechti (182), making it a strong choice for our panel.

CD4 BV605 (V610) – CD4 is widely expressed on tissue MNP populations, including DCs and macrophages, and has long been used to identify antigen presenting cells in peripheral tissues (200). While CD4 is ubiquitous, it is relatively dim on MNPs, hence BV605 was selected as a bright fluorophore to resolve MNP populations without interfering with gating on other cell populations.

CD206 (MR) BV750 (V750) – CD206 is a key C-type lectin receptor often used to distinguish macrophage and DC subsets in tissue. It is not expressed in blood-derived cells but has variable expression in tissue. As BV750 was one few remaining spots available in the 700-800 emission

range and we wanted to saturate this wavelength with macrophage markers, it was a suitable fluorophore for CD206.

CD86 APC (R670) and CCR7 BUV661 (U670) – The Red 670/30 detectors and UV 670/30 detectors were chosen to measure functional markers relating to DC maturation and activation. BUV661, a bright fluorophore, has spillover into the Red 670/30 detector; however, CCR7 expression is relatively low compared to many other markers on MNPs, making this a suitable assignment. Based on our experience, CD86 is the most differential of the three maturation markers (CD80, CD83 and CD86) and commonly used to assess DC maturation status. Therefore, we placed CD86 on APC with the potential to swap for other markers of interest.

HLA-DQ BUV563 (U586) – HLA-DQ was included based on findings from Duterte et al (2019) (42), which demonstrated that FcεR1α and HLA-DQ could effectively delineate cDC2s. While BUV563 posed a problematic interference risk with Slan PE, the impact was minimised by the fact Slan+ monocytes were the only subset expressing Slan, reducing the likelihood of significant spillover from the highly expressed HLA-DQ.

Autofluorescence Blue 610/20 – Once all the other fluorophores were allocated, we evaluated the remaining channels for their autofluorescence detection. B610 was a good candidate as autofluorescence has a strong peak around 600nm and this channel has limited fluorophore availability.

One detector was left intentionally open in this first iteration design. U515, most often used with BUV496, was chosen as this fluorophore is dim and has minimal spillover. Keeping this spot open provided flexibility to relocate any highly expressed markers that proved problematic in subsequent iterations. We also optimised blocking reagents to reduce non-specific antibody binding to Fc receptors on MNPs (**Online Figure 3**). Following the recommendations of Kristensen et al. (201), we utilised a dual-blocking approach by titrating Human Antibody serum and Oligo-block to suit our tissue samples.

4.3.4 Iteration 2

Once the markers were titrated and the panel run on samples, it became apparent that our objective to restrict the most severe spillover to the 700-800 wavelengths was more problematic than expected. We encountered extreme spillover and difficulty achieving good resolution on CD14 APC Fire 810 and CD45 BB790, despite extensive optimisation of acquisition voltages and attempts to maintain a low antibody concentration, as per our previous successful experiments

on lymphocytes (**Online Figure 4a**). Additionally, excessive spillover in the red detectors prevented the resolution of viability on FVS700 (R710) (**Online Figure 4b**). To address this, we repositioned several markers to attempt to improve gating and resolution. HLA-DR was moved to APC Fire 810 (R820) to shift the spillover from this fluorophore higher in the gating strategy. CD14 was moved to BUV737 (U740), a well-established position used in our previous panels, and CD11c, originally on BUV737, was moved to BUV395 (U379) – the spot previously held by HLA-DR.

Additionally, markers assigned to the 600-670nm wavelength were challenging to resolve. The markers causing spillover were CCR7 BUV661 (U670), CD103 PE Vio615 (Y610), CD169 BUV615 (U610) and Calprotectin AF594 (O616) (**Online Figure 5**). Of these markers, Calprotectin had the brightest signal, significantly brighter than originally anticipated for such a relatively dull fluorophore. We endeavoured to minimise this signal by switching from intracellular staining to surface staining, which we had performed successfully in previous panels to decrease calprotectin signal. As we preferred to keep CD103 and CD169 on their assigned detectors, we opted to removed CCR7 from this iteration. This allowed a more accurate assessment of how the calprotectin staining change impacted the two markers. We additionally included Ki67 to the panel assigned to Dylight 800 (N820), using a biotinylated anti-Ki67 to accommodate for this very dim detector. The biotinylated Ki67 conjugated to Dylight 800 was not used in our initial testing to simplify the workflow by avoiding the more complex two-step intracellular staining procedure.

We observed that the CD16 signal was not bright enough on tissue cells to resolve with BV570. Accordingly, we moved CD16 to BUV496, the fluorophore we had left unallocated for necessary changes. Furthermore, we replaced CD89 with CD88 as our designated monocyte marker as CD88 proved a more reliable marker in tissue (**Online Figure 6**). While we kept it in the same detector (Y710), we could only source it on PerCP-efluor710.

4.3.5 Iteration 3

Despite the changes made in the previous iteration, spillover issues persisted, particularly for markers allocated to the ~600 and ~800nm wavelengths. APC Fire 810 exhibited the most troublesome spillover at its wavelength, leading us to exclude it from the panel. As a result, HLA-DR was moved back to BUV395 (U379), displacing CD11c, which we moved to BB515 (B515), removing FcεR1α from the panel. We further found HLA-DQ BUV563 to be highly expressed by most tissue antigen presenting cells and not exclusively cDC2s. Given its brightness, this caused greater spectral spillover errors than anticipated. Since HLA-DQ contributed little phenotypic

information whilst introducing significant compensation and spreading errors, it was removed from the panel. We also decided to move CD45 from the ~800 wavelength as we were unable to maintain a consisting low staining across highly varied tissues. Due to its high expression and limited alternative placement options that would not cause spreading errors, we posited it could be effectively resolved on AF350, utilising a previously unused dim detector (U450).

Additionally, we observed that the three macrophage markers on adjacent Violet detectors: CD11b BV711 (BV711), CD206 BV750 (V750) and Axl BV756 (V820), were spilling into each other and compromising their resolution. To introduce more space into this wavelength we removed the middle marker and reassigned CD206 to RB780 (B820), which became available after moving CD45 from BB790. Additionally, RB780 had a tighter spectral footprint than BB790, further reducing panel interactions.

Despite reducing the calprotectin signal by utilising surface staining, the interactions between AF594 and CD103 PE Vio615 and CD169 BUV615 still posed a problem as spillover persisted at the voltages required for optimal marker resolution. Given our previous success using Calprotectin on PE (Y586) (163), we reassigned it to this fluorophore. Slan was subsequently relinquished to accommodate this change, meaning Slan$^+$ monocytes could no longer be specifically identified. However, as Calprotectin no longer occupied the ~600 wavelength, we reintroduced CCR7 BUV661 to this iteration, as we anticipated the overall changes would now accommodate its inclusion.

4.3.6 Iteration 4

For CD45 AF350, we found two available pre-conjugated clones (I430I and I430u). After testing and titrating, we found clone I430u to most effectively resolved CD45$^+$ cells and selected a high concentration to provide the best resolution to account for donor variability (**Online Figure 7a**).

However, from the first run of the previous iteration, it became clear that CD45 could not be reliably resolved on AF350 with the current panel, even after multiple titrations attempts across different tissue donors. We conducted FMO comparisons and examined CD45$^+$ selected cells (but not stained for CD45 AF350) and were still unable to resolve the CD45$^+$ cells.

With no other suitable alternative for CD45 in the panel, we decided to remove it. We were confident we could use HLA-DR in combination with FSC and SSC for gating strategies and determined CD45 was not essential for identifying our target populations (**Online Figure 7b**).

Moving Calprotectin from AF594 to PE corrected the resolution issues with Siglec-1 BUV615 and CD103 PE Vio615 (**Online Figure 8**). However, this correction revealed another previously masked problem – XCR1 was not being properly resolved on APC Fire 750. Among the only three available fluorophores for our selected clone; PE, BV421 and APC, we determined APC (R670) to be the most suitable option. This meant sacrificing CD86 from the panel as we were hesitant to disrupt other successfully working markers. These final adjustments allowed for the resolution of all markers and creation of gating strategies across all tissue types. The final spillover matrix is provided in **Online Table 9**.

Separate gating strategies identifying all known MNPs have been created for skin (**Online Figure 9**), type II mucosa (**Online Figure 10**) and Type I mucosa (**Online Figure 11a**), considering the MNP subsets present in each tissue. All MNP subsets across the different tissues were identified with the same defining markers regardless of gating order.

4.3.7 Correction of Autofluorescence post-acquisition

While spectral flow cytometry enables background signal correction in the acquisition software, conventional flow cytometry lacks this capability. As such, an unstained donor-and-tissue-matched sample is necessary to be acquired with all samples. This sample serves as an exogenous single-colour control and, when added to the bead controls to create a new compensation matrix, removes spilled autofluorescence signal while allowing it to be quantified in its allocated detector (163) . All gating strategies presented in this OMIP have been designed on autofluorescence corrected samples. As gut tissue has the highest autofluorescence of all the tissues contained herein, an example gating strategy without autofluorescence correction has been included in **Online Figure 11b**.

4.3.8 Tissue digestion and Flow Cytometry Staining Protocol

Materials

- Roswell Park Memorial Institute (RPMI) 1640 (Lonza, Switzerland)
- Neutral Protease (Dispase) (Worthington, USA)
- Gentamicin (Life Technologies, USA)
- Dulbecco’s Phosphate-Buffered Saline (PBS) without Ca2+ and Mg2+ (Lonza, Switzerland)
- Collagenase Type IV (Worthington, USA)
- DNase I (Sigma-Aldrich, USA)
- Ficoll-Paque Plus (GE Healthcare, USA)

- Human AB serum (Sigma Aldrich, USA)
- Phosphorothioate-oligodeoxynucleotides (Oligoblock) (Sigma-Aldrich, USA)
- Brilliant Stain Buffer PLUS (BD Bioscience, USA)
- EDTA (Sigma-Aldrich, USA)
- Sodium azide (Sigma-Aldrich, USA)
- Cytofix (BD Biosciences, USA)
- Cytofix/Cytoperm (BD Biosciences, USA)
- Foetal Bovine Serum (FBS) (Sigma-Aldrich, Missouri, USA)
- Dithiothreitol (DTT) (Sigma-Aldrich)
- Derma Carriers Skin Graft Carriers, (Zimmer, USA)
- Zimmer Skin Graft Mesher, (Zimmer, USA)
- MACSmix Tube Rotators, (Miltenyi Biotec, Germany)
- Easy Strainer 100 µm, (Greiner Bio-One, Austria)

Solutions

- **FACS wash:** PBS supplemented with 0.1% w/v sodium azide + 2 mM EDTA + 1% v/v human AB serum (filter sterilised)
- **Perm Wash:** PBS supplemented with 1% w/v BSA + 0.1% w/v saponin + 0.1% w/v sodium azide + 1% v/v FCS
- **RF10:** 10% FBS in RPMI 1640
- **Epithelial Strip Solution:** 0.3% DTT and 2 mM EDTA in RF10
- **Collagenase Solution 1:** 525 U/mL Collagenase IV with 750 U/mL DNase I in RPMI
- **Collagenase Solution 2:** 640 U/mL Collagenase IV with 750 U/mL DNase I in RPMI
- **Dispase Solution 1:** 0.8 mU/mL Dispase in RPMI with 50 ug/mL Gentamicin and filter sterilised with 0.22 µm filter
- **Dispase Solution 2:** 1.6 mU/mL Dispase in RPMI with 50 ug/mL Gentamicin and filter sterilised with 0.22 µm filter

Intestinal tissue digestion (type I mucosa) (as per **Chapter 2**)

4. Using curved surgical scissors and forceps, remove any staples, open intestinal tube, and clean with PBS if necessary.
5. With the luminal surface on a PBS-dampened cutting board, remove any fat or mesentery.

6. Remove the muscle layer in small strips with surgical scissors and forceps, keeping the tissue section whole, and leaving the entire submucosal thickness.
7. Use a scalpel to cut the tissue into 5 mm x 5 mm square pieces and place in 50 mL Falcon tube, no higher than the 5 mL mark.
8. Add 20 mL of Epithelial Strip Solution into the tube containing the tissue.
9. Vortex for 10 seconds and incubate for 15 mins in 37°C water bath.
10. Using tea strainer, strain tissue into a waste container to remove epithelial components and place tissue back in the tube, a P1000 pipette tip can be used to manoeuvre the tissue.
11. Repeat steps 5-7 once more.
12. After second epithelial strip solution is removed, wash tissue briefly in PBS and strain again, placing the tissue into a clean 50 mL Falcon tube.
13. To the tissue, add 20 mL Collagenase Solution 1.
14. Vortex for 10 seconds, seal tube with Parafilm, and incubate for 30 mins at 37°C (incubator) in a rotator, placing the tubes askew to maximise movement in the tube.
15. Strain tissue with tea strainer, collecting the cell suspension in a new 50 mL Falcon tube, placing the tissue back into its original tube.
16. Repeat steps 6-8 with the tissue tube.
17. Dilute the collected cell solution to 50 mL and pass over a 100 µm cell strainer, before a 5 minutes 300 x g spin.
18. Wash cells again in 50 mL PBS. Resuspend cell pellet in 5 mL RPMI and store on ice until second collection.
19. For second collections, strain tissue with tea strainer, collecting the cell suspension in a new 50 mL Falcon tube, placing the tissue back into its original tube.
20. Add 20 mL PBS to tissue and gently vortex to collect all liberated cells from the tissue. Strain tissue again into the same collection tube and discard tissue.
21. Repeat steps 14-15, combining the resuspended pellet with the pellet from the first collection for target cell enrichment.
22. Dilute the combined cells in 35 mL of RPMI, underlay with 15 mL of Ficoll-Paque, and centrifuge at 400 x g for 20 mins without breaks. Collect the cells from the RPMI:Ficoll interface using a transfer pipette and wash twice in PBS, first at 400 x g, then at 300 × g for 5 mins. Count the cells for staining on a haemocytometer.

Abdomen skin tissue digestion

1. Stretch skin samples until taut using large surgical forceps and graft to a 1mm thickness using a skin grafting knife.
2. Pass grafted skin through a skin graft mesher to increase the surface area and distributed evenly the resultant meshed skin across 50 mL Falcon tubes.
3. Fill each tube with 30 mL of **Dispase Solution 1** and incubate at 4°C on a rotator. Dispase cleaves the bonds between the epidermis and dermis. The following morning, place tubes in a 37°C water bath for 15 mins to initiate enzymatic activity.
4. Wash skin by dunking in 40 mL of PBS and using surgical tweezers peel the epidermis from the dermis. Keep the epidermis moist in a 50mL Falcon tube of PBS on ice. On peeling completion, centrifuge the epidermis (300 x g for 5 mins), tip off supernatant and cut epidermis into small pieces using long surgical scissors. Cut dermis into 5 x 5 mm pieces using a scalpel and collect in separate tubes, filled up to the 5 mL mark.
5. Fill each tube with 20 mL of warmed **Collagenase Solution 2** and incubate for 120 mins at 37°C on a MACSmix Tube Rotator. Collagenase liberates the cells from the connective tissue.
6. Collect the supernatants of each tube by pouring through a tea strainer. Wash the undigested tissue with 10 mL PBS and strain again. Filter the strained supernatants using a 100 µm cell strainer and centrifuge at 300 x g for 5 mins.
7. Wash the cells twice more using PBS (300 x g for 5 mins).
8. Count the dermal cells and resuspend in 100 µL PBS, ready for antibody staining.
9. Enrich the epidermal cells further using Ficoll-Paque. Resuspend the cells in 35 mL of RPMI, underlay with 15 mL of Ficoll-Paque, and centrifuge at 400 x g for 20 mins without breaks. Collect the cells from the RPMI:Ficoll interface using a transfer pipette and wash twice in PBS, first at 400 x g, then at 300 x g for 5 mins. Count the epidermal cells and prepare for staining.

Genital tissue digestion (skin and type II mucosa)

Genital skin and Type II mucosa samples cannot be grafted or passed through the skin graft mesher due to their small size.

1. Remove the underlying connective tissue and fatty layers using surgical scissors, thinning the sample to no more than 3 mm thick.
2. Make small cuts using a scalpel to mimic the action of a mesher.

3. Place the tissue in either a 50 mL or 15 mL Falcon tube, depending on sample size, and fill with **Dispase Solution 2** to a volume of either 30 mL or 10 mL accordingly.
4. From herein, process the tissue identically to abdominal skin from steps 3–8. Adjust all volumes to 10 mL if using a 15 mL tube.

Note: The epidermal cell yield from these samples is often low, and Ficoll-Paque enrichment in step 9 is only performed on a large pellet. In this case, resuspend the cells in 10 mL RPMI and underlay with 5 mL Ficoll-Paque.

Staining protocol

1. Place isolated cells in a 5 mL FACS tube in 100 µL PBS.
2. Stain cells with Fixable Viability Stain FVS700 for 30 mins at 4˚C.

Note*:* Set aside a small number of cells for an unstained control tube for each sample.

3. Wash cells with 2 mL FACS wash (300 x g for 5 mins) and resuspend in 100 µL.
4. Incubate cells with 10 µL human AB serum and 3.2 µL Oligoblock for 10 mins at 4°C in the dark.
5. Add the antibody cocktail containing all surface stain antibodies (outlined in **Online Table 2**) and 10 µL Brilliant Buffer PLUS per test (one test = 2.5 x 10^6 cells) without washing. Incubate for 30 mins at 4°C in the dark.
6. Wash cells twice with FACS wash.
7. Add 100 µL of Cytofix/Cytoperm to cells and incubate for 20 mins at 4˚C in the dark.
8. Wash cells once with Perm wash and repeat step 4.
9. Add biotin KI67 as per **Online Table 2** and incubate for 30 mins at 4˚C.
10. Repeat step 8 with two washes.
11. Add streptavidin DyLight800 as per **Online Table 2** and incubate for 30 mins at 4˚C.
12. Wash cells twice with Perm wash.
13. Repeat step 7 with 100 µL of Cytofix.
14. Wash cells with FACS wash and resuspend in 100 µL, ready for acquisition on FACSymphony A5.
15. Pass cells through a 100 µm cell strainer immediately before acquisition on the flow cytometer.

4.4 Supplemental: Online Tables

Online table 1: Instrument Configuration – BD FACSymphony A5

Laser	Wavelength [nm]	Laser Type	Laser Power [mW]	Dichroic mirror	Notch filter [nm]	Bandpass Filter [nm]	Spectral Range	Detector	Assigned Fluorochrome
Red	637	Solid State, OBIS 637 LX	140	800 LP		820/60 BP	800-850	R820	
				750 LP	785	780/60 BP	750-800	R780	
				685 LP		710/40 BP	690-730	R710	FVS700
				665 LP		670/30 BP	665-685	R670	APC
UV	355	Solid State, Genesis CX-355	100	800 LP	785	820/60 BP	800-850	U820	BUV805
				770 LP		780/60 BP	770-800	U780	
				710 LP		740/35 BP	722.5-757.5	U740	BUV737
				685 LP		695/40 BP	685-710	U695	
				635 LP		670/30 BP	655-685	U670	BUV661
				600 LP		610/20 BP	600-620	U610	BUV615
				570 LP	594	586/15 BP	578.5-593.5	U586	
				450 LP		515/30 BP	500-530	U515	BUV496
				410 LP		450/50 BP	425-450	U450	
						379/28 BP	365-393	U379	BUV395
Yellow	561	Solid State, OBIS 561 LS	150	800 LP		820/60 BP	800-850	Y820	
				750 LP	785	780/60 BP	750-800	Y780	PE Vio770
				685 LP		710/50 BP	685-735	Y710	PE Cy5.5
				635 LP		670/30 BP	655-685	Y670	PE Cy5
				600 LP		610/20 BP	600-620	Y610	PE Vio615
				570 LP	594	586/15 BP	578.5-593.5	Y586	PE
Blue	488	Solid State, Sapphire 488 LP	200	800 LP		820/60 BP	800-850	B820	RB780
				770 LP	785	780/60 BP	770-800	B780	
				735 LP		750/30 BP	735-765	B750	
				685 LP		710/50 BP	685-735	B710	PerCP eF710
				635 LP		670/30 BP	655-685	B670	NovaBlue 660-120s
				600 LP	594	610/20 BP	600-620	B610	
				505 LP		515/30 BP	505-530	B515	BB515
						488/10 BP	483-493	SSC	
Orange	594	Solid State OBIS 594 LS	100	635 LP		660/20 BP	650-670	O660	
				610 LP		616/23 BP	610-627.5	O616	

Laser	Wavelength [nm]	Laser Type	Laser Power [mW]	Dichroic mirror	Notch filter [nm]	Bandpass Filter [nm]	Spectral Range	Detector	Assigned Fluorochrome
Violet	406	Solid State, OBIS 405 LX	200	800 LP		820/60 BP	800-850	V820	BV786
				770 LP	785	780/60 BP	770-800	V780	
				735 LP		750/30 BP	735-765	V750	
				685 LP		710/50 BP	685-735	V710	BV711
				635 LP		677/20 BP	667-685	V677	BV650
				600 LP		610/20 BP	600-620	V610	BV605
				550 LP	594	586/15 BP	578.5-593.5	V586	
				505 LP		525/50 BP	505-550	V525	BV510
				450 LP		474/25 BP	462.5-485.5	V474	BV480
				410 LP		427/25 BP	415.5-438.5	V427	BV421
						405/10 BP	400-410	V405	Violet SSC
Indigo/ NIR Collinear	446/779	Solid State, OBIS 785 LX	75/100	800 LP		820/60 BP	800-850	N820	DyLight 800
				635 LP		660/20 BP	650-670	I660	
				600 LP		605/40 BP	600-625	I605	
				500 LP		515/30 BP	500-530	I515	
				450 LP		470/15 BP	462.5-477.5	I470	

Online table 2: Commercial reagents used in OMIP. All dilutions

Specificity	Fluorochrome	Clone	Catalogue #	Manufacturer	Dilution (µL) (antibody volume in µL/100µL of stain buffer per 2.5 x 10^6 cells)
HLA-DR	BUV395	G46-6	564040	BD Biosciences	1.5
CD16	BUV496	3GB	564653	BD Biosciences	2.5
Siglec-1	BUV615	7-239	751124	BD Biosciences	2
CCR7	BUV661	2-L1-A	749824	BD Biosciences	5
CD14	BUV737	B-ly6	612763	BD Biosciences	1
CD163	BUV805	GHI/61	749201	BD Biosciences	2
CD209	BV421	DCN46	564127	BD Biosciences	2.5
Siglec-6	BV480	767329	767329	BD Biosciences	1
CD1a	BV510	HI149	563481	BD Biosciences	1
CD4	BV605	OKT4	317436	Biolegend	4
CD1c	BV650	F10/21A3	742749	BD Biosciences	3
CD11b	BV711	ICRF44	301344	Biolegend	2
Axl	BV785	108724	747857	BD Biosciences	2.5
CD11c	BB515	B-ly6	564490	BD Biosciences	1.5
CD3	NovaFluor Blue 660-120S	UCHT1	H002T03B08-A	ThermoFisher scientific	0.5
CD19	NovaFluor Blue 660-120S	HIB19	H004T03B08-A	ThermoFisher scientific	2.5
CD88	PerCP eFluor710	20/70	46-0882-82	ThermoFisher scientific	2.5
CD206	RB780	19.2	755605	BD Biosciences	0.5
Calprotectin	PE	MAC387	MA5-28130	ThermoFisher scientific	4
CD103	PE Vio615	REA803	130-111-837	Miltenyi Biotec	2.5
C123	PE-Cy5	6H6	306008	Biolegend	0.5
CD5	PE-Cy5.5	CD5-5D7	MHCD0518	ThermoFisher scientific	0.5
CD207	PE Vio770	REA770	130-100-586	Miltenyi Biotec	1
XCR1	APC	S15046E	372606	Biolegend	4
Viability	FVS700	N/A	564997	BD Biosciences	0.01
KI67 biotin (Intracellular)	Streptavidin DyLight800	MKI67/2465	ab21811	AbCam	2.5 (KI67) 0.5 (Streptavidin)

Online table 3: Experiment iterations of panel development. Reagents that were removed after an individual iteration are highlighted in **blue**. Reagents that remained constant across all four iterations are highlighted in green.

		Iterations			
Detector	**Fluorochrome**	**1**	**2**	**3**	**4**
R670	APC	CD86	CD86	CD86	XCR1
R730	FVS700	LiveDead	LiveDead	LiveDead	LiveDead
R780	APC Fire 750	XCR1	XCR1	XCR1	
R820	APC Fire 810	CD14	HLA-DR		
U379	BUV395	HLA-DR	CD11c	HLA-DR	HLA-DR
U450	AF350			CD45	
U515	BUV496		CD16	CD16	CD16
U586	BUV563	HLA-DQ	HLA-DQ		
U610	BUV615	CD169	CD169	CD169	CD169
U670	BUV661	CCR7		CCR7	CCR7
U740	BUV737	CD11c	CD14	CD14	CD14
U820	BUV803	CD163	CD163	CD163	CD163
Y586	PE	Slan/ MDC8	Slan/ MDC8	Calprotectin	Calprotectin
Y610	PE Vio615	CD103	CD103	CD103	CD103
Y670	PE Cy5	CD123	CD123	CD123	CD123
Y710	PE Cy5.5	CD5	CD5	CD5	CD5
Y780	PE Vio770	CD207	CD207	CD207	CD207
B515	BB515	FcER1a AF488	FcER1a AF488	CD11c	CD11c
B610	Autofluorescence	Autofluorescence	Autofluorescence	Autofluorescence	Autofluorescence
B670	NovaBlue660 / 120S	CD3 CD19	CD3 CD19	CD3 CD19	CD3 CD19
B710	PerCP eF710	CD89 BB700	CD88	CD88	CD88
B820	RB780	CD45 BB790	CD45 BB790	CD206	CD206
O616	AF594	Calprotectin	Calprotectin		
V427	BV421	CD209	CD209	CD209	CD209
V474	BV480	CD327	CD327	CD327	CD327
V525	BV510	CD1a	CD1a	CD1a	CD1a
V586	BV570	CD16			
V610	BV605	CD4	CD4	CD4	CD4
V677	BV650	CD1c	CD1c	CD1c	CD1c
V710	BV711	CD11b	CD11b	CD11b	CD11b
V750	BV750	CD206	CD206		
V820	BV785	Axl	Axl	Axl	Axl
N820	Dylight 800		Ki67 biotin	Ki67 biotin	Ki67 biotin

Online table 4: Antibodies tested but not included

Specificity	Fluorochrome	Clone	Reason for inclusion	Reason for removal
CD89	BB700	A59	MDDC	CD88 was shown to be more reliable than CD89 in identifying tissue monocytes
CD45	BB790	HI30	All immune cells	The bright CD45 signal spilled over into too many detectors of a similar wavelength. Moved to AF350.
CD45	AF350	I430u	All immune cells	The signal from AF350 was not bright enough to be able to get clean separation, even at high titre
HLA-DR	APC Fire 810	L243	All MNPs	HLA-DR was moved to BUV395 after the bright signal spilled over into other detectors of a similar wavelength
CD14	APC Fire 810	63D3	Macrophage, monocyte, MDM, MDDC	CD14 was moved to BUV737 after the bright signal spilled over into other detectors of a similar wavelength
XCR1	APC Fire 750	S15046E	cDC1	XCR1 was moved to APC to reduce spillover in the red detectors
CD83	APC	HB15e	Mature DC	CD86 was removed from the panel to make space for XCR1 after it was removed from APCFire750
CD11c	BUV737	B-ly6	DC	CD11c was moved to BUV395 to make space for CD14 after it was removed from APCFire810
CD11c	BUV395	B-ly6	DC	CD11c was moved to BB515 to make space for HLA-DR after it was removed from APCFire810
FcER1A	AF488	9E1	cDC2	FcER1A was removed to free up the B515 detector for CD11c, after it was removed from BUV395
HLA-DQ	BUV563	Tu169	cDC2	HLA-DQ was removed with FcER1A as they were to be used in conjunction to isolate a subset of DC
Calprotectin	AF594	MAC387	Monocyte, MDM	Calprotectin was moved to PE as there was too much spillover with PEVio615 and BUV615
SLAN	PE	S15046E	Slan DC	SLAN was removed to free up the Y586 detector for Calprotectin, after it was removed from AF594
CD206	BV750	19.2	DC, macrophage	CD206 was moved to RB780 to reduce the spillover in the higher violet wavelength, allowing for better resolution of CD11b and Axl on BV711 and BV786 respectively

Online table 5: Compensation reagents. For each compensation control, 50 µL of positive and 5 0µL of negative beads were combined in a 5 mL FACS tube and washed (350 x *g* for 5 mins) in FACS wash (1% FBS (v/v), 2 mM EDTA, 0.1% sodium azide (w/v) in PBS). The beads were resuspended in 100 µl of FACs wash and stained for 15 mins at 25°C. Beads were then washed twice using FACS wash. Dilution is shown as antibody volume in µL/100 µL.

Specificity	Fluorochrome	Compensation bead	Dilution (µL)
HLA-DR	BUV395	BD CompBeads Plus Anti-Mouse Ig (P)	1
CD16	BUV496	P	1
Siglec-1	BUV615	P	1
CD163	BUV805	P	1
Calprotectin	PE	P	0.5
CD5	PE Cy5.5	P	0.5
CD207	PE Vio770	P	1
CD3	NovaFluor Blue 660-120S	P	0.8
CD19	NovaFluor Blue 660-120S	CD3 antibody used for compensation	-
CD88	PerCP eFluor710	P	1
CD206	RB780	P	0.4
Siglec-6	BV480	P	0.5
CD1a	BV510	P	1.3
CD4	BV605	P	0.8
CD1c	BV650	P	1
Axl	BV785	P	0.5
CCR7	BUV661	BD CompBeads Normal Anti-Mouse Ig (N)	1
CD14	BUV737	N	1
CD209	BV421	N	1
CD11b	BV711	N	1
CD11c	BB515	N	1
C123	PE Cy5	N	0.5
CD103	PE Vio615	MACS Comp Bead Kit, anti-REA	1
XCR1	APC	Slingshot SpectraComp	1.3
Viability	FVS700	Arc Amine Reactive Compensation Bead Kit	1
KI67	Streptavidin DyLight800	Cells (HEKS293 cell line)	As per table 2

Online table 6: Summary of titration panels including reagents and fluorochromes used. Cell preparations and titrations performed summarised in online figure 1.

Antibody titrated	Titration panel	Gated population
HLA-DR BUV395	CD45 AF350, CD45 BB790, FVS700, HLA-DR BUV395	Cells, live, FSC-H high
CD16 BUV496	FVS700, CD16 BUV496, CD45 PE	Cells, live, CD45+
Siglec-1 BUV615	HLA-DR BUV395, Siglec-1 BUV615, CD163 BUV805, CD14 BV421, LiveDead Aqua, MR BV750	Cells, live, HLA-DR+, autofluorescence-
CD163 BUV805	HLA-DR BUV395, Siglec-1 BUV615, CD163 BUV805, CD14 BV421, LiveDead Aqua, MR BV750	Cells, live, HLA-DR+, autofluorescence-
Calprotectin PE	Calprotectin PE, CD14 BUV737, CD16 BUV496, FVS700, HLAD-DR BUV395, XCR1 APC	Cells, live, autofluorescent-
CD5 PE Cy5.5	CD3 NovaFluor Blue 660-120S, CD5 PE Cy5.5, FVS700, HLA-DR BUV395	Cells, live, HLA-DR+, autofluorescent-, CD1a-
CD207 PE Vio770	CD1c BV650, CD11b BV711, CD16 BV570, CD19 NovaFluor Blue 660-120S, CD45 BB790, DC-SIGN BV421, FVS700, Langerin PE Vio770	Cells, live, HLA-DR+
CD3 NovaFluor Blue 660-120S	CD3 NovaFluor Blue 660-120S, CD5 PE Cy5.5, FVS700, HLA-DR BUV395	Cells, live, CD14-
CD19 NovaFluor Blue 660-120S	CD1c BV650, CD11b BV711, CD16 BV570, CD19 NovaFluor Blue 660-120S, CD45 BB790, DC-SIGN BV421, FVS700, Langerin PE Vio770	Cells, live, autofluorescent-
CD88 PerCP eFluor710	CD11c BUV395, CD14 BUV737, CD45 PE, CD88 PerCP-eFluor710, HLA-DR APC fire810, HLA-DER BB515, NIR R780	Cells, live, HLA-DR+, CD45+
CD206 RB780	HLA-DR BUV395, MR RB780, UV440	Cells, live, HLA-DR+, autofluorescent-
Siglec-6 BV480	Axl BV785, CD11c BUV661, CD123 PE Cy5, FVS700, HLA-DR BUV395, Siglec-6 BV480	Cells, live, HLA-DR+, CD11c+
CD1a BV510	CD1a BV510, Langerin PE Vio770, FVS700, HLA-DR BUV395	Cells, live, HLA-DR+
CD4 BV605	FVS700, HLA-DR BUV395, CD14 APC Fire810, CD89 BB700, CD4 BV605, CCR5 VioBright B515, Calprotectin AF594	Cells, live, HLA-DR-, autofluorescent-
CD1c BV650	CD1c BV650, CD11b BV711, CD16 BV570, CD19 NovaFluor Blue 660-120S, CD45 BB790, DC-SIGN BV421, FVS700, Langerin PE Vio770	Cells, live, HLA-DR+, autofluorescent-
Axl BV785	FVS700, HLA-DR BUV395, CD11c BUV661, Siglec-6 BV480, Axl BV785	Cells, live, HLA-DR+, CD11c+
CCR7 BUV661	UV440, NIR R780, HLA-DR BUV395, CD83 APC, CD45 BB790, CD11c BB515, CCR7 BUV661	Cells, live, HLA-DR+, CD11c+
CD14 BUV737	CD11c BUV395, CD14 BUV737, CD45 PE, CD88 PerCP-eFluor710, HLA-DR APC fire810, HLA-DER BB515, NIR R780	Cells, live, CD45+, autofluorescence-
CD209 BV421	CD1c BV650, CD11b BV711, CD16 BV570, CD19 NovaFluor Blue 660-120S, CD45 BB790, DC-SIGN BV421, FVS700, Langerin PE Vio770	Cells, live, HLA-DR+, AF-
CD11b BV711	CD1c BV650, CD11b BV711, CD16 BV570, CD19 NovaFluor Blue 660-120S, CD45 BB790, DC-SIGN BV421, FVS700, Langerin PE Vio770	Cells, live, HLA-DR+, autofluorescent-
CD11c BB515	FVS700, HLA-DR BUV395, CD3 BUV486, CD14 BUV737, CD45 PE Cy7, CD11c BB515, CD19 BV750	Cells, live, HLA-DR+, CD45+, CD3-, CD19-, autofluorescent-
C123 PE-Cy5	CD11c BV421, CD14 BUV737, CD45 BB790, CD123 PE Cy5, FVS700, HLA-DR BUV395	Cells, live, HLA-DR+
CD103 PE Vio615	CD3 BUV496, CD103 PE Vio615, HLA-DR BUV395, LiveDead Violet, XCR1 APC Fire750	Cells, live, HLA-DR-, CD3+
XCR1 APC	CD1a BV510, CD1c PE Vio770, CD11c PE-CF594, CD14 BUV737, CD45 BV786, CD141 BV711, HLA-DR BUV395, Langerin Vioblue, LiveDead NIR, XCR1 APC	Cells, live, CD45+, HLA-DR+, Autofluorescent-, CD141+, CD14-
Viability FVS700	FCER1a APC, FVS700, HLA-DR BUV395, CD3 BUV496, CD11c BUV661, CD14 BUV737, CD123 PE-Cy5, XCR1 BV421, CD16 BV570, CD1c BV650, CD19 BV750	Cells, live
1' KI67-biotin 2' streptavidin Dylight800	Streptavidin AF647, LiveDead Violet, KI67 Biotin	Cells, live

Online table 7: Summary of antigen expression across all MNP subsets in human skin and mucosa.

	cDC1	cDC2	DC3	pDC	ASDC	LC	Monocyte	MDDC	MDM (skin & type II mucosa)	MDM (type I mucosa)	t-MDM (type I mucosa)	Autofluorescent macrophage
HLA-DR												
XCR1												
CD11c	+/-				+/-				+/-		+/-	
CD1c					+/-							
CD1a	+/-	+/-	+/-		+/-			+/-				
CD5		+/-										
CD14			+/-									
CD163									+/-			
CD123		+/-	+/-		+/-			+/-	+/-			
Axl												
Siglec-6												
Siglec-1					+/-							
CD88												
CD11b		+/-										
CD16												
CD206		+/-	+/-		+/-			+/-	+/-			
CD207	+/-	+/-			+/-							
CD209			+/-									
CD103	+/-	+/-										
Calprotectin		+/-	+/-									
CD4												
CCR7	+/-	+/-	+/-	+/-	+/-	+/-	+/-	+/-				
FcεR1α												
CD89												
HLA-DQ												

Very high	High	Moderate	Low	None	+/- can be expressed or not expressed

Online Table 8: Preliminary stain index for BD Symphony A5. All fluorophores were conjugated to CD4 and stained on PBMCs, except DYLIGHT800 and AF350 which were stained on beads.

JAN-2021-V2 SYMPHONY-SSM		BB515	BB630	BB660	BB700	BB755	BB790	DYLIGHT800	AF594	APC	APCR700	APCH7	APCFIRE810	BUV395	AF350	BUV496	BUV563	BUV615	BUV661	BUV737	BUV805	BV421	BV480	BV510	BV570	BV605	BV650	BV711	BV750	BV786	BYG584	PECF594	PECY5	PECY7
		B515_30-A	B610_20-A	B670_30-A	B710_50-A	B750_30-A	B820_60-A	N820_60-A	O616_23-A	R670_30-A	R710_40-A	R780_60-A	R820_60-A	U379_28-A	U450_50-A	U515_30-A	U586_15-A	U610_20-A	U670_30-A	U740_35-A	U820_60-A	V427_25-A	V474_25-A	V525_50-A	V586_15-A	V610_20-A	V677_20-A	V710_50-A	V750_30-A	V820_60-A	Y586_15-A	Y610_20-A	Y670_30-A	Y820_60-A
BB515	B515_30-A	0.00	0.60	0.40	0.26	0.30	0.14	0.00	0.28	0.35	0.05	0.02	0.00	0.10	0.00	0.08	0.31	0.17	0.13	0.04	0.00	0.00	0.05	0.11	0.13	0.25	0.16	0.09	0.06	0.00	0.31	0.00	0.02	0.00
BB630	B610_20-A	0.06	0.00	1.99	1.19	1.74	0.75	0.00	1.92	1.67	0.79	0.06	0.01	0.18	0.00	0.00	0.34	0.90	1.14	0.51	0.29	0.00	0.00	0.00	0.34	2.28	2.05	1.06	0.96	0.59	0.62	2.76	0.78	0.35
BB660	B670_30-A	0.03	0.41	0.00	1.85	2.81	1.37	0.16	0.32	4.82	2.58	0.54	0.47	0.11	0.00	0.00	0.18	0.17	1.48	0.85	0.44	0.02	0.00	0.00	0.22	0.38	3.27	1.50	1.48	0.87	0.29	0.17	1.62	0.61
BB700	B710_50-A	0.07	0.37	2.54	0.00	4.87	2.36	0.39	0.26	2.65	4.04	0.75	0.68	0.20	0.00	0.00	0.21	0.21	1.42	1.52	0.83	0.22	0.00	0.06	0.23	0.39	2.86	2.74	2.73	1.66	0.29	0.10	0.88	0.75
BB755	B750_30-A	0.06	0.36	0.65	0.99	0.00	2.85	0.48	0.27	0.48	0.72	0.41	0.42	0.19	0.00	0.00	0.16	0.19	0.25	1.10	0.99	0.10	0.00	0.03	0.16	0.36	0.52	0.64	2.83	1.93	0.29	0.00	0.00	0.72
BB790	B820_60-A	0.19	0.87	0.98	1.01	16.1	0.00	1.21	0.39	0.67	0.73	0.52	0.47	0.22	0.00	0.00	0.24	0.26	0.38	1.25	1.61	0.20	0.00	0.06	0.28	0.45	0.74	0.60	3.39	3.01	0.37	0.12	0.18	0.85
DYLIGHT800	N820_60-A	0.00	0.00	0.00	0.01	0.52	0.51	0.00	0.01	0.00	0.02	0.28	0.41	0.00	0.00	0.00	0.00	0.05	0.00	0.13	0.84	0.00	0.00	0.00	0.05	0.04	0.00	0.03	0.78	0.89	0.05	0.05	0.00	1.11
AF594	O616_23-A	0.00	0.76	0.70	0.29	0.33	0.05	0.00	0.00	0.68	0.32	0.03	0.05	0.00	0.00	0.00	0.24	0.65	0.70	0.32	0.22	0.00	0.00	0.00	0.00	0.48	0.63	0.42	0.42	0.26	0.38	2.76	0.82	0.54
APC	R670_30-A	0.00	0.04	1.04	0.24	0.40	0.28	0.00	0.28	0.00	2.31	0.62	0.56	0.15	0.00	0.00	0.05	0.16	1.52	0.71	0.38	0.00	0.00	0.00	0.00	0.07	1.28	0.61	0.69	0.52	0.10	0.24	1.74	0.89
APCR700	R710_40-A	0.00	0.01	0.30	0.31	0.63	0.42	0.00	0.05	0.86	0.00	0.75	0.65	0.12	0.00	0.02	0.04	0.08	0.36	0.82	0.41	0.00	0.00	0.00	0.00	0.02	0.36	0.54	0.75	0.54	0.00	0.00	0.37	0.98
APCH7	R780_60-A	0.00	0.00	0.00	0.02	1.44	1.59	2.56	0.06	0.40	0.48	0.00	2.03	0.40	0.00	0.00	0.13	0.31	0.28	0.70	2.04	0.00	0.00	0.00	0.14	0.09	0.00	0.08	2.18	2.16	0.36	0.00	0.12	4.27
APCFIRE810	R820_60-A	0.00	0.00	0.23	0.08	1.61	1.75	3.57	0.03	0.92	0.87	0.65	0.00	0.35	0.07	0.00	0.15	0.22	0.33	0.39	2.44	0.00	0.00	0.07	0.01	0.03	0.02	0.18	2.52	2.77	0.11	0.00	0.41	5.20
BUV395	U379_28-A	0.00	0.00	0.00	0.00	0.00	0.00	0.00	0.12	0.00	0.00	0.01	0.00	0.00	0.32	0.10	0.14	0.08	0.06	0.01	0.00	0.00	0.00	0.00	0.00	0.00	0.00	0.01	0.01	0.00	0.13	0.00	0.01	0.00
AF350	U450_50-A	0.05	0.01	0.02	0.05	0.09	0.00	0.00	0.62	0.23	0.00	0.03	0.00	0.00	0.00	0.65	0.95	0.69	0.52	0.23	0.07	0.00	0.00	0.43	0.47	0.29	0.22	0.22	0.14	0.11	0.86	0.00	0.00	0.00
BUV496	U515_30-A	0.28	0.10	0.07	0.00	0.00	0.00	0.00	1.50	0.52	0.14	0.02	0.00	1.49	0.28	0.00	1.66	1.04	1.11	0.40	0.14	0.00	0.39	0.42	0.69	0.56	0.46	0.23	0.00	0.16	1.73	0.10	0.00	0.00
BUV563	U586_15-A	0.00	0.78	0.59	0.33	0.27	0.16	0.00	2.33	1.19	0.20	0.00	0.02	1.20	0.15	0.12	0.00	1.83	1.61	0.52	0.25	0.00	0.00	0.00	0.48	0.51	0.38	0.20	0.05	0.01	3.36	1.75	0.47	0.16
BUV615	U610_20-A	0.00	0.96	0.75	0.33	0.42	0.22	0.00	3.92	1.91	0.60	0.06	0.02	0.79	0.11	0.03	0.78	0.00	2.71	1.18	0.57	0.00	0.00	0.00	0.15	0.71	0.88	0.49	0.42	0.29	0.83	3.20	0.99	0.63
BUV661	U670_30-A	0.00	0.06	0.82	0.23	0.37	0.22	0.15	0.42	3.95	2.31	0.54	0.46	0.51	0.08	0.00	0.11	0.32	0.00	1.26	0.65	0.00	0.00	0.00	0.00	0.09	0.97	0.47	0.53	0.39	0.09	0.25	1.23	0.62
BUV737	U740_35-A	0.00	0.00	0.20	0.37	1.66	0.71	0.28	0.01	0.20	0.90	0.52	0.46	0.43	0.10	0.01	0.07	0.06	0.20	0.00	1.12	0.00	0.00	0.00	0.00	0.02	0.05	0.27	0.78	0.56	0.13	0.00	0.02	0.43
BUV805	U820_60-A	0.00	0.00	0.00	0.00	0.40	0.39	1.71	0.11	0.07	0.00	0.22	0.30	0.73	0.10	0.00	0.07	0.12	0.09	0.27	0.00	0.00	0.03	0.00	0.00	0.00	0.00	0.00	0.58	0.68	0.05	0.00	0.02	0.64
BV421	V427_25-A	0.00	0.00	0.00	0.00	0.00	0.00	0.00	0.11	0.04	0.00	0.00	0.00	0.06	0.48	0.05	0.15	0.14	0.07	0.01	0.00	0.00	1.08	0.75	0.27	0.14	0.12	0.04	0.11	0.04	0.39	0.00	0.00	0.00
BV480	V474_25-A	0.23	0.12	0.06	0.02	0.06	0.00	0.00	0.55	0.14	0.18	0.00	0.03	0.28	0.04	0.47	0.58	0.46	0.43	0.19	0.04	0.11	0.00	1.46	0.92	0.79	0.72	0.34	0.34	0.16	1.08	0.32	0.01	0.00
BV510	V525_50-A	0.00	0.16	0.03	0.00	0.08	0.00	0.00	1.24	0.56	0.55	0.03	0.00	0.48	0.09	0.40	1.35	0.96	1.04	0.59	0.40	0.31	1.43	0.00	1.50	1.43	1.78	0.86	0.94	0.80	1.91	0.62	0.00	0.10
BV570	V586_15-A	0.00	0.83	0.72	0.39	0.38	0.16	0.00	1.46	0.77	0.66	0.00	0.00	0.45	0.12	0.03	1.87	1.11	1.19	0.53	0.37	0.67	0.32	0.43	0.00	1.93	2.28	1.05	1.10	0.72	3.30	2.24	0.60	0.11
BV605	V610_20-A	0.00	0.79	0.76	0.42	0.57	0.40	0.00	1.85	1.16	1.02	0.04	0.00	0.20	0.06	0.00	0.64	1.31	1.79	0.92	0.55	0.32	0.12	0.13	0.70	0.00	3.09	1.56	1.66	1.07	1.00	2.66	0.86	0.70
BV650	V677_20-A	0.00	0.14	0.47	0.20	0.26	0.13	0.00	0.50	1.54	1.53	0.29	0.26	0.19	0.03	0.00	0.06	0.33	1.77	0.97	0.48	0.33	0.16	0.12	0.10	0.62	0.00	1.71	1.58	0.96	0.15	0.53	0.66	0.46
BV711	V710_50-A	0.00	0.00	0.35	0.54	1.14	0.59	0.16	0.07	0.66	2.89	0.73	0.60	0.18	0.08	0.00	0.03	0.07	0.60	2.10	1.14	0.43	0.11	0.08	0.09	0.07	1.33	0.00	3.17	2.11	0.05	0.00	0.19	0.71
BV750	V750_30-A	0.00	0.00	0.03	0.25	1.34	0.71	0.18	0.05	0.05	0.58	0.40	0.44	0.22	0.06	0.00	0.00	0.12	0.13	1.84	1.31	0.43	0.29	0.11	0.16	0.08	0.16	0.65	0.00	2.78	0.16	0.00	0.00	0.59
BV786	V820_60-A	0.00	0.00	0.04	0.06	1.05	0.75	0.71	0.07	0.09	0.51	0.45	0.48	0.24	0.08	0.00	0.11	0.13	0.19	1.48	2.17	1.28	0.22	0.22	0.13	0.08	0.36	0.59	7.37	0.00	0.14	0.00	0.00	0.83
BYG584	Y586_15-A	0.00	0.56	0.39	0.15	0.23	0.15	0.00	0.30	0.23	0.11	0.01	0.02	0.09	0.00	0.00	0.27	0.20	0.18	0.09	0.03	0.02	0.00	0.00	0.30	0.28	0.29	0.14	0.13	0.09	0.00	1.84	0.51	0.34
PECF594	Y610_20-A	0.00	1.50	1.17	0.76	1.09	0.49	0.00	1.23	0.94	0.41	0.05	0.00	0.10	0.00	0.00	0.16	0.52	0.64	0.28	0.16	0.00	0.00	0.00	0.09	0.76	0.79	0.46	0.43	0.25	0.66	0.00	0.81	0.61
PECY5	Y670_30-A	0.00	0.16	2.69	1.53	2.43	1.20	0.06	0.10	3.63	1.64	0.37	0.32	0.10	0.00	0.00	0.08	0.07	1.36	0.59	0.28	0.04	0.01	0.00	0.04	0.16	1.84	0.91	0.88	0.51	0.35	0.29	0.00	1.38
PECY7	Y820_60-A	0.00	0.12	0.17	0.25	2.81	2.14	0.49	0.04	0.04	0.12	0.22	0.24	0.05	0.00	0.00	0.03	0.08	0.06	0.33	0.61	0.05	0.00	0.00	0.01	0.02	0.04	0.08	1.05	1.01	0.31	0.21	0.07	0.00

Online table 9: Spill-over spreading error (SSE) matrix (SSM) obtained with compensation beads and cells in the case of DyLight 800. The reagents from the final panel (**Online table 3**, iteration 4) were used.

	B515_30	B670_30	B710_50	B820_60	N820_60	R670_30	R710_40	U379_28	U515_30	U610_20	U670_30	U740_35	U820_60	V427_25	V474_25	V525_50	V610_20	V677_20	V710_50	V820_60	Y586_15	Y610_20	Y670_30	Y710_50	Y780_60
B515_30	1.00	0.01	0.00	0.00	0.00	0.00	0.00	0.00	0.02	0.00	0.00	0.00	0.00	0.00	0.00	0.00	0.00	0.00	0.00	0.00	0.00	0.00	0.00	0.00	0.00
B670_30	0.16	1.00	0.31	0.03	0.00	0.72	0.49	0.00	0.00	0.00	0.01	0.01	0.00	0.00	0.00	0.00	0.00	0.07	0.02	0.01	0.00	0.00	0.07	0.02	0.01
B710_50	0.00	0.19	1.00	0.18	0.11	0.06	0.94	0.00	0.00	0.00	0.05	0.46	0.12	0.00	0.00	0.00	0.00	0.19	0.79	0.33	0.00	0.00	0.10	0.48	0.19
B820_60	0.10	0.01	0.02	1.00	0.29	0.00	0.00	0.00	0.00	0.00	0.00	0.08	0.36	0.00	0.00	0.00	0.00	0.00	0.00	0.21	0.00	0.00	0.00	0.00	0.02
N820_60	0.05	0.01	0.01	0.01	1.00	0.00	0.01	0.04	0.04	0.01	0.01	0.02	0.07	0.04	0.06	0.06	0.04	0.02	0.02	0.08	-0.11	0.00	0.01	0.01	0.01
R670_30	0.00	0.02	0.00	0.00	0.00	1.00	0.66	0.00	0.00	0.00	0.14	0.10	0.02	0.00	0.01	0.01	0.00	0.12	0.05	0.02	0.00	0.01	0.49	0.13	0.05
R710_40	0.00	0.01	0.01	0.00	0.00	0.22	1.00	0.00	0.00	0.00	0.02	0.08	0.02	0.00	0.00	0.00	0.00	0.02	0.05	0.02	0.00	0.00	0.03	0.07	0.03
U379_28	0.00	0.00	0.00	0.00	0.00	0.00	0.00	1.00	0.08	0.00	0.00	0.00	0.00	0.01	0.00	0.00	0.00	0.00	0.00	0.00	0.00	0.00	0.00	0.00	0.00
U515_30	0.07	0.00	0.00	0.00	0.00	0.00	0.00	0.27	1.00	0.11	0.03	0.02	0.01	0.01	0.08	0.15	0.03	0.01	0.00	0.00	0.00	0.00	0.00	0.00	0.00
U610_20	0.00	0.02	0.01	0.00	0.00	0.00	0.00	0.05	0.01	1.00	0.43	0.24	0.04	0.00	0.00	0.00	0.16	0.06	0.02	0.01	0.19	0.70	0.31	0.12	0.04
U670_30	0.00	0.02	0.01	0.00	0.00	0.77	0.72	0.03	0.01	0.03	1.00	0.66	0.12	0.00	0.00	0.00	0.00	0.08	0.04	0.01	0.00	0.01	0.25	0.09	0.03
U740_35	0.00	0.00	0.02	0.01	0.00	0.00	0.11	0.02	0.00	0.00	0.00	1.00	0.26	0.00	0.00	0.00	0.00	0.00	0.02	0.02	0.00	0.00	0.00	0.01	0.01
U820_60	0.00	0.00	0.00	0.01	0.53	0.00	0.00	0.07	0.02	0.00	0.00	0.06	1.00	0.00	0.00	0.00	0.00	0.00	0.00	0.06	0.00	0.00	0.00	0.00	0.00
V427_25	0.00	0.00	0.00	0.00	0.00	0.00	0.00	0.00	0.01	0.00	0.00	0.00	0.00	1.00	0.13	0.02	0.00	0.00	0.00	0.00	0.00	0.00	0.00	0.00	0.00
V474_25	0.07	0.00	0.00	0.00	0.00	0.00	0.00	0.00	0.23	0.03	0.01	0.00	0.00	0.00	1.00	0.80	0.17	0.03	0.01	0.00	0.00	0.00	0.00	0.00	0.00
V525_50	0.02	0.00	0.00	0.00	0.00	0.00	0.00	0.00	0.36	0.15	0.06	0.05	0.01	0.01	0.37	1.00	0.54	0.17	0.08	0.03	0.00	0.00	0.00	0.00	0.00
V610_20	0.00	0.03	0.01	0.00	0.00	0.00	0.00	0.00	0.00	0.24	0.13	0.09	0.02	0.14	0.02	0.00	1.00	0.39	0.18	0.06	0.17	0.35	0.19	0.07	0.02
V677_20	0.00	0.02	0.01	0.00	0.00	0.20	0.20	0.00	0.00	0.05	0.33	0.21	0.04	0.25	0.04	0.01	0.17	1.00	0.49	0.11	0.00	0.03	0.19	0.08	0.02
V710_50	0.00	0.01	0.08	0.02	0.00	0.05	0.94	0.00	0.00	0.00	0.04	0.77	0.19	0.23	0.03	0.01	0.00	0.13	1.00	0.41	0.00	0.00	0.01	0.05	0.02
V820_60	0.00	0.00	0.00	0.01	0.09	0.00	0.00	0.00	0.00	0.00	0.00	0.14	0.36	0.21	0.03	0.01	0.00	0.00	0.02	1.00	0.00	0.00	0.00	0.00	0.01
Y586_15	0.00	0.02	0.01	0.00	0.00	0.00	0.00	0.00	0.00	0.01	0.00	0.00	0.00	0.00	0.00	0.00	0.02	0.00	0.00	0.00	1.00	0.11	0.03	0.01	0.00
Y610_20	0.00	0.36	0.16	0.01	0.01	0.01	0.01	0.00	0.00	0.10	0.06	0.04	0.01	0.00	0.00	0.00	0.14	0.07	0.04	0.01	0.42	1.00	0.64	0.28	0.08
Y670_30	0.00	0.57	0.21	0.02	0.00	0.26	0.21	0.00	0.00	0.00	0.08	0.06	0.01	0.00	0.00	0.00	0.00	0.08	0.03	0.01	0.07	0.01	1.00	0.36	0.13
Y710_50	0.00	0.17	0.48	0.06	0.00	0.07	0.34	0.00	0.00	0.00	0.03	0.13	0.04	0.00	0.00	0.00	0.00	0.05	0.11	0.03	0.23	0.03	0.35	1.00	0.37
Y780_60	0.00	0.00	0.01	0.30	0.12	0.00	0.00	0.00	0.00	0.00	0.00	0.06	0.16	0.00	0.00	0.00	0.00	0.00	0.00	0.16	0.12	0.02	0.01	0.01	1.00

4.5 Supplemental: Online Figures

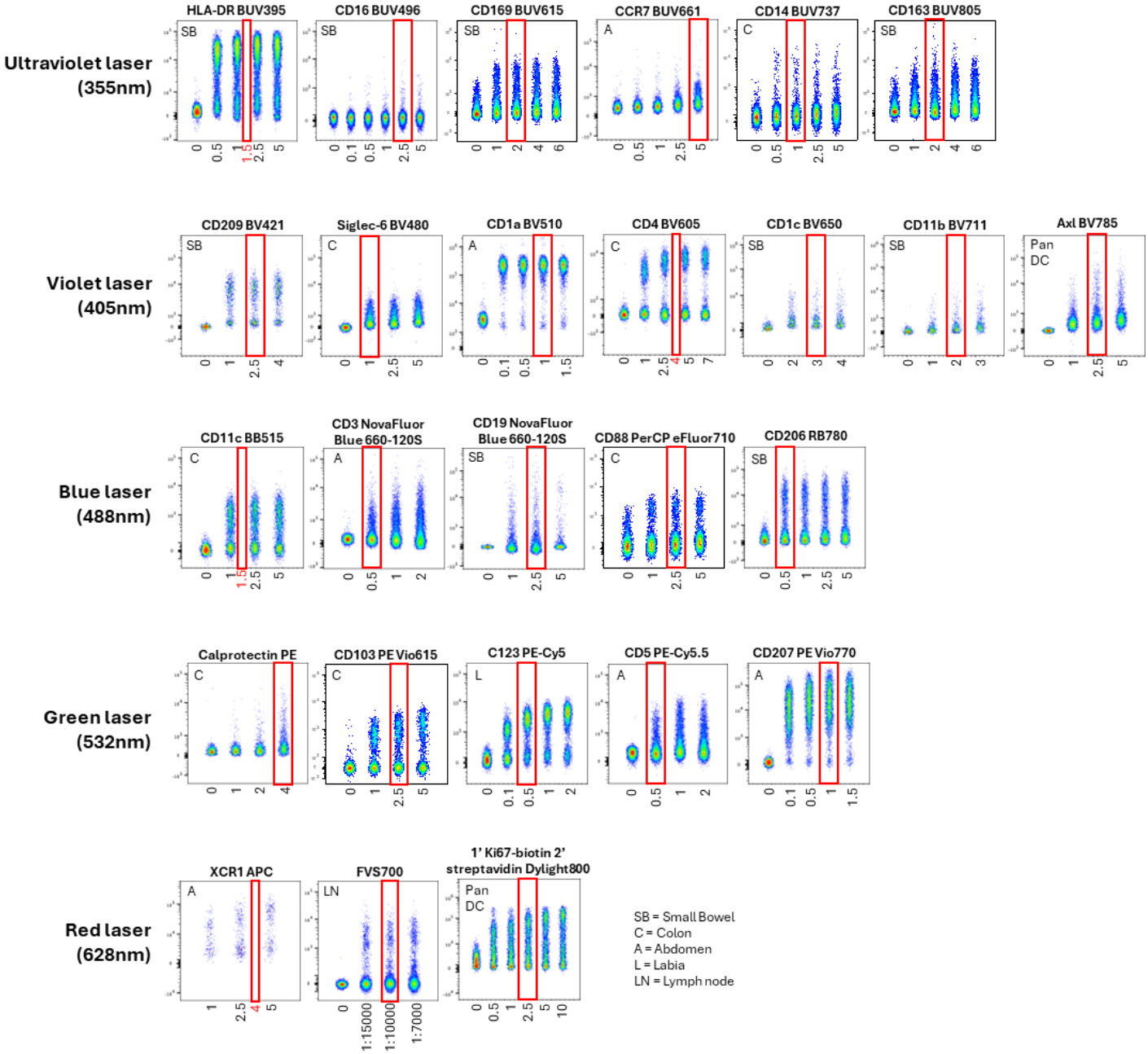

Online Figure 1: Titration experiments of the antibodies used in the optimised 26 parameter panel. All titrations were performed on a human tissue, including small bowel (SB), colon (C), abdomen (A), labia (L) or lymph nodes (LN), or on isolated blood derived Pan DCs, indicated in the top left corner of each plot. The specific titre selected for the OMIP is highlighted by the red box and volume indicated below. Optimal concentrations were chosen based on maximal separation between positive and negative populations and minimal shifting of the negative population. All titrations were optimised for 2.5 x 10^6 cells with a final staining volume of x µL/100 µL, except for FVS700 which is displayed as a dilution.

Online Figure 2: Autofluorescent signal across all FACSymphony A5 detectors in tissues of the skin, type II and type I mucosa. All cells were isolated from fresh samples and not stained with any antibodies (unstained samples). The autofluorescent positive population was gated using detectors B610 and Y586, and histograms generated.

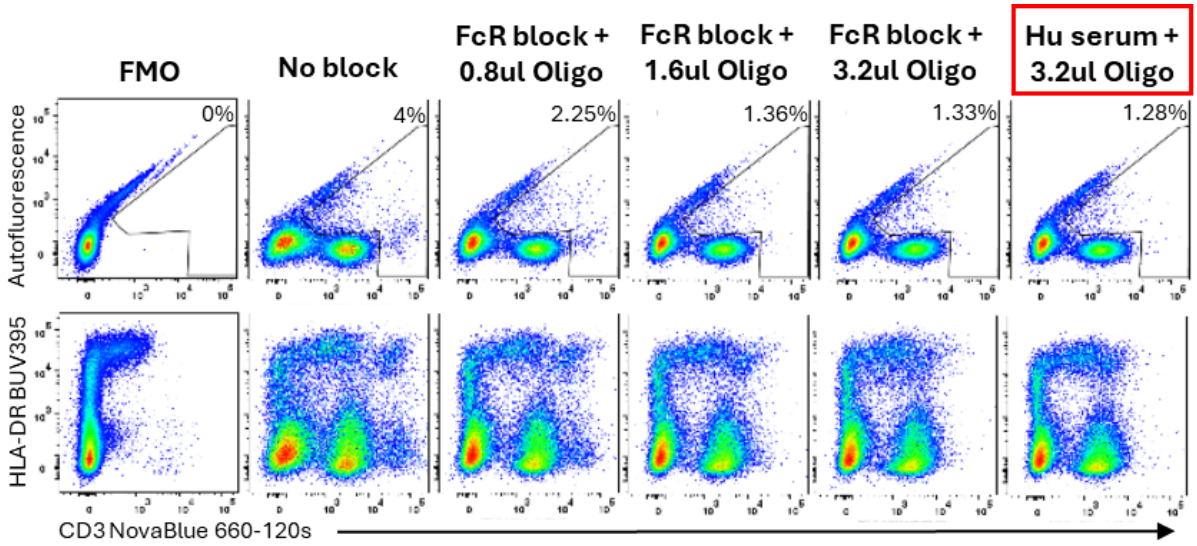

Online Figure 3: Optimisation of blocking reagents in human tissue as demonstrated by cells isolated from colon lamina propria. The testing assessed the non-specific binding (background staining) picked up by CD3 NovaBlue 660-120s and the sample was divided into a CD3 NovaBlue 660-120s FMO, and differing dual combinations of FcR block (5 uL), Human antibody serum (10 uL) and Oligo-block. Cells were gated as live (FVS700$^-$), single (FSC-A vs FSC-H and SSC-A vs SSC-W), CD45$^+$ cells. The most optimal blocking combination was 10ul human antibody serum and 3.2 uL Oligo-block (boxed in red).

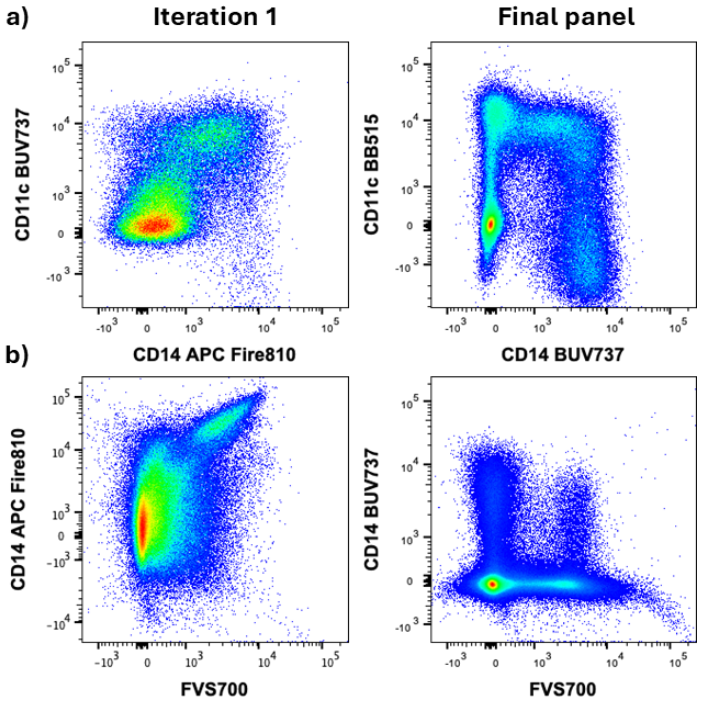

Online Figure 4: Unresolved staining of a) CD14 APC Fire810 and b) FVS700 in iteration 1 compared to resolved CD14 and live cell populations in the final panel as demonstrated by human skin dermis (left: labia, right: outer foreskin). Cells in iteration 1 were gated as live (FVS700$^-$), single (FSC-A vs FSC-H and SSC-A vs SSC-W), CD3$^-$ CD19$^-$ and cells in final panel as single cells (FSC-A vs FSC-H and SSC-A vs SSC-W). Data is shown with compensation matrix generated at acquisition.

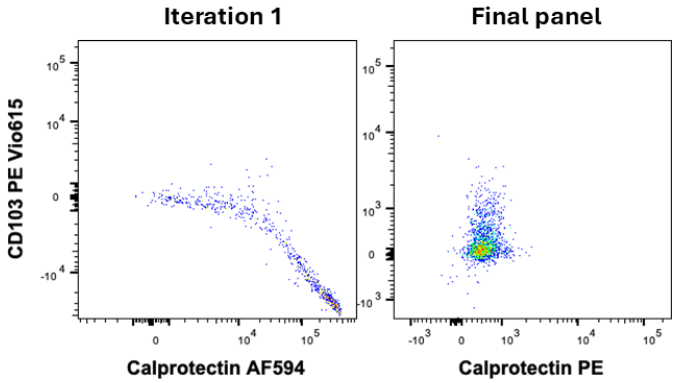

Online Figure 5:
CD103 PE Vio615 interaction with calprotectin AF594 in iteration 1 compared to resolved expression of CD103 PE Vio615 and calprotectin PE in the final panel. Cells were isolated from colon lamina propria and gated as live (FVS700$^-$), single (FSC-A vs FSC-H and SSC-A vs SSC-W), CD3$^-$ CD19$^-$ XCR1$^+$ cDC1s

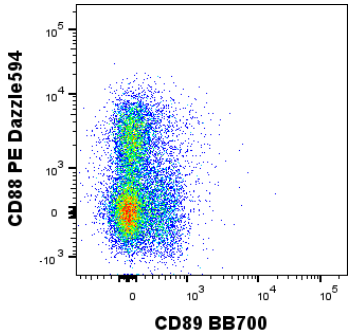

Online Figure 6:
Marker comparison of CD88 and CD89 to identify monocytes in human tissue (demonstrated in colon lamina propria). Cells were gated as live (FVS700$^-$), single (FSC-A vs FSC-H and SSC-A vs SSC-W), CD3$^-$ CD19$^-$ XCR1$^-$. CD88 was selected for the final panel due to its superior staining.

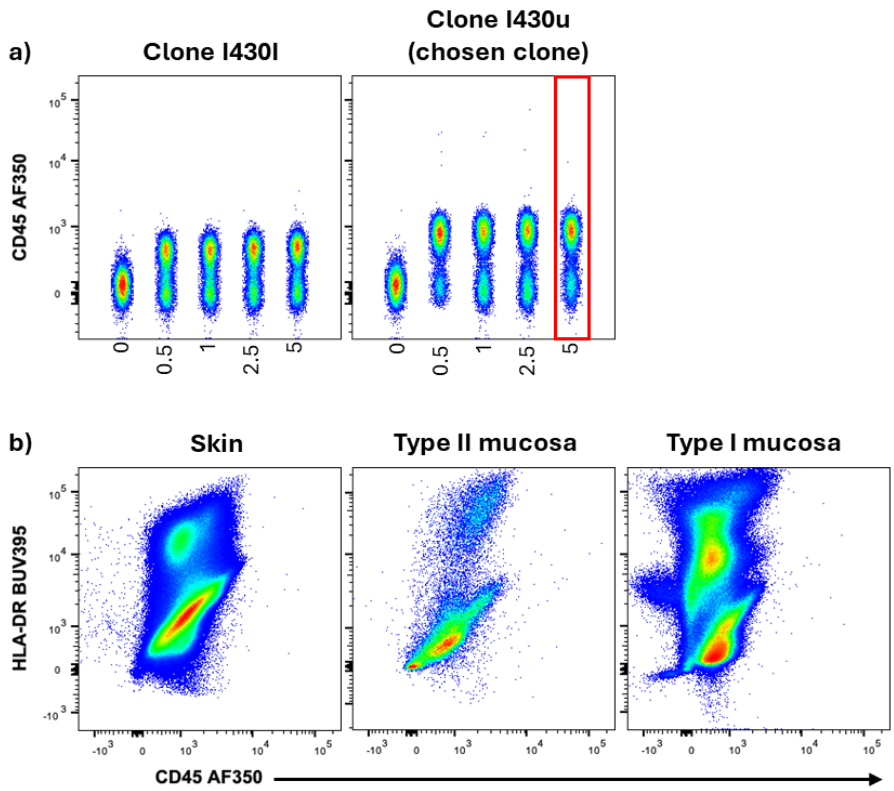

Online Figure 7:
Optimisation of CD45 AF350. a) Two clones of CD45 AF350, I430I and I430u, were titrated on human colon cells. The clone I430u was selected for its higher staining with a volume of 5ul (boxed in red). All titrations were performed on 2.5 x 10^6 cells with a final staining volume of x µL/100 µL. b) Unresolved CD45 AF350 staining across skin dermis (labia), type II lamina propria (vagina) and type I mucosa lamina propria (colon) despite using the favourable clone and optimised volume. Cells were gated as live (FVS700$^-$), single (FSC-A vs FSC-H and SSC-A vs SSC-W). Data is shown with compensation matrix generated at acquisition.

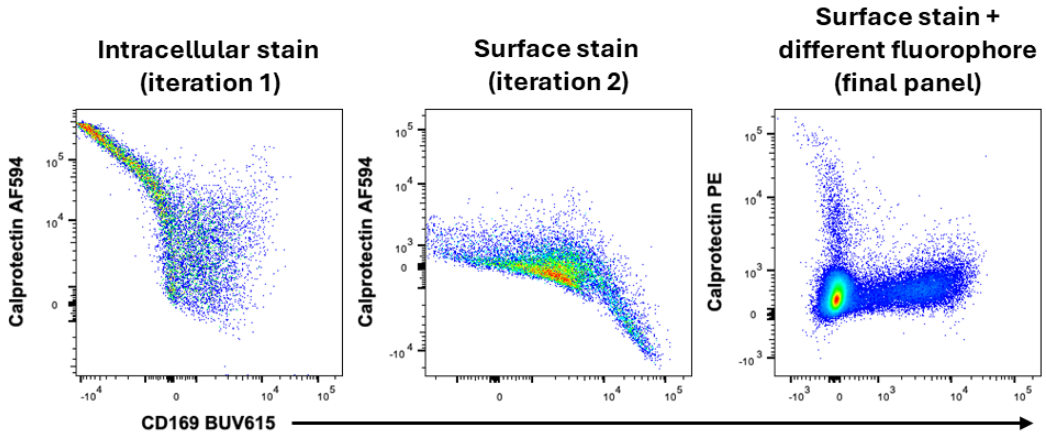

Online Figure 8:
Calprotectin resolution and interaction with CD169 BUV615 across multiple panel iterations as demonstrated by colon lamina propria. Cells were gated as live (FVS700$^-$), single (FSC-A vs FSC-H and SSC-A vs SSC-W), CD3$^-$ CD19$^-$. Data is shown with compensation matrix generated at acquisition.

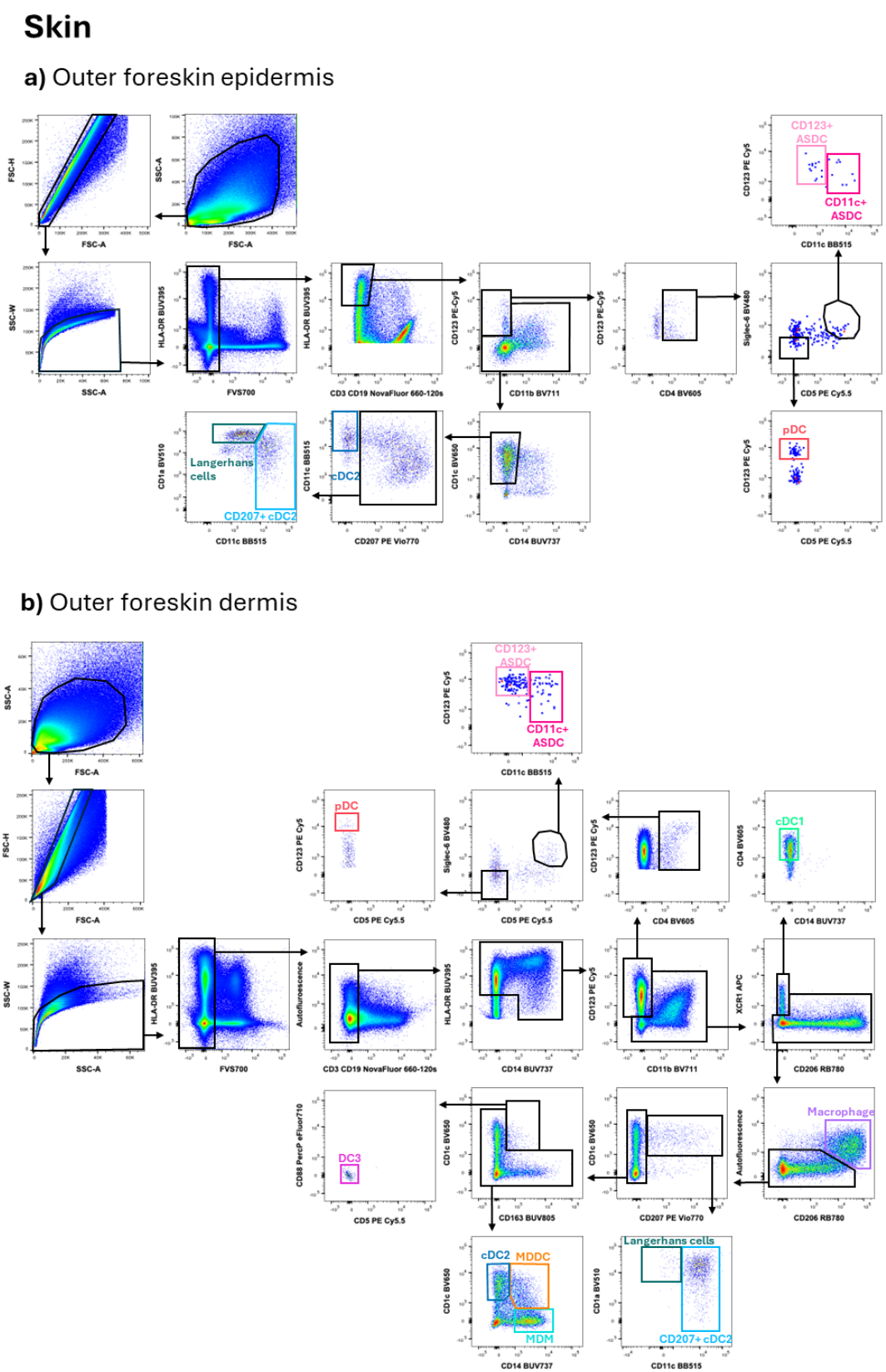

Online Figure 9: Complete gating strategy of the 26 colour optimised panel identifying all known MNPs in skin, as demonstrated by outer foreskin in the **a)** epidermis and **b)** dermis. Cells were freshly processed and isolated from the tissue, stained and acquired on a BD FACSymphony A5. A comprehensive description of gating can be found in **figure 1**.

Type II mucosa

a) Inner foreskin epithelium

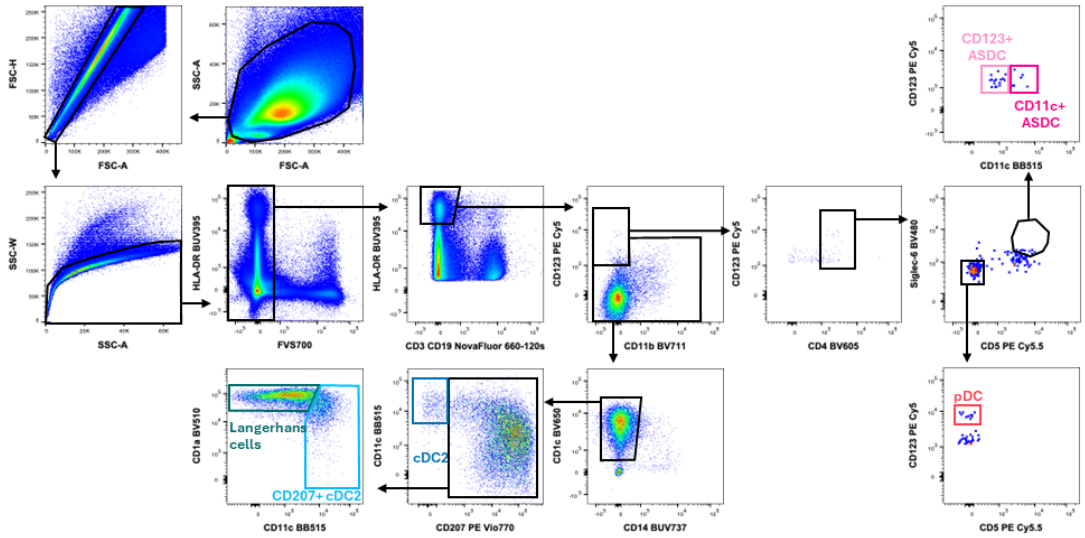

b) Inner foreskin lamina propria

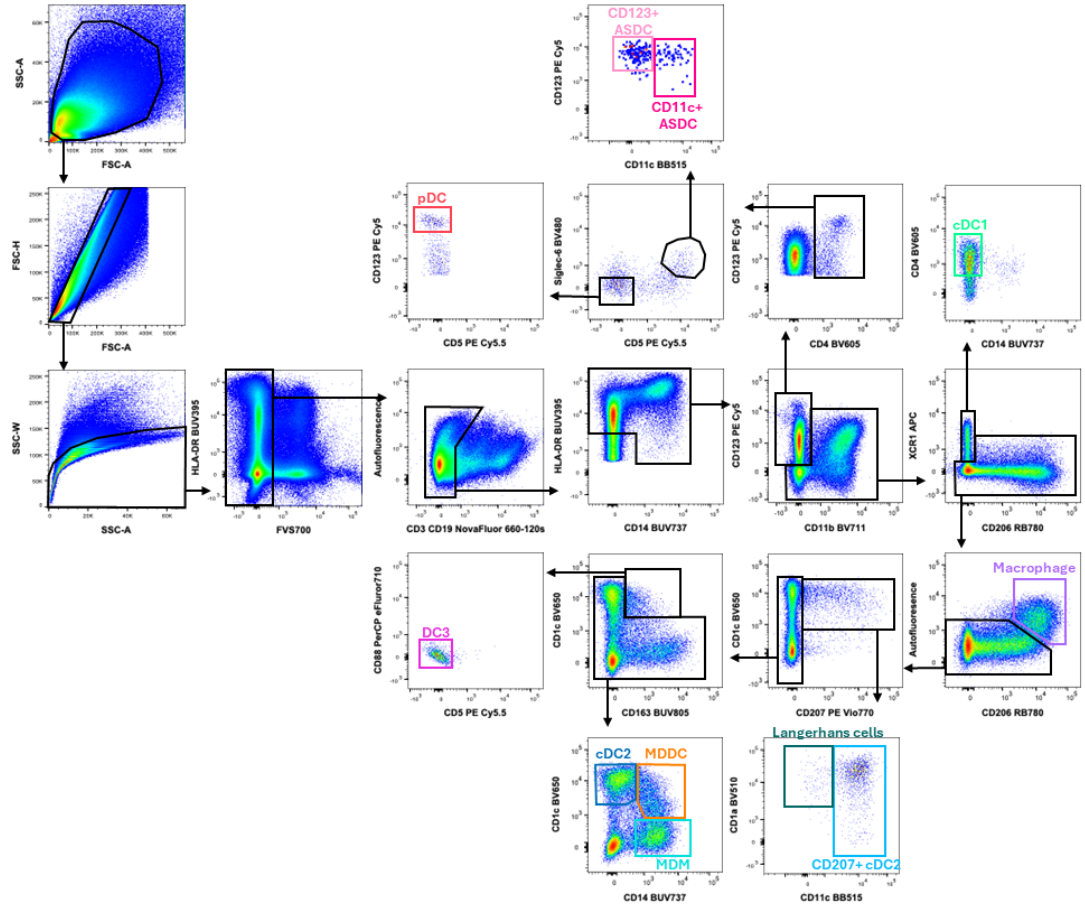

continued over page

c) Vagina epithelium

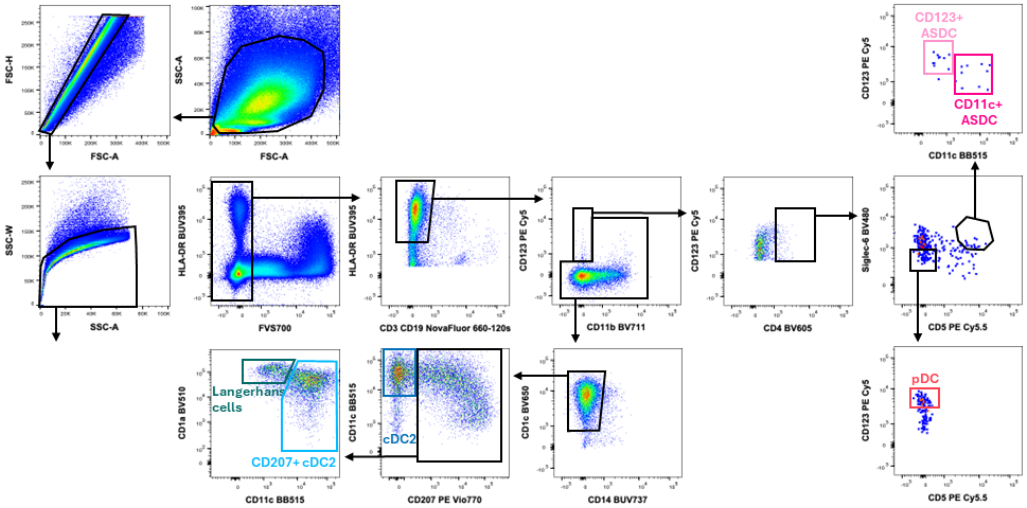

d) Vagina lamina propria

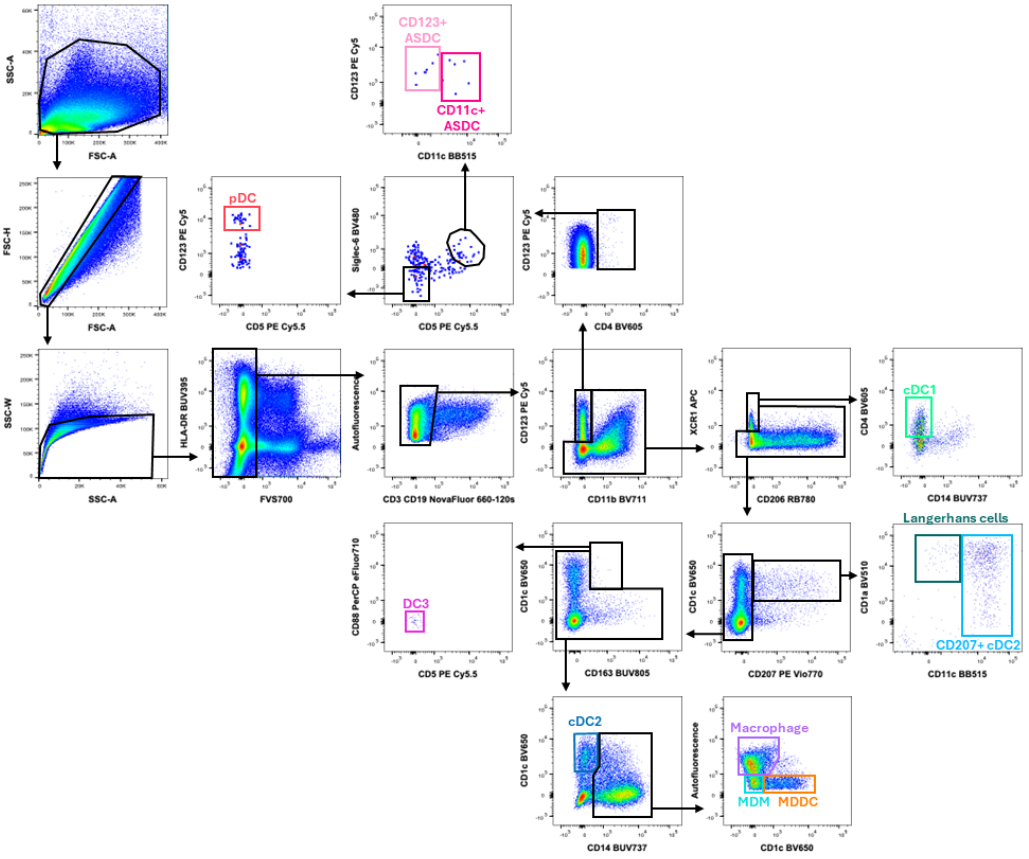

Online Figure 10: Complete gating strategy of the 26 colour optimised panel identifying all known MNPs in type II mucosa, as demonstrated by inner foreskin **a)** epidermis and **b)** lamina propria and vagina **c)** epidermis and **d)** lamina propria. Whilst the epithelial gating strategy remains identical across both type II mucosal tissue types, the lamina propria strategy differs due to the strong autofluorescent macrophage signal in inner foreskin. Cells were freshly processed and isolated from the tissue, stained and acquired on a BD FACSymphony A5. A comprehensive description of gating can be found in **figure 1**.

Type I mucosa

a) Colon lamina propria acquisition compensation

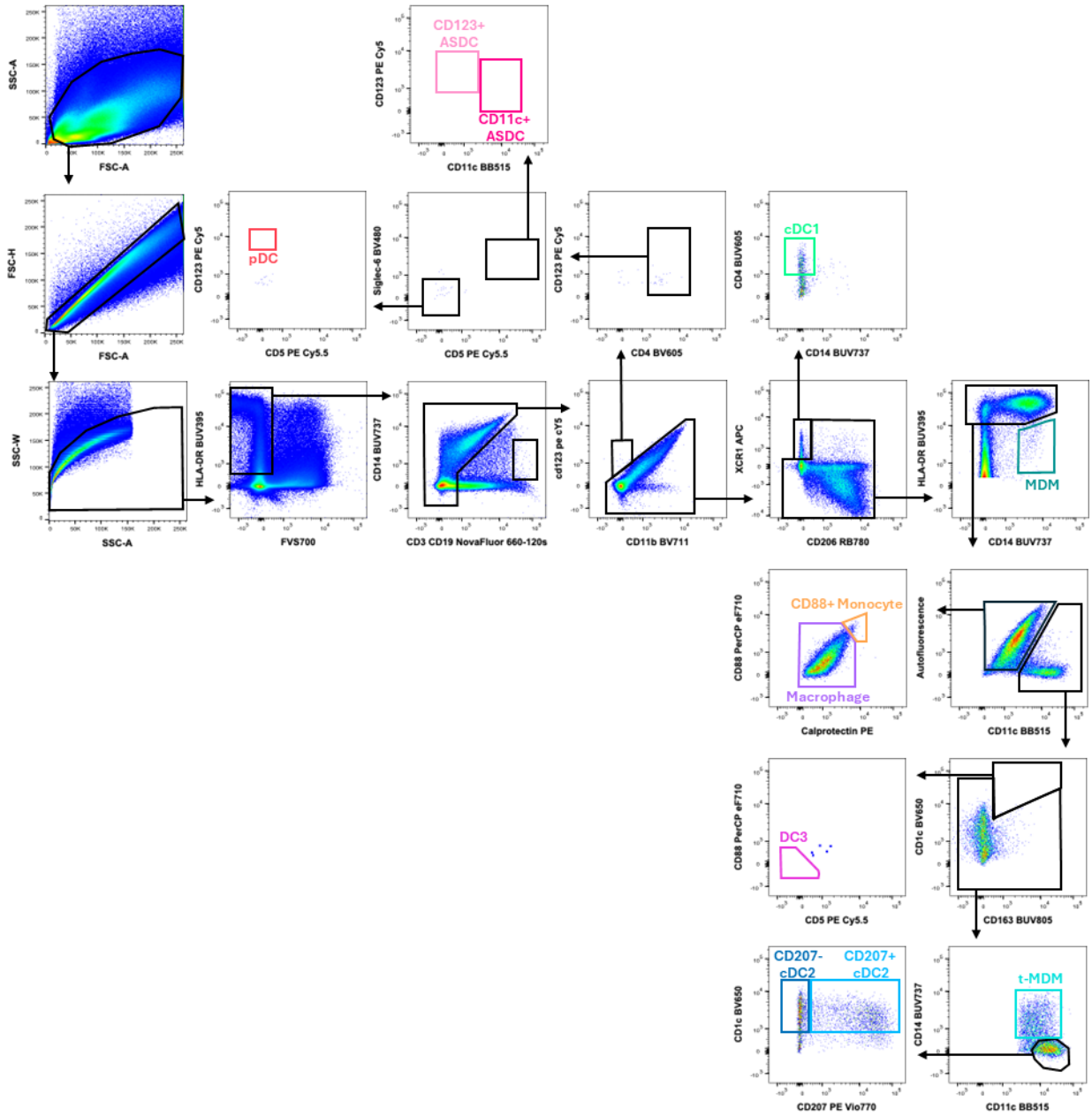

continued over page

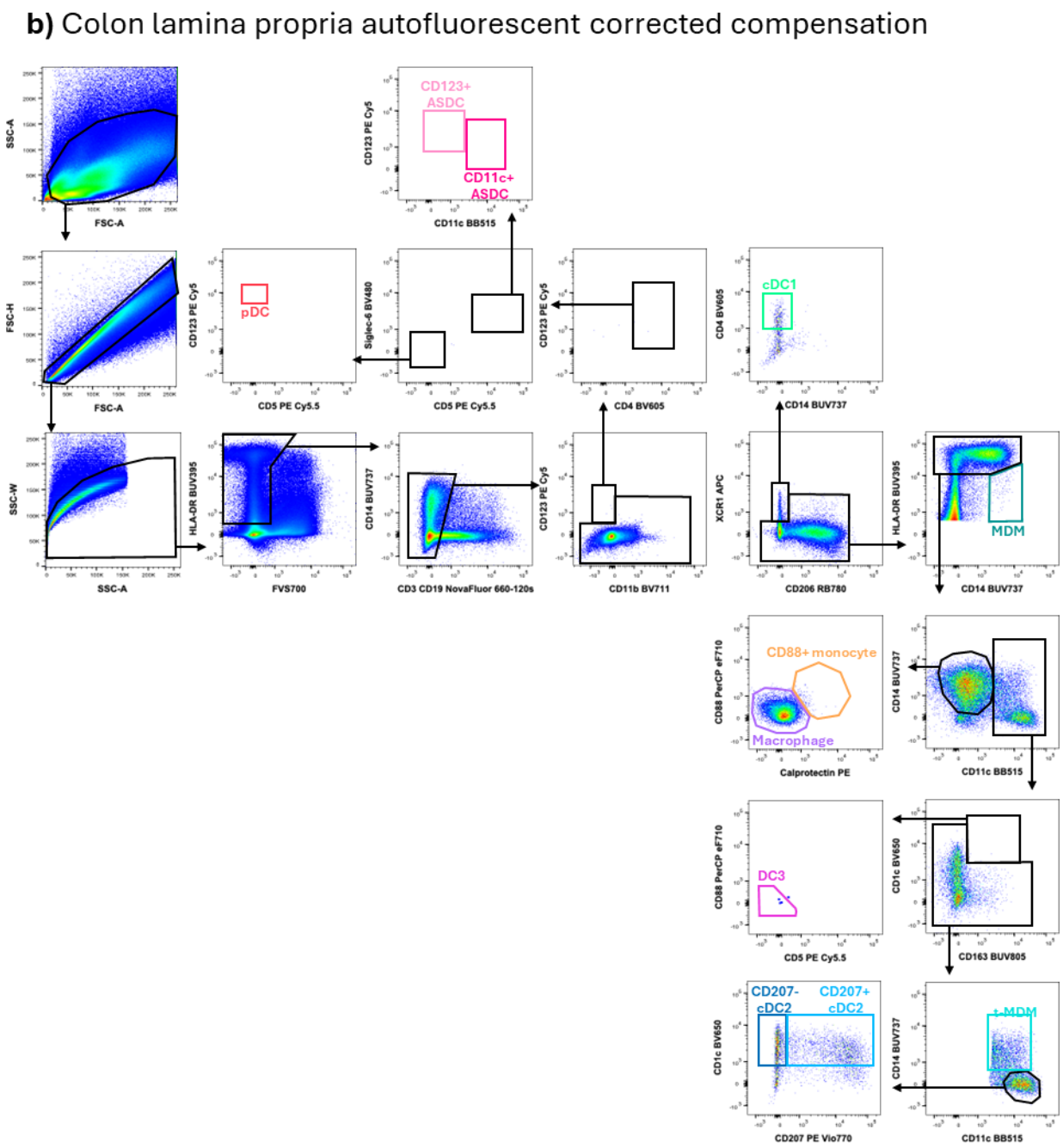

Online Figure 11: Complete gating strategy of the 26 colour optimised panel identifying all known MNPs in type I mucosa, as demonstrated by colon lamina propria using either **a)** acquisition compensation or **b)** autofluorescent corrected compensation. All gates downstream of cDC1 identification differ to those of skin and type II mucosa due to the presence of different cell populations, particularly monocyte and macrophage populations. Cells were freshly processed and isolated from the tissue, stained and acquired on a BD FACSymphony A5. A comprehensive description of gating can be found in **figure 1**.

Chapter 5. Overall conclusions and future directions

To elucidate the role of colorectal mononuclear phagocytes (MNPs) in HIV transmission, it is essential to examine them in their tissue-resident state. A main limitation of working with tissue-liberated cells is the alteration to the cells that can occur as a result of the enzymatic digestion. This includes enzymatic cleavage of the surface proteins that allow for the cell's classification as well as their ability to perform in functional assays that require the binding of surface receptors. Additionally, the digestion process can trigger the activation and maturation of immune cells, altering their phenotype and their function. For over two decades, our group has had experience extracting cells from explants taken from all human tissues that are involved in the transmission of sexual disease. This experience has led to publications demonstrating not only these processes in human skin and type II mucosa but also to the discovery of a dendritic cell (DC) that was previously overlooked due to digestion protocols (7,8). In **Chapter 2**, we presented an optimised intestinal tissue digestion protocol, which was published with this author as co-first author (163) . The protocol, consisting of two short sequential digestions, utilised collagenase type IV due to its low tryptic activation formulation. This enzymatic liberation is advantageous over other liberation methods such as spontaneous migration, which we have shown to activate tissue DCs (8). We also demonstrated that the liberated cells remained functional, with MNPs able to upregulate maturations markers (CD54, CD80, CD83 and CD86) as well as producing cytokines (TNF, IL-23p40, IL-6) for 14 hours post-extraction. To be able to examine the different anatomic compartments in intestinal tissue, building on previous studies (141,150) we offered a method to mechanically separate the mucosa and submucosa layers, as well as extract lymphoid follicles under light microscopy, Additionally, we presented a high-parameter flow cytometry panel to investigate the human intestinal MNPs that were known at the time of publication (109,139,140), with an optimised gating strategy and method to correct autofluorescence. Furthermore, a FACS panel was also presented to allow for the individual interrogation of each MNP subset.

Utilising these methods, we were able to investigate the MNPs of the colorectum and their interactions with HIV and CD4 T cells in early HIV infection (**Chapter 3**). Intestinal DC subsets have been previously described and characterised in the small intestine (139,140), divided by CD103 and SIRPa. We have shown herein an alternative gating strategy that allowed for Intestinal DCs to be gated similarly to other tissue types, using XCR1, CD1c and CD207. Additionally, small intestine macrophages had been previously interrogated (109), with four distinct subsets presented. Here, we presented three subsets of colorectal DC, cDC1, $CD207^{+}$ cDC2, and $CD207^{-}$ cDC2, in addition to three macrophage subsets, MDM, t-MDM and Macrophages. Newly defined DC3s were not found in our non-inflamed samples, and they have been suggested to be an

inflammatory cell (169). Tissue-resident Macrophages were significantly abundant in the colon, a trend that was also seen in other sections of the small intestine and rectum. The MNP subsets displayed unique profiles of HIV-entry co-receptor CCR5, with cDC2 and t-MDM displaying the highest levels, suggesting the highest susceptibility to HIV infection, though this data was not available at the time of this thesis submission. HIV-binding lectin receptors CD169 (Siglec-1), CD206 (Mannose Receptor), CD207 (langerin) and CD209 (DC-SIGN) were examined on each MNP subset, and while CD206 was highly expressed by all MNPs except cDC1 and MDM, CD207 was only expressed by $CD207^+$ cDC2, and CD169 and CD209 were expressed by t-MDM and Macrophages, while low levels of CD209 were seen on $CD207^+$ cDC2. Interestingly, the high expression of CD207 on $CD207^+$ cDC2 did not correspond to an increase of HIV uptake compared to $CD207^-$ cDC2, in contrast to dermal $CD207^+$ cDC2 (9). However, while all MNPs demonstrated the capacity for HIV uptake, Macrophages and t-MDM exhibited significantly higher levels of uptake. Notably, the expression of CD169 and CD209 appeared to correlate with elevated HIV uptake by t-MDM and Macrophages. Furthermore, blocking CD169 significantly reduced the ability of Macrophages to take up HIV. We subsequently investigated the interaction between colorectal MNPs and CD4 T cells in HIV transmission. First, we demonstrated that the presence of the bulk DCs, MDM and Macrophages in co-culture enhances HIV infection rates in CD4 T cells. Secondly, we showed that bulk DC and t-MDM were efficient in transferring HIV to CD4 T cells at 2 hours post-exposure. Interestingly, the infection of the CD4 T cells did not correlate to the infectious HIV particles collected from the supernatants, with higher quantities of HIV seen from t-MDMs and Macrophages. This suggests that macrophages are releasing HIV in an infection-independent manner, most likely from CD169-mediated uptake into VCC. Testing this viral release in the presence of a CCR5 inhibitor such as maraviroc would demonstrate this, as is a future direction of this study. This ability of colorectal macrophages to persist with internalised HIV supports existing tissue studies that establish macrophages as a key contributor to the HIV reservoir (47,176).

Our investigation into MNPs in non-inflamed colorectal tissue provides a crucial foundation for understanding the early infection events in this transmission site. However, given the correlation between inflammation and increased transmission of sexual disease (164–166,168) , the study of non-inflamed tissues provides only a partial view of the events of transmission. Additionally, investigating the colorectum in isolation restricts correlation and comparisons to MNPs from other transmission tissues. Representing an unprecedented approach, we endeavoured to design and optimise a high-parameter flow cytometry panel to identify all known MNPs in all inflamed and non-inflamed human sexual transmission tissues. While this idea originally

seemed insurmountable, the broadening range of commercially available fluorophores made the attempt possible. The progress of the panel was hampered by the compounding limitations of human tissue availability, with each interaction requiring samples from at least one of each tissue type (skin, type II mucosa, type I mucosa). Though the panel required four years and two dedicated PhD students, the finalised panel has been submitted to Cytometry A as an OMIP with this author as co-first author (presented here as **Chapter 4**). We were successful in creating one panel that would not only be able to identify all MNPs presented above, but also inflammatory DCs: plasmacytoid DCs (pDC), both $CD123^+$ and $CD11c^+$ Axl^+/ Siglec-6^+ (CD327) DCs (ASDC) and DC3s. Our group was the first to define ASDCs in human anogenital tissue (111), and this panel will enable their detection in multiple tissue types. In addition to phenotype characterisation, we included markers for activation (CD83) and DC migration (CCR7) and proliferation (Ki67), as well as the HIV-binding lectin receptors examined above. The panel was designed to allow for HIV capsid protein p24 to be added to the panel to investigate HIV uptake. Most importantly, this panel was optimised to resolve the highest and lowest expression of each marker across the tissues. Therefore, data from all transmission tissues can be acquired on a single set of flow cytometer settings, allowing for direct correlation of quantitative data from the same MNP subset between different tissues from different donors. Due to time constraints of this PhD, and the extensive optimisation that was required, these experiments will be conducted by my collaborating student colleague and will form part of her thesis submission.

Being able to interrogate *ex vivo* colorectal MNPs offers opportunities to isolate specific cell interactions in controlled conditions. However, to fully understand the events as they occur in tissue, we must utilise spatial data. This *ex vivo* study was originally conceived as a companion study to an existing *in situ* colorectal investigation in our group. This study utilised RNAscope with immunofluorescence microscopy to elucidate the first 2 hours of interactions between HIV and key target cells: CD4 T cells, DCs and tissue-resident macrophages, supported by early *ex vivo* data from this thesis (116). Both studies found that DCs and macrophages ($FXIIIA^+$ macrophages, that are here called tissue-resident Macrophages) both bind and take up more HIV in 2 hours than CD4 T cells, both in total amount of HIV and number of HIV particles per cell. DCs contained significantly higher proportion of HIV compared to their cell number in the lamina propria, while the same was true for Macrophages in the submucosa. Furthermore, DCs were found in greater density adjacent to HIV particles in the epithelium, lamina propria and lymphoid follicles, whereas Macrophages were more densely found near HIV particles in the submucosa. As our *ex vivo* HIV uptake occurs in a suspended culture, all MNPs have equal access to the virus. Due to the higher density of lectin receptors on macrophages, this set up facilitates superior HIV uptake

by macrophages compared to DCs. In contrast, in the lamina propria, DCs exhibit greater mobility within tissues, which favours their capacity for HIV uptake. This mobility and migration are further shown by HIV^+ DCs being concentrated near lymphoid follicles, whereas HIV^- DC, Macrophages and CD4 T cells were not. This migration of HIV^+ DCs would not only facilitate antigen presentation to the CD4 T cells contained therein but also allow for HIV to be trafficked deeper into the tissue via lymphoid follicles, facilitating submucosal macrophage interactions. This and our findings above highlight the importance of continued research into tissue macrophages, as the high density of HIV associated with submucosal macrophages at this 2-hour timepoint suggests that HIV infection of tissue macrophages occurs very early in transmission which, untreated, leads to the establishment of the tissue reservoir.

A limitation of the *ex vivo* data presented is the absence of tissue compartment breakdown. In Chapter 2, we offered a method to separate the colorectal mucosa into three compartments, lamina propria, lymphoid follicle and submucosa, with digestion protocols optimised for each compartment, and differences between lymphocyte and MNP proportions were presented to show enrichment for each compartment. Regrettably, the interrogation of these compartments for MNP identification, proportions, HIV-binding receptors profiles and HIV uptake was intended to utilise the high-parameter flow cytometry panel presented in **Chapter 4**. However, due to delays in panel optimisation, analysis of tissue compartments will need to be pursued as a direction for future research. To further enhance and integrate high-parameter with *in situ* investigation, our group has recently optimised a 35-parameter imaging mass cytometry panel to detect immune cells and HIV in intestinal tissues (202). Developed by Kevin Hu as part of his PhD thesis, his analysis of this panel focused only on lymphocyte interactions with HIV. As the panel contains all the markers necessary to identify the subsets of MNPs presented here, analysing this data will yield spatial insights relevant to the forthcoming HIV uptake experiments within the tissue compartments.

Single-cell RNA sequencing (ScRNA) has recently been conducted on human intestinal tissues (203), infected in vitro-derived MDMs (204), and PBMCs isolated from HIV+ individuals (205,206). However, no dataset currently exists for investigating early HIV infection in human tissue-liberated MNPs. To address this, we intend to develop our own ScRNA dataset on human tissue structural cells, lymphocytes and in particular enriched MNPs. Of interest to the conclusion of this study, MNPs will be exposed to the previously mentioned dual-fluorescent HIV and collected at early and late timepoints to elucidate the transcriptional changes that occur during the first few hours and days of HIV infection. This will be conducted in conjunction with antibody

sequencing (AbSeq, BD), employing a multi-omics approach to correlate transcriptional shifts with surface phenotype changes. This strategy will assist cell identification by facilitating the comparison of known surface marker expression rather than relying solely on transcriptomic profiles. This is particularly important as transcriptomic profiles of tissue MNPs in the first hours of HIV uptake and infection are not currently available for cross-reference. The dual-fluorescent virus enables the distinction between HIV taken up via non-infection pathways and infection resulting in integrated viral DNA. The collection of this unique dataset, across all sexual transmission tissues, will elucidate the changes tissue MNPs undergo in early HIV infection. Additionally, multiple timepoints will allow for the mapping of the kinetics of HIV uptake, infection and the establishment of HIV latency.

Antiretroviral pre-exposure prophylactics (PrEP) has successfully led to reduced rates of HIV transmission. However, as there are still over 1 million new infections every year, understanding the early events in HIV transmission remains a global priority. By understanding how to better block HIV acquisition, an effective vaccine could be developed, but in the meantime could contribute to improved prophylaxis. This is particularly important in cases of genital inflammation, where PrEP has been shown to have reduced effectiveness. To this end, it is crucial to identify the immune cells that are present in human sexual transmission tissues and investigate their contributions to HIV transmission at each relevant site. While specific MNP subsets have been extensively investigated for their early interactions with HIV in human anogenital tissues (7,9,18,155), an understanding of the composition of MNPs and their function during HIV transmission in colorectal tissue lacks the same depth. The investigations performed within this thesis have allowed for the identification all non-inflammatory MNP subsets in the human colorectum and investigated their role in HIV transmission. Using optimised tissue digestion protocols and flow cytometry panels (163), we demonstrated that tissue-resident macrophages are predominant over DCs in this tissue, both in abundance and in their capacity for HIV uptake. Blocking CD169 significantly reduces HIV uptake on Macrophages confirming that it serves as a key receptor for HIV uptake. However, despite the higher levels of HIV uptake, DCs and t-MDMs are more efficient than Macrophages and MDMs at transferring HIV to CD4 T cells, though further investigations into t-MDMs are warranted as they may contain DC-like cells. Additionally, we have presented a high-parameter flow cytometry panel to facilitate ongoing research into inflammatory MNPs from the colorectum asm well as all transmission tissues.

In conclusion, this thesis addresses a significant gap in the understanding of the composition of MNP in the human colorectum and their role in HIV transmission, while outlining clear future directions to further advance HIV transmission research. Moreover, we have emphasised that tissue-resident macrophages, through their interactions with HIV during transmission events, are likely to play a substantial role in the establishment of HIV reservoirs.

Chapter 6. References

1. Andrade VM, Stevenson M. Host and Viral Factors Influencing Interplay between the Macrophage and HIV-1. J Neuroimmune Pharm. 2018;1–11.

2. King HL, Keller SB, Giancola MA, Rodriguez DA, Chau JJ, Young JA, et al. Pre-Exposure Prophylaxis Accessibility Research and Evaluation (PrEPARE Study). Aids Behav. 2014;18(9):1722–5.

3. Schueler K, Ferreira M, Nikolopoulos G, Skaathun B, Paraskevis D, Hatzakis A, et al. Pre-exposure Prophylaxis (PrEP) Awareness and Use Within High HIV Transmission Networks. Aids Behav. 2019;1–11.

4. Hladik F, Doncel GF. Preventing mucosal HIV transmission with topical microbicides: Challenges and opportunities. Antivir Res. 2010;88:S3–9.

5. Nunes R, Sarmento B, Neves J das. Formulation and delivery of anti-HIV rectal microbicides: Advances and challenges. J Control Release. 2014;194:278–94.

6. Burgener A, McGowan I, Klatt NR. HIV and mucosal barrier interactions: consequences for transmission and pathogenesis. Curr Opin Immunol. 2015;36:22–30.

7. Bertram KM, Botting RA, Baharlou H, Rhodes JW, Rana H, Graham JD, et al. Identification of HIV transmitting CD11c+ human epidermal dendritic cells. Nat Commun. 2019;10(1):2759.

8. Botting RA, Bertram KM, Baharlou H, Sandgren KJ, Fletcher J, Rhodes JW, et al. Phenotypic and functional consequences of different isolation protocols on skin mononuclear phagocytes. J Leukocyte Biol. 2017;101(6):1393–403.

9. Rhodes JW, Botting RA, Bertram KM, Vine EE, Rana H, Baharlou H, et al. Human anogenital monocyte-derived dendritic cells and langerin+cDC2 are major HIV target cells. Nat Commun. 2021;12(1):2147.

10. Monin L, Whettlock EM, Male V. Immune responses in the human female reproductive tract. Immunology. 2020;160(2):106–15.

11. Liu A, Yang Y, Liu L, Meng Z, Li L, Qiu C, et al. Differential Compartmentalization of HIV-Targeting Immune Cells in Inner and Outer Foreskin Tissue. Plos One. 2014;9(1):e85176.

12. Rhodes JW, Tong O, Harman AN, Turville SG. Human Dendritic Cell Subsets, Ontogeny, and Impact on HIV Infection. Front Immunol. 2019;10:1088.

13. Neidleman JA, Chen JC, Kohgadai N, Müller JA, Laustsen A, Thavachelvam K, et al. Mucosal stromal fibroblasts markedly enhance HIV infection of CD4+ T cells. Plos Pathog. 2017;13(2):e1006163.

14. Murakami T, Kim J, Li Y, Green G, Shikanov A, Ono A. Secondary lymphoid organ fibroblastic reticular cells mediate trans-infection of HIV-1 via CD44-hyaluronan interactions. Nature Communications. 2018;9(1):2436.

15. Egedal JH, Xie G, Packard TA, Laustsen A, Neidleman J, Georgiou K, et al. Hyaluronic acid is a negative regulator of mucosal fibroblast-mediated enhancement of HIV infection. Mucosal Immunol. 2021;14(5):1203–13.

16. Real F, Sennepin A, Ganor Y, Schmitt A, Bomsel M. Live Imaging of HIV-1 Transfer across T Cell Virological Synapse to Epithelial Cells that Promotes Stromal Macrophage Infection. Cell Reports. 2018;23(6):1794–805.

17. Hladik F, Sakchalathorn P, Ballweber L, Lentz G, Fialkow M, Eschenbach D, et al. Initial Events in Establishing Vaginal Entry and Infection by Human Immunodeficiency Virus Type-1. Immunity. 2007;26(2):257–70.

18. Pena-Cruz V, Agosto LM, Akiyama H, Olson A, Moreau Y, Larrieux JRR, et al. HIV-1 replicates and persists in vaginal epithelial dendritic cells. The Journal of clinical investigation. 2018;128(8):3439–44.

19. Maher D, Wu X, Schacker T, Horbul J, Southern P. HIV binding, penetration, and primary infection in human cervicovaginal tissue. P Natl Acad Sci Usa. 2005;102(32):11504–9.

20. Perez-Zsolt D, Cantero-Pérez J, Erkizia I, Benet S, Pino M, Serra-Peinado C, et al. Dendritic Cells From the Cervical Mucosa Capture and Transfer HIV-1 via Siglec-1. Front Immunol. 2019;10:825.

21. Brenchley JM, Douek DC. HIV infection and the gastrointestinal immune system. Mucosal Immunol. 2008;1(1):mi20071.

22. Mueller SN, Mackay LK. Tissue-resident memory T cells: local specialists in immune defence. Nat Rev Immunol. 2015;16(2):79–89.

23. Ruelas DS, Greene WC. An Integrated Overview of HIV-1 Latency. Cell. 2013;155(3):519–29.

24. Eriksson S, Graf EH, Dahl V, Strain MC, Yukl SA, Lysenko ES, et al. Comparative Analysis of Measures of Viral Reservoirs in HIV-1 Eradication Studies. Plos Pathog. 2013;9(2):e1003174.

25. Ganor Y, Zhou Z, Bodo J, Tudor D, Leibowitch J, Mathez D, et al. The adult penile urethra is a novel entry site for HIV-1 that preferentially targets resident urethral macrophages. Mucosal Immunology. 2012;6(4):776–86.

26. Cavarelli M, Foglieni C, Rescigno M, Scarlatti G. R5 HIV-1 envelope attracts dendritic cells to cross the human intestinal epithelium and sample luminal virions via engagement of the CCR5. Embo Mol Med. 2013;5(5):776–94.

27. Stieh DJ, Matias E, Xu H, Fought AJ, Blanchard JL, Marx PA, et al. Th17 Cells Are Preferentially Infected Very Early after Vaginal Transmission of SIV in Macaques. Cell Host Microbe. 2016;19(4):529–40.

28. Stannah J, Silhol R, Elmes J, Owen B, Shacklett BL, Anton P, et al. Increases in HIV Incidence Following Receptive Anal Intercourse Among Women: A Systematic Review and Meta-analysis. AIDS Behav. 2020;24(3):667–81.

29. Silhol R, Nordsletten A, Maheu-Giroux M, Elmes J, Staunton R, Owen B, et al. The association between heterosexual anal intercourse and HIV acquisition in three prospective cohorts of women. medRxiv. 2022;2022.09.07.22279674.

30. Underhill DM, Gordon S, Imhof BA, Núñez G, Bousso P. Élie Metchnikoff (1845–1916): celebrating 100 years of cellular immunology and beyond. Nat Rev Immunol. 2016;16(10):651–6.

31. Cunningham RS, Sabin FR, Doan CA. The differentiation of two distinct types of phagocytic cells in the spleen of the rabbit. P Soc Exp Biol Med. 1924;21(6):326–9.

32. Barreda DR, Neely HR, Flajnik MF. Evolution of Myeloid Cells. Microbiol Spectr. 2016;4(3).

33. Langerhans P. Uber die nerven der menschlichen haut. Archives of Pathological Anatomy. 1868;44:325–7.

34. Silberberg I. Apposition of mononuclear cells to langerhans cells in contact allergic reactions. An ultrastructural study. Acta Derm-venereol. 1973;53(1):1–12.

35. Steinman RM, Cohn ZA. IDENTIFICATION OF A NOVEL CELL TYPE IN PERIPHERAL LYMPHOID ORGANS OF MICE. J Exp Medicine. 1973;137(5):1142–62.

36. Steinman RM, Cohn ZA. IDENTIFICATION OF A NOVEL CELL TYPE IN PERIPHERAL LYMPHOID ORGANS OF MICE. J Exp Medicine. 1974;139(2):380–97.

37. Haniffa M, Ginhoux F, Wang XN, Bigley V, Abel M, Dimmick I, et al. Differential rates of replacement of human dermal dendritic cells and macrophages during hematopoietic stem cell transplantation. J Exp Medicine. 2009;206(2):371–85.

38. McGovern N, Schlitzer A, Gunawan M, Jardine L, Shin A, Poyner E, et al. Human dermal $CD14^+$ cells are a transient population of monocyte-derived macrophages. Immunity. 2014;41(3):465–77.

39. Villani AC, Satija R, Reynolds G, Sarkizova S, Shekhar K, Fletcher J, et al. Single-cell RNA-seq reveals new types of human blood dendritic cells, monocytes, and progenitors. Sci New York N Y. 2017;356(6335):eaah4573.

40. Cytlak U, Resteu A, Pagan S, Green K, Milne P, Maisuria S, et al. Differential IRF8 Transcription Factor Requirement Defines Two Pathways of Dendritic Cell Development in Humans. Immunity. 2020;53(2):353-370.e8.

41. Bourdely P, Anselmi G, Vaivode K, Ramos RN, Missolo-Koussou Y, Hidalgo S, et al. Transcriptional and Functional Analysis of CD1c+ Human Dendritic Cells Identifies a CD163+ Subset Priming CD8+CD103+ T Cells. Immunity. 2020;53(2):335-352.e8.

42. Dutertre CA, Becht E, Irac SE, Khalilnezhad A, Narang V, Khalilnezhad S, et al. Single-Cell Analysis of Human Mononuclear Phagocytes Reveals Subset-Defining Markers and Identifies Circulating Inflammatory Dendritic Cells. Immunity. 2019;(3):573-589.e8.

43. Sharova N, Swingler C, Sharkey M, Stevenson M. Macrophages archive HIV-1 virions for dissemination in trans. Embo J. 2005;24(13):2481–9.

44. Turville SG, Santos JJ, Frank I, Cameron PU, Wilkinson J, Miranda-Saksena M, et al. Immunodeficiency virus uptake, turnover, and 2-phase transfer in human dendritic cells. Blood. 2004;103(6):2170–9.

45. Nasr N, Lai J, Botting RA, Mercier SK, Harman AN, Kim M, et al. Inhibition of Two Temporal Phases of HIV-1 Transfer from Primary Langerhans Cells to T Cells: The Role of Langerin. J Immunol. 2014;193(5):2554–64.

46. Hendricks CM, Cordeiro T, Gomes AP, Stevenson M. The Interplay of HIV-1 and Macrophages in Viral Persistence. Front Microbiol. 2021;12:646447.

47. Ganor Y, Real F, Sennepin A, Dutertre CA, Prevedel L, Xu L, et al. HIV-1 reservoirs in urethral macrophages of patients under suppressive antiretroviral therapy. Nat Microbiol. 2019;1–12.

48. Sattentau QJ, Stevenson M. Macrophages and HIV-1: An Unhealthy Constellation. Cell Host Microbe. 2016;19(3):304–10.

49. Tan J, Sattentau QJ. The HIV-1-containing macrophage compartment: a perfect cellular niche? Trends Microbiol. 2013;21(8):405–12.

50. Pelchen-Matthews A, Giese S, Mlčochová P, Turner J, Marsh M. β2 Integrin Adhesion Complexes Maintain the Integrity of HIV-1 Assembly Compartments in Primary Macrophages. Traffic. 2012;13(2):273–91.

51. Mlcochova P, Pelchen-Matthews A, Marsh M. Organization and regulation of intracellular plasma membrane-connected HIV-1 assembly compartments in macrophages. Bmc Biol. 2013;11(1):89.

52. Vine EE, Austin PJ, O'Neil TR, Nasr N, Bertram KM, Cunningham AL, et al. Epithelial dendritic cells vs. Langerhans cells: Implications for mucosal vaccines. Cell Rep. 2024;43(4):113977.

53. Harman AN, Kraus M, Bye CR, Byth K, Turville SG, Tang O, et al. HIV-1-infected dendritic cells show 2 phases of gene expression changes, with lysosomal enzyme activity decreased during the second phase. Blood. 2009;114(1):85–94.

54. Cavrois M, Neidleman J, Kreisberg JF, Greene WC. In Vitro Derived Dendritic Cells trans-Infect CD4 T Cells Primarily with Surface-Bound HIV-1 Virions. Plos Pathog. 2007;3(1):e4.

55. McDonald D, Wu L, Bohks SM, KewalRamani VN, Unutmaz D, Hope TJ. Recruitment of HIV and Its Receptors to Dendritic Cell-T Cell Junctions. Science. 2003;300(5623):1295–7.

56. Dupont M, Sattentau QJ. Macrophage Cell-Cell Interactions Promoting HIV-1 Infection. Viruses. 2020;12(5):492.

57. Aggarwal A, Iemma TL, Shih I, Newsome TP, McAllery S, Cunningham AL, et al. Mobilization of HIV Spread by Diaphanous 2 Dependent Filopodia in Infected Dendritic Cells. Plos Pathog. 2012;8(6):e1002762.

58. Eugenin EA, Gaskill PJ, Berman JW. Tunneling nanotubes (TNT) are induced by HIV-infection of macrophages: A potential mechanism for intercellular HIV trafficking. Cell Immunol. 2009;254(2):142–8.

59. Hammonds JE, Beeman N, Ding L, Takushi S, Francis AC, Wang JJ, et al. Siglec-1 initiates formation of the virus-containing compartment and enhances macrophage-to-T cell transmission of HIV-1. PLOS Pathogens. 2017;13(1):e1006181.

60. Nguyen DG, Hildreth JEK. Involvement of macrophage mannose receptor in the binding and transmission of HIV by macrophages. Eur J Immunol. 2003;33(2):483–93.

61. Preza GC, Tanner K, Elliott J, Yang OO, Anton PA, Ochoa MT. Antigen-Presenting Cell Candidates for HIV-1 Transmission in Human Distal Colonic Mucosa Defined by CD207 Dendritic Cells and CD209 Macrophages. AIDS Research and Human Retroviruses. 2014;30(3):241–9.

62. Turville SG, Cameron PU, Handley A, Lin G, Pöhlmann S, Doms RW, et al. Diversity of receptors binding HIV on dendritic cell subsets. Nat Immunol. 2002;3(10):975–83.

63. Jong MAWP de, Geijtenbeek TBH. Langerhans cells in innate defense against pathogens. Trends Immunol. 2010;31(12):452–9.

64. Cunningham AL, Abendroth A, Jones C, Nasr N, Turville S. Viruses and Langerhans cells. Immunol Cell Biol. 2010;88(4):416–23.

65. Ahmed Z, Kawamura T, Shimada S, Piguet V. The Role of Human Dendritic Cells in HIV-1 Infection. J Invest Dermatol. 2015;135(5):1225–33.

66. Valladeau J, Ravel O, Dezutter-Dambuyant C, Moore K, Kleijmeer M, Liu Y, et al. Langerin, a Novel C-Type Lectin Specific to Langerhans Cells, Is an Endocytic Receptor that Induces the Formation of Birbeck Granules. Immunity. 2000;12(1):71–81.

67. Ganor Y, Zhou Z, Tudor D, Schmitt A, Vacher-Lavenu MC, Gibault L, et al. Within 1 h, HIV-1 uses viral synapses to enter efficiently the inner, but not outer, foreskin mucosa and engages Langerhans–T cell conjugates. Mucosal Immunology. 2010;3(5):506–22.

68. Kawamura T, Cohen SS, Borris DL, Aquilino EA, Glushakova S, Margolis LB, et al. Candidate Microbicides Block HIV-1 Infection of Human Immature Langerhans Cells within Epithelial Tissue Explants. J Exp Medicine. 2000;192(10):1491–500.

69. Geijtenbeek TBH, Kwon DS, Torensma R, Vliet SJ van, Duijnhoven GCF van, Middel J, et al. DC-SIGN, a Dendritic Cell–Specific HIV-1-Binding Protein that Enhances trans-Infection of T Cells. Cell. 2000;100(5):587–97.

70. Geijtenbeek TBH, Torensma R, Vliet SJ van, Duijnhoven GCF van, Adema GJ, Kooyk Y van, et al. Identification of DC-SIGN, a Novel Dendritic Cell–Specific ICAM-3 Receptor that Supports Primary Immune Responses. Cell. 2000;100(5):575–85.

71. Steinman RM. DC-SIGN A Guide to Some Mysteries of Dendritic Cells. Cell. 2000;100(5):491–4.

72. Bernhard OK, Lai J, Wilkinson J, Sheil MM, Cunningham AL. Proteomic Analysis of DC-SIGN on Dendritic Cells Detects Tetramers Required for Ligand Binding but No Association with CD4*. J Biol Chem. 2004;279(50):51828–35.

73. Wu L, Martin TD, Han YC, Breun SK, KewalRamani VN. Trans-dominant cellular inhibition of DC-SIGN-mediated HIV-1 transmission. Retrovirology. 2004;1(1):14.

74. Arrighi JF, Pion M, Wiznerowicz M, Geijtenbeek TB, Garcia E, Abraham S, et al. Lentivirus-Mediated RNA Interference of DC-SIGN Expression Inhibits Human Immunodeficiency Virus Transmission from Dendritic Cells to T Cells. J Virol. 2004;78(20):10848–55.

75. Arrighi JF, Pion M, Garcia E, Escola JM, Kooyk Y van, Geijtenbeek TB, et al. DC-SIGN–mediated Infectious Synapse Formation Enhances X4 HIV-1 Transmission from Dendritic Cells to T Cells. J Exp Medicine. 2004;200(10):1279–88.

76. Bracq L, Xie M, Benichou S, Bouchet J. Mechanisms for Cell-to-Cell Transmission of HIV-1. Front Immunol. 2018;9:260.

77. Prasad A, Kulkarni R, Jiang S, Groopman JE. Cocaine Enhances DC to T-cell HIV-1 Transmission by Activating DC-SIGN/LARG/LSP1 Complex and Facilitating Infectious Synapse Formation. Scientific Reports. 2017;7(1):srep40648.

78. Ribeiro CMS, Sarrami-Forooshani R, Setiawan LC, Zijlstra-Willems EM, Hamme JL van, Tigchelaar W, et al. Receptor usage dictates HIV-1 restriction by human TRIM5α in dendritic cell subsets. Nature. 2016;540(7633):448–52.

79. Gringhuis SI, Vlist M van der, Berg LM van den, Dunnen J den, Litjens M, Geijtenbeek TBH. HIV-1 exploits innate signaling by TLR8 and DC-SIGN for productive infection of dendritic cells. Nat Immunol. 2010;11(5):419–26.

80. Gurney KB, Elliott J, Nassanian H, Song C, Soilleux E, McGowan I, et al. Binding and Transfer of Human Immunodeficiency Virus by DC-SIGN+ Cells in Human Rectal Mucosa. Journal of Virology. 2005;79(9):5762–73.

81. Lai J, Bernhard OK, Turville SG, Harman AN, Wilkinson J, Cunningham AL. Oligomerization of the Macrophage Mannose Receptor Enhances gp120-mediated Binding of HIV-1. J Biol Chem. 2009;284(17):11027–38.

82. Izquierdo-Useros N, Naranjo-Gómez M, Archer J, Hatch SC, Erkizia I, Blanco J, et al. Capture and transfer of HIV-1 particles by mature dendritic cells converges with the exosome-dissemination pathway. Blood. 2009;113(12):2732–41.

83. Hatch SC, Archer J, Gummuluru S. Glycosphingolipid Composition of Human Immunodeficiency Virus Type 1 (HIV-1) Particles Is a Crucial Determinant for Dendritic Cell-Mediated HIV-1 trans-Infection ▿ . J Virol. 2009;83(8):3496–506.

84. Puryear WB, Akiyama H, Geer SD, Ramirez NP, Yu X, Reinhard BM, et al. Interferon-Inducible Mechanism of Dendritic Cell-Mediated HIV-1 Dissemination Is Dependent on Siglec-1/CD169. Plos Pathog. 2013;9(4):e1003291.

85. Puryear WB, Yu X, Ramirez NP, Reinhard BM, Gummuluru S. HIV-1 incorporation of host-cell–derived glycosphingolipid GM3 allows for capture by mature dendritic cells. Proc National Acad Sci. 2012;109(19):7475–80.

86. Izquierdo-Useros N, Lorizate M, Puertas MC, Rodriguez-Plata MT, Zangger N, Erikson E, et al. Siglec-1 Is a Novel Dendritic Cell Receptor That Mediates HIV-1 Trans-Infection Through Recognition of Viral Membrane Gangliosides. Plos Biol. 2012;10(12):e1001448.

87. Rempel H, Calosing C, Sun B, Pulliam L. Sialoadhesin Expressed on IFN-Induced Monocytes Binds HIV-1 and Enhances Infectivity. Plos One. 2008;3(4):e1967.

88. Brenchley JM, Price DA, Schacker TW, Asher TE, Silvestri G, Rao S, et al. Microbial translocation is a cause of systemic immune activation in chronic HIV infection. Nat Med. 2006;12(12):1365–71.

89. Pino M, Erkizia I, Benet S, Erikson E, Fernández-Figueras MT, Guerrero D, et al. HIV-1 immune activation induces Siglec-1 expression and enhances viral trans-infection in blood and tissue myeloid cells. Retrovirology. 2015;12(1):37.

90. Sigal A, Kim JT, Balazs AB, Dekel E, Mayo A, Milo R, et al. Cell-to-cell spread of HIV permits ongoing replication despite antiretroviral therapy. Nature. 2011;477(7362):95.

91. Hu ZB, Ma W, Zaborski M, MacLeod R, Quentmeier H, Drexler HG. Establishment and characterization of two novel cytokine-responsive acute myeloid and monocytic leukemia cell lines, MUTZ-2 and MUTZ-3. Leukemia. 1996;10(6):1025–40.

92. Harman AN, Bye CR, Nasr N, Sandgren KJ, Kim M, Mercier SK, et al. Identification of Lineage Relationships and Novel Markers of Blood and Skin Human Dendritic Cells. J Immunol. 2013;190(1):66–79.

93. Liu X, Zhu R, Luo Y, Wang S, Zhao Y, Qiu Z, et al. Distinct human Langerhans cell subsets orchestrate reciprocal functions and require different developmental regulation. Immunity. 2021;54(10):2305-2320.e11.

94. Cimarelli A, Zambruno G, Marconi A, Girolomoni G, Bertazzoni U, Giannetti A. Quantitation by competitive PCR of HIV-1 proviral DNA in epidermal Langerhans cells of HIV-infected patients. J Acq Immun Def Synd. 1994;7(3):230–5.

95. Compton CC, Kupper TS, Nadire KB. HIV-Infected Langerhans Cells Constitute a Significant Proportion of the Epidermal Langerhans Cell Population Throughout the Course of HIV Disease. J Invest Dermatol. 1996;107(6):822–6.

96. Dezutter-Dambuyant C, Charbonnier AS, Schmitt D. [Epithelial dendritic cells and HIV-1 infection in vivo and in vitro]. Pathologie-biologie. 1995;43(10):882–8.

97. Giannetti A, Zambruno G, Cimarelli A, Marconi A, Negroni M, Girolomoni G, et al. Direct detection of HIV-1 RNA in epidermal Langerhans cells of HIV-infected patients. J Acq Immun Def Synd. 1993;6(4):329–33.

98. Henry M, Uthman A, Ballaun C, Stingl G, Tschachler E. Epidermal Langerhans Cells of AIDS Patients Express HIV-1 Regulatory and Structural Genes. J Invest Dermatol. 1994;103(4):593–6.

99. Sugaya M, Loré K, Koup RA, Douek DC, Blauvelt A. HIV-Infected Langerhans Cells Preferentially Transmit Virus to Proliferating Autologous CD4+ Memory T Cells Located within Langerhans Cell-T Cell Clusters. J Immunol. 2004;172(4):2219–24.

100. Pope M, Betjes MGH, Romani N, Hirmand H, Cameron PU, Hoffman L, et al. Conjugates of dendritic cells and memory T lymphocytes from skin facilitate productive infection with HIV-1. Cell. 1994;78(3):389–98.

101. AYEHUNIE S, GROVES RW, BRUZZESE AM, RUPRECHT RM, KUPPER TS, LANGHOFF E. Acutely Infected Langerhans Cells Are More Efficient than T Cells in Disseminating HIV Type 1 to Activated T Cells Following a Short Cell-Cell Contact. Aids Res Hum Retrov. 1995;11(8):877–84.

102. Berger Rudolf, Gartner Suzanne, Rappersberger Kiemens, Foster CA, Wolff Klaus, Stingl Georg. Isolation of Human Immunodeficiency Virus Type 1 from Human Epidermis: Virus Replication and Transmission Studies. J Invest Dermatol. 1992;99(3):271–7.

103. Zhou Z, Longchamps NB de, Schmitt A, Zerbib M, Vacher-Lavenu MC, Bomsel M, et al. HIV-1 Efficient Entry in Inner Foreskin Is Mediated by Elevated CCL5/RANTES that Recruits T Cells and Fuels Conjugate Formation with Langerhans Cells. Plos Pathog. 2011;7(6):e1002100.

104. Witte L de, Nabatov A, Pion M, Fluitsma D, Jong MAWP de, Gruijl T de, et al. Langerin is a natural barrier to HIV-1 transmission by Langerhans cells. Nat Med. 2007;13(3):367–71.

105. Eckstein DA, Penn ML, Korin YD, Scripture-Adams DD, Zack JA, Kreisberg JF, et al. HIV-1 Actively Replicates in Naive CD4+ T Cells Residing within Human Lymphoid Tissues. Immunity. 2001;15(4):671–82.

106. Münch J, Rücker E, Ständker L, Adermann K, Goffinet C, Schindler M, et al. Semen-Derived Amyloid Fibrils Drastically Enhance HIV Infection. Cell. 2007;131(6):1059–71.

107. Wollenberg A, Oppel T, Schottdorf EM, Günther S, Moderer M, Mommaas M. Expression and Function of the Mannose Receptor CD206 on Epidermal Dendritic Cells in Inflammatory Skin Diseases. Journal of Investigative Dermatology. 2002;118(2):327–34.

108. Wollenberg A, Kraft S, Hanau D, Bieber T. Immunomorphological and Ultrastructural Characterization of Langerhans Cells and a Novel, Inflammatory Dendritic Epidermal Cell (IDEC) Population in Lesional Skin of Atopic Eczema. J Invest Dermatol. 1996;106(3):446–53.

109. Bujko A, Atlasy N, Landsverk OJB, Richter L, Yaqub S, Horneland R, et al. Transcriptional and functional profiling defines human small intestinal macrophage subsets. J Exp Med. 2017;215(2):jem.20170057.

110. Rodriguez-Garcia M, Shen Z, Barr FD, Boesch AW, Ackerman ME, Kappes JC, et al. Dendritic cells from the human female reproductive tract rapidly capture and respond to HIV. Mucosal Immunology. 2016;

111. Dijk FAW van, Tong O, O'Neil TR, Bertram KM, Hu K, Baharlou H, et al. Characterising plasmacytoid and myeloid AXL+ SIGLEC-6+ dendritic cell functions and their interactions with HIV. PLOS Pathog. 2024;20(6):e1012351.

112. Ruffin N, Gea-Mallorquí E, Brouiller F, Jouve M, Silvin A, See P, et al. Constitutive Siglec-1 expression confers susceptibility to HIV-1 infection of human dendritic cell precursors. Proc National Acad Sci. 2019;116(43):21685–93.

113. Shen R, Kappes JC, Smythies LE, Richter HE, Novak L, Smith PD. Vaginal Myeloid Dendritic Cells Transmit Founder HIV-1. J Virol. 2014;88(13):7683–8.

114. Shen R, Smythies LE, Clements RH, Novak L, Smith PD. Dendritic cells transmit HIV-1 through human small intestinal mucosa. J Leukocyte Biol. 2010;87(4):663–70.

115. Trifonova RT, Bollman B, Barteneva NS, Lieberman J. Myeloid Cells in Intact Human Cervical Explants Capture HIV and Can Transmit It to CD4 T Cells. Front Immunol. 2018;9:2719.

116. Baharlou H, Canete N, Vine EE, Hu K, Yuan D, Sandgren KJ, et al. An in situ analysis pipeline for initial host-pathogen interactions reveals signatures of human colorectal HIV transmission. Cell Rep. 2022;40(12):111385.

117. Bertram KM, O'Neil TR, Vine EE, Baharlou H, Cunningham AL, Harman AN. Defining the landscape of human epidermal mononuclear phagocytes. Immunity. 2023;56(3):459–60.

118. Vine EE, Rhodes JW, Dijk FAW van, Byrne SN, Bertram KM, Cunningham AL, et al. HIV transmitting mononuclear phagocytes; integrating the old and new. Mucosal Immunol. 2022;1–9.

119. Shen R, Richter HE, Smith PD. Early HIV-1 Target Cells in Human Vaginal and Ectocervical Mucosa. Am J Reprod Immunol. 2011;65(3):261–7.

120. Ganor Y, Real F, Sennepin A, Dutertre CA, Prevedel L, Xu L, et al. HIV-1 reservoirs in urethral macrophages of patients under suppressive antiretroviral therapy. Nat Microbiol. 2019;1–12.

121. Woottum M, Yan S, Sayettat S, Grinberg S, Cathelin D, Bekaddour N, et al. Macrophages: Key Cellular Players in HIV Infection and Pathogenesis. Viruses. 2024;16(2):288.

122. Stevenson M. HIV persistence in macrophages. Nat Med. 2017;23(5):538–9.

123. Esra RT, Olivier AJ, Passmore JAS, Jaspan HB, Harryparsad R, Gray CM. Does HIV Exploit the Inflammatory Milieu of the Male Genital Tract for Successful Infection? Front Immunol. 2016;7:245.

124. Powers KA, Poole C, Pettifor AE, Cohen MS. Rethinking the heterosexual infectivity of HIV-1: a systematic review and meta-analysis. Lancet Infect Dis. 2008;8(9):553–63.

125. Passmore JAS, Jaspan HB, Masson L. Genital inflammation, immune activation and risk of sexual HIV acquisition. Curr Opin Hiv Aids. 2016;11(2):156–62.

126. Cheu RK, Gustin AT, Lee C, Schifanella L, Miller CJ, Ha A, et al. Impact of vaginal microbiome communities on HIV antiretroviral-based pre-exposure prophylaxis (PrEP) drug metabolism. PLoS Pathog. 2020;16(12):e1009024.

127. Adapen C, Réot L, Menu E. Role of the human vaginal microbiota in the regulation of inflammation and sexually transmitted infection acquisition: Contribution of the non-human primate model to a better understanding? Front Reprod Heal. 2022;4:992176.

128. Torcia MG. Interplay among Vaginal Microbiome, Immune Response and Sexually Transmitted Viral Infections. Int J Mol Sci. 2019;20(2):266.

129. Lewis FMT, Bernstein KT, Aral SO. Vaginal Microbiome and Its Relationship to Behavior, Sexual Health, and Sexually Transmitted Diseases. Obstet Gynecol. 2017;129(4):643–54.

130. Tang-Huau TL, Segura E. Human in vivo-differentiated monocyte-derived dendritic cells. Semin Cell Dev Biol. 2018;86:44–9.

131. See P, Dutertre CA, Chen J, Günther P, McGovern N, Irac SE, et al. Mapping the human DC lineage through the integration of high-dimensional techniques. Science. 2017;356(6342):eaag3009.

132. Caër C, Wick MJ. Human Intestinal Mononuclear Phagocytes in Health and Inflammatory Bowel Disease. Front Immunol. 2020;11:410.

133. Chow A, Brown BD, Merad M. Studying the mononuclear phagocyte system in the molecular age. Nat Rev Immunol. 2011;11(11):788–98.

134. Haniffa M, Bigley V, Collin M. Human mononuclear phagocyte system reunited. Semin Cell Dev Biol. 2015;41:59–69.

135. Artyomov MN, Munk A, Gorvel L, Korenfeld D, Cella M, Tung T, et al. Modular expression analysis reveals functional conservation between human Langerhans cells and mouse cross-priming dendritic cells. J Exp Med. 2015;212(5):743–57.

136. Carpentier S, Manh TPV, Chelbi R, Henri S, Malissen B, Haniffa M, et al. Comparative genomics analysis of mononuclear phagocyte subsets confirms homology between lymphoid tissue-resident and dermal XCR1+ DCs in mouse and human and distinguishes them from Langerhans cells. J Immunol Methods. 2016;432:35–49.

137. Chu CC, Ali N, Karagiannis P, Meglio PD, Skowera A, Napolitano L, et al. Resident CD141 (BDCA3)+ dendritic cells in human skin produce IL-10 and induce regulatory T cells that suppress skin inflammation. J Exp Med. 2012;209(5):935–45.

138. Haniffa M, Shin A, Bigley V, McGovern N, Teo P, See P, et al. Human Tissues Contain CD141hi Cross-Presenting Dendritic Cells with Functional Homology to Mouse CD103+ Nonlymphoid Dendritic Cells. Immunity. 2012;37(1):60–73.

139. Richter L, Landsverk OJB, Atlasy N, Bujko A, Yaqub S, Horneland R, et al. Transcriptional profiling reveals monocyte-related macrophages phenotypically resembling DC in human intestine. Mucosal Immunol. 2018;11(5):1512–23.

140. Watchmaker PB, Lahl K, Lee M, Baumjohann D, Morton J, Kim SJ, et al. Comparative transcriptional and functional profiling defines conserved programs of intestinal DC differentiation in humans and mice. Nat Immunol. 2013;15(1):ni.2768.

141. Fenton TM, Jørgensen PB, Niss K, Rubin SJS, Mörbe UM, Riis LB, et al. Immune Profiling of Human Gut-Associated Lymphoid Tissue Identifies a Role for Isolated Lymphoid Follicles in Priming of Region-Specific Immunity. Immunity. 2020;52(3):557-570.e6.

142. Bachem A, Güttler S, Hartung E, Ebstein F, Schaefer M, Tannert A, et al. Superior antigen cross-presentation and XCR1 expression define human CD11c+CD141+ cells as homologues of mouse CD8+ dendritic cells. J Exp Med. 2010;207(6):1273–81.

143. Roca CP, Burton OT, Gergelits V, Prezzemolo T, Whyte CE, Halpert R, et al. AutoSpill is a principled framework that simplifies the analysis of multichromatic flow cytometry data. Nat Commun. 2021;12(1):2890.

144. Harman AN, Wilkinson J, Bye CR, Bosnjak L, Stern JL, Nicholle M, et al. HIV Induces Maturation of Monocyte-Derived Dendritic Cells and Langerhans Cells. J Immunol. 2006;177(10):7103–13.

145. Banchereau J, Briere F, Caux C, Davoust J, Lebecque S, Liu YJ, et al. Immunobiology of Dendritic Cells. Annu Rev Immunol. 2000;18(1):767–811.

146. Stagg AJ. Intestinal Dendritic Cells in Health and Gut Inflammation. Front Immunol. 2018;9:2883.

147. Lefrançois L, Lycke N. Isolation of Mouse Small Intestinal Intraepithelial Lymphocytes, Peyer's Patch, and Lamina Propria Cells. Curr Protoc Immunol. 1996;17(1):3.19.1-3.19.16.

148. Durack J, Lynch SV. The gut microbiome: Relationships with disease and opportunities for therapy. J Exp Med. 2019;216(1):20–40.

149. Ahn H, Kang SG, Yoon S il, Ko HJ, Kim PH, Hong EJ, et al. Methylene blue inhibits NLRP3, NLRC4, AIM2, and non-canonical inflammasome activation. Sci Rep. 2017;7(1):12409.

150. Jørgensen PB, Fenton TM, Mörbe UM, Riis LB, Jakobsen HL, Nielsen OH, et al. Identification, isolation and analysis of human gut-associated lymphoid tissues. Nat Protoc. 2021;16(4):2051–67.

151. Bigley V, McGovern N, Milne P, Dickinson R, Pagan S, Cookson S, et al. Langerin-expressing dendritic cells in human tissues are related to CD1c + dendritic cells and distinct from Langerhans cells and CD141 high XCR1 + dendritic cells. J Leukocyte Biol. 2014;97(4):627–34.

152. Collin M, Bigley V. Human dendritic cell subsets: an update. Immunology. 2018;154(1):3–20.

153. McKinnon LR, Liebenberg LJ, Yende-Zuma N, Archary D, Ngcapu S, Sivro A, et al. Genital inflammation undermines the effectiveness of tenofovir gel in preventing HIV acquisition in women. Nat Med. 2018;24(4):491–6.

154. Spinner CD, Boesecke C, Zink A, Jessen H, Stellbrink HJ, Rockstroh JK, et al. HIV pre-exposure prophylaxis (PrEP): a review of current knowledge of oral systemic HIV PrEP in humans. Infection. 2016;44(2):151–8.

155. Parthasarathy S, Lara LM de, Carrillo-Salinas FJ, Werner A, Borchers A, Iyer V, et al. Human genital dendritic cell heterogeneity confers differential rapid response to HIV-1 exposure. Front Immunol. 2024;15:1472656.

156. Silhol R, Nordsletten A, Maheu-Giroux M, Elmes J, Staunton R, Owen B, et al. The Association Between Heterosexual anal Intercourse and HIV Acquisition in Three Prospective Cohorts of Women. AIDS Behav. 2023;27(12):4010–21.

157. Shen R, Richter HE, Clements RH, Novak L, Huff K, Bimczok D, et al. Macrophages in Vaginal but Not Intestinal Mucosa Are Monocyte-Like and Permissive to Human Immunodeficiency Virus Type 1 Infection. Journal of Virology. 2009;83(7):3258–67.

158. Domanska D, Majid U, Karlsen VT, Merok MA, Beitnes ACR, Yaqub S, et al. Single-cell transcriptomic analysis of human colonic macrophages reveals niche-specific subsets. J Exp Med. 2022;219(3).

159. Deymier MJ, Ende Z, Fenton-May AE, Dilernia DA, Kilembe W, Allen SA, et al. Heterosexual Transmission of Subtype C HIV-1 Selects Consensus-Like Variants without Increased Replicative Capacity or Interferon-α Resistance. Plos Pathog. 2015;11(9):e1005154.

160. Hao Y, Stuart T, Kowalski MH, Choudhary S, Hoffman P, Hartman A, et al. Dictionary learning for integrative, multimodal and scalable single-cell analysis. Nat Biotechnol. 2024;42(2):293–304.

161. Trapnell C, Cacchiarelli D, Grimsby J, Pokharel P, Li S, Morse M, et al. The dynamics and regulators of cell fate decisions are revealed by pseudotemporal ordering of single cells. Nat Biotechnol. 2014;32(4):381–6.

162. Chen Y, Hwang SL, Chan VSF, Chung NPY, Wang SR, Li Z, et al. Binding of HIV-1 gp120 to DC-SIGN promotes ASK-1-dependent activation-induced apoptosis of human dendritic cells. Plos Pathog. 2013;9(1):e1003100.

163. Doyle CM, Vine EE, Bertram KM, Baharlou H, Rhodes JW, Dervish S, et al. Optimal Isolation Protocols for Examining and Interrogating Mononuclear Phagocytes From Human Intestinal Tissue. Front Immunol. 2021;12:727952.

164. Masson L, Passmore JAS, Liebenberg LJ, Werner L, Baxter C, Arnold KB, et al. Genital Inflammation and the Risk of HIV Acquisition in Women. Clin Infect Dis. 2015;61(2):260–9.

165. Lemos MP, Lama JR, Karuna ST, Fong Y, Montano SM, Ganoza C, et al. The Inner Foreskin of Healthy Males at Risk of HIV Infection Harbors Epithelial CD4+ CCR5+ Cells and Has Features of an Inflamed Epidermal Barrier. PLoS ONE. 2014;9(9):e108954.

166. Hearps AC, Tyssen D, Srbinovski D, Bayigga L, Diaz DJD, Aldunate M, et al. Vaginal lactic acid elicits an anti-inflammatory response from human cervicovaginal epithelial cells and inhibits production of pro-inflammatory mediators associated with HIV acquisition. Mucosal Immunol. 2017;10(6):1480–90.

167. Rana H, Truong NR, Johnson B, Baharlou H, Herbert JJ, Kandasamy S, et al. Herpes simplex virus spreads rapidly in human foreskin, partly driven by chemokine-induced redistribution of Nectin-1 on keratinocytes. PLOS Pathog. 2024;20(6):e1012267.

168. Cruz NCDL, Möckel M, Wirtz L, Sunaoglu K, Malter W, Zinser M, et al. Ex Vivo Infection of Human Skin with Herpes Simplex Virus 1 Reveals Mechanical Wounds as Insufficient Entry Portals via the Skin Surface. J Virol. 2021;95(21):10.1128/jvi.01338-21.

169. Dijk FAW van, Bertram KM, O'Neil TR, Li Y, Buffa DJ, Harman AN, et al. Recent Advances in Our Understanding of Human Inflammatory Dendritic Cells in Human Immunodeficiency Virus Infection. Viruses. 2025;17(1):105.

170. Izquierdo-Useros N, Lorizate M, McLaren PJ, Telenti A, Kräusslich HG, Martinez-Picado J. HIV-1 Capture and Transmission by Dendritic Cells: The Role of Viral Glycolipids and the Cellular Receptor Siglec-1. Plos Pathog. 2014;10(7):e1004146.

171. Gummuluru S, Ramirez NGP, Akiyama H. CD169-Dependent Cell-Associated HIV-1 Transmission: A Driver of Virus Dissemination. J Infect Dis. 2014;210(suppl_3):S641–7.

172. Perez-Zsolt D, Raïch-Regué D, Muñoz-Basagoiti J, Aguilar-Gurrieri C, Clotet B, Blanco J, et al. HIV-1 trans-Infection Mediated by DCs: The Tip of the Iceberg of Cell-to-Cell Viral Transmission. Pathogens. 2021;11(1):39.

173. Sewald X, Ladinsky MS, Uchil PD, Beloor J, Pi R, Herrmann C, et al. Retroviruses use CD169-mediated trans-infection of permissive lymphocytes to establish infection. Science. 2015;350(6260):563–7.

174. Berre S, Gaudin R, Alencar BC de, Desdouits M, Chabaud M, Naffakh N, et al. CD36-specific antibodies block release of HIV-1 from infected primary macrophages and its transmission to T cells. J Exp Med. 2013;210(12):2523–38.

175. Gaudin R, Alencar BC de, Jouve M, Bèrre S, Bouder EL, Schindler M, et al. Critical role for the kinesin KIF3A in the HIV life cycle in primary human macrophages. J Cell Biol. 2012;199(3):467–79.

176. Zalar A, Figueroa MI, Ruibal-Ares B, Baré P, Cahn P, Bracco MM de E de, et al. Macrophage HIV-1 infection in duodenal tissue of patients on long term HAART. Antivir Res. 2010;87(2):269–71.

177. Bain CC, Schridde A. Origin, Differentiation, and Function of Intestinal Macrophages. Front Immunol. 2018;9:2733.

178. Duluc D, Gannevat J, Anguiano E, Zurawski S, Carley M, Boreham M, et al. Functional diversity of human vaginal APC subsets in directing T-cell responses. Mucosal Immunol. 2013;6(3):626–38.

179. Segura E, Durand M, Amigorena S. Similar antigen cross-presentation capacity and phagocytic functions in all freshly isolated human lymphoid organ–resident dendritic cells. J Exp Med. 2013;210(5):1035–47.

180. Battivelli E, Dahabieh MS, Abdel-Mohsen M, Svensson JP, Silva ITD, Cohn LB, et al. Distinct chromatin functional states correlate with HIV latency reactivation in infected primary CD4+ T cells. eLife. 2018;7:e34655.

181. Segura E, Touzot M, Bohineust A, Cappuccio A, Chiocchia G, Hosmalin A, et al. Human Inflammatory Dendritic Cells Induce Th17 Cell Differentiation. Immunity. 2013;38(2):336–48.

182. Mair F, Liechti T. Comprehensive Phenotyping of Human Dendritic Cells and Monocytes. Cytom Part A. 2021;99(3):231–42.

183. Arnold KB, Burgener A, Birse K, Romas L, Dunphy LJ, Shahabi K, et al. Increased levels of inflammatory cytokines in the female reproductive tract are associated with altered expression of proteases, mucosal barrier proteins, and an influx of HIV-susceptible target cells. Mucosal Immunol. 2016;9(1):194–205.

184. Borgdorff H, Gautam R, Armstrong SD, Xia D, Ndayisaba GF, Teijlingen NH van, et al. Cervicovaginal microbiome dysbiosis is associated with proteome changes related to alterations of the cervicovaginal mucosal barrier. Mucosal Immunol. 2016;9(3):621–33.

185. Zevin AS, Xie IY, Birse K, Arnold K, Romas L, Westmacott G, et al. Microbiome Composition and Function Drives Wound-Healing Impairment in the Female Genital Tract. PLoS Pathog. 2016;12(9):e1005889.

186. Silvin A, Yu CI, Lahaye X, Imperatore F, Brault JB, Cardinaud S, et al. Constitutive resistance to viral infection in human CD141+ dendritic cells. Sci Immunol. 2017;2(13):eaai8071.

187. Ziegler-Heitbrock L, Ancuta P, Crowe S, Dalod M, Grau V, Hart DN, et al. Nomenclature of monocytes and dendritic cells in blood. Blood. 2010;116(16):e74–80.

188. Zaba LC, Fuentes-Duculan J, Eungdamrong NJ, Abello MV, Novitskaya I, Pierson KC, et al. Psoriasis Is Characterized by Accumulation of Immunostimulatory and Th1/Th17 Cell-Polarizing Myeloid Dendritic Cells. J Investig Dermatol. 2009;129(1):79–88.

189. Eguíluz-Gracia I, Bosco A, Dollner R, Melum GR, Lexberg MH, Jones AC, et al. Rapid recruitment of CD14+ monocytes in experimentally induced allergic rhinitis in human subjects. J Allergy Clin Immunol. 2016;137(6):1872-1881.e12.

190. Tang-Huau TL, Gueguen P, Goudot C, Durand M, Bohec M, Baulande S, et al. Human in vivo-generated monocyte-derived dendritic cells and macrophages cross-present antigens through a vacuolar pathway. Nat Commun. 2018;9(1):2570.

191. Chen W, Jin B, Cheng C, Peng H, Zhang X, Tan W, et al. Single-cell profiling reveals kidney CD163+ dendritic cell participation in human lupus nephritis. Ann Rheum Dis. 2024;83(5):608–23.

192. Nakamizo S, Dutertre CA, Khalilnezhad A, Zhang XM, Lim S, Lum J, et al. Single-cell analysis of human skin identifies CD14+ type 3 dendritic cells co-producing IL1B and IL23A in psoriasis. J Exp Med. 2021;218(9):e20202345.

193. Jardine L, Wiscombe S, Reynolds G, McDonald D, Fuller A, Green K, et al. Lipopolysaccharide inhalation recruits monocytes and dendritic cell subsets to the alveolar airspace. Nat Commun. 2019;10(1):1999.

194. Reynolds G, Vegh P, Fletcher J, Poyner EFM, Stephenson E, Goh I, et al. Developmental cell programs are co-opted in inflammatory skin disease. Science. 2021;371(6527).

195. Ohl L, Mohaupt M, Czeloth N, Hintzen G, Kiafard Z, Zwirner J, et al. CCR7 Governs Skin Dendritic Cell Migration under Inflammatory and Steady-State Conditions. Immunity. 2004;21(2):279–88.

196. Doyle CM, Fewings NL, Ctercteko G, Byrne SN, Harman AN, Bertram KM. OMIP 082: A 25-color phenotyping to define human innate lymphoid cells, natural killer cells, mucosal-associated invariant T cells, and γδ T cells from freshly isolated human intestinal tissue. Cytom Part A. 2022;101(3):196–202.

197. O'Neil TR, Harman AN, Cunningham AL, Nasr N, Bertram KM. OMIP-096: A 24-color flow cytometry panel to identify and characterize CD4+ and CD8+ tissue-resident T cells in human skin, intestinal, and type II mucosal tissue. Cytom Part A. 2023;103(11):851–6.

198. Cohen E, Mariotton J, Rozenberg F, Sams A, Kuppevelt TH van, Delongchamps NB, et al. CGRP inhibits human Langerhans cells infection with HSV by differentially modulating specific HSV-1 and HSV-2 entry mechanisms. Mucosal Immunol. 2022;15(4):762–71.

199. Shimizu K, Libby P, Rocha VZ, Folco EJ, Shubiki R, Grabie N, et al. Loss of Myeloid Related Protein-8/14 Exacerbates Cardiac Allograft Rejection. Circulation. 2011;124(25):2920–32.

200. Jardine L, Barge D, Ames-Draycott A, Pagan S, Cookson S, Spickett G, et al. Rapid Detection of Dendritic Cell and Monocyte Disorders Using CD4 as a Lineage Marker of the Human Peripheral Blood Antigen-Presenting Cell Compartment. Front Immunol. 2013;4:495.

201. Kristensen MW, Kejlberg-Jensen S, Sørensen AS, Vorup-Jensen T, Kragstrup TW, Hokland M, et al. Behold Cytometrists: One Block Is Not Enough! Cyanine-Tandems Bind Non-Specifically to Human Monocytes. Cytom Part A. 2021;99(3):265–8.

202. Hu K, O'Neil T, Canete N, Baharlou H, Harman A. OMIP-103: A 35-marker imaging mass cytometry panel for the co-detection of HIV and immune cell populations in human formalin fixed paraffin embedded intestinal tissue. Cytom Part A. 2024;105(7):488–92.

203. Oliver AJ, Huang N, Bartolome-Casado R, Li R, Koplev S, Nilsen HR, et al. Single-cell integration reveals metaplasia in inflammatory gut diseases. Nature. 2024;635(8039):699–707.

204. Calado M, Pires D, Conceição C, Ferreira R, Santos-Costa Q, Anes E, et al. Cell-to-Cell Transmission of HIV-1 and HIV-2 from Infected Macrophages and Dendritic Cells to CD4+ T Lymphocytes. Viruses. 2023;15(5):1030.

205. Lee D, Choi SY, Shin SI, An H, Choi BS, Park J. Multi-Omics Single-Cell Analysis Reveals Key Regulators of HIV-1 Persistence and Aberrant Host Immune Responses in Early Infection. 2025;

206. Zaongo SD, Harypursat V, Chen Y. Single-Cell Sequencing Facilitates Elucidation of HIV Immunopathogenesis: A Review of Current Literature. Front Immunol. 2022;13:828860.